UNIVERSITÀ DEGLI STUDI DI MILANO
DOCTORAL SCHOOL OF CHEMICAL SCIENCES AND TECHNOLOGIES
DEPARTMENT OF CHEMISTRY
PHD COURSE IN INDUSTRIAL CHEMISTRY, XXVIII CYCLE

Tumor Targeting via Integrin Ligands: Synthesis and Biological Evaluation of RGD Peptidomimetic-Drug Conjugates

CHIM/06 Organic Chemistry

Alberto DAL CORSO
R10075

Tutor: Prof. Dr. Cesare GENNARI
Academic Co-Tutor: Dr. Luca PIGNATARO
Industrial Co-Tutor: Dr. Michele CARUSO (Nerviano Medical Sciences S.R.L.)

Co-ordinator: Prof. Dr. Dominique ROBERTO

A.Y. 2014/2015

The present work was led by:	Prof. C. Gennari, Dr. L. Pignataro and Dr. M. Caruso	
Doctoral Final Oral Examination:	December, 1st 2015	
Examination Committee:	Chairperson:	Prof. Dr. L. Colombo Università degli Studi di Pavia (I)
	Second Member:	Prof. Dr. P. Seneci Università degli Studi di Milano (I)
	Third Member:	Prof. Dr. M. Zanda University of Aberdeen (UK)

The work herein described was performed at the University of Milan at the Department of Chemistry, in collaboration with Nerviano Medical Sciences, in the period from November 2012 to October 2015 under the supervision of Prof. Cesare Gennari.

I sincerely acknowledge my supervisors, Prof. Gennari, Dr. Pignataro and Dr. Caruso, for giving me the opportunity to work in a challenging and multidisciplinary project, for their steady support and for their huge contribution to my scientific education. I gratefully thank Dr. Daniele Donati and all the NMS staff, without whom this project would not have been possible. A special thanks is given to all the chemists I've been working and living with every day at UNIMI, for being my second family for 4 years. This work is dedicated to my sweet parents, Bianca and Gianni, and to my beloved sister, Ilaria.

Table of Contents

Abbreviations

Aba	Azabicycloalkane
Ac	Acetyl
ADC	Antibody-drug conjugate
Alloc	Allyloxycarbonyl
Ampro	4-Aminoproline
aq.	Aqueous solution
Bn	Benzyl
Boc	*tert*-Butyloxycarbonyl
BSA	Bovine serum albumin
Bu	Butyl
Bz	Benzoyl
Cit	Citrulline
CPT	Camptothecin
DAVB	Desacetyl vinblastine
DAVBH	Desacetyl vinblastine hydrazide
DCC	*N*,*N*'-Dicyclohexylcarbodiimide
DIC	*N*,*N*'-Diisopropylcarbodiimide
DKP	Diketopiperazine
DMAP	4-Dimethylaminopyridine
DME	Dimethoxyethane
DMF	*N*,*N*-Dimethylformamide
DMSO	Dimethyl sulfoxide
DNR	Daunorubicin
DOX	Doxorubicin
EDC	1-Ethyl-3-(3-dimethylaminopropyl)carbodiimide
EEDQ	*N*-Ethoxycarbonyl-2-ethoxy-1,2-dihydroquinoline
EPR	Enhanced permeability and retention
eq	Equivalents
ESI	Electrospray ionisation
Et	Ethyl
FAK	Focal adhesion kinase
FDA	Food and Drug Administration
Fmoc	9-Fluorenylmethoxycarbonyl
FRET	Fluorescence Resonance Energy Transfer
HATU	O-(7-azabenzotriazol-1-yl)-tetramethyl-uronium hexafluorophosphate
HOAt	1-Hydroxy-7-azabenzotriazole
HPLC	High performance liquid chromatography
HRMS	High resolution mass spectrometry
IC	Inhibitory capacity
ID	Injected dose
IgG	Immunoglobulin G
*i*Pr	Isopropyl
J	Scalar coupling constants
LC	Lethal concentration
mAb	Monoclonal antibody
MALDI	Matrix-assisted laser desorption ionization
Me	Methyl
MMAE	Monomethyl auristatin E
MMP	Matrix metalloproteinase
MS	Mass spectroscopy
MW	Molecular weight
Naph.	Naphthalimide
NMR	Nuclear Magnetic Resonance
NHS	*N*-Hydroxysuccinimide
PBS	Phosphate-buffered saline
PEG	Polyethylene glycol
PET	Positron emission tomography

Ph	Phenyl		of caspases
ppm	Part per million	SMDC	Small molecue-drug conjugate
PSMA	Prostate specific membrane antigen	*t*Bu	*tert*-Butyl
		tert	Tertiary
PTX	Paclitaxel	TFA	Trifluoroacetic acid
quant.	Quantitative	THF	Tetrahydrofuran
R_f	Retention factor	TK	Tyrosine kinase
RPMI	Roswell Park Memorial Institute	TMS	Tetramethylsilane
		t_R	Retention time
RT	Room temperature	unc	Uncleavable
SMAC	Second mitochondrial activator	δ	Chemical shift

Amino acid*	**One-letter code**	**Three-letter code**
Alanine	A	Ala
Arginine	R	Arg
Asparagine	N	Asn
Aspartic	D	Asp
Cysteine	C	Cys
Glutamine	Q	Gln
Glutamic acid	E	Glu
Glycine	G	Gly
Histidine	H	His
Isoleucine	I	Ile
Leucine	L	Leu
Lysine	K	Lys
Methionine	M	Met
Phenylalanine	F	Phe
Proline	P	Pro
Serine	S	Ser
Threonine	T	Thr
Tryptophan	W	Trp
Tyrosine	Y	Tyr
Valine	V	Val

* D-amino acids are described by D-Xaa in the three-letter code and with the small letter in the one-letter code.

General Introduction

The administration of cytotoxic agents traditionally represents a significant component of pharmacologic approaches for tumor therapy. These compounds induce cell death by interfering with fundamental steps of cell growth and replication, but their efficiency as anticancer agents is often limited by their non-exclusive activity against tumor cells. This drawback typically results in severe side-effects, limiting therapeutic benefits.

Different approaches to overcome the limitations of conventional chemotherapy have been investigated so far, aiming at the selective delivery of cytotoxic agents to cancer cells. Among these strategies, promising results have been achieved with the covalent conjugation of anticancer drugs to different ligands, capable of binding to proteins or other receptors overexpressed on the surface of tumor cells. In the so-called small molecule-drug conjugate (SMDC) technology, a variety of natural compounds, but also synthetic peptides and peptidomimetics are exploited as drug-targeting vehicles, due to their high affinity for specific tumor antigens.

This PhD thesis describes the synthesis of new SMDCs targeting $\alpha_v\beta_3$ integrin, a heterodimeric transmembrane glycoprotein overexpressed in several tumor cells. These new anticancer devices consist of three fundamental components:

- *Ligand* - The *cyclo*[DKP-RGD] peptidomimetic, developed by the Gennari and Piarulli group, has been used as integrin-targeting module in all the new SMDCs;
- *Drug* - Three different cytotoxic agents (i.e. paclitaxel, daunorubicin and camptothecin) have been included as anticancer payloads;
- *Linker* - Specific functional groups (i.e. peptides and disulfide bonds) have been used to connect the drug and ligand modules, aiming at the selective drug release in the intracellular environment.

These new SMDCs have been subjected to a panel of biochemical and biological assays, for the assessment of both their structural features (e.g. stability, kinetics of drug release, etc.) and biological activity (e.g. affinity for the purified receptor, selective cytotoxicity against $\alpha_v\beta_3$-expressing cells, etc.).

The structure of the present work is described here. Chapter 1 introduces the tumor-targeting research area through a survey of the most relevant and recent literature in the field. Chapter 2 describes the synthesis of RGD-paclitaxel conjugates bearing peptide linkers and their full

biological evaluation *in vitro*. The results achieved with these first compounds prompted the design of a next-generation RGD-paclitaxel conjugate, whose synthesis and preliminary biological evaluation is reported in Chapter 3. Moving from the “traditional” concept of SMDC, Chapter 4 describes the synthesis of new RGD-drug conjugates bearing fluorescent properties, aimed at the direct monitoring of the compounds’ interactions with cancer cells. Finally, all the experimental details of synthetic and biological procedures are included in Experimental Section, together with spectroscopic data and HPLC profiles of the newly synthesized compounds.

Drug Targeting To Tumors

1.1. Introduction

Chemotherapy has been one of the main approaches for the treatment of cancer for more than half a century and it consists in the administration of drugs which cause the cell death by interfering with fundamental steps of cell lifecycle.

The first cytotoxic compounds to be administered in human patients in late 1940s were the nitrogen mustards chlorambucil and cyclophosphamide, which are able to alkylate DNA irreversibly. Around the same time, the observation that folic acid stimulated cancer growth prompted the development of folate analogues, which could prevent DNA synthesis by inhibiting dihydrofolate reductase (DHFR).

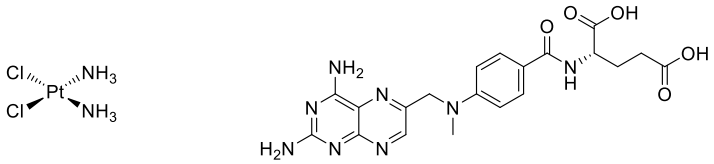

Cisplatin (*Platinum complexes*) (**1**)
DNA-crosslinking
av. IC_{50}(M):[a] $4.3 \cdot 10^{-6}$ (13 cell lines)
min. IC_{50}(M):[b] $2.2 \cdot 10^{-7}$

Methotrexate (*antimetabolites*) (**2**)
Dihydrofolate reductase inhibition
av. IC_{50}(M):[a] $7.3 \cdot 10^{-8}$ (97 cell lines)
min. IC_{50}(M):[b] $2.4 \cdot 10^{-8}$

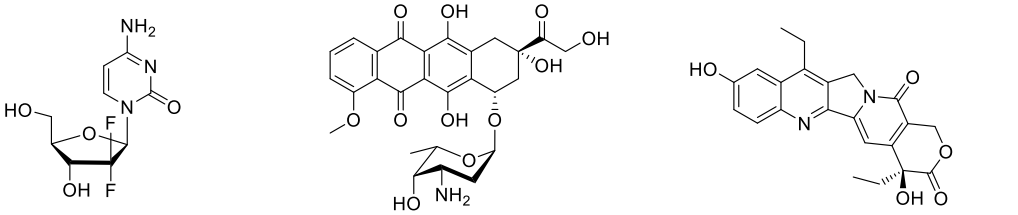

Gemcitabine (*nucleoside analogue*) (**3**)
Ribonucleotide reductase inhibition
av. IC_{50}(M):[a] $6.0 \cdot 10^{-7}$ (13 cell lines)
min. IC_{50}(M):[b] $3.0 \cdot 10^{-9}$

Doxorubicin (*anthracyclines*) (**4**)
DNA-intercalation (multitarget)[c]
av. IC_{50}(M):[a] $8.4 \cdot 10^{-8}$ (85 cell lines)
min. IC_{50}(M):[b] $2.5 \cdot 10^{-9}$

SN-38 (*camptothecins*) (**5**)
Topoisomerase I inhibition
av. IC_{50}(M):[a] $4.0 \cdot 10^{-10}$ (11 cell lines)
min. IC_{50}(M):[b] $5.1 \cdot 10^{-9}$

Figure 1. Molecular structures, mechanism of action and growth inhibition data of common cytotoxic agents, currently used in chemotherapy. [a] average (av.) of IC_{50} values reported for a variable number of human cancer cell lines (in brackets): [b] IC_{50} values reported for the most sensitive cell line (min.); multitarget: additional mechanisms of induction of apoptosis are known.[1]

This early example of rational drug design resulted in the development of methotrexate (Fig. 1), one of the first drugs to cure a solid tumor in 1950.[2] The elucidation of DNA structure led to development of nucleoside analogues (e.g. thioguanine, 5-fluoruracil, gemcitabine) that

induce apoptosis by means of blocking the elongation of DNA strands. Later on, the serendipitously-discovered cytotoxic effects of cisplatin (Fig. 1), gave rise to the biological evaluation of different platinum(II) complexes, which are able to crosslink DNA strands by binding to guanine and adenine residues.[3] Besides the use of DNA-interacting agents, significant anticancer effects were provided by the administration of inhibitors of repair proteins topoisomerase I and II. These proteins are involved in fundamental arrangements of the DNA structure, being able to break the single- (topoisomerase I) or double-strand (topoisomerase II) and then rejoin the DNA ends.[4] Drugs such as etoposide, teniposide and camptothecins (see Fig. 1) are able to stabilize DNA-topoisomerase complexes, thus blocking the progression of the replication fork.[5] Among topoisomerase inhibitors, anthracyclines (e.g. daunorubicin and doxorubicin) are known to cause cell death by additional means (e.g. intercalation into DNA, generation of free radicals, DNA cross linking and interference with helicase activity).[6] In addition to DNA and DNA-interacting proteins, microtubules represent a validated target in chemotherapy. Vinca alkaloids (e.g. vincristine and vinblastine) and their derivatives were initially found to bind tubulin, inhibiting the microtubule formation and inducing cell apoptosis.

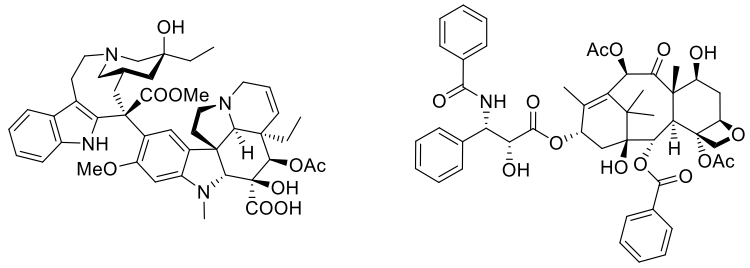

Vinblastine (*vinca alkaloids*) (**6**)
Inhibition of microtubule polymerization
av. IC_{50}(M):[a] $6.4 \cdot 10^{-10}$ (99 cell lines)
min. IC_{50}(M):[b] $2.5 \cdot 10^{-10}$

Paclitaxel (*taxanes*) (**7**)
Microtubule stabilization
av. IC_{50}(M):[a] $9.6 \cdot 10^{-9}$ (94 cell lines)
min. IC_{50}(M):[b] $2.8 \cdot 10^{-9}$

Figure 2. Molecular structures, mechanism of action and growth inhibition data of two well-known tubulin-targeted chemotherapeutics. [a] average (av.) of IC_{50} values reported for a variable number of human cancer cell lines (in brackets): [b] IC_{50} values reported for the most sensitive cell line (min.).[7]

The isolation of paclitaxel from the pacific yew, *Taxus brevifolius* in 1971, gave rise to the successful use of taxanes for cancer treatment. While vinca alkaloids affect the rates of tubulin polymerization, taxanes inhibit microtubule depolymerization (Fig. 2).[8] Due to the presence of preferential targets for cancer treatment in both healthy and diseased cells, the antitumor efficacy of these conventional chemotherapeutics is limited by their nonspecific action against normal cells, especially to rapidly growing cells such as bone marrow, cells of hair follicles and mucous membrane cells. As a result, these anticancer agents are characterized by a narrow therapeutic window, that is, the quantitative relationship between efficacy and safety. Moreover, the ability of low-molecular weight cytotoxic compounds to reach cancer cells is often impaired by different physiological barriers (e.g. tumor interstitial

pressure, diffusion through the tumor endothelium or extracellular matrix) as well as by degradation processes that convert the anticancer drugs into inactive metabolites.[9] Besides, the occurrence of drug resistance strongly limits the chemotherapy efficacy: tumor cells can be considered as a rapidly changing target because of their heterogeneity, genetic instability, and high rate of mutation, resulting in a selection and overgrowth of drug-resistant tumor cells.

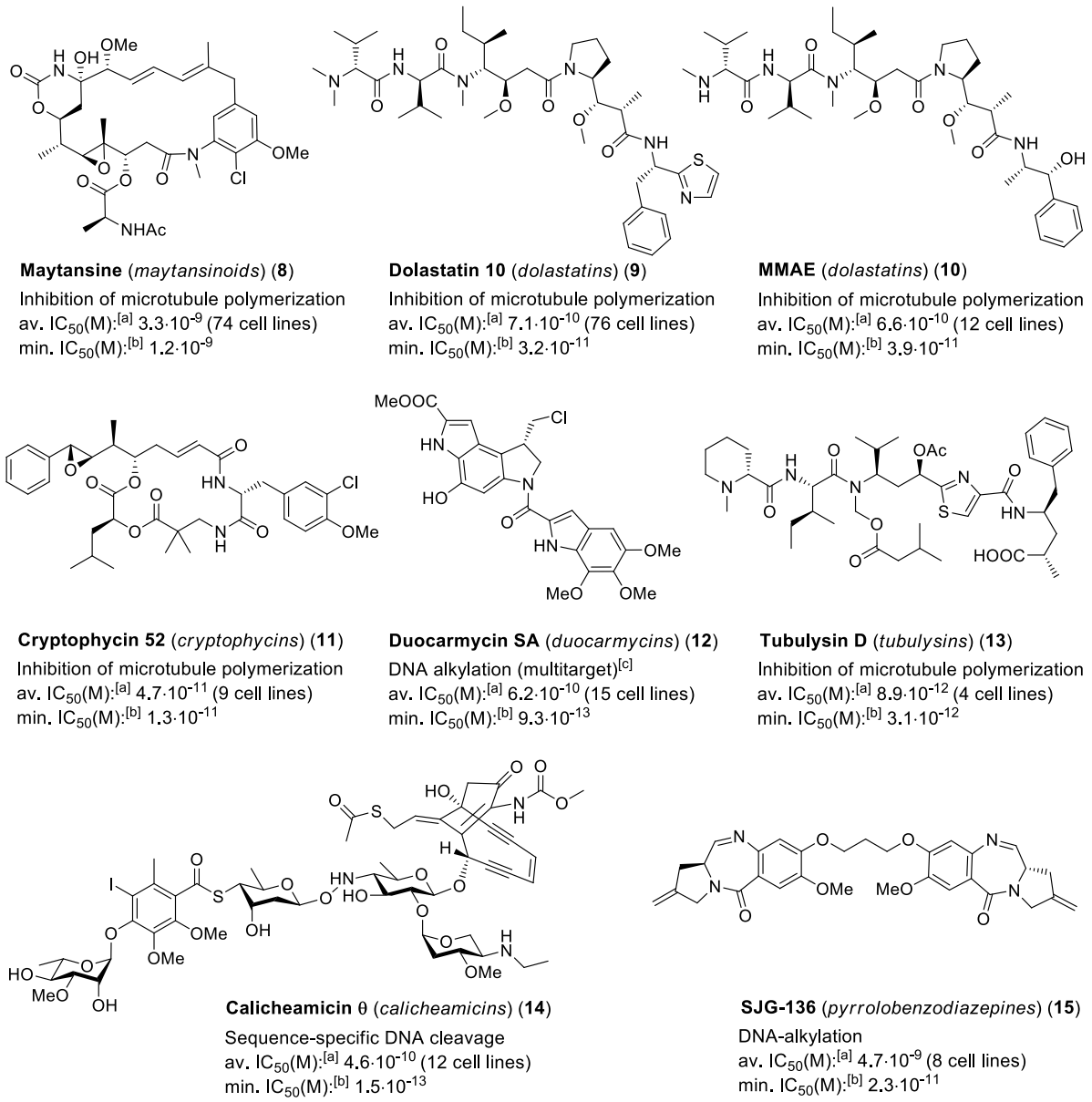

Maytansine (*maytansinoids*) (**8**)
Inhibition of microtubule polymerization
av. IC_{50}(M):[a] $3.3 \cdot 10^{-9}$ (74 cell lines)
min. IC_{50}(M):[b] $1.2 \cdot 10^{-9}$

Dolastatin 10 (*dolastatins*) (**9**)
Inhibition of microtubule polymerization
av. IC_{50}(M):[a] $7.1 \cdot 10^{-10}$ (76 cell lines)
min. IC_{50}(M):[b] $3.2 \cdot 10^{-11}$

MMAE (*dolastatins*) (**10**)
Inhibition of microtubule polymerization
av. IC_{50}(M):[a] $6.6 \cdot 10^{-10}$ (12 cell lines)
min. IC_{50}(M):[b] $3.9 \cdot 10^{-11}$

Cryptophycin 52 (*cryptophycins*) (**11**)
Inhibition of microtubule polymerization
av. IC_{50}(M):[a] $4.7 \cdot 10^{-11}$ (9 cell lines)
min. IC_{50}(M):[b] $1.3 \cdot 10^{-11}$

Duocarmycin SA (*duocarmycins*) (**12**)
DNA alkylation (multitarget)[c]
av. IC_{50}(M):[a] $6.2 \cdot 10^{-10}$ (15 cell lines)
min. IC_{50}(M):[b] $9.3 \cdot 10^{-13}$

Tubulysin D (*tubulysins*) (**13**)
Inhibition of microtubule polymerization
av. IC_{50}(M):[a] $8.9 \cdot 10^{-12}$ (4 cell lines)
min. IC_{50}(M):[b] $3.1 \cdot 10^{-12}$

Calicheamicin θ (*calicheamicins*) (**14**)
Sequence-specific DNA cleavage
av. IC_{50}(M):[a] $4.6 \cdot 10^{-10}$ (12 cell lines)
min. IC_{50}(M):[b] $1.5 \cdot 10^{-13}$

SJG-136 (*pyrrolobenzodiazepines*) (**15**)
DNA-alkylation
av. IC_{50}(M):[a] $4.7 \cdot 10^{-9}$ (8 cell lines)
min. IC_{50}(M):[b] $2.3 \cdot 10^{-11}$

Figure 3. Molecular structures, mechanism of action and growth inhibition data of some of the most potent cytotoxic agents. [a] average (av.) of IC_{50} values reported for a variable number of human cancer cell lines (in brackets): [b] IC_{50} values reported for the most sensitive cell line (min.); multitarget: additional mechanisms of induction of apoptosis are known.[10]

In principle, the treatment efficiency can be improved by increasing the doses, but this approach commonly results in severe side-effects. The administration of combinations of anticancer drugs with different mechanisms of action and non-overlapping toxicity profiles

has been one of the first strategies to improve the efficacy of conventional chemotherapeutics: multidrug therapy became a standard modality for the treatment of most cancers. Anticancer drugs derived from natural sources became the object of an intense research aiming at the discovery of new cytotoxic agents with improved anticancer activity. These significant efforts led to the development of a variety of both tubulin-targeted (e.g. maytansinoids, tubulysins, dolastatins, cryptophycins) and DNA-interacting agents (e.g. derivatives of calicheamicin, pyrrolobenzodiazepines and duocarmycin) with higher antiproliferative activity than conventional chemotherapeutics (Fig. 3), besides being worse substrates of P-glycoprotein (Pgp, associated with drug resistance). However, the mere enhancement of the cell-killing power of cytotoxic drugs did not result in increased therapeutic indexes. Indeed, the clinical evaluations of these new cytotoxic agents were discontinued immediately, due to the occurrence of severe side-toxicities at low administration doses.

1.2. Targeted Chemotherapy

These important drawbacks of cytotoxic agents prompted the development of “targeted” therapies, which may selectively kill the diseased tissue while sparing healthy cells. Based on the understanding of molecular principles of genetic and pathological processes that contribute to tumor growth, a large variety of new tumor targeting strategies could be developed. For example, it has been found that the altered activity or the overexpression of key tyrosine kinase (TK) proteins in tumors result in the abnormal phosphorylation of target effectors that activate signaling pathways and drive the cancer growth. Therefore, the use of selective kinase inhibitors as “targeted” anticancer agents has gained popularity among the pharmaceutical industries. In general, these small molecules interact with the cytoplasmic domain of transmembrane receptor TKs and inhibit the activity of the catalytic domain by interfering with the binding of ATP.[11] Approved by the FDA in 2001, imatinib (Gleevec™, compound **16**, Fig. 4) was the first compound of this class to enter the market. This drug is indicated for the treatment of chronic myelogenous leukemia patients expressing the BCR-ABL fusion protein, which is the result of an abnormal gene translocation. While imatinib was the 5th best-selling anticancer drug in 2014,[12] at least 20 other receptor TK inhibitors (e.g. sunitinib, erlotinib, crizotinib, axitinib and gefitinib) have broken into the market as inhibitors of aberrant phosphorilations in various cancers, such as renal cell carcinoma, and non-small-cell lung cancer (NSCLC).[13]

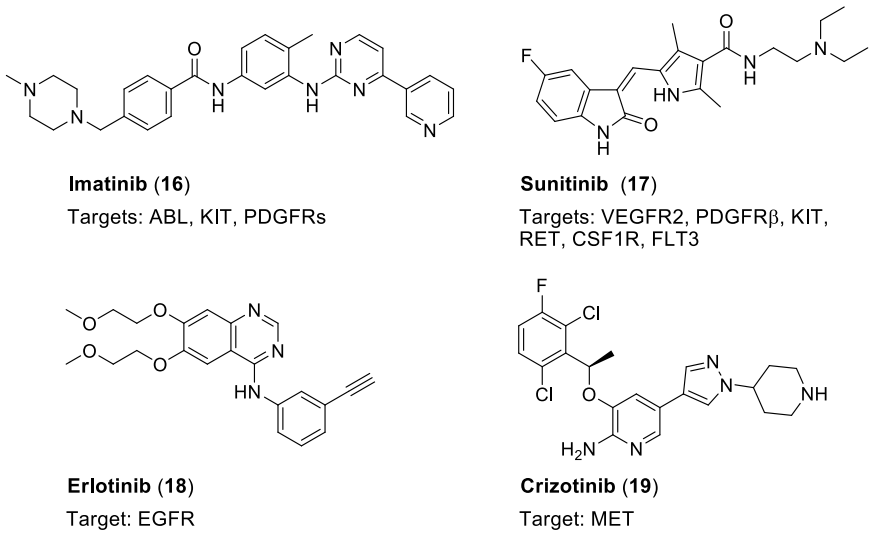

Figure 4. Examples of current FDA-approved multi-targeted as well as selective tyrosine kinase inhibitors (TKIs) targeting receptor tyrosine kinases (RTKs).[11]

Besides the active research on inhibitors of receptor tyrosine kinases, a large variety of "targeted" pharmacological approaches still relies on the administration of traditional cytotoxic agents, which are chemically modified or incorporated in suitable macromolecular structures to improve their therapeutic window. For example, anticancer agents have been incorporated into nanoparticles (e.g. liposomes, polymers and micelles) to exploit the tortuous and poorly differentiated vasculature of several tumor masses. Unlike the vasculature in normal tissues, solid tumor vasculature allows the extravasation of these large nanomedicines, resulting in a more selective drug accumulation at the tumor site (i.e. the enhanced permeability and retention (EPR) effect).

Among the known hallmarks of cancer, the EPR effect is arguably the most exploited strategy to improve the delivery of cytotoxic agents to tumors and, relying on the pathological features of the targeted tissue, it is generally classified as a "passive drug targeting" approach.[14] Examples of passively-targeted nanomedicines that have been approved for clinical use are both PEGylated (Doxil™/Caelyx™) and non-PEGylated (Myocet™/, Daunoxome™) liposomal anthracyclines, and albumin-based pacitaxel (Abraxane™). Alternatively to "passive drug targeting" approaches, the evidence that tumors often express different receptors, enzymes and other proteins in higher amounts than normal tissues, gave rise to the so-called "active drug targeting" strategies. Here, recognition of tumor cells is made possible by the covalent conjugation of cytotoxic agents to targeting vehicles (e.g. monoclonal antibodies, vitamins, peptides and substrate analogues) that bind specific tumor antigens. These drug delivery systems (DDS) are designed to release the cytotoxic payload only after the ligand binding to the target.

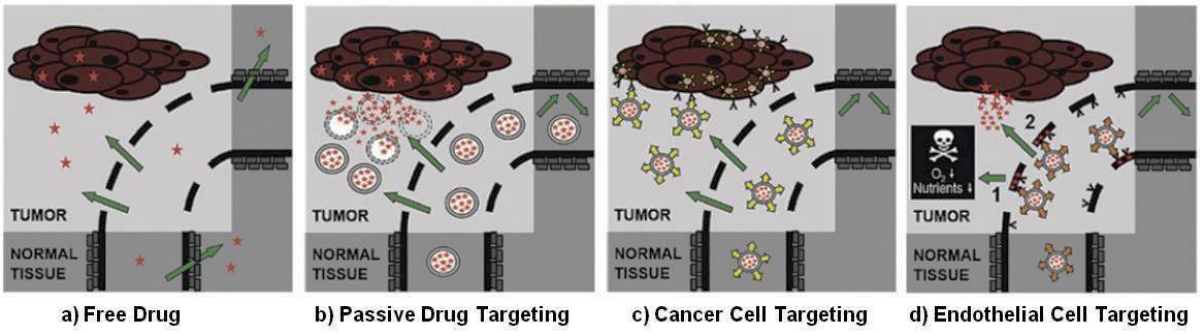

Figure 5. Schematic representation of common strategies used for drug targeting to tumors: while the traditional chemotherapeutic agent (**a**, free drug) is often rapidly cleared from the blood, it accumulates at low levels in the tumor and its localization to normal organs and tissues can be relatively high, the use of passively targeted drug delivery systems (**b**) enhances the drug accumulation in tumors by means of the EPR effect. Active drug targeting strategies exploit the molecular recognition of specific receptors, expressed either on tumor (**c**) or on the surface of endothelial cells (**d**).[14]

Depending on the exact localization of the receptor, different "active targeting" approaches have been introduced:

- *Active targeting to cancer cells*: the target is expressed on the plasma membrane of tumor cells. In general, the transmembrane receptor promotes the internalization of the drug through receptor-mediated endocytosis (described in the following paragraphs). This strategy is particularly useful to improve the cellular uptake of a specific payload;
- *Active targeting to endothelial cells*: the target is highly expressed on cells of tumor blood vessels (i.e. endothelial cells). This strategy overcomes the need for extravasation and penetration into the tumor mass. As a result of the cytotoxic action against endothelial cells, the tumor is deprived of oxygen, nutrients and other growth factors, which are required for cancer progression. Moreover, upon binding to tumor blood vessels, the payload can also diffuse within the tumor vasculature, thus enabling low-molecular weight drugs to penetrate deeply into the tumor environment.[14]

A newly-reported strategy, often referred to as *"non-internalizing" tumor targeting*, must be mentioned here. In this approach, the target is either expressed in the tumor extracellular matrix (ECM) or is a transmembrane protein that is not efficiently internalized by the tumor cell. Ideally, the cytotoxic agent released in the extracellular space diffuses in the immediate surroundings and, due to a "bystander effect", it is able to kill a broad variety of cells (e.g. both tumor and endothelial cells).[15,16]

A variety of drug delivery systems have been successfully developed to treat cancer according to these strategies. While some of these devices have already reached the market, others can be considered as promising technologies for future oncology.

1.3. Antibody-Drug Conjugates

1.3.1. Monoclonal Antibodies

Antibodies are the most used devices to target specific antigens that are either overexpressed or present in mutated forms in cancer cells. At first, antibodies were obtained from immunization of mice with human cancer cells (or with the purified antigens), followed by recovery of the final target-specific antibodies in the sera of the animals. This procedure afforded in poor yields a mixture of antibodies, as binders of different epitopes of the desired antigen. Moreover, these mixtures also encompassed undesired antibodies that bind different antigens expressed by the human cancer cells. In 1984, Georges Köhler and César Milstein were awarded the Nobel Prize in Medicine for the development of the hybridoma technology: here, the synthesis of large amounts of a single-purified antibody, targeting the antigen of interest was made possible.[17,18] Mice immunization with a specific antigen is followed by the isolation of lymphocytes B from the mice spleen. These antibody-producing cells are immortalized by fusion with myeloma cells (i.e. cancerous plasma cells) and diluted into multi-well plates to such an extent that only one cell is contained in each well. The subsequent screening and *in vitro* culture of the resulting pure hybridoma cells affords monoclonal antibodies (mAbs), which are able to bind a single epitope of the antigen of interest.[19] Antibodies can induce cancer cell death by a multitude of mechanisms, which can involve a direct action of the antibody towards the tumor cell (e.g. through receptor blockade or agonist activity, with induction of apoptosis) or against the tumor vasculature or stroma. Moreover, mAbs can promote immune-mediated cell killing mechanisms (e.g. complement-dependent cytotoxicity, antibody-dependent cellular cytotoxicity and regulation of T cell function).[20]

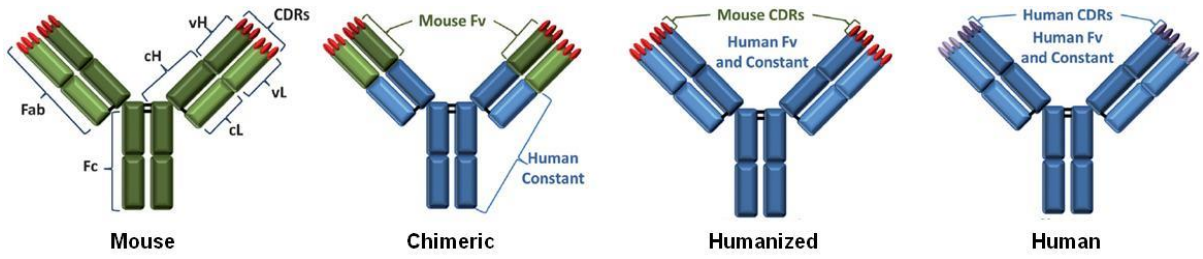

Figure 6. Representation of mouse (green), chimeric, humanized, and human (blue) mAbs. The mAb subdomains are reported. Fab: Fragment antigen-binding; Fc: fragment crystallizable region; vH: heavy-chain variable; vL: light-chain variable; cH: heavy-chain constant; cL: light-chain constant; CDR: complementarity determining regions.[21]

In early 1980s, the first clinical evaluations of antibodies as anticancer agents revealed that murine mAbs were easily identified as foreign proteins by the immune system, resulting in rapid clearance of the drug from circulation. Advances in recombinant DNA technology made possible the modification of the mAb structure, leading to “chimeric” antibodies (Fig. 6): in

these structures, the protein sequences of the murine mAb were replaced by typical sequences of human antibodies, without affecting the specific binding affinity for its target antigen. Later on, "humanized" antibodies were developed, in which the number of human residues in the mAb were further increased and murine residues were only limited to the essential antigen recognition moieties, that is, the complementarity determining regions (CDRs). The development of phage display technology and the advent of transgenic mice bearing the human repertoire led to "fully human" mAbs, which show prolonged survival in the blood stream ($T_{1/2}$ up to three weeks, compared to the typical 2/3 days half-lives of murine analogues). Since the first approval of a mAb for anticancer therapy in 1997, mAbs have been successfully used as single agents, to such an extent that mAbs such as rituximab (Rituxan™), bevacizumab (Avastin™) and trastuzumab (Herceptin™) were the first 3 best-selling anticancer drugs in 2014.[12] On the other hand, mAbs approved for solid tumors are not sufficiently potent and are typically used in combination with traditional chemotherapeutic agents.[21]

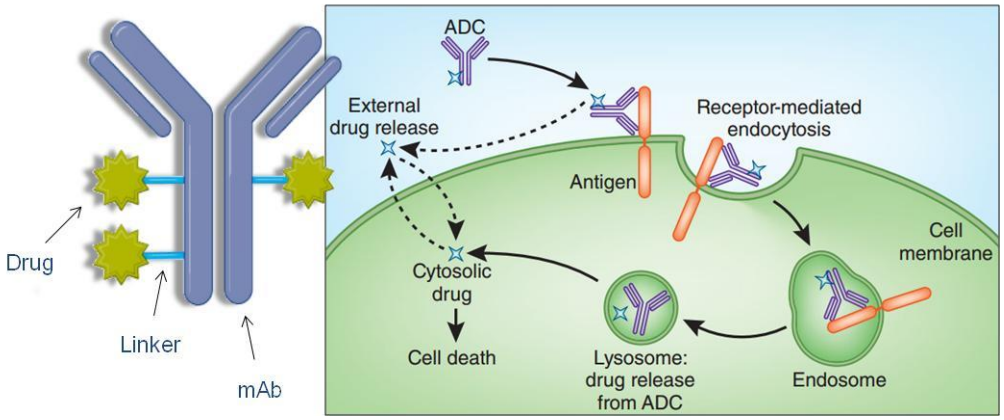

Figure 7. Structure and drug delivery mechanism of ADCs. Upon binding to tumor cell surface antigens, the ADC-receptor complex is internalized into the cell. This receptor-mediated endocytosis leads to drug release in intracellular compartments (e.g. lysosomes). Alternatively, in case of non-internalizing antigens, the ADC remains bound to the receptor on the cell surface. Here, depending on the linker, the anticancer drug may be released in the extracellular environment and enter the cell by passive diffusion.[22]

1.3.2. The Success of ADCs

The concept of antibody-drug conjugate (ADC) originates from the necessity to selectivity target a variety of known cytotoxic agents against the diseased cells, by exploiting the cancer recognition displayed by mAbs. In the ADC technology, the antibody and the cytotoxic agent are connected by a third fundamental moiety, the linker (Fig. 7). In general, the linker-drug system is endowed with an electrophilic moiety (e.g. a *N*-hydroxysuccinimidyl ester or a maleimide) which are then coupled to nucleophilic residues of the mAb (e.g. lysine and cysteine side chains). The linker is responsible for drug release from the targeting vehicle: since cytotoxic drugs are generally active only once released from the mAb, a non-specific

linker cleavage would result in side toxicity against healthy tissues. For this reason, the linker should be stable in the blood stream and, at the same time, it should be rapidly cleaved once the tumor site is reached. In particular, due to the fact that virtually all small-molecule anticancer drugs act at the intracellular level (i.e. by binding to tubulin, DNA, etc.), most of the ADCs that have been developed so far were designed to be internalized by the cancer cell and to release the drug within the intracellular environment. This has been achieved by developing mAbs which bind specific proteins widely expressed on the surface of tumor cells and known to promote receptor-mediated endocytosis of the ADC. Through this mechanism (Fig. 7), the ADC binding to the target protein is followed by folding of the ADC-receptor complex into membrane vesicles, that drive to endosomes and lysosomes. The environmental conditions typical of these intracellular compartments (e.g. acidic pH, high expression of proteases, high concentration of antioxidants) are responsible for the linker cleavage. Finally, the released drug is free to enter the cytoplasm and to bind its molecular target, resulting in cell cycle arrest and apoptosis.[23]

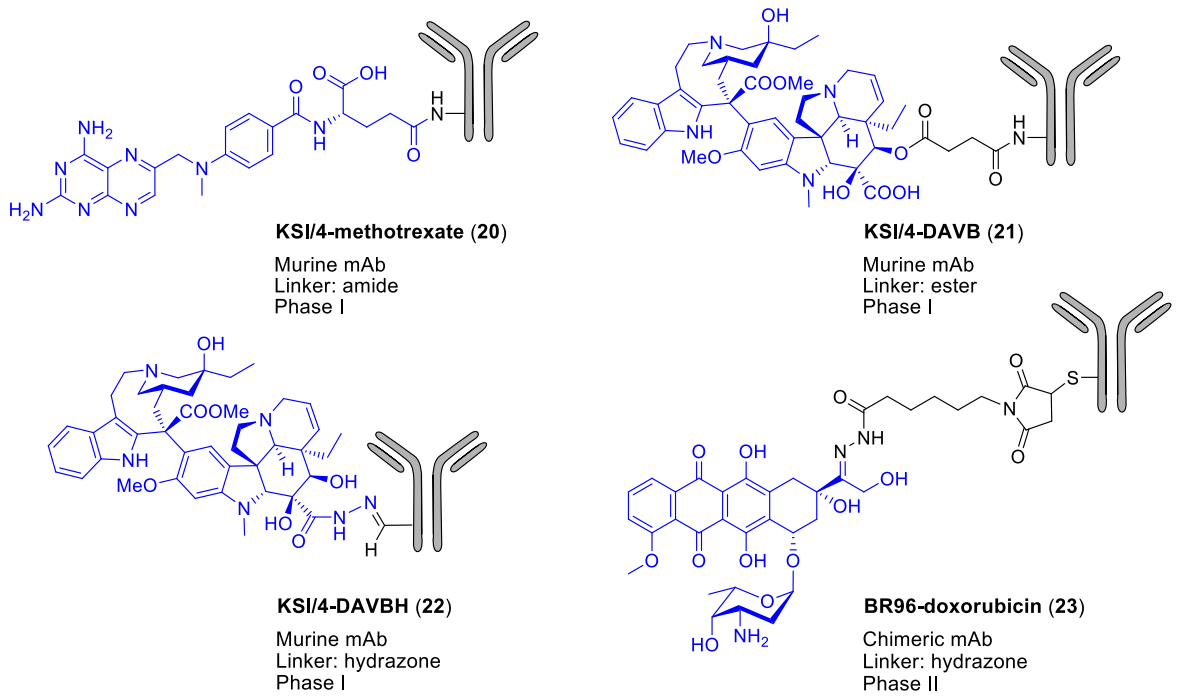

Figure 8. Molecular structures, mAb/linker adopted and clinical phase reached of first-generation ADCs. DAVB: desacetyl vinblastine: DAVBH: desacetyl vinblastine hydrazide.[21]

The first ADCs that were prepared and tested were introduced as an attempt to enhance the tumor selectivity of conventional anticancer agents, such as methotrexate, desacetylvinblastine and doxorubicin.[21] These cytotoxic agents were linked to chimeric mAbs through acid-labile linkers (i.e. esters, hydrazones and amides, Fig. 8).These ADCs substantially failed to demonstrate a significant target-selective potency towards cell lines expressing different levels of the target antigens. The *in vivo* evaluation of radiolabeled

analogues provided a convincing evidence of the tumor localization of the ADCs, but little therapeutic benefit was observed. Moreover, due to the non-human nature of the mAbs, ADCs often elicited a strong immune response in patients and, as a result, the clinical evaluation of this first-generation ADCs was discontinued before Phase III.

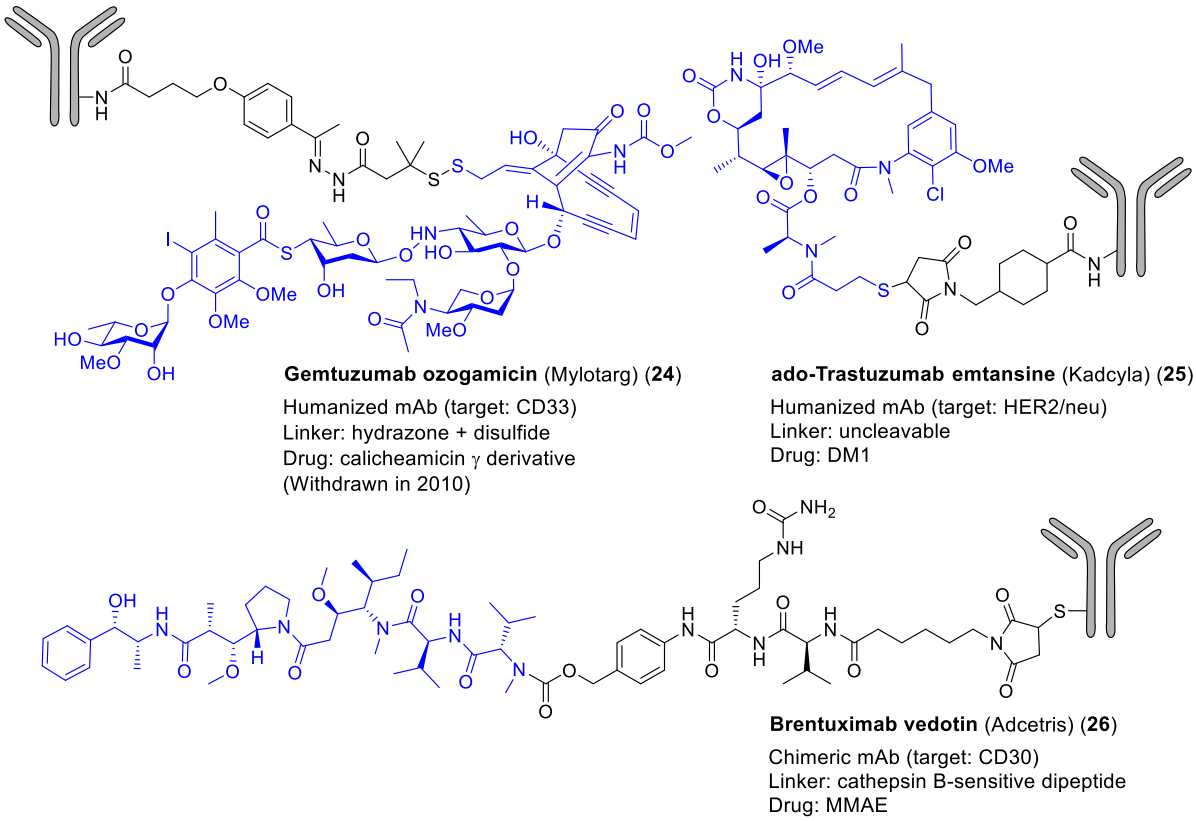

Figure 9. Molecular structures and mAb/linker/drug adopted of ADCs that were approved for cancer treatment. DM1: mertansine (i.e. a thiol-bearing maitansinoid); MMAE: monomethyl auristatin E.[21]

An intense research activity in this field highlighted the structural basis for the development of efficient ADCs, that can be listed as follows:

- *Humanized mAb*: humanized and fully human antibodies were used to reduce or avoid immunogenicity;
- *Improved linker system*: dipeptides that are recognized and cleaved selectively by intracellular proteases were preferred to more labile acid-sensitive linkers, with a significant minimization of drug release in the blood stream;
- *Increased drug potency*: the anticancer activity of the administered ADC depends on the number of compounds that reach the tumor site, to the number of antigens per cell and on the internalization process, which may be ineffective. Moreover, the number of molecules of a moderately potent cytotoxic agent required to kill a cell can be relatively high (e.g. > 10^6 molecules/cell). For these reasons, cytotoxic agents with potency in the picomolar range are required to elicit a significant anticancer activity.

These findings allowed the development of second-generation ADCs, which proceeded through the clinical steps, until reaching the market: although gemtuzumab ozogamicin (Mylotarg™ compound **24**) was withdrawn in 2010, due to an inadequate efficacy/side effect relationship,[24] ado-trastuzumab emtansine (Kadcyla™ compound **25**) is currently indicated for the treatment of metastatic breast cancer, while brentuximab vedotin (Adcetris™ compound **26**) has been approved for the treatment of Hodgkin lymphoma and anaplastic large cell lymphoma (Fig. 9). Nowadays, the number of ADCs in clinical trials has climbed to more than 30, while between 100 and 150 are in the preclinical stage.[25]

1.3.3. Limitations of Antibodies

Despite the increasing interest that ADCs are catching among the pharmaceutical industry, this technology is still far from being optimal. Indeed, although mAbs are able to preferentially localize at the tumor site in patients, the vast majority of the injected ADC do not end up in the tumor. This is due to the big dimensions of the antibody, that lead to a delayed extravasation and result in a poor drug accumulation at the tumor site.[26] Moreover, ADCs that are synthesized through the traditional thiol-maleimide strategy are heterogeneous mixtures of compounds bearing varying numbers of drugs attached at different positions on the antibody. In addition to the relatively low stability of the resulting Michael adduct,[27] the pharmacokinetic properties of the mixture components may vary significantly. Finally, the large-scale assembly of ADCs is a challenging and expensive process, requiring manufacturers to simultaneously handle biologic materials in sterile conditions and highly potent cytotoxic compounds.[25]

Owing to these limitations, the research in this field is now seeking to improve the ADC technology, mainly through the following strategies:

- Synthesis of ADCs bearing a smaller mAb portion, which would impart better pharmacokinetic properties;[28]
- Evaluation of extracellular proteins and non-internalizing receptors as targets for ADCs, which would avoid the difficulties related to the receptor-mediated endocytosis step;[15,29]
- Development of site-specific conjugation procedures, which would allow the synthesis of ADCs as singular entities, with a defined and optimized drug/antibody ratio.[30]

1.4. Small Molecule-Drug Conjugates

1.4.1. Advantages and Structure of SMDCs

Although ADCs are currently at the cutting-edge of “active” tumor-targeting technology, the above-mentioned drawbacks prompted the development of smaller devices, which could

maintain the tumor-targeting skills of mAbs, while showing better pharmacokinetic properties.[31] In particular, smaller targeting vehicles would easily extravasate and penetrate deeply in the tumor mass. Moreover, the defined molecular structure of the resulting small molecule-drug conjugate (SMDC) would be suitable for hit-to-lead optimizations as well as be more sustainable in terms of production costs.[32] SMDCs maintain significant structural similarity to ADCs. In both the technologies, linker and drug fragments are attached to a targeting vehicle (in the case of SMCs, a small ligand), which binds tumor antigens with high affinity. Similarly to the ADC technology, the prodrug nature of the ligand-drug conjugate allows the employment of ultrapotent cytotoxic agents, which would result too toxic to be given for therapy as free drugs. Finally, the drug release from both mAbs and small ligands often requires a proper spacer (see Spacer 2 in Fig. 10) to install suitable functional groups for conjugation chemistry and to improve the kinetic of drug release.

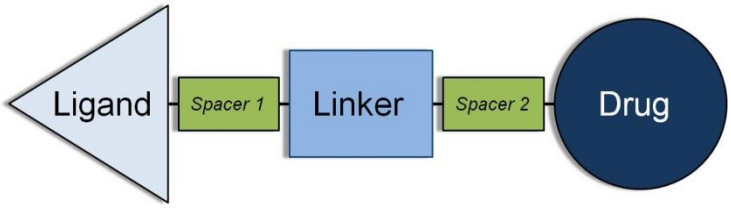

Figure 10. Structure of small molecule-drug conjugates (SMDCs). Besides the three fundamental modules ligand, linker and drug, additional spacers are often present at both sides of the linker (Spacer 1 and Spacer 2), to modify the conjugate's physicochemical properties (e.g. solubility) or to improve the kinetic of drug release.

Remarkably, due to the lack of large hydrophilic structures (such as the mAb), the ligand and linker fragments in SMDCs do not sufficiently solubilize the cytotoxic agent, which is usually highly lipophilic. For this reason, the water solubility in SMDCs is often improved by the addition of hydrophilic spacers (e.g. PEG chains or short peptide sequences bearing hydrophilic residues), which are commonly installed between the ligand and the drug modules (see Spacer 1 in Fig. 10).[33,34] In most cases, SMDCs are designed to enter the cell by receptor-mediated endocytosis but, as for ADCs, examples of SMDCs that are targeted to non-internalizing receptors are now emerging.[35] According to the physiological features of the targeted receptors, a variety of linkers have been used to promote drug release from SMDCs. These can be grouped as follows:

- *Acid labile linkers:* functional groups (e.g. esters and hydrazones, see Scheme 1) that are hydrolyzed under the acidic conditions of endosomes (pH 6.0-6.8) and lysosomes (pH 4.5-5.5).[36] importantly, tumors are often characterized by a remarkable acidity of their extracellular milieu,[16] where the cleavage of these linkers can easily occur. Ideally, hydrolysis should be slow enough to allow significant drug accumulation at the tumor site and negligible release of the payload into the blood stream;

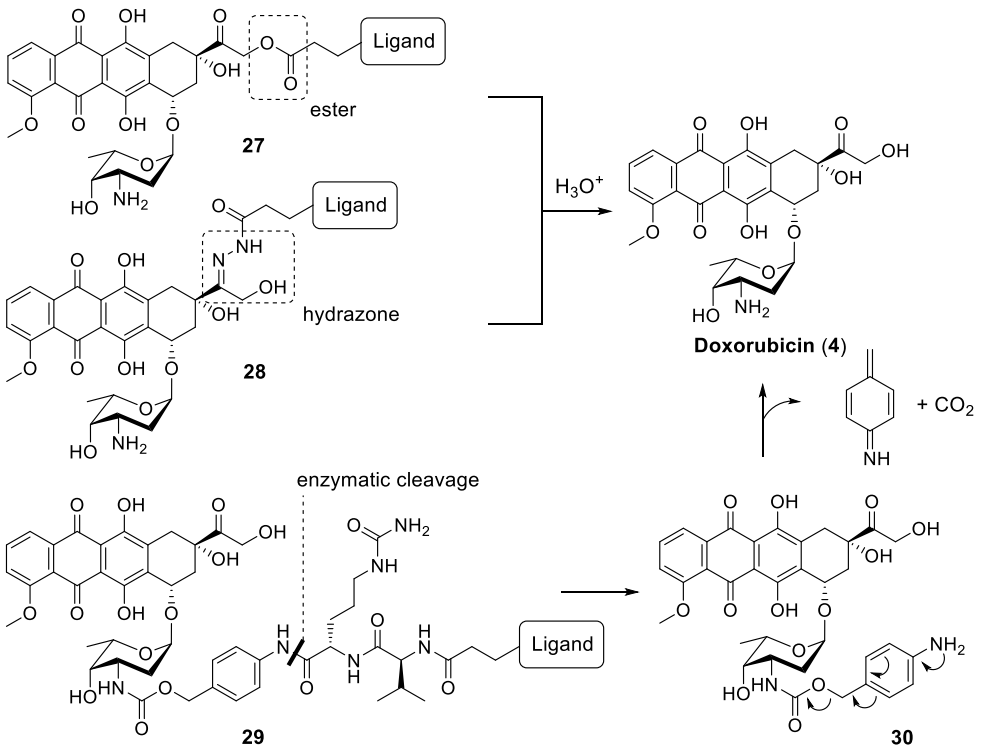

Scheme 1. Examples of acid-labile linkers (ester in compound **27**, hydrazone in compound **28**) and protease-sensitive linker (compound **29**) installed in doxorubicin. While the first two release the free drug upon hydrolysis, in compound **29** the enzymatic dipeptide cleavage at the C terminus releases metabolite **30**, which rapidly undergoes 1,6-elimination over an aromatic ring (i.e. mechanism of a common a self-immolative spacer).

- *Enzimatically-cleavable linkers:* short peptide sequences and sugar moieties that are selectively cleaved by specific proteases or glycoside hydrolases. Some known dipeptides (e.g. Val-Cit, Phe-Lys, Val-Ala, etc…) have been particularly exploited, due to their high stability in plasma and to their fast cleavage in the presence of a variety of proteases (e.g. cathepsins, legumain, matrix metalloproteinases, etc…) that are expressed in the extracellular tumor milieu or in different intracellular compartments. When these linkers are used, a "self-immolative spacer" is often present to reduce the steric hindrance around the peptide sequence, thus allowing a more efficient enzymatic action (Scheme 1);[37]
- *Reducible linkers:* functional groups (mainly disulfide bonds, but also metal complexes)[38] that take advantage of the highly reducing environment of the intracellular compartment (Scheme 2). This is due to an increased expression of antioxidants in cancer cells, such as cysteine, reduced glutathione, thioredoxin, peroxiredoxins, and nicotinamide adenine dinucleotides.[39,40]
- *Uncleavable linkers:* functional groups that are not appreciably cleaved either in plasma or at the tumor site (e.g. amides, triazoles, carbamates) are often used to link fluorescent dyes to the ligand, for imaging purposes. Although these linkers have found

limited success in SMDCs, they have been often used in ADCs (e.g. in the form of spacers attached to the antibody through a maleimide and to the drug as an amide), showing remarkable potency (e.g. in ado-trastuzumab emtansine, **25**). It is hypothesized that, in the case of ADCs, the entire mAb is proteolytically degraded once inside the cell, thus releasing the cytotoxic agent.[26]

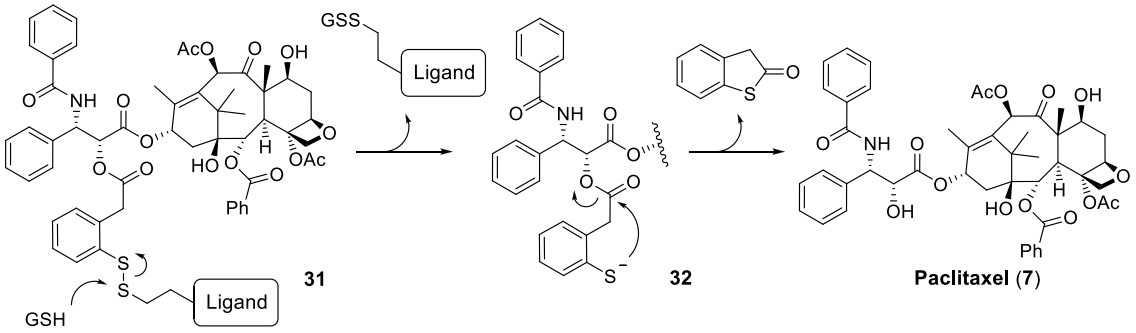

Scheme 2. Examples of reduction of a disulfide linker mediated by glutathione (GSH): the free thiol **32** undergoes cyclization onto an electrophile moiety (in this case, an ester group). This kinetically favoured 5-membered ring closure releases the free hydroxyl group of paclitaxel.

While in the ADC technology it is possible to identify monoclonal antibodies that are specific for virtually all proteins of interest, the isolation of low-molecular weight ligands of a specific protein is often a troublesome process. So far, traditional approaches to develop tumor-targeting ligands have focused on naturally-occurring small molecules (i.e. vitamins, substrates, hormones, etc.) that are well-known binders of tumor-overexpressed receptors.

Besides the conjugation of anticancer drugs to the natural ligands as such, synthetic analogues can be also created (e.g. by molecular modeling, if the X-ray structure of the receptor or related receptors is available), in order to mimic the binding affinity of the natural ligand as well as to introduce specific pharmacokinetic properties. Advances in the preparation and screening of large combinatorial libraries are now providing powerful tools for the development of peptides[41] and other small molecules[42,43] to target an increasing number of antigens.

1.4.2. SMDCs targeting Vitamin Receptors

Vitamins are often required in large amounts by fast-growing tumors, being essential for biosynthesis and nutrient metabolism: this results in the pronounced expression of receptors involved in the uptake of these molecules.

Folic acid is considered the first small molecule to be used as ligand in SMDCs and the research activity carried out on folate-drug conjugates represents a milestone in the development of tumor-targeting cytotoxic agents. Folate receptor (FR) is expressed at low levels in most normal tissues, whereas it is upregulated in several human tumors, including cancers of the ovary, lung, breast, kidney, brain, endometrium, colon, and hematopoietic

cells of myelogenous origin.[44] Folate-based SMDCs have shown selective cytotoxic activities against FR-expressing cell lines. Folate-drug conjugates are known to enter the cell by receptor-mediated endocytosis and, during this internalization pathway, the compounds are driven to the endosome. Importantly, a significant transition of the internalized compounds through lysosomes has never been observed.

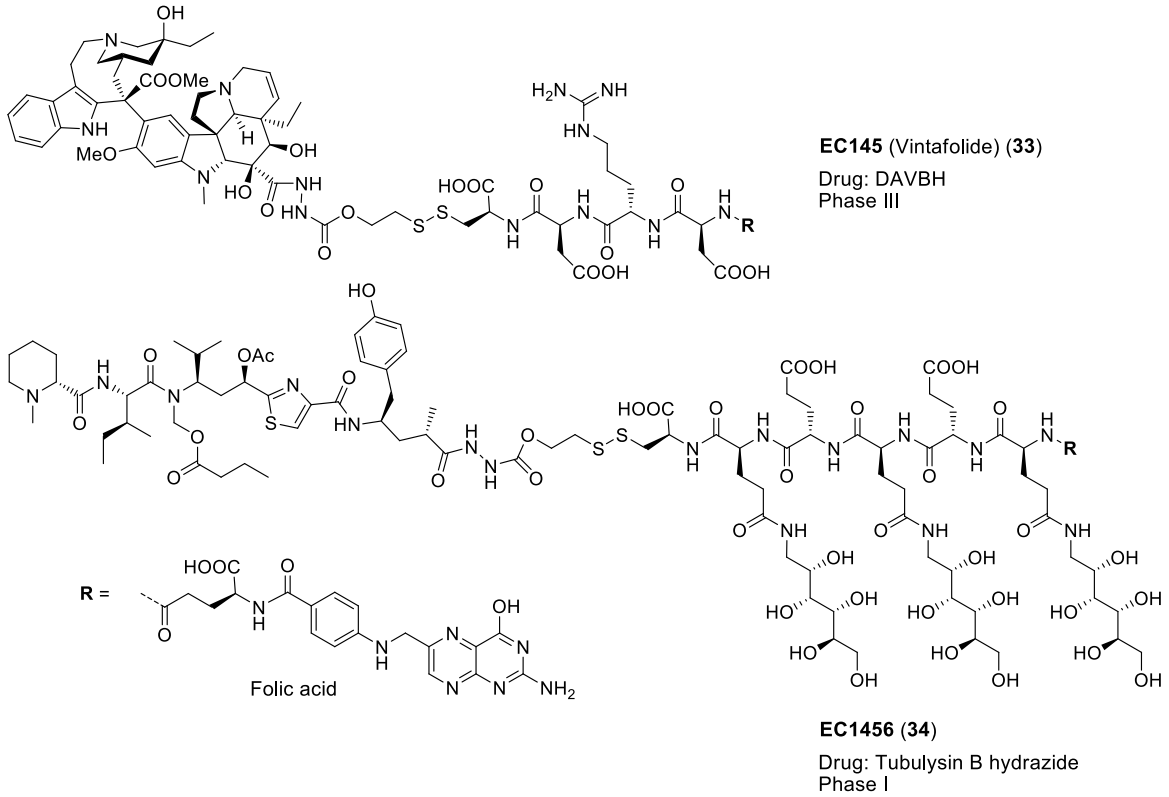

Figure 11. Molecular structures and clinical phase reached of two FR-targeted SMDCs.

This accurate analysis of the endocytic pathway is fundamental for the choice of an efficient linker: as a matter of fact, while a variety of linkers showed efficient drug release (e.g. hydrazones, disulfide and β-galactosidase sensitive linkers),[45] the lack of lysosomal access explains the low-efficacy of lysosomally-cleavable linkers.[33] The intense research activity of FR-targeted SMDCs led to the development of EC145 (vintafolide, Vynfinit™ compound **33**), a folate-desacetylvinblastine hydrazide (DAVBH) conjugate, bearing a disulfide linker (Fig. 11): this compound was the first folate-based SMDC to enter clinical trials and early-stage data in lung and ovarian cancer suggest that vintafolide has the potential for combination with other anticancer agents.[46] These results stirred up an increasing interest in this field, to such an extent that a large variety of FR-targeted SMDCs are now being developed.[45,47,48,49]

The conjugation of cytotoxic agents to biotin is being catching increasing interest, due to the overexpression of biotin receptors (BR) in tumor cells.[50] Similarly to folate-based SMDCs, analogues featuring biotin are internalized into the early endosome through receptor-mediated endocytosis, even though examples of lysosomal localization of fluorescent-labeled

biotin-drug conjugates have been reported.[51] Among the linkers that have been installed on these compounds, the use of an acid-labile hydrazone linker in a biotin-doxorubicin conjugate has been reported recently.[52] However, the intensive research carried out by the Ojima research group strongly promoted the use of disulfide linkers in biotin-based SMDCs. A variety of conjugates has been prepared, showing high cytotoxic activities against BR-expressing cells. Moreover, the use of "theranostic" devices (Fig. 12) provided a real-time monitoring of the BR-targeted accumulation and internalization.[53,54,55]

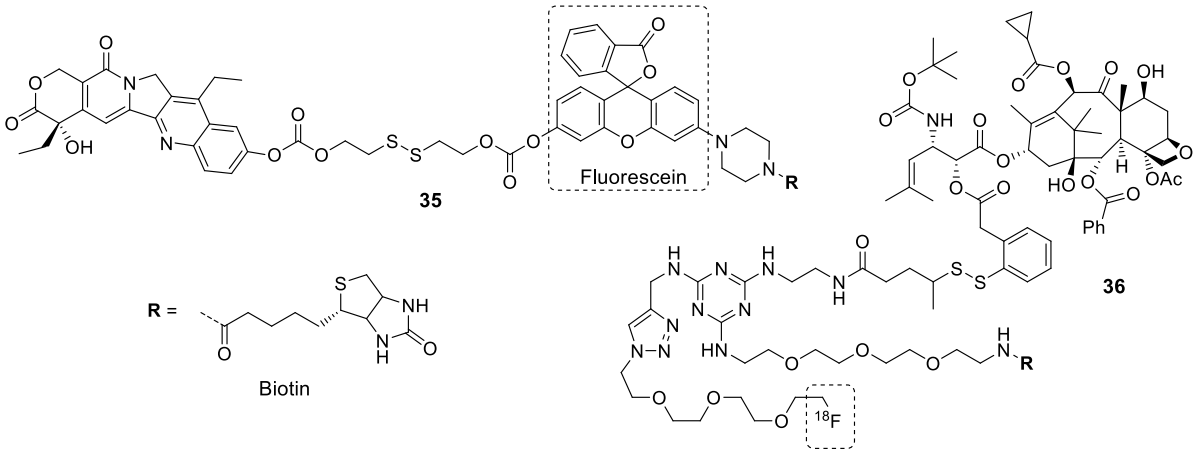

Figure 12. Molecular structures of two recently-reported "theranostic" SMDCs targeting biotin receptor. Compound **35**: biotin-SN38 conjugate, labeled with fluorescein;[56] compound **36**: biotin-taxoid conjugate, featuring a ^{18}F label, for PET imaging.[55]

A recent *ex-vivo* evaluation of a fluorescein-labeled BR-targeted SN-38 (compound **35**) showed a preferential accumulation of the conjugate in the tumor, compared to the labeled drug alone. However, the administration of **35** to tumor-bearing mice resulted in a modest tumor-volume inhibition, confirming that the development of this class of anticancer agents is still in its early stages.[56]

1.4.3. SMDCs Targeting Enzymes

Small molecules that act as substrate analogues of tumor-expressed enzymes are valuable tumor-targeting carriers of cytotoxic agents. A well-established marker of prostate carcinoma is the prostate-specific membrane antigen (PSMA), also known as folate hydrolase I or glutamate carboxypeptidase II. This transmembrane glycoprotein cleaves glutamate residues from biological substrates (e.g. *N*-acetylaspartyl glutamate) and, upon ligand binding, the receptor is internalized into clathrin-coated pits, that are driven to the lysosomes.[57] The remarkably higher expression of this enzyme by prostate carcinoma cells, compared to the cells of healthy prostate, gave rise to the development of PSMA-targeted anticancer agents. A variety of analogues of *N*-acetylaspartyl glutamate have been prepared and linked to cytotoxic agents. In 2009, the ligand 2-[3-(1,3-dicarboxypropyl)ureido]pentanedioic acid (DUPA, see Fig. 13) was linked to radiotracers and evaluated in biodistribution studies,

showing rapid clearance from blood vessels (tumor/blood ratio = 33:1) and high accumulation of the injected dose in the xenografted tumor (11.2% ID g^{-1}). However, the high expression of PSMA in murine kidneys resulted in a strong accumulation of the radiolabeled DUPA in these organs (28.9% ID g^{-1}).

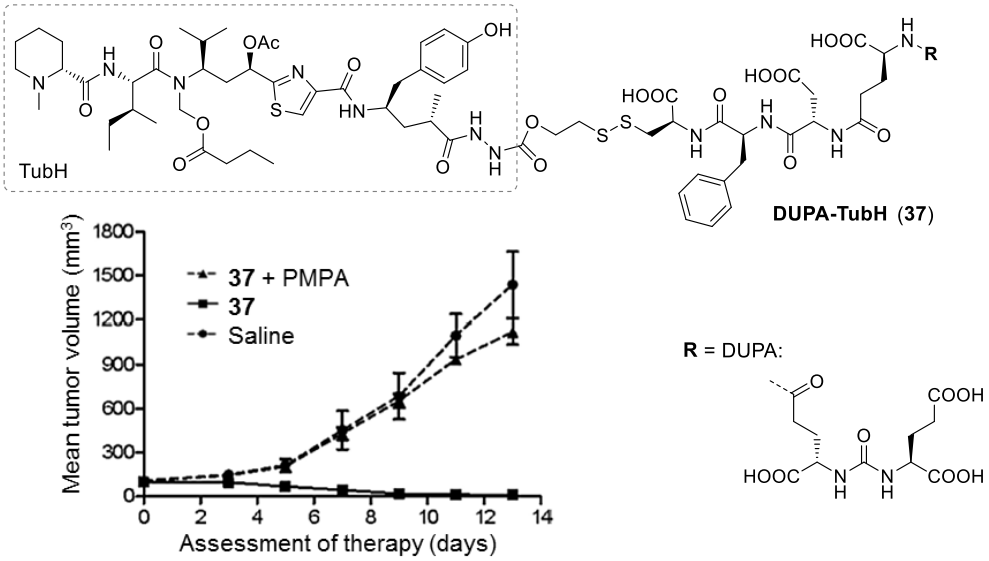

Figure 13. Molecular structures of DUPA-TubH conjugate (**37**) and effect on the growth of subcutaneous LNCaP tumors (mice treated with 1.5 μmol/kg of **37**); PMPA: PSMA inhibitor 2-(phosphonomethyl)-pentanedioic acid.[58]

The ligand was then conjugated to the potent antimitotic agent tubulysin hydrazide through a disulfide linker: this DUPA-TubH conjugate (compound **37**) showed remarkable tumor regression in LNCaP xenografts (Fig. 13) with no observable toxicity *in vivo*.[58] These results prompted the conjugation of a large variety of potent anticancer drugs to DUPA,[59,60] showing the high potential of this therapeutic approach. Besides PSMA, other enzymes have been recently introduced as suitable targets for SMDCs. For example, the metalloenzyme α-carbonic anhydrase catalyzes the reversible hydration of carbon dioxide to hydrogen carbonate and H^+ ($CO_2 + H_2O \leftrightarrow H^+ + HCO_3^-$). In humans, this enzyme is expressed in 15 known isoforms, which are involved in acid-base homeostasis and in the transport of CO_2 and hydrogen carbonate.[61] Among these isoforms, carbonic anhydrase IX (CAIX) is considered an excellent tumor antigen, being overexpressed in different tumors (e.g. glioblastoma, colorectal and breast cancer) as a marker of hypoxia. Although it is known that CAIX-targeting ligands do not enter the cell through receptor-mediated endocytosis, two different CAIX-targeted SMDCs bearing disulfide linkers were recently developed, and their antitumor properties were evaluated *in vivo*.[62] In this non-internalizing tumor-targeting approach, a strong dependence on the cytotoxic payload was observed: while the SMDC bearing a duocarmycin displayed only modest tumor volume inhibition, a maytansinoid-bearing analogue (compound **38**, Fig. 14) showed a potent antitumor effect. The ligand

fragment of this compound has been recently improved through an innovative affinity-maturation experiment, performed through development and screening of encoded self-assembling chemical (ESAC) libraries. Although biodistribution analysis of this new ligand showed an improved accumulation in the tumor, the anticancer properties of an analogue SMDC have not been reported yet.[63]

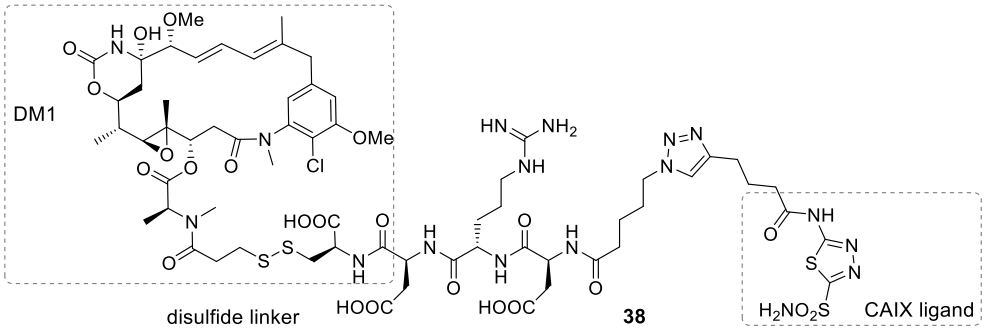

Figure 14. Molecular structures of the CAIX-targeted SMDC **38**, bearing a maytansinoid warhead.[62,58]

1.4.4. SMDCs Targeting Hormone Receptors

Specific hormone receptors are considered suitable targets for anticancer therapy, due to their high expression in different cancer cells.

A variety of synthetic peptides as analogues of hormones such as gonadotropin-releasing hormone (GnRH, often referred to as luteinizing hormone-releasing hormone, LH-RH), somatostatin and bombesin, have been conjugated to anticancer drugs.[64,65] The resulting SMDCs showed promising results in terms of significant tumor volume inhibition and low toxicities.[66] GnRH receptor (GnRHR) is expressed in tissues of male and female reproductive organs and, to a higher extent, in a variety of human malignancies, such as breast, prostate, ovarian, and endometrial cancers.[67] To date, different cytotoxic drugs such as doxorubicin,[68] paclitaxel,[69] and gemcitabine[70] have been coupled to GnRHR-targeting peptides, showing promising tumor-targeting performances. In particular, a peptide-doxorubicin conjugate (AN-152, compound **39** in Fig. 15) has been the first compound of this class to enter clinical trials.[26] In this conjugate, the anthracycline is coupled through an ester bond to a decapeptide, able to target GnRHR and enter the cell through receptor-mediated endocytosis.[64]

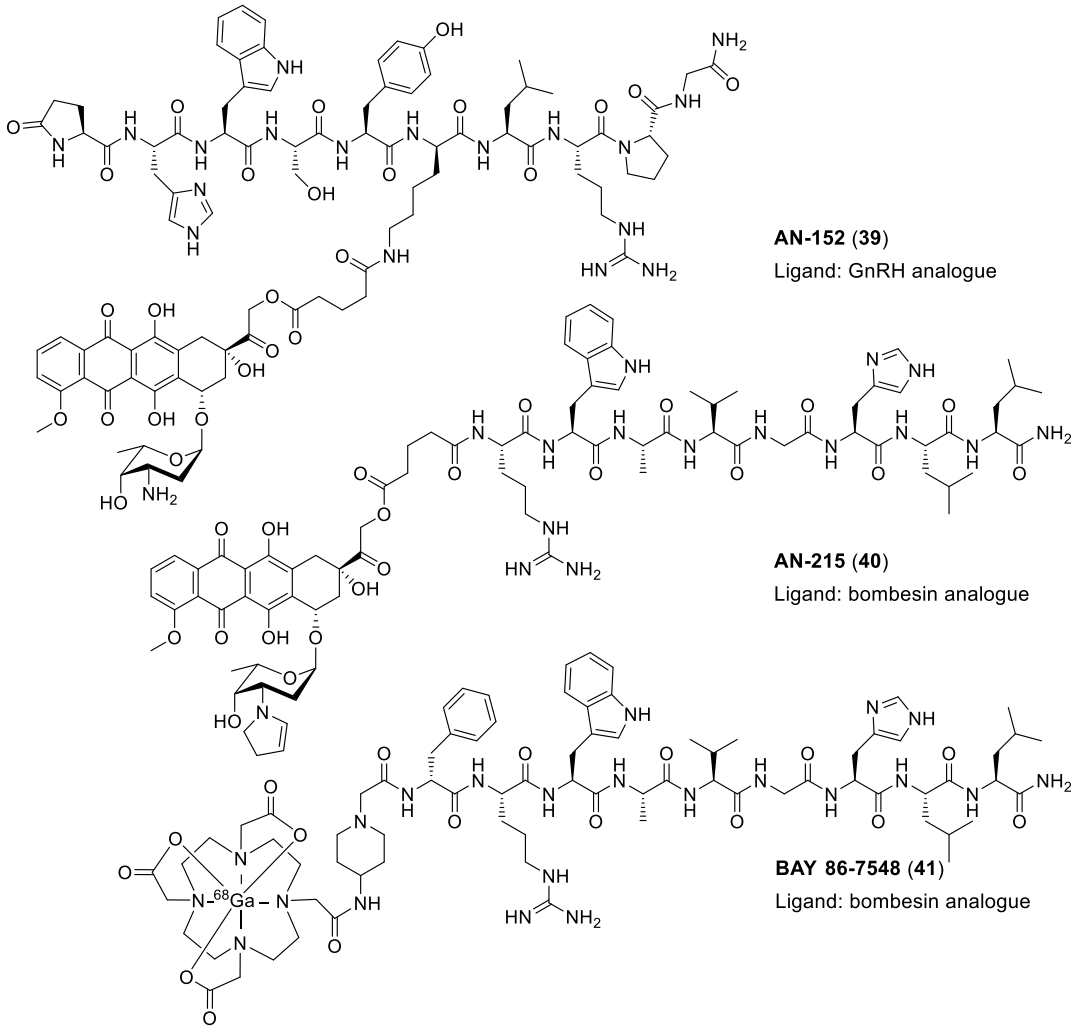

Figure 15. Molecular structures of two peptide hormone derivatives (**39** and **40**),[65] coupled to anthracycline drugs and of the clinically-evaluated ^{68}Ga-labeled bombesin analogue **41**.[76]

Similarly to GnRHR, receptors of hormone somatostatin (SSTRs, in particular subtypes 2, 3 and 5) are widely expressed in cancer cells, in particular in neuroendocrine tumors.[71] Peptidic somatostatin analogues have been successfully used as tumor-homing devices: while a ^{111}In-labeled cyclic peptide is commercially available for cancer imaging,[72] similar peptides have been incorporated into SMDCs and evaluated at preclinical levels. For instance, somatostatin analogues have been coupled to paclitaxel, showing stronger antitumor efficacy and lower systemic toxicity compared to PTX alone.[73,74] Moreover, peptidic SSTR ligands have been also used to improve the anticancer efficacy of liposomal doxorubicin against SSTR2-expressing tumor model.[75]

Finally, peptidic analogues of bombesin and gastrin hormones have been coupled to anticancer drugs to target cancer cells expressing the gastrin releasing peptide receptor (GRPR), the neuromedin B receptor (NMBR), and the bombesin receptor subtype 3 (BRS-3).[64] In particular, a bombesin analogue endowed with 2-pyrrolinodoxorubicin through an ester bond (SMDC: AN-215, compound **40** in Fig. 15),[76] showed remarkable anticancer

effects in mice xenografted with human prostate carcinoma cells, as well as being much more tolerated than the free drug.[77,78] Similar peptidic bombesin analogues have been functionalized with chelating moieties,[79] and the ^{68}Ga-labeled peptide BAY 86-7548 (compound **41**, Fig. 15) is currently running clinical trials for the imaging of GRPR-expressing prostate cancers.[80] Non-peptidic ligands of hormone receptors have been often preferred to peptide analogues, due to the well-known poor plasma stability of conventional peptide sequences. Besides the development of non-peptidic SSTR binders,[81] a synthetic non-peptidic ligand (CLR, see Fig. 16) of cholecystokinin 2 receptor (CCK2R) has been recently developed as tumor-targeting ligand. CCK2R is a g protein-coupled receptor that is overexpressed in several cancers (e.g. lung, pancreas, liver, esophagus, colon, and gastrointestinal stromal tumors), where it plays important roles in carcinogenesis and tumor progression.

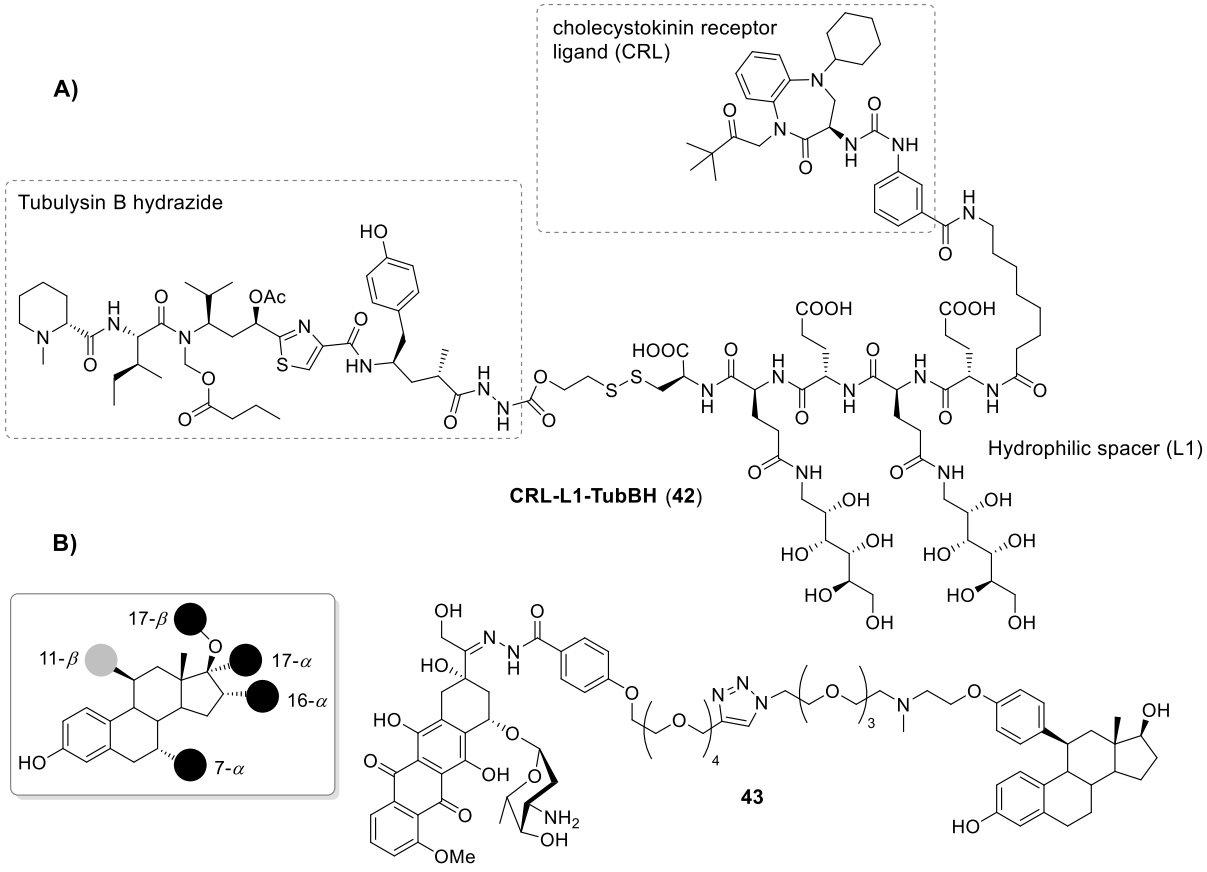

Figure 16. A) Molecular structures of CLR-L1-TubH conjugate (**42**).[83] **B**) Schematic representation of the estradiol scaffold (in the square), showing the variety of positions that have been used for conjugation chemistry: the black spot indicate low ER-binding affinity, whereas the functionalization of the 11-β position (grey spot) led to the development of SMDC **43**, which showed selective cytotoxic activity *in vitro* against ER-expressing cells.[86]

CCK2R-transfected HEK 293 cells were injected in mice and evaluated as antigen-positive control: upon the *in vivo* biodistribution evaluation of the selected ligand, coupled with a ^{99}Tc-radiotracer,[82] an analogue tubulysin B-bearing SMDC (SMDC **42**, Fig. 16A) showed

inhibition of tumor growth, followed by regression to an undetectable level.[83]Receptors of steroid hormones have also been studies as targets for SMDCs. For instance, estrogen receptors (ERs, in particular the α-subtype) are overexpressed by different breast cancer cells. At first, the estrogen estradiol has been derivatized in different positions (i.e. the 17β-, 17α-, 16α-, and 7α-positions, see Fig. 16B) and endowed with a variety of anticancer drugs.[84] These modifications were synthetically accessible through simple transformations of estradiol or its derivatives but not suitable for SMDCs, since a poor selective anticancer activity towards ER-expressing cells was observed.[84] X-ray analysis of the ligand-receptor complexes suggested that modifications in these positions of estradiol strongly affected the ligand binding. The 11β-position of estradiol was identified as suitable for the conjugation of anticancer drugs, but the installation of uncleavable linkers still resulted in the lack of selectivity against ER-expressing cells.[85] Finally, 11β-modified estradiol was linked to the anticancer drug doxorubicin through a hydrazone linker: the resulting SMDC (compound **43**, Fig. 16B) showed remarkable selectivity *in vitro* towards ER-expressing lines.[86] In a control experiment, the observed selectivity was completely abolished by the addition of free-estradiol, which competes with **43** for the ER-binding site. This experiment confirmed the receptor-mediated endocytosis of the SMDC and the high potential of this anticancer approach.[86]

1.5. $\alpha_v\beta_3$ Integrin-Targeted Delivery of Chemotherapeutics

1.5.1. Integrins

Integrins are heterodimeric transmembrane glycoproteins formed by non-covalently associated α- and β- subunits: in vertebrates, the integrin family is composed of 18 α and 8 β subunits that can assemble leading to 24 identified heterodimers (Fig. 17). Integrins are particularly important in areas where cell adhesion is necessary for function and in those involving tissue growth.

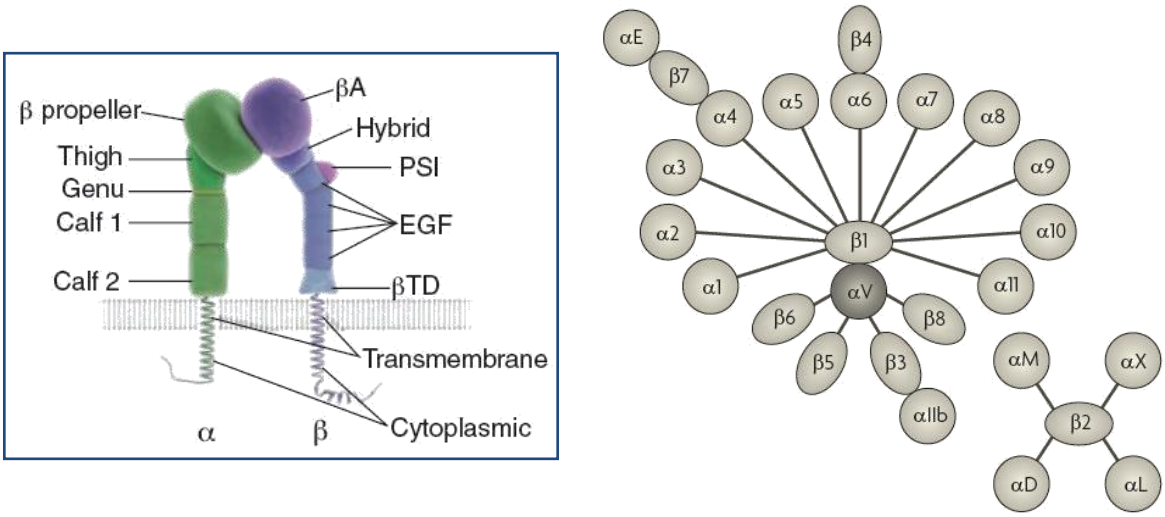

Figure 17. Schematic representation of the two integrin subunits and the 24-membered integrin family.[87,88]

The primary functions of integrins as cell transmembrane proteins are to mediate cell-cell and cell-extracellular matrix (ECM) adhesion, with pivotal roles in the organization and remodeling of the cytoskeleton during cell adhesion and migration.

Moreover, integrins mediate fundamental steps of cell life by transmitting both mechanical and chemical signals across the cell membrane: in general, these signaling pathways are promoted by specific growth factors and cytokines and mediate the integrin interaction with a variety of tyrosine kinase proteins (e.g. focal adhesion kinase and Src kinase family), resulting in the control of cell proliferation, activation, migration and homeostasis.[89]

The complexity of signals in which integrins are involved makes them play vital roles in both healthy and diseased tissues. For instance, integrin signaling is important for tumorigenesis and progression: since cells that have undergone neoplastic transformation are less dependent on ECM adhesion for their survival and proliferation, it has been demonstrated that cancer cells enhance the expression of specific integrins that favor their proliferation, survival and migration. Among these, $\alpha_v\beta_3$ integrin has been widely investigated as receptor for tumor-targeting strategies.

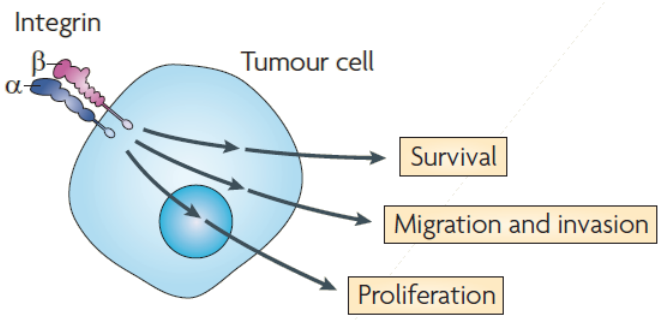

Figure 18. Integrins expressed in tumour cells contribute to tumour progression and metastasis by increasing tumour cell migration, invasion, proliferation and survival.

1.5.2. $\alpha_v\beta_3$ Integrin as Tumor Antigen

The interactions of $\alpha_v\beta_3$ integrin with several receptor tyrosine kinases (RTKs), including the receptors for EGF, PDGF, insulin and vascular endothelial growth factor (VEGF) control the behavior of endothelial cells.[90,91] The involvement in these complex "cross-talk" networks makes $\alpha_v\beta_3$ integrin a principal marker of angiogenesis, that is the formation of new blood vessels in avascular tissues. This latter is a fundamental step not only for physiological processes (e.g. embryogenesis, tissue remodeling, female reproductive cycle, and wound healing), but also for survival and growth of tumor masses. Moreover, $\alpha_v\beta_3$ is involved in ECM remodeling and degradation, which are key processes for tumor invasion and metastasis. For instance, this integrin heterodimer has been shown to facilitate the transition from the radial to the vertical phase of cell growth, therefore facilitating the penetration of the basement membrane and invasion into the underlying stroma.[92] These special roles of $\alpha_v\beta_3$ integrin seem to arise from its ability to recruit and activate specific extracellular proteases (i.e. MMP2 and plasmin) which degrade different components of the extracellular and interstitial matrixes, thus promoting the migration of cancer cells.[89] As a result of these key roles in cell proliferation, survival and migration, $\alpha_v\beta_3$ integrin is not only upregulated in angiogenic endothelial cells, but it is also overexpressed in various tumors, such as melanoma, glioblastoma, breast, pancreatic, cervical and prostate carcinomas.[93]

The evaluation of $\alpha_v\beta_3$ integrin as pharmacological target for antitumor applications started with the understanding of the molecular basis of the adhesion of ECM protein to cells. In particular, Ruoslahti and coworkers discovered that cell adhesion of particular domains of fibronectin and other ECM proteins takes place by means of an Arg-Gly-Asp (RGD) sequence (Fig. 19), which was identified as specific binding motif of certain integrin receptors.[94,95]

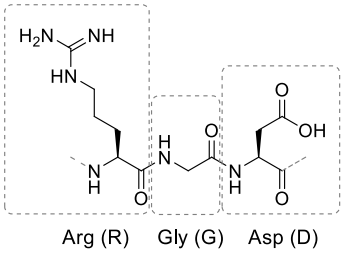

Figure 19. The arginine-glycine-aspartic acid (RGD) peptide sequence.

Later on, the development of peptide libraries led to the identification of series of RGD-bearing compounds, which were able to bind $\alpha_v\beta_3$ integrin at low-nanomolar concentrations. In these peptide ligands, the inclusion of the RGD tripeptide into cyclic sequences impaired lower conformational flexibility to the integrin ligands, resulting in a higher affinity for the integrin receptor.[96,97,98] An important milestone in this research field is the X-ray analysis of the co-crystals obtained from integrin $\alpha_v\beta_3$ and cilengitide (compound **44**, Fig. 20), the well-known integrin ligand developed by Kessler.[99] In this crystal structure, an extended conformation of the RGD sequence in the integrin binding pocket was observed, with a 9-Å distance between C-β atoms of the Arg and Asp residues: this arrangement allows the interaction of the arginine side chain with two anionic aspartic acid residues in the α-subunit, whereas the aspartic acid binds to divalent metal cation in the metal ion-dependent adhesion site (MIDAS) region of the β-subunit.[100] The understanding of these structural requirements prompted the development of peptidic, peptidomimetic and non-peptidic $\alpha_v\beta_3$ integrin ligands.[101,102,103] These potent integrin binders were originally designed as antiangiogenic compounds to be directly used in anticancer therapy.

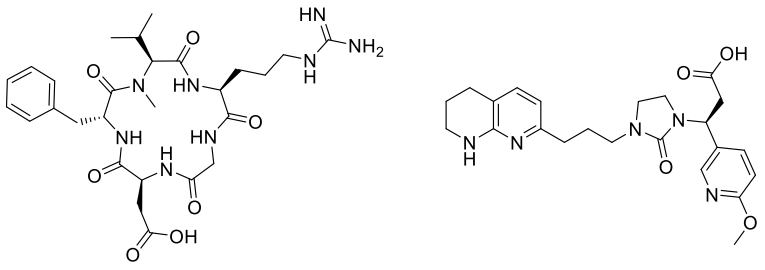

Figure 20. Molecular structures of integrin-targeting small molecules cilengitide (**44**, non-selective) and MK-0429 (**45**, $\alpha_v\beta_3$ selective), that have been evaluated in clinical trials as inhibitors of tumor angiogenesis.

In addition to the humanized, $\alpha_v\beta_3$ integrin-targeted mAb etaracizumab (Abegrin™), the small molecules cilengitide and MK-0429 (**45**) have been evaluated in clinical trials as anticancer drugs.[104] Although all of these integrin antagonists were demonstrated to be non-toxic and well-tolerated, some doubts have recently emerged concerning their anticancer efficacy. Indeed, a paradoxical pro-angiogenic activity of **44** under certain experimental conditions has

been reported.[105,106] Moreover, the failure of cilengitide in improving overall survival in patients with newly-diagnosed glioblastoma and methylated MGMT promoter status[107] stimulated the debate on the feasibility of anticancer treatments based on the administration of integrin-targeted antiangiogenic compounds.[108,109,110]

Nevertheless, owing to the high expression of $\alpha_v\beta_3$ integrin in cancer cells, several RGD-bearing peptides and peptidomimetics have been investigated as promising carriers for the delivery of lyposomes,[111,112,113] nanoparticles.[114,115] and imaging agents,[116,117,118] which were the first RGD-conjugated payloads to enter the clinic.

1.5.3. RGD Ligands in Tumor Imaging and Therapy

Small ligands of $\alpha_v\beta_3$ integrin found widespread applications in positron emission tomography (PET) imaging. In particular, [^{18}F]-Galacto-RGD (**46**, Fig. 21) was the first compound of this class to be studied in patients. Later on, due to the short half-life of ^{18}F isotope, novel integrin-targeted radiotracers were developed in which the ^{18}F label is rapidly installed by "click" reactions (e.g. triazole and oxime formations in compound **47** and **48**, respectively). These structural modifications allow easy labeling procedures and increase the availability of the radiotracer, making these compounds suitable for diagnostic applications. Besides the use of RGD ligands in PET imaging, the ^{99m}Tc-labeled compound **49** is currently evaluated in clinical trials as probe for single photon emission computed tomography (SPECT).[119,120] In general, all these targeted imaging agents are well tolerated by patients and their *in vivo* accumulation have shown good correlation with the $\alpha_v\beta_3$ expression in tumor vasculature as well as in integrin-expressing cancer cells. To increase the tumor uptake and reduce side accumulation to organs (mainly kidneys and intestine), radiotracers have been coupled to dimeric RGD peptides.[121] Such a multivalent approach is known to enhance the ligand affinity for a specific receptor:[122] in the field of $\alpha_v\beta_3$ imaging, it led to the FDA approval for clinical evaluation of [^{18}F]-FPPRGD$_2$ ([^{18}F]-Alfatide, compound **50**)[123] and of its more stable analogue [^{18}F]-Alfatide II (compound **51**).[124]

The increasing interest in this research area led to the development of a large variety of new-generation RGD-coupled radiotracers, which are being evaluated at preclinical levels. In general, the conjugation to integrin ligands is often shown to induce a pronounced accumulation of the imaging agent in the tumor, resulting in some cases in a preferential probe localization in the tumor (Fig. 22).[125] This selectivity for the diseased tissue is completely abolished by the co-injection of unlabeled integrin ligand, indicating the involvement of $\alpha_v\beta_3$ in the tumor recognition.[126,127,128]

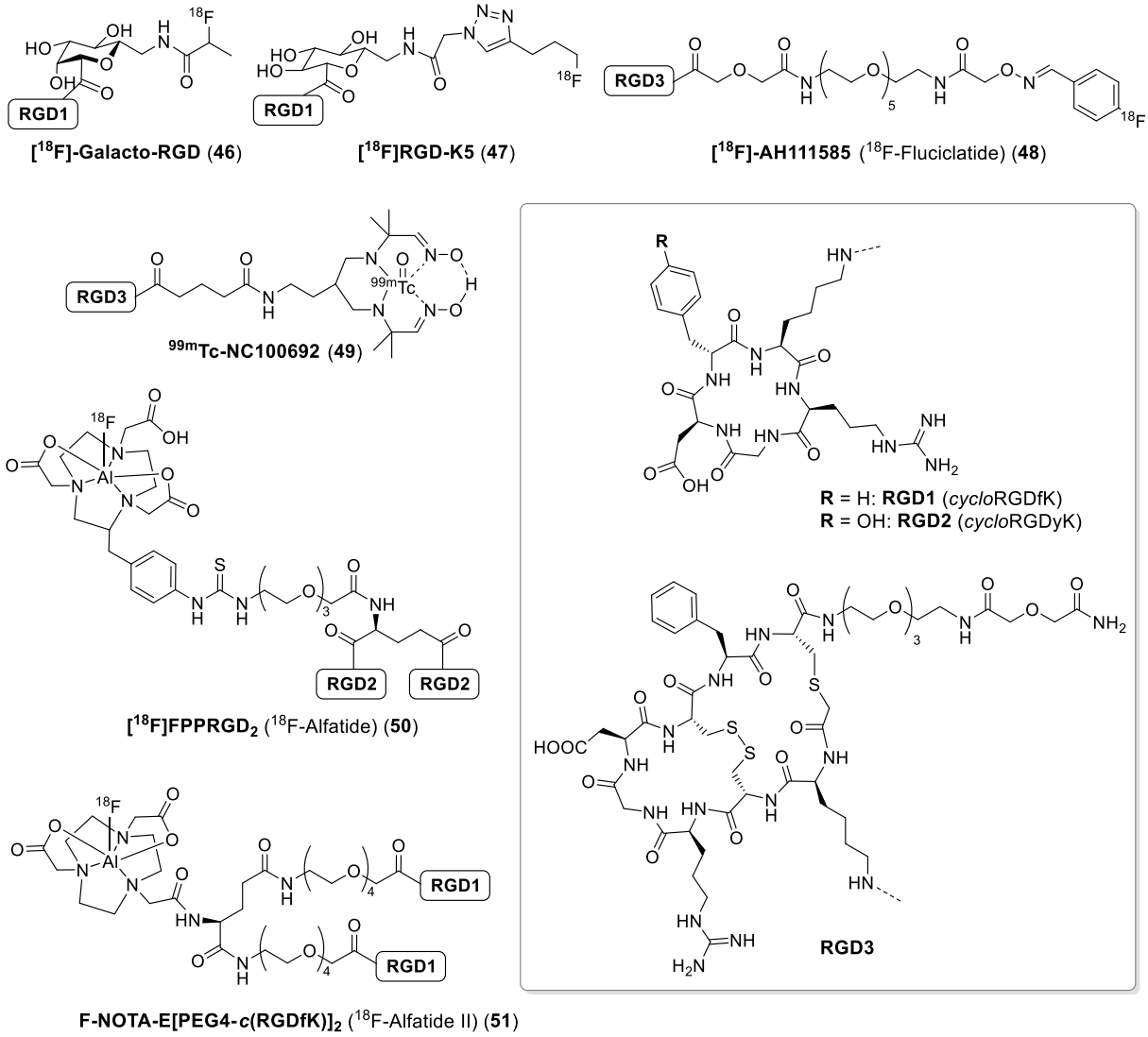

[^{18}F]-Galacto-RGD (**46**) **[^{18}F]RGD-K5** (**47**) **[^{18}F]-AH111585** (^{18}F-Fluciclatide) (**48**)

^{99m}Tc-NC100692 (**49**)

[^{18}F]FPPRGD$_2$ (^{18}F-Alfatide) (**50**)

F-NOTA-E[PEG4-*c*(RGDfK)]$_2$ (^{18}F-Alfatide II) (**51**)

Figure 21. Molecular structures of integrin-targeted imaging agents that are currently evaluated in clinical trials.

While cancer imaging strategies based on the administration of radiolabeled RGD peptides are being investigated at the clinical level, the use of these small compounds as ligands in SMDCs is still far from being validated for therapy.

Due to the expression of $\alpha_v\beta_3$ integrin in angiogenic tumor vasculature, RGD ligands can exert anticancer activity by targeting endothelial cells. However, therapeutic approaches targeting cancer cells expressing the integrin receptor can also be devised. Integrins are commonly considered as internalizing receptors, and a variety of endocytic pathways mediated by integrins have been described.[129]

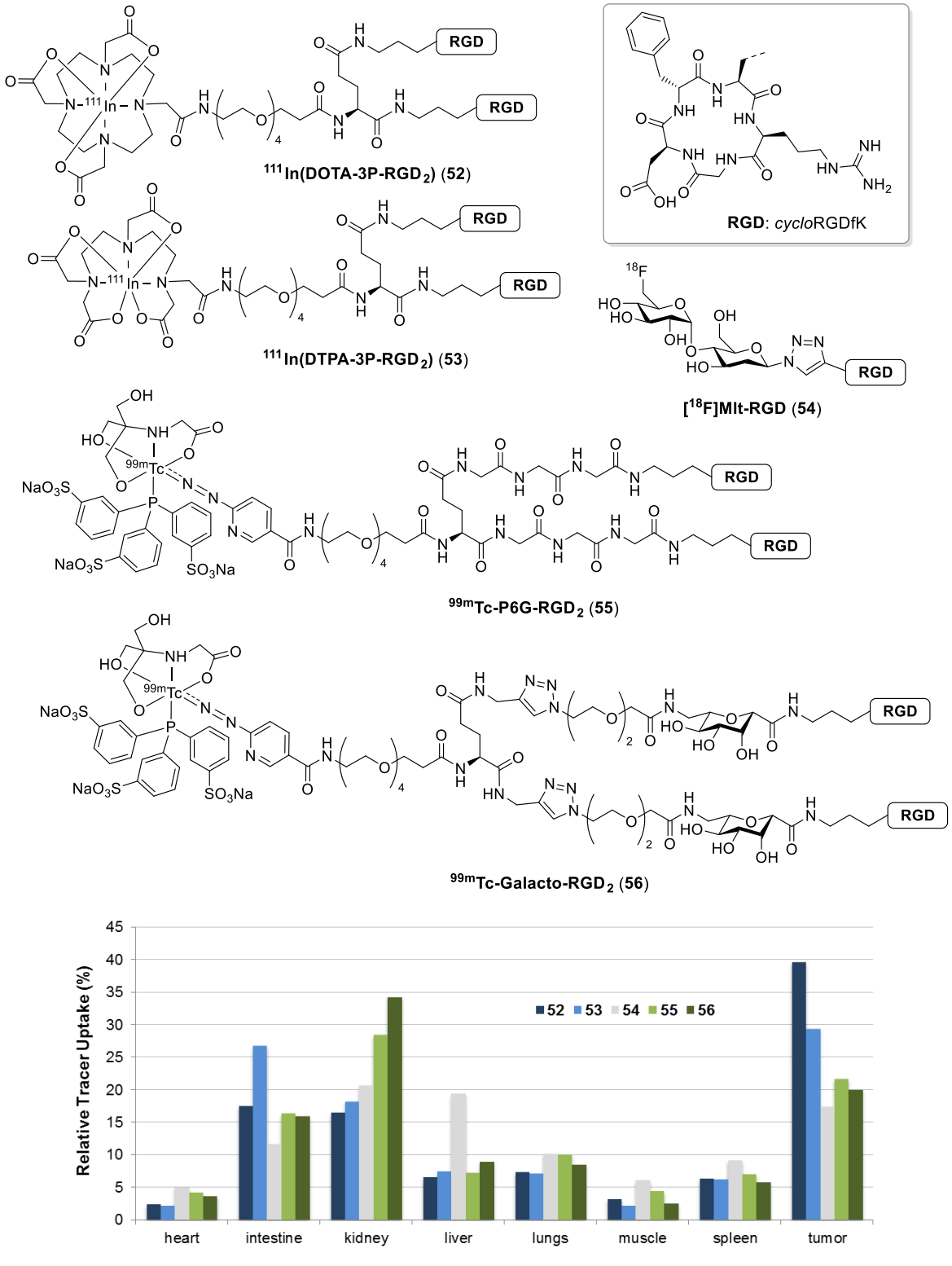

Figure 22. Molecular structures of the recently-reported $\alpha_v\beta_3$-targeted radiotracers ^{111}In(DOTA-3P-RGD$_2$) (**52**),[125] ^{111}In(DTPA-3P-RGD$_2$) (**53**),[125] [^{18}F]Mlt-RGD (**54**),[126] ^{99m}Tc-P6G-RGD$_2$ (**55**)[126] and ^{99m}Tc-Galacto-RGD$_2$ (**56**).[128] Chart: comparison of the 60-min biodistribution data in athymic nude mice bearing U87MG human glioma xenografts.

Specific proteins (i.e. caveolin and clathrin) are known to interact with the intracellular domain of $\alpha_v\beta_3$ integrin and promote the receptor folding into membrane vesicles that travel to early endosomes. Here, $\alpha_v\beta_3$ integrin can be either driven to intracellular compartments responsible for protein degradation (e.g. endosomes and lysosomes), or recycled to the plasma membrane. These trafficking pathways are involved in different processes, such as cell migration (by detachment of integrins from the extracellular matrix), integrin recycling and activation of different receptors (e.g. VEGFR-2, involved in angiogenesis).[130]

Cleavage type	**Linker[a]**	**Drug**	**$\alpha_v\beta_3$ Ligand**	**Ref.[b]**
Hydrolysis	*N*-Mannich base	DOX	RGD4C	[131]
	ester	PTX	E[*cyclo*(RGDyK)]$_2$	[132],[133]
	ester	PTX	E[*cyclo*(RGDfK)]$_2$	[134]
	ester	PTX	AbaRGD; AmproRGD	[135]
	ester	PTX	multimeric AbaRGD	[136]
	amide, hydrazone	CPT analogues	RGD cyclopentapeptides	[137]
	hydrazone	DOX	E[*cyclo*(RGDfK)]$_2$	[138]
Enzymatic cleavage	D-Ala-Phe-Lys	DOX	RGD4C	[139]
	Pro-Leu-Gly	DOX	E[*cyclo*(RGDfK)]$_2$	[140]
	Pro-Leu-Gly; Val-Cit	MMAE	*cyclo*(RGDfC)	[141]
	Ala-Cit	NMT	RGD cyclopentapeptides	[142]
	Ala-Ala-Asn	MMAE	Non-peptidic $\alpha_v\beta_3$ inhibitor	[143]
Reduction	Disulfide	CPT	*cyclo*(RGDyK)	[144]
	Pt(IV) complex	Cisplatin	Linear RGD and cyclopentapeptides	[145]
	Pt(IV) complex	Cisplatin, DOX	RGD cyclopentapeptide	[146]

Table 1. $\alpha_v\beta_3$ integrin-targeted SMDCs, grouped by type of linker. [a] specific functional group that is cleaved during drug release from SMDCs. [b] Contribution from our group is not reported here. DOX: doxorubicin; PTX: paclitaxel; CPT: camptothecin; SMAC: second mitochondrial activator of caspases; NMT: ST 1968 (namitecan).

Doxorubicin was the first anticancer drug to be coupled to an integrin ligand. In 1998, Ruoslahti and coworkers injected an RGD-DOX conjugate in mice xenografted with MDA-MB-435 human cancer cell line: owing to the high expression of α_v integrins in this cell line, this compound showed enhanced volume inhibition and lower toxicity, compared to the free anthracycline drug.[147] Although the conjugate's mechanism of action was not discussed at that time, these findings inspired the conjugation of different anticancer agents to a variety of peptidic, peptidomimetic and non-peptidic $\alpha_v\beta_3$ ligands. Moreover, different drug release mechanisms have been investigated through the installation of linkers that are cleaved upon hydrolysis, chemical reduction or enzymatic action (an overview of the drug-linker-ligand combinations that have been reported in the literature is shown in Table 1).

Paclitaxel and doxorubicin are the most common anticancer drugs to be evaluated as payloads in $\alpha_v\beta_3$-targeted SMDCs: the first has been mostly conjugated to integrin ligands by esterification of the drug's 2'-hydroxyl group. Although this drug design was often found to improve the efficacy of paclitaxel *in vivo*,[132,135] the use of this linker-payload combination is limited by the poor stability of the ester bond towards hydrolysis.[148] For instance, SMDC **57** (Fig. 23) showed a half-life of only ~2 h at 37 °C in glucose phosphate buffer solution at pH 7. This poor stability had a strong influence on antiproliferation assays against HUVECs: the cytotoxic effects of **57** and those of the poor integrin binder RAD-PTX conjugate (compound **58**) were significantly different only within a very short time exposure (i.e. less than 1 hour), indicating a swift loss of the integrin-targeting effect.[134]

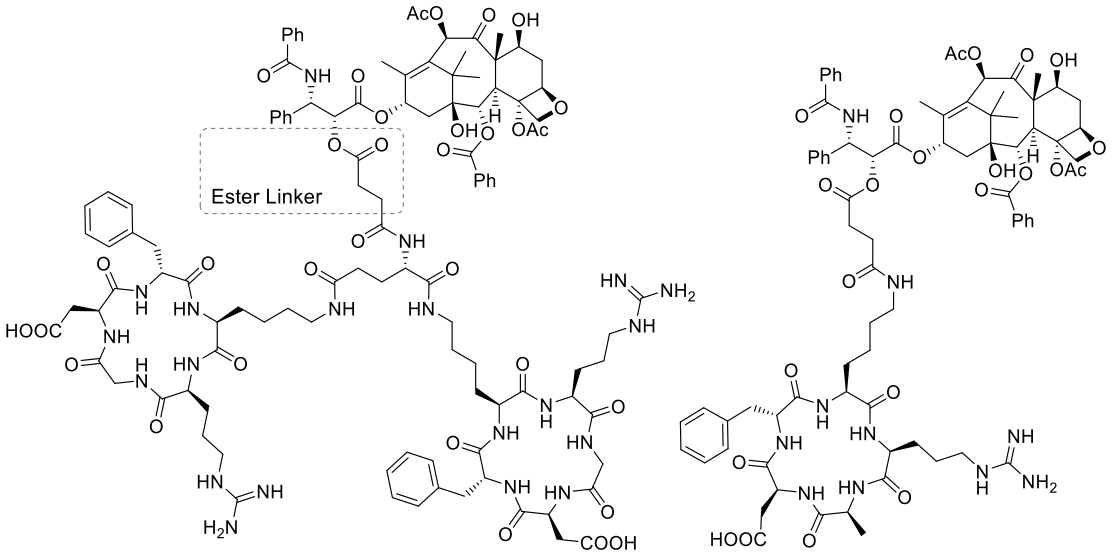

Figure 23. Molecular structures of the dimeric E[*cyclo*(RGDfK)]$_2$-PTX conjugate **57** and the control compound *cyclo*(RADfK)-PTX **58**, unable to bind $\alpha_v\beta_3$ integrin.[134]

The ketone and amino groups in doxorubicin allowed the conjugation of this anthracycline drug to RGD ligands through a wider group of linkers. Similarly to hemisuccinate esters of PTX, hydrazone derivatives of doxorubicin have shown a poor stability towards hydrolysis, when coupled to integrin ligands.[137,138] On the other hand, the daunosamine moiety of doxorubicin was used as anchoring point for enzymatically-cleavable peptide linkers.[139,140] Due to their stability, these peptide sequences have been recently used in integrin-targeted SMDCs, in which the drug potency is sensibly increased, compared to conventional anticancer agents.[141,143] For instance, the Liu and Sinha group conjugated MMAE to a non-peptidic $\alpha_v\beta_3$ ligand through the peptide linker Ala-Ala-Asn. This sequence acts as specific substrate of legumain, an intracellular protease which was found to co-localize with $\alpha_v\beta_3$ integrin in integrin-expressing breast carcinoma MDA-MB-435 cells. Due to its targeting properties, the resulting SMDC (compound **59**, Fig. 24) was administered to tumor-bearing

mice at 30 fold higher dose (11,7 if the different molecular weights of MMAE and SMDC are taken into account) than the maximum tolerated dose of free MMAE. This resulted in improved tumor response and much lower toxicity compared to the free MMAE (Fig. 24 A and B).[143]

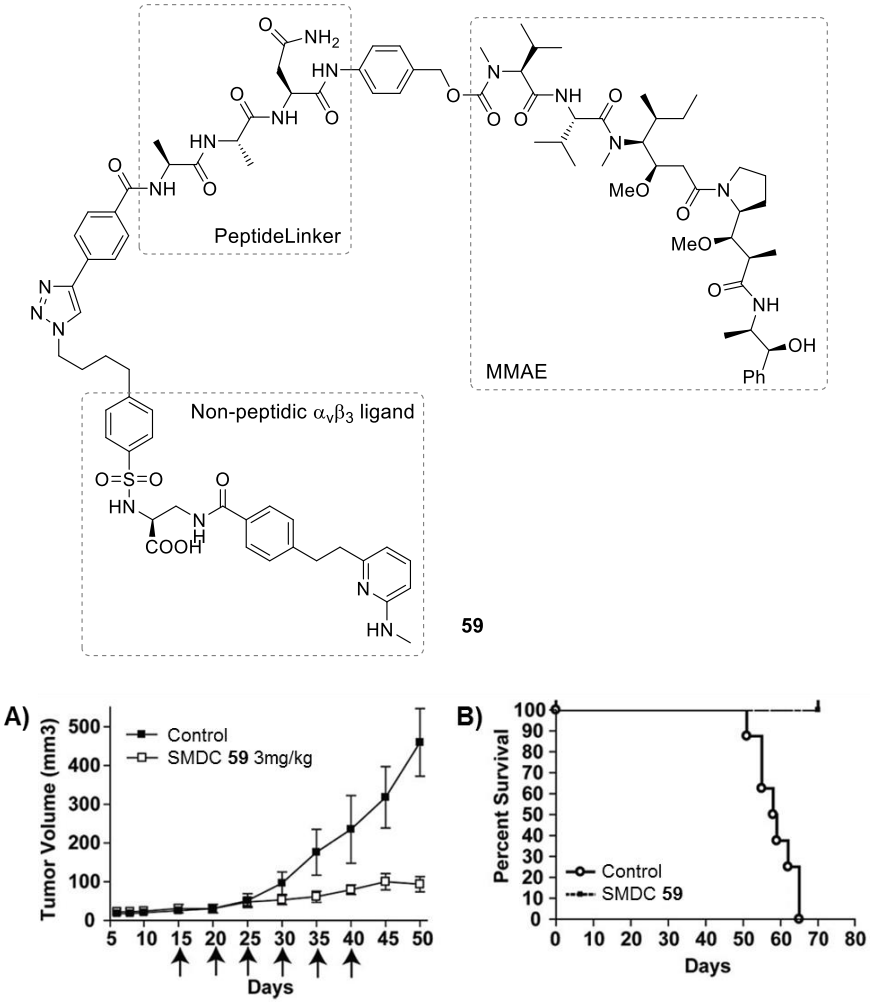

Figure 24. Molecular structures of the integrin-targeted SMDC **59**, reported by Liu and Sinha; A) *In vivo* effect of **59** on MDA-MB-435 carcinoma; B) survival curves of mice bearing MDA-MB-435 tumors in control and **59** groups.[143]

If the increase in drug's potency is important to improve the therapeutic effects of the conjugate, the development of "theranostic" devices is now facilitating the overall understanding of the mechanism of $\alpha_v\beta_3$-targeted drug delivery. In a recent paper, Liu and coworkers reported the synthesis and biological evaluation of a RGD-drug conjugate (compound **60**, Fig. 25), whose endocytosis in $\alpha_v\beta_3$-expressing cells is followed by the reduction of a Pt(IV) complex, resulting in the release of cisplatin and doxorubicin from a fluorescent tetraphenylene (TPE) moiety. In addition to the benefit of the multi-drug administration, this conjugate was designed to be analyzed by Fluorescence Resonance Energy Transfer (FRET) microscopy. Due to energy transfer to doxorubicin, the TPE

fluorescence is quenched before platinum reduction, whereas the separation between the two fluorophores leads to an enhanced intensity of the TPE signal.

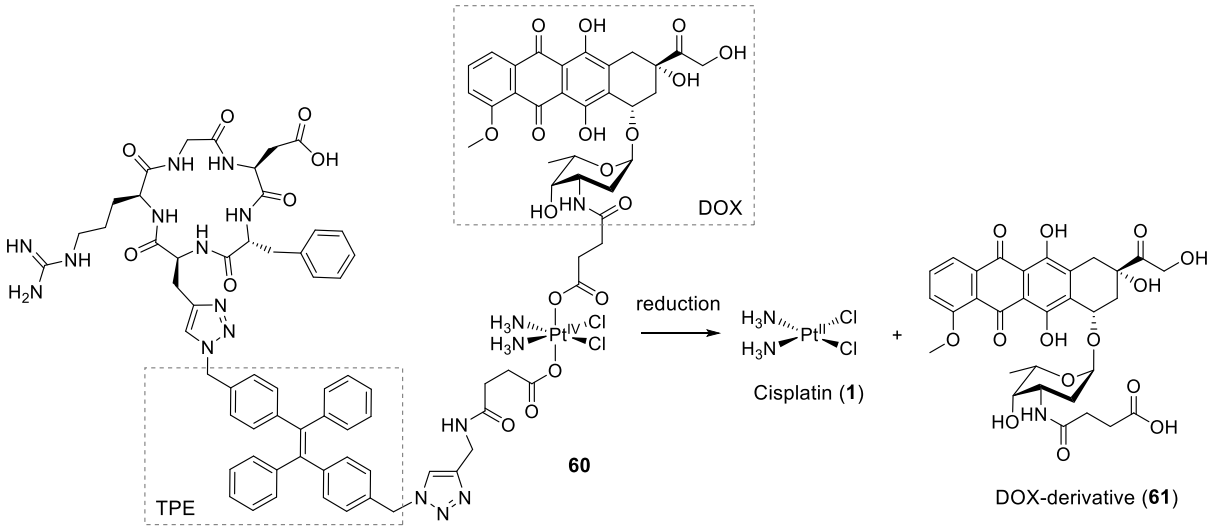

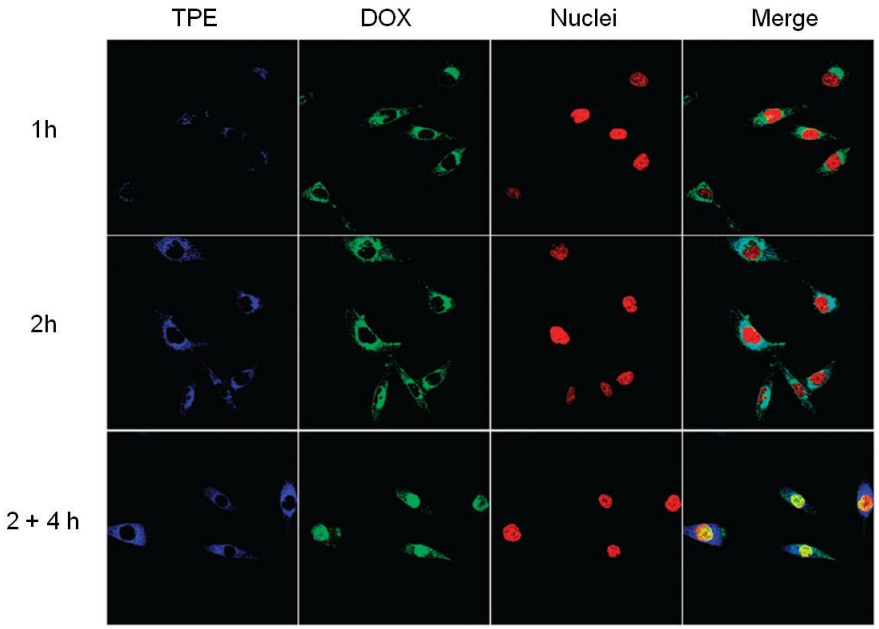

Figure 25. Molecular structure and mechanism of action of tetraphenylene (TPE)-labeled SMDC **60**. The intracellular Pt(IV)-Pt(II) reduction is exploited to deliver cisplatin (**1**) and doxorubicin derivative **61**. The separation between TPE and doxorubicin is monitored by FRET imaging owing to the enhancement of TPE's fluorescence. Picture: confocal images of MDA-MB-231 cells after incubation with **60** for 1 h, 2 h, and 2 h followed by incubation in fresh medium for additional 4 h.

This technique allowed a real-time monitoring of both the endocytosis in MDA-MB-231 cells and the release of doxorubicin from the vehicle (Fig. 25): by confocal microscopy, the migration of DOX from the cytosol to the nuclei was observed over a period of 6 h (i.e. cell incubation with SMDC for 2 h, followed by incubation in fresh medium for additional 4 h). On the other hand, the initial weak blue fluorescence of TPE increases significantly after 2h incubation, indicating the reductive linker cleavage and the separation between the two

fluorescent dyes. Unlike DOX, the TPE fluorescence is not observed in the nuclei, indicating that the RGD-TPE aggregate is not able to diffuse from the endocytic vesicle. Compound **60** revealed stronger antiproliferative activity, compared to free cisplatin and doxorubicin, against $\alpha_v\beta_3$-expressing cell line MDA-MB-231. Although conjugate **60** was reported to be remarkably less potent against cell lines showing low integrin expression (i.e. MCF-7 and 293T cells), a clear quantification of this integrin-targeting effect was not provided. Other "theranostic" RGD-drug conjugates have been reported in the literature and will be extensively discussed in the next chapters.

The development of "theranostic" devices as well as the evaluation of new linker systems for the selective drug release from integrin ligands are now providing better understanding of the potentialities of $\alpha_v\beta_3$-targeting SMDCs.

1.6. Previous Work of Our Research Group in the Field

1.6.1. Peptidomimetic cyclo[DKP-RGD] ligands

In 2009, the Gennari and Piarulli group entered this research area with the development of new integrin ligands in which the RGD sequence is constrained into a cycle by bifunctional 2,5-diketopiperazine (DKP) scaffolds. DKPs (Fig. 26) are the smallest cyclic peptides and their capability of altering the properties of traditional peptides led medicinal chemists to investigate them as important tools for biological target recognitions and drug design. Indeed, the DKP ring constrains the nitrogen atom of an α-amino amide: this modification of the two peptide bonds results in remarkable alterations of their physical-chemical properties. In particular, the 6-membered ring reduces the susceptibility of peptide bonds to metabolic cleavage and confers conformational rigidity.

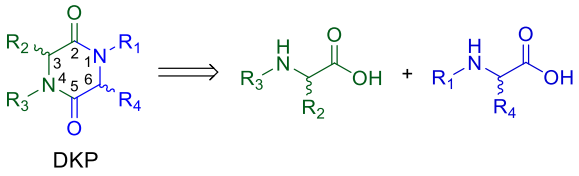

Figure 26. General structure of a 2,5-Diketopiperazine (DKP) and retrosynthetic analysis.

These changes in structural and physical properties, as well as the presence of functional groups that can act as donors (amide proton) and acceptors (carbonyl groups) of hydrogen bonds enhance favorable interactions with biological targets. Moreover, DKPs are simple heterocyclic scaffolds in which structural diversity can be introduced at up to four positions (N1, N4, C3, C6) and their preparation from enantiopure α-amino acids allows to control the stereochemical configuration in two positions (C3, C6, Fig. 26).[149] Due to all of these features, the Gennari and Piarulli group synthesized eight different diketopiperazines bearing

an amino and an acidic group. These scaffold were derived from combination of L- and D-amino acids, bearing carboxy (i.e. aspartic and glutamic acids) or amino groups in their side chains. Furthermore, the amino groups of the DKP ring were differently functionalized with benzylic moieties. The Arg-Gly-Asp sequence was coupled to each DKP, resulting in a library of 8 peptidomimetics (Fig. 27).[150,151]

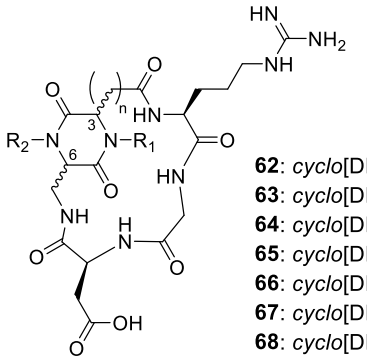

62: *cyclo*[DKP-1-RGD] = 3*S*, 6*S*, R_1=H, R_2=CH_2Ph, n=1
63: *cyclo*[DKP-2-RGD] = 3*R*, 6*S*, R_1=H, R_2=CH_2Ph, n=1
64: *cyclo*[DKP-3-RGD] = 3*S*, 6*R*, R_1=H, R_2=CH_2Ph, n=1
65: *cyclo*[DKP-4-RGD] = 3*R*, 6*S*, R_1=CH_2Ph, R_2=H, n=1
66: *cyclo*[DKP-5-RGD] = 3*R*, 6*S*, R_1=CH_2Ph, R_2=CH_2Ph, n=1
67: *cyclo*[DKP-6-RGD] = 3*S*, 6*R*, R_1=CH_2Ph, R_2=H, n=1
68: *cyclo*[DKP-7-RGD] = 3*S*, 6*R*, R_1=CH_2Ph, R_2=CH_2Ph, n=1
69: *cyclo*[DKP-8-RGD] = 3*S*, 6*R*, R_1=H, R_2=CH_2Ph, n=2

Figure 27. Schematic representation of the *cyclo*[DKP-RGD] library.[151]

The library members were tested *in vitro* for their ability to compete with fibronectin for the binding to the purified $\alpha_v\beta_3$ and $\alpha_v\beta_5$ receptors: IC_{50} values in the 10^{-10}-10^{-6} molar range demonstrated that the DKP ring strongly influences the ligand affinity for the receptor. NMR and *in silico* conformational studies completed the panel of SAR studies, providing the structural basis of the affinity observed *in vitro*. Due to its low-nanomolar affinity for the $\alpha_v\beta_3$ receptor and to its synthetic accessibility, the *cyclo*[DKP-RGD] ligand **64** (i.e. the *cyclo*[DKP-3-RGD]) was selected among the library members as hit compound for further biological evaluations. While this compound was found to inhibit the capillary network formation in human umbilical vein endothelial cells (HUVEC), it did not interfere with the production of mRNA for the α_v, β_3, and β_5 subunits.[152] Moreover, due to its inhibitory effect on integrin-mediated FAK/Akt transduction pathways and cell infiltration processes, ligand **64** has been recently classified as a pure $\alpha_v\beta_3$, antagonist.[153] These results highlighted the differences between the *cyclo*[DKP-RGD] ligand and the well-known cilengitide (**44**), whose agonist-like activity has been mentioned in Paragraph 1.5.2.

1.6.2. First-generation cyclo[DKP-RGD]-PTX conjugates

In order to explore the functionalization of the *cyclo*[DKP-RGD] ligand with bioactive molecules, the DKP scaffold of compound **64** was endowed with a benzylamino moiety. This nucleophilic functional group installed on the new *cyclo*[DKP-RGD]-CH_2NH_2 ligand (compound **70**, Fig. 28)[154] has then been used as anchoring point for the conjugation of different compounds, such as paclitaxel,[154] a pro-apoptotic SMAC mimetic compound[155] and an anti-angiogenic peptide.[156] Despite the increased molecular weight of these

conjugates, all new compounds were found to maintain an appreciable binding affinity towards $\alpha_v\beta_3$ integrin (nanomolar IC_{50} values), proving the feasibility of the ligand functionalization in the aromatic portion of the DKP scaffold. Among these compounds, the SMDC *cyclo*[DKP-RGD]-PTX (compound **71**, Fig. 28) was endowed with an acid-labile ester linker.

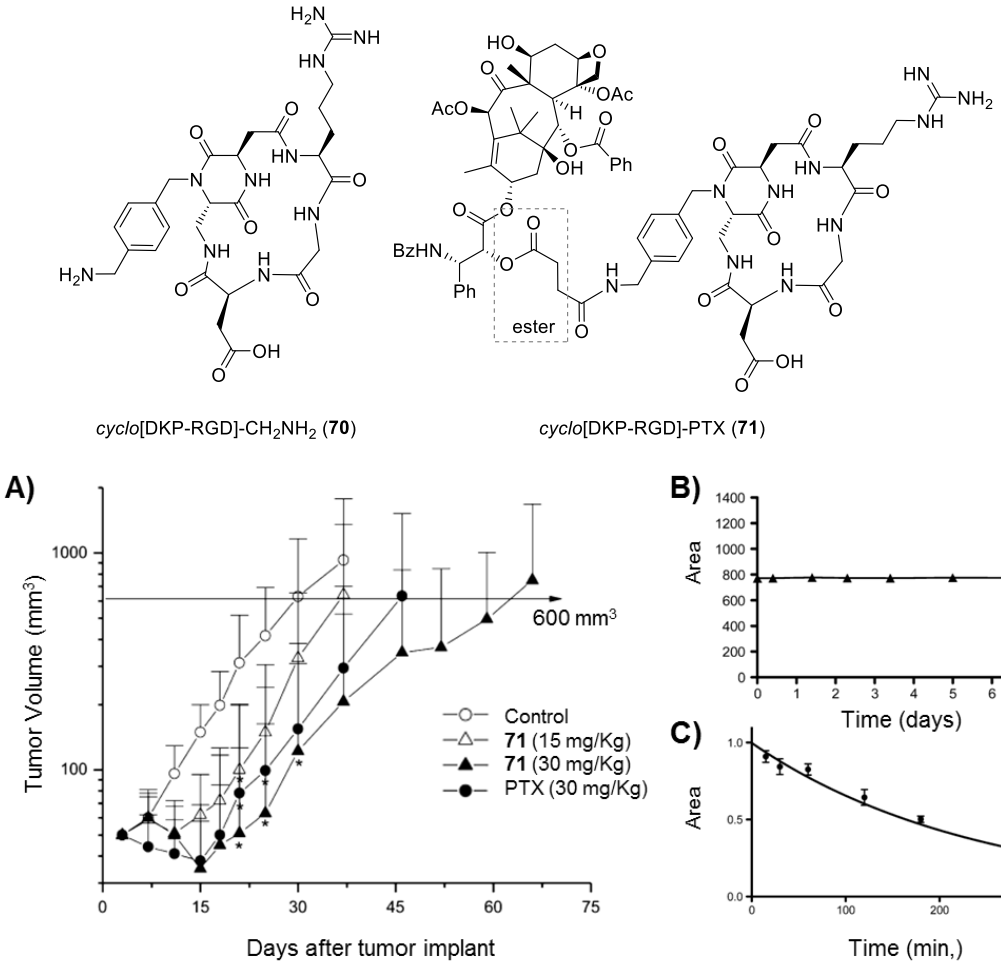

Figure 28. Molecular structures of the functionalized integrin ligand *cyclo*[DKP-RGD]-CH_2NH_2 **70** and the SMDC *cyclo*[DKP-RGD]-PTX **71**; **A**) *In vivo* antitumor activity studies of **71** compared to paclitaxel (PTX) on IGROV-1/Pt1 ovarian carcinoma; **B**) stability of **71** (1.28 mM) in physiological solution; **C**) stability of **71** in murine plasma.[154]

The anticancer properties of **71** were tested *in vivo* against the $\alpha_v\beta_3$ integrin-expressing cancer cells IGROV-1/Pt1 xenografted in nude mice. A remarkable tumor-targeting effect was observed: when injected at doses of 15 mg/kg-mouse, compound **71** displayed a higher inhibition of tumor growth, compared to the same dose of free PTX (Fig. 28A). Moreover, considering the different molecular weights of the SMDC and the free drug, it was possible to assert that **71** was more efficient than PTX at minor molar dosages, thus revealing that the conjugation with the *cyclo*[DKP-RGD] ligand improves the antitumor performances of PTX. As discussed in Paragraph 1.5.3, the low stability of PTX-hemisuccinate esters has been often reported. Although compound **71** revealed to be stable for days in physiological

solution (Fig. 28B), the ester linker was found to be cleaved in both murine and human plasma, with half-lives of 165 and 143 min, respectively (Fig. 28C).[154] These data are consistent with the observed antitumor activity: indeed, the stability assays revealed that the ester linker is sufficiently stable in plasma to allow a significant accumulation of intact **71** at the integrin-expressing tumor mass, where PTX is then released to exert its "targeted" cytotoxic activity. On the other hand, the plasma stability of this ester linker was found to be too low to exclude a premature drug release in circulation. This limitation of the ester linker would have an even stronger impact in the case of the conjugation of more potent cytotoxic agents to the *cyclo*[DKP-RGD] ligand, aimed at the development of highly efficient SMDCs. Arguably, the severe side effects derived from partial drug release in plasma would strongly restrict the application of this $\alpha_v\beta_3$-targeted anticancer approach.

A deep analysis of the linker technology thus appears mandatory for the evaluation of *cyclo*[DKP-RGD]-drug conjugates, in order to develop efficient integrin-targeted prodrugs.

Second-Generation *cyclo*[DKP-RGD]-PTX Conjugates

Part of the work described in this Chapter was published in the following articles:

- A. Dal Corso, M. Caruso, L. Belvisi, D. Arosio, U. Piarulli, C. Albanese, F. Gasparri, A. Marsiglio, F. Sola, S. Troiani, B. Valsasina, L. Pignataro, D. Donati, C. Gennari, *Chem. Eur. J.* **2015**, *21*, 6921-6929;
- Open Access Review: A. Dal Corso, L. Pignataro, L. Belvisi, C. Gennari, *Curr. Top. Med. Chem.* **2016**, *16*, 314-329.

2.1. Introduction

The biological evaluation of the RGD-PTX conjugate **71** revealed that the peptidomimetic ligand *cyclo*[DKP-RGD] can efficiently promote the accumulation of the cytotoxic payload at the tumor site. Besides the variety of integrin-targeting agents that have been reported in the literature, different approaches for the release of cytotoxic payloads from integrin ligands have been investigated so far. As discussed in Paragraphs 1.3.2 and 1.4.1, these linker moieties are fundamental for the SMDC efficacy, which is derived from the correct equilibrium between the linker stability in circulation and its fast cleavage at the tumor site. Peptide linkers have been extensively used for the release of cytotoxic payloads from targeting vehicles (e.g. mAbs and small ligands) and for the activation of anticancer prodrugs. The efficiency of peptide linkers is ascribable to their high plasma stability and to their selective cleavage at the site of disease, which is the result of their interaction with specific proteases. These target enzymes can be either expressed on the surface of tumor cells (e.g. MMP-2 and -9) or in the endosomal/lysosomal compartment (e.g. cathepsin B and other cysteine proteases).

We focused on lysosomally-cleavable linkers: this choice was made in order to exploit the endocytic pathways of $\alpha_v\beta_3$ integrin, which make possible the drug release in the intracellular environment, thus minimizing the linker cleavage in the extracellular milieu. Importantly, these linkers would allow the rapid screening *in vitro* of the synthesized SMDCs, aiming at the evaluation of their cytotoxic activity depending on the targeted $\alpha_v\beta_3$ receptor. Moreover, in 2013 Sewald and coworkers analyzed by confocal microscopy the intracellular localization of

a fluorescein-labeled RGD-chryptophycin conjugate.[157] This experiment highlighted the transition of the RGD-labeled compound through the lysosomal compartment, where the compound accedes upon $\alpha_v\beta_3$-mediated endocytosis. This observation strongly supports the feasibility of lysosomally-degradable linkers in RGD-drug conjugates.

With the aim of designing 2nd-generation *cyclo*[DKP-RGD]-PTX conjugates, significant importance was given to the self-immolative spacer: as discussed in Paragraph 1.4.1, this moiety connects the drug to the cleavable linker, reducing steric hindrance and allowing better protease activity. Unlike the ester bond in SMDC **71**, this spacer module has to be connected to the drug through more stable functional groups, in order to allow drug release only upon the enzymatic action. We focused on different self-immolative spacers reported in the literature for paclitaxel release from peptide moieties in both targeted and non-targeted prodrugs.

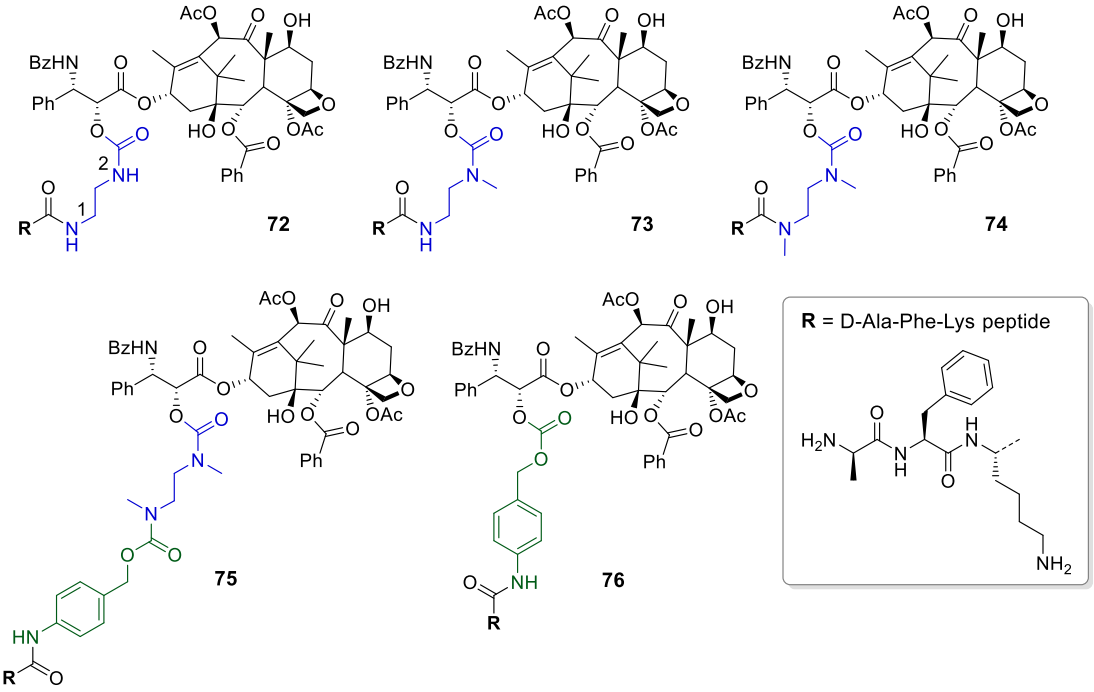

Figure 29. Molecular structures of the protease-activable paclitaxel prodrug reported by Scheeren and coworkers.[158,159]

In particular, Scheeren and coworkers developed a group of protease-activable paclitaxel prodrugs, in which a substrate of the serine protease plasmin (i.e. the D-Ala-Phe-Lys peptide) was coupled to the drug's 2'-position through carbamate (compounds **72**-**75** in Fig. 29) and carbonate (compound **76**) bonds.[158,159] The carbonate group in compound **76** connects directly the drug to the *p*-aminobenzyl alcohol (green moiety in Fig. 29), which is a well-known self-immolative spacer, already discussed in Paragraph 1.4.1. On the other hand, the formation of carbamate bonds in the other prodrugs has been made by using ethylenediamine derivatives (blue moiety in Fig. 29). The two nitrogen atoms are named here

as N1 and N2 (see compound **72**). Upon deprotection of N1, the free amine undergoes cyclization onto the carbonyl group of the carbamate bond, releasing the free PTX and a cyclic urea. This cyclization mechanism has been reported to be significantly slower than the electronic cascade mechanism of self-immolative spacers. In order to improve the kinetic and stability of drug release from these cyclization spacers, the presence of substituents on N1 and N2 atoms have been extensively investigated. For instance, the methylation of the N2 atom in compound **73** has been devised to avoid the undesired reaction described for compound **72**, which was found to completely degrade to baccatin III (**77**, Scheme 3A**Scheme**) within 24h under neutral pH conditions.

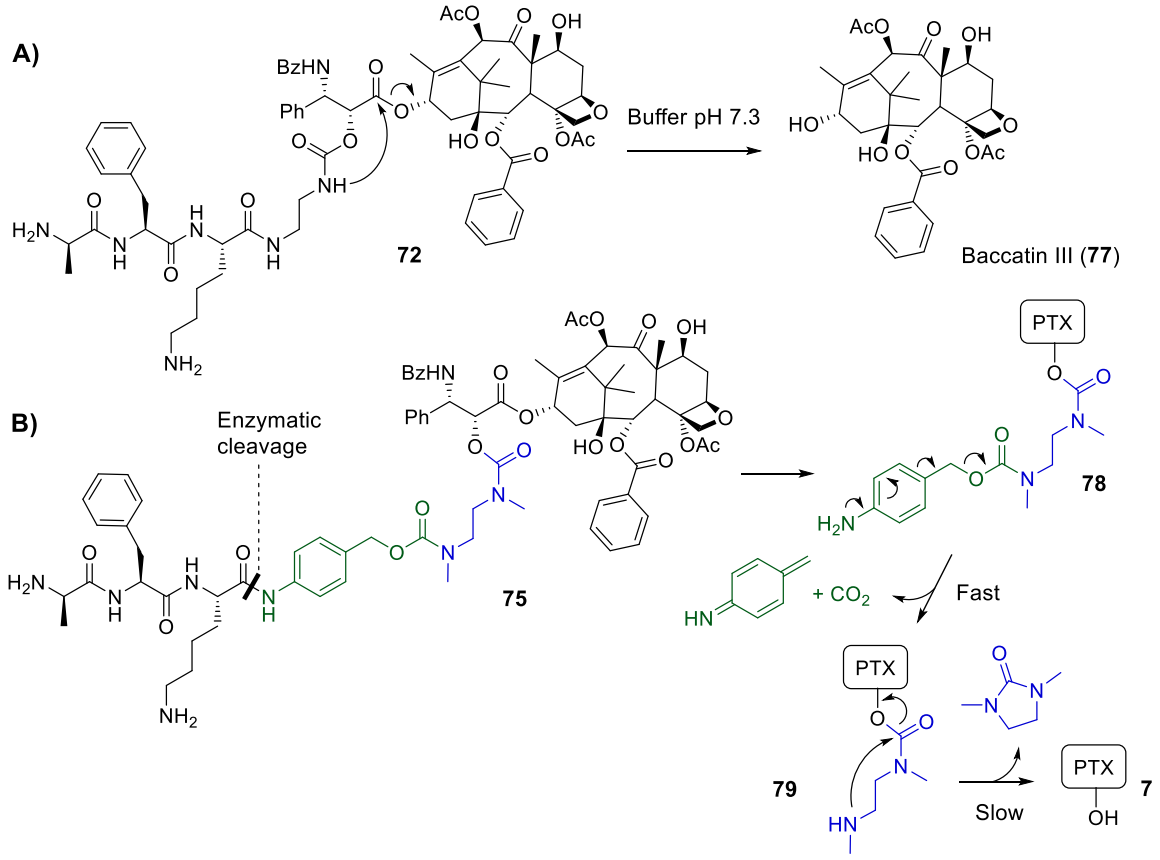

Scheme 3. A) degradation mechanism of prodrug **72**; **B**) two-step drug release mechanism of prodrug **75** upon enzymatic cleavage.

On the other hand, the methyl group on N1 atom has been installed (i.e. in compounds **74** and **75**) in order to achieve a faster PTX release compared to what observed with prodrug **73**. However, no drug release in the presence of plasmin has been observed from prodrug **74**, indicating that the amide bond between methylated N1 and the C terminus of the peptide sequence is not recognized by the proteolytic enzyme. We focused on the self-immolative spacer of prodrug **75**: in this compound, the ethylenediamino moiety bears two methyl groups at both N1 and N2 atoms and the enzymatic activity is made possible by the elongation of the dimethylethylenediamino chain with a *p*-aminobenzylcarbamate (PABC)

spacer (green moiety in Fig. 29). The two self-immolative spacers are connected through a physiologically-stable carbamate bond and the mechanism of drug release is depicted in Scheme 3B: the enzymatic cleavage leads to aniline **78**, which rapidly releases CO_2 and paclitaxel metabolite **79**. The final PTX release occurs by cyclization of the methylamine group onto the 2'-carbamate group and it was indicated as the rate-determining step of the release process. From its development in 2001, this two-step self-immolative spacer has been widely applied in the field of triggered-drug release from polymers, dendrimers, and nano-scale assemblies.[160]

Inspired by this work, we developed second-generation *cyclo*[DKP-RGD]-PTX conjugates (Fig. 30) in which the self-immolative spacer of prodrug **75** connects the payload to lysosomally-cleavable peptide linkers.

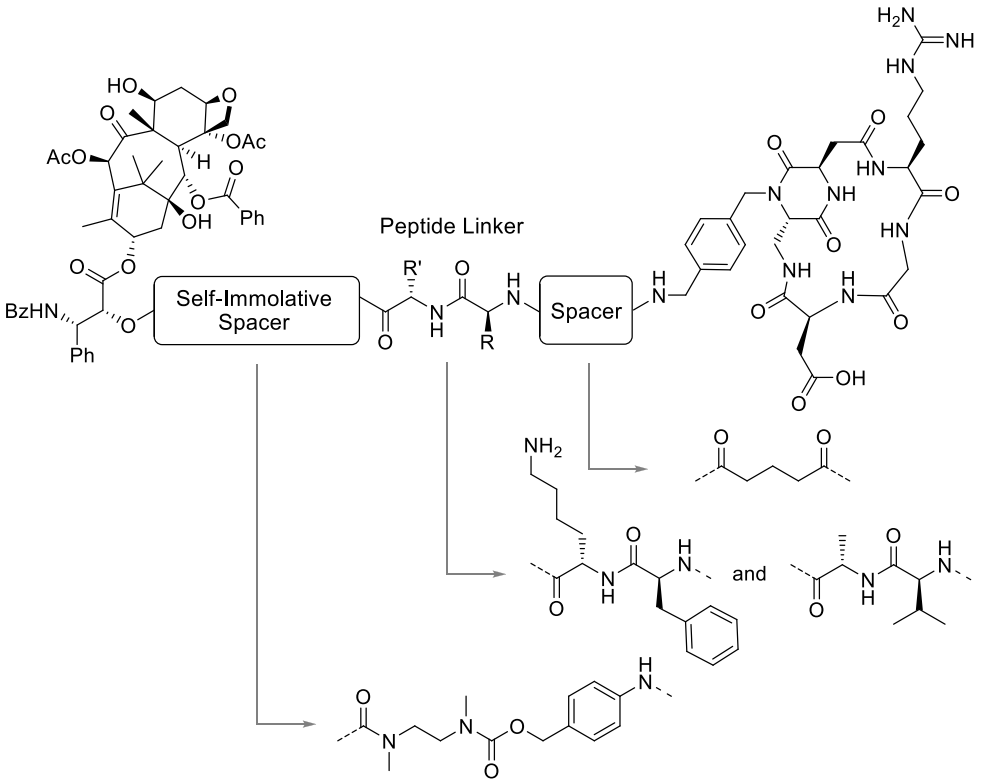

Figure 30. Schematic representation of second-generation *cyclo*[DKP-RGD]-PTX conjugates, bearing peptide linkers.

Among the plethora of dipeptide linkers that are known to be specific substrates of lysosomal proteases, we chose the Phe-Lys and the Val-Ala sequences, whose engagement as linkers in SMDCs was well documented in the literature.[142,161] Moreover, a di-carboxylate spacer (derived from a cyclic anhydride) allowed the connection of the *cyclo*[DKP-RGD]-CH_2NH_2 ligand (**70**) to the N-terminus of the peptide linker (Fig. 30).

2.2. Synthesis of RGD Peptidomimetic-Paclitaxel Conjugates bearing Lysosomally Cleavable Linkers

Three different *cyclo*[DKP-RGD]-PTX conjugates have been synthesized, and their molecular structures are reported in Fig. 31.[162]

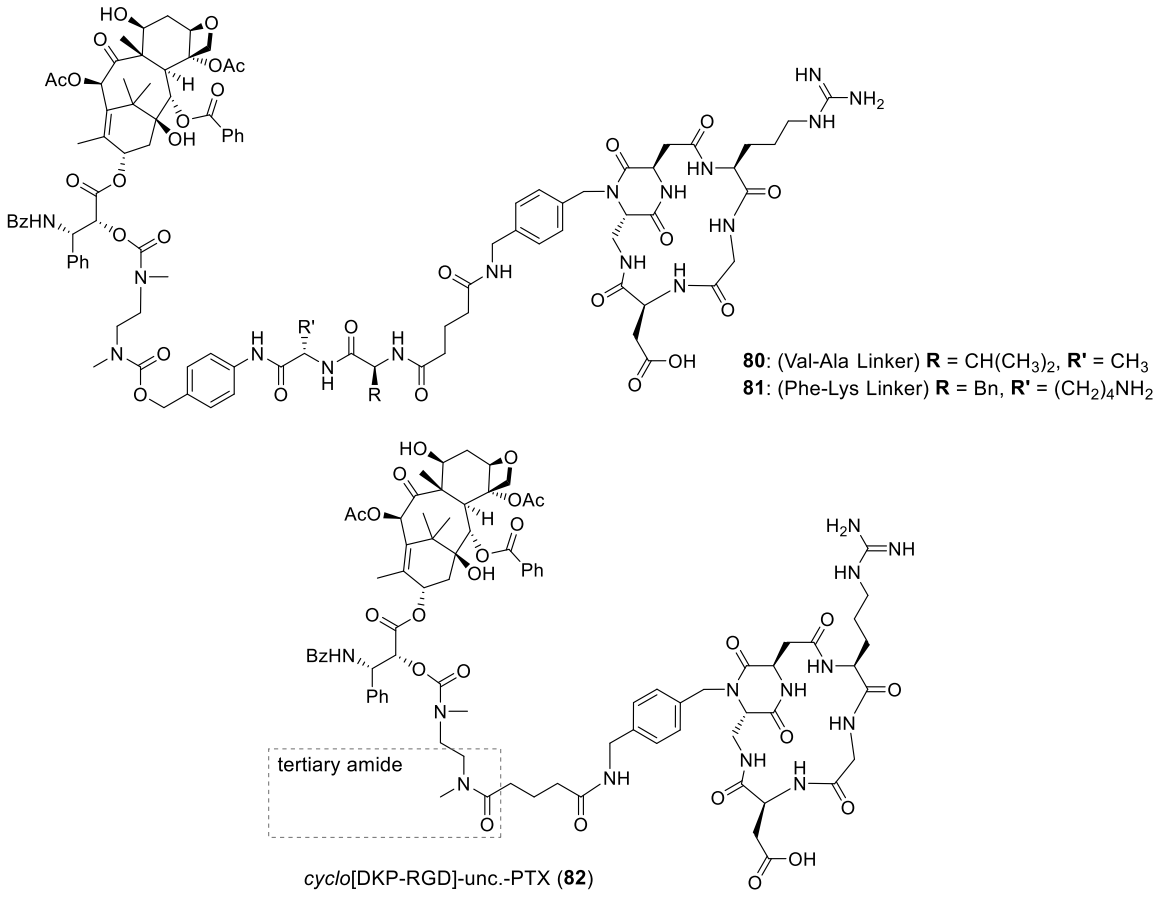

Figure 31. Molecular structures of the SMDCs *cyclo*[DKP-RGD]-Val-Ala-PTX **80**, *cyclo*[DKP-RGD]-Phe-Lys-PTX **81**, and *cyclo*[DKP-RGD]-uncleavable-PTX **82**.

In addition to the peptide linker-bearing compounds *cyclo*[DKP-RGD]-Val-Ala-PTX (SMDC **80**) and *cyclo*[DKP-RGD]-Phe-Lys-PTX (**81**), a third conjugate (compound **82**) was prepared, in which the dipeptide moiety is replaced by a tertiary amide bond. This proteolytically-stable or "uncleavable" linker was designed in order to use compound **82** as a negative control for evaluating the biological performances of conjugates **80** and **81**.

2'-(4-Nitrophenoxycarbonyl)paclitaxel (compound **83** in Scheme 4) and *N*-(Boc)-*N*,*N'*-dimethylethylenediamine (**86**) have been synthesized as common intermediates for the preparation of SMDCs **80**-**82**. While the diamine spacer was prepared according to a previously reported methodology,[163] the reaction of paclitaxel with *p*-nitrophenylchloroformate was optimized, resulting in a 69% conversion to carbonate **83** and

minimizing the functionalization of the hindered 7-hydroxyl group (i.e. conversion to compound **84**).

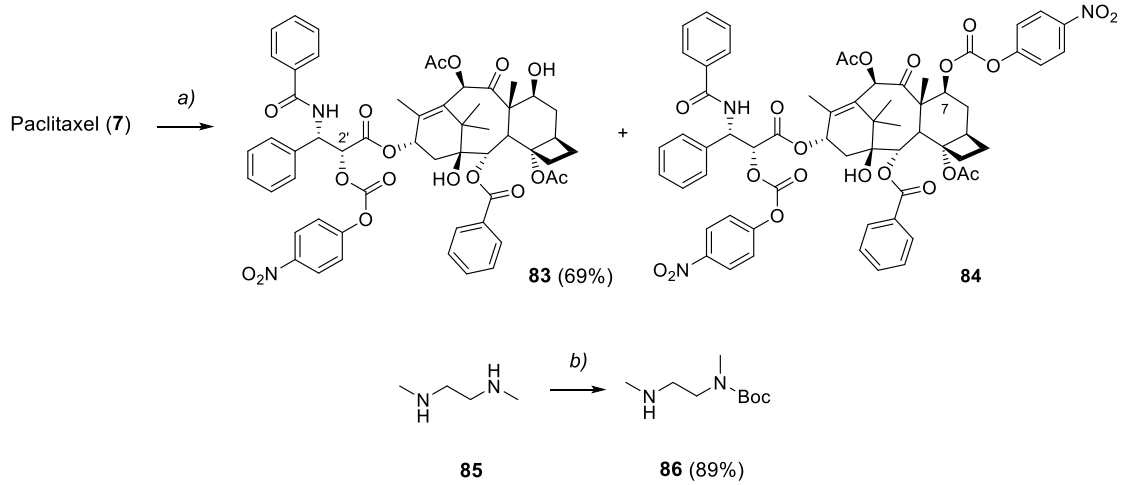

Scheme 4. Synthesis of intermediates **83** and **86**. Reagents and conditions: *a) p*-nitrophenyl chloroformate, pyridine, CH_2Cl_2, -50 °C to -20 °C, 4 h; *b)* Boc_2O, CH_2Cl_2, 0 °C to RT, overnight.

SMDCs **80** was obtained through the synthetic pathway shown in Scheme 5. The Fmoc-Val-Ala-OH (**87a**) intermediate, synthesized according to a procedure reported by Kratz and coworkers,[161] was coupled to 4-aminobenzyl alcohol, affording compound **88a**. The synthesis of the self-immolative spacer continued with the activation of the benzyl alcohol group by conversion into the corresponding 4-nitrophenyl carbonate **89a**. The latter was then reacted with the mono Boc-protected diamine **86**, affording compound **90a**. The Fmoc protecting group was removed in solution and without purification: after removing DMF and piperidine from the reaction mixture, the crude amine was re-dissolved and treated with glutaric anhydride. Flash chromatography afforded the resulting hemigluatarate **91a** in high yields. This carboxylic acid was activated as *N*-hydroxysuccinimidyl (NHS) ester and coupled with the integrin ligand *cyclo*[DKP-RGD]-CH_2NH_2 (**70**). As a well-established procedure from our group, this conjugation step was run at controlled pH, since at pH < 7.0 the reaction does not proceed, whereas at pH > 7.6 the hydrolysis of the NHS ester competes significantly with the desired coupling. The pH was maintained in the 7.3-7.6 range by adding aliquots of 0.2 M aq. NaOH to the reaction mixture. Boc cleavage at this stage yielded the free secondary amine **92a**, as trifluoroacetate salt. This amine was reacted with 2'-(4-nitrophenoxycarbonyl)-paclitaxel (**83**) affording the final *cyclo*[DKP-RGD]-Val-Ala-PTX conjugate (**80**). This synthetic strategy has been also applied to the preparation of compound **81**. Unlike the Val-Ala-bearing analogue **80**, the synthesis of SMDC **81** required the protection of the amino group on the lysine side chains: the allyloxycarbonyl (Alloc) protecting group was chosen, in order to take advantage of its stability under the cleavage conditions of both Boc- and Fmoc-protecting groups.

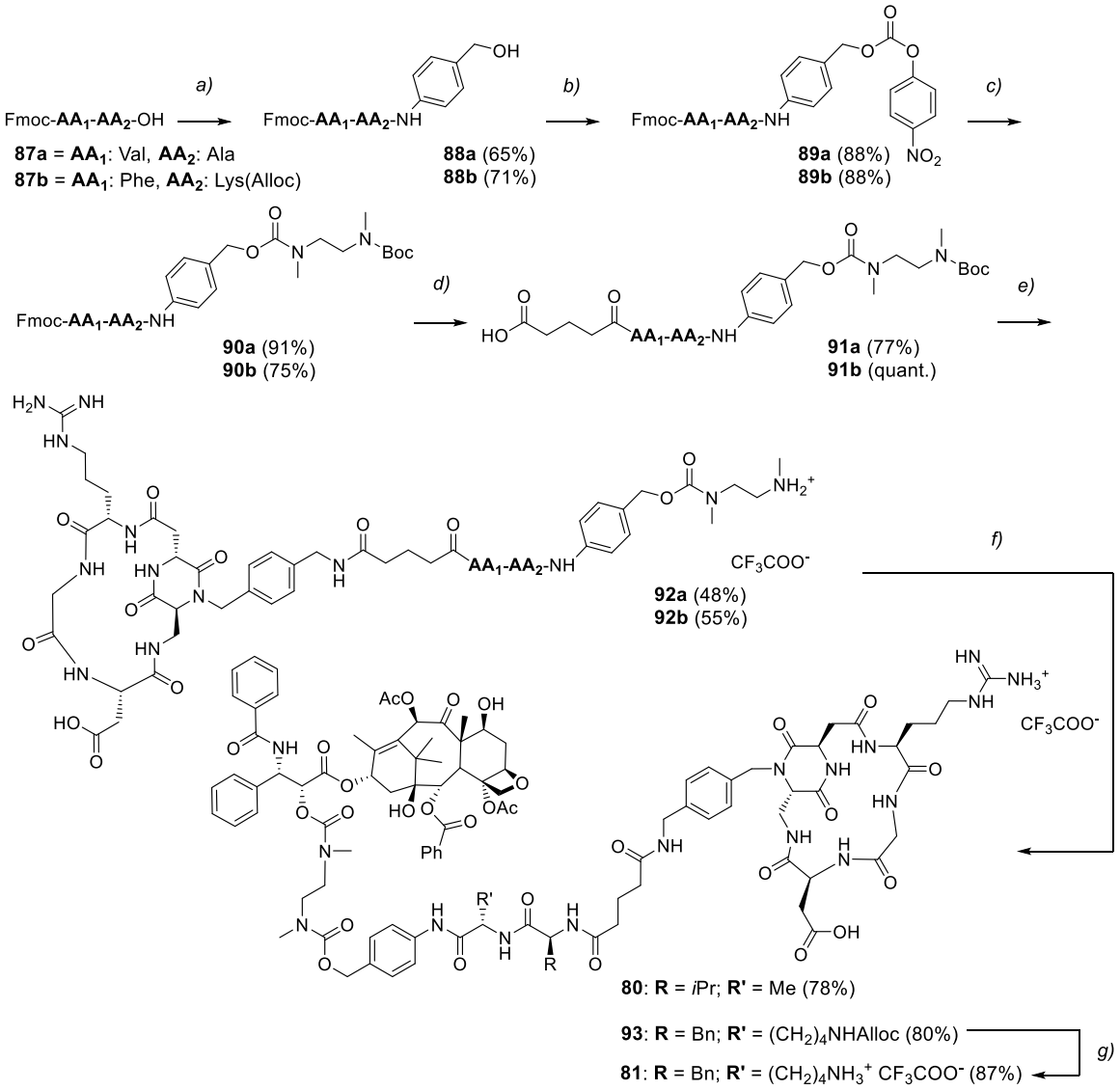

Scheme 5. Synthesis of SMDCs **80** and **81**. Reagents and conditions: *a)* 4-aminobenzyl alcohol, EEDQ, CH_2Cl_2/MeOH (2:1), overnight (**88a**); 4-aminobenzyl alcohol, EDC·HCl, HOAt, *N*-methylmorpholine, THF, 4 h (**88b**); *b)* 4-nitrophenylchloroformate, pyridine, THF, 4 h; *c)* **86**, *i*Pr_2NEt, THF, overnight; *d)* [1] piperidine, DMF, 2 h; [2] glutaric anhydride, DMAP, *i*Pr_2NEt, DMF, overnight; *e)* [1] DIC, NHS, DMF, overnight (**92a**); EDC·HCl, NHS, DMF, overnight (**92b**); [2] *cyclo*[DKP-RGD]-CH_2NH_2 (**70**), CH_3CN/PBS (1:1; pH 7.5), overnight; [3]. TFA/CH_2Cl_2 (1:2), 45 min; *f)* **83**, *i*Pr_2NEt, DMF, 24 h; *g)* [$Pd(PPh_3)_4$], Bu_3SnH, AcOH, DMF, RT, overnight.

The final Alloc-deprotection of compound **93** was carried out on a 10-mg scale, affording the final *cyclo*[DKP-RGD]-Phe-Lys-PTX conjugate (**81**) in 87% yield. This was achieved after an optimization of the relative stoichiometric amounts of the Pd(0) complex and the scavenger of the π-allyl Pd(II) complex (i.e. Bu_3SnH), which avoids the irreversible allylation reactions of the deprotected amine.

The synthesis of the RGD-paclitaxel conjugate featuring the “uncleavable” linker (**82**) is reported in Scheme 6. In this case, glutaric anhydride was reacted with the mono-protected diamine **86**. The Boc group was removed at this stage, and the resulting secondary amine **94** was reacted with paclitaxel derivative **83** to yield compound **95**. Unlike SMDCs **80** and **81**,

the conjugation of the integrin ligand *cyclo*[DKP-RGD]-CH_2NH_2 (**70**) was performed at the end of the synthesis, affording the *cyclo*[DKP-RGD]-unc.-PTX (**82**) in 50% yield.

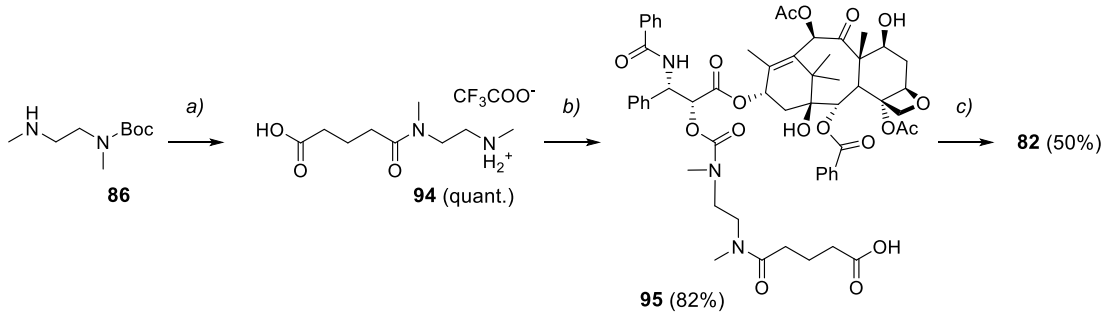

Scheme 6. Synthesis of the "uncleavable" SMDC **82**. Reagents and conditions: *a)* [1] Glutaric anhydride, *i*Pr_2NEt, DMF, 6 h; [2] TFA/CH_2Cl_2 1:2, 45 min; *b)* **83**, *i*Pr_2NEt, DMF, 24 h; *c)* [1] DIC, NHS, DMF, overnight; [2] **2**, 1:1 CH_3CN/PBS (pH 7.5), overnight.

The final compounds **80**-**82** were all purified by semi-preparative HPLC and lyophilized before being subjected to biological assays.

2.3. In vitro Biological Evaluation

2.3.1. Integrin Receptor Competitive Binding Assays

The functionalization of the *cyclo*[DKP-RGD] ligand with linker and drug modules resulted in an over-3-fold increase of the final molecular weight. In order to assess the effects of this increased steric hindrance on the ligand's affinity for the receptor, *cyclo*[DKP-RGD]-PTX conjugates **80**-**82** were examined *in vitro* for their ability to inhibit biotinylated vitronectin binding to the purified $\alpha_v\beta_3$ and $\alpha_v\beta_5$ receptors. The calculated IC_{50} values are listed in Table 2, together with the previous data relative to the free-ligand **64**.

	IC_{50} (nM)[a]	
Structure	**$\alpha_v\beta_3$**	**$\alpha_v\beta_5$**
cyclo[DKP-RGD]-Val-Ala-PTX (**80**)	13.3 ± 3.6	924 ± 290
cyclo[DKP-RGD]-Phe-Lys-PTX (**81**)	52.4 ± 14.4	n.d.
cyclo[DKP-RGD]-unc.-PTX (**82**)	10.8 ± 1.7	1050 ± 270
cyclo[DKP-RGD] (**64**)[151]	4.5 ± 1.1	149 ± 25

Table 2. Inhibition of biotinylated vitronectin binding to isolated $\alpha_v\beta_3$ and $\alpha_v\beta_5$ receptors. [a] IC_{50} values relative to compounds **80**-**82** were calculated as the concentration of compound required for 50% inhibition of biotinylated vitronectin binding as estimated by GraphPad Prism software. All values are the arithmetic mean ± the standard deviation (SD) of triplicate determinations. n.d.: not determined.

Screening assays were carried out through incubation of the immobilized integrin receptors with solutions of the tested compounds at different concentrations (10^{-12}-10^{-5} M) in the presence of biotinylated vitronectin (1 μg/mL), and measuring the concentration of bound

vitronectin. The results showed that despite their remarkable steric bulk, the conjugates' affinity for the purified $\alpha_v\beta_3$ receptor is comparable to that of the free ligand **64**. Indeed, low-nanomolar IC_{50} values were obtained throughout the series. Moreover, SMDCs **80**-**82** showed micromolar IC_{50} values for the binding to the $\alpha_v\beta_5$ receptor, indicating their selectivity towards the $\alpha_v\beta_3$ heterodimer. This selectivity has been also observed with other derivatives of *cyclo*[DKP-RGD] previously developed by our group.[154–156] Notably, besides showing the highest IC_{50} binding values in the series towards integrin $\alpha_v\beta_3$, the RGD-PTX conjugate **81** did not allow to obtain reproducible binding curves to $\alpha_v\beta_5$ integrin. This unusual behavior is possibly due to the poor solubility of conjugate **81** in the aqueous medium, that might interfere with the binding process, especially at the highest concentration (10^{-5} M).

2.3.2. Stability Assays and Lysosome Extract Digestion

The stability of the different linker systems installed in *cyclo*[DKP-RGD]-PTX conjugates **80**-**82** was assessed under different conditions. At first, the compounds were dissolved in neutral (pH 7.4) and acidic (pH 5.5) buffers. After 4 h exposure, HPLC-MS analysis revealed the perfect stability of the three SMDCs under the different pH conditions.

To evaluate the effective cleavage of the peptide linkers and the subsequent paclitaxel release in the presence intracellular proteases, conjugates **80**-**82** were treated with lysosome extract, and metabolites were detected by HPLC-MS analysis. The enzymatic cleavage of the peptide linkers in compounds **80** and **81** was observed over a 2 h period. In particular, the metabolite analysis of these two compounds revealed the presence of *N*,*N'*-dimethylethylenediamine spacer-bearing paclitaxel (i.e. compound **79**, reported in Scheme 3B, pag. 41) as the main product.

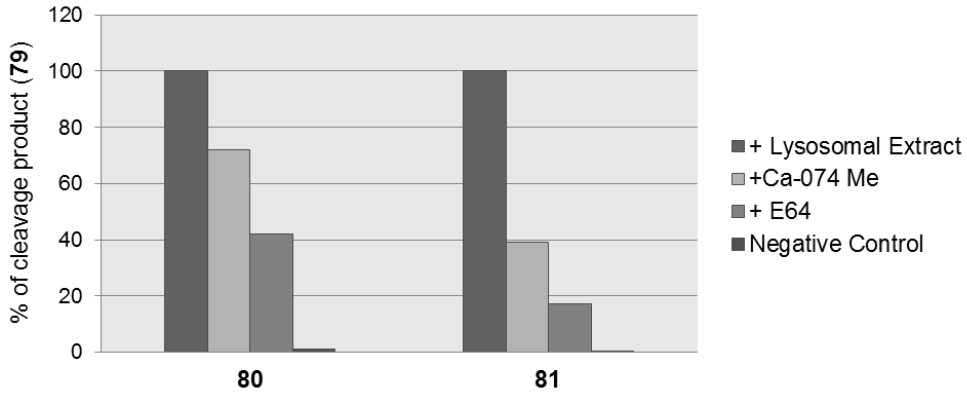

Figure 32. Analysis of lysosomal extract digestion of SMDCs **80** and **81** in the presence of cathepsin B specific inhibitor (CA-074-Me), cysteine proteases inhibitor (E-64) and inactivated lysosomal extract (negative control). Signal detected for m/z 968.4 (attributed to compound **79**) expressed in percentage relative to that obtained with lysosomal extract (set to 100%).

This is consistent with the drug release mechanism described by Scheeren for prodrug **75** (Scheme 3B), in which the cyclization of the diamine spacer was claimed as the rate-limiting

step of the drug release. On the other hand, the exposure of the *cyclo*[DKP-RGD]-unc.-PTX conjugate (**82**) to lysosome extract did not lead to any drug release, due to the absence of peptide linkers. In order to analyze more in detail the selectivity of the linker cleavage, SMDCs **80** and **81** were treated with lysosome extract in the presence of a cathepsin B specific inhibitor (CA-074-Me) and of a broader-scope cysteine protease inhibitor (E-64). The effect of protease inhibition, evaluated by HPLC-MS, is shown in Fig. 32. The digestion of the two RGD-PTX conjugates was impaired by both CA-074-Me and E-64 compounds, with the latter being more effective than the catepsin B-specific inhibitor. However, the lysosome digestion was not completely abolished by treatment with these inhibitors. This data indicate that the cleavage of the Val-Ala and Phe-Lys linkers is not exclusively ascribable to the enzymatic action of cysteine proteases, but it can rather occur in the presence of other lysosomal proteases.

2.3.3. Cell Proliferation Analysis

With the aim of verifying the ability of the synthesized compounds to selectively target $\alpha_v\beta_3$ integrin in human cancer cells, two isogenic cell lines were selected, expressing the integrin receptor at different levels: the acute lymphoblastic leukemia cell line CCRF-CEM ($\alpha_v\beta_3$ −) and its subclone CCRF-CEM $\alpha_v\beta_3$ ($\alpha_v\beta_3$ +). This latter antigen-positive cancer cell line was generated by transfection of the antigen-negative CCRF-CEM with a DNA vector, resulting in the stable expression of the $\alpha_v\beta_3$ integrin receptor. The different $\alpha_v\beta_3$ expressions on the cell membrane of the two cell lines was confirmed by treatment the cells with a fluorescein-labeled $\alpha_v\beta_3$-selective mAb, followed by cell immunofluorescence analysis and flow cytometry.

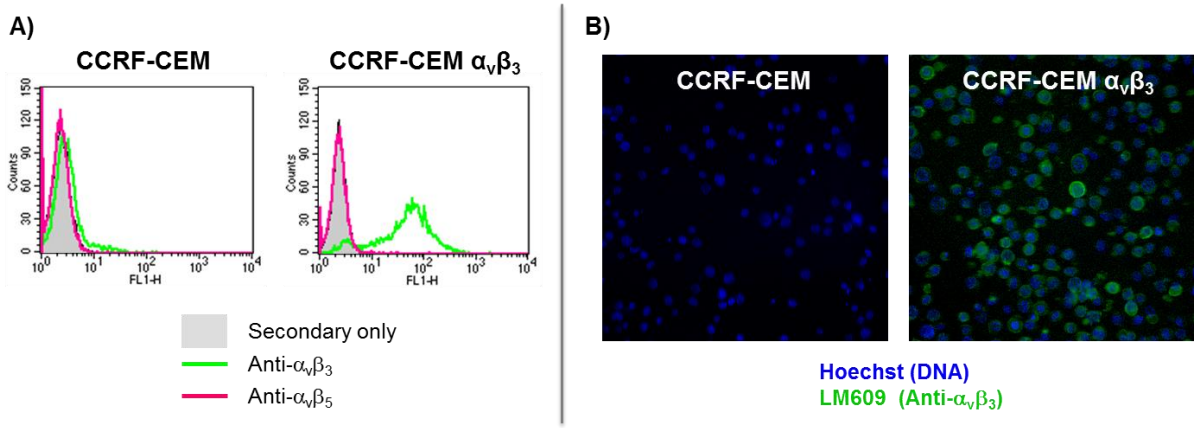

Figure 33. Confocal microscopy (**A**) and immunofluorescence (**B**) analyses of integrin expressions on the two isogenic leukemia cell lines CCRF-CEM ($\alpha_v\beta_3$ –) and subclone CCRF-CEM $\alpha_v\beta_3$ ($\alpha_v\beta_3$ +).

The two isogenic cell lines were incubated with increasing doses of free PTX and SMDCs **80**-**82**. After 144 hours, the cell viability was analyzed by CellTiter-GLO™ luciferase-based ATP detection assay. Under these conditions, “cleavable” conjugates **80** and **81** showed no

significant targeting towards CCRF-CEM $\alpha_v\beta_3$, as compared with CCRF-CEM. These results were interpreted in terms of an undesired linker cleavage in the extracellular environment, which may take place over the long period of time. A modified antiproliferative assay was devised, consisting in a short-time exposure of tumor cells (6 h) to the tested compounds, followed by cell washout and incubation in fresh medium for additional 138 hours. As previously reported in the SMDC field,[58,60,143] this experiment aimed at mimicking the *in vivo* conditions, characterized by a rapid clearance of the administered drug from the tumor extracellular environment. With this procedure, the fraction of *cyclo*[DKP-RGD]-PTX conjugates unbound to the integrin receptors was removed from the medium. This led to a minimization of the extracellular release of paclitaxel, thus maximizing the cytotoxic activity of PTX through the integrin-mediated endocytosis of the SMDCs.

The calculated IC_{50} values are shown in Table 3.

	IC_{50} (nM)[a]			
Structure	**CCRF-CEM ($\alpha_v\beta_3$ −)**	**CCRF-CEM $\alpha_v\beta_3$ ($\alpha_v\beta_3$ +)**	***S*[b]**	**T.I.[c]**
Paclitaxel (PTX, **7**)	155 ± 55	21 ± 2	7.4	1
RGD-Val-Ala-PTX (**80**)	5153 ± 977	77 ± 20	66.9	9.0
RGD-Phe-Lys-PTX (**81**)	535 ± 70	34 ± 2	15.7	2.1
RGD-unc.-PTX (**82**)	> 10000	> 10000	n.d.	n.d.

Table 3. Antiproliferative activity of PTX and conjugates **80**-**82** in CCRF-CEM and CCRF-CEM $\alpha_v\beta_3$ after 6 hour-treatment followed by compound washout and 138 hour-long growth in fresh medium. [a] IC_{50} values were calculated as the concentration of compound required for 50% inhibition of cell viability in culture, based on quantitation of the ATP present as estimated by CellTiter-GLO™; cells were treated for 6 h in U-bottomed 96-well plates, then washed and incubated for 138 h in compound-free medium in 96-well flat-bottomed plates. [b] Selectivity (*S*): $IC_{50}(\alpha_v\beta_3$ −)/$IC_{50}(\alpha_v\beta_3$ +). [c] Targeting index (T.I.): selectivity/selectivity observed with free paclitaxel.

While the ability of free PTX to inhibit the proliferation of CCRF-CEM $\alpha_v\beta_3$ cells was found to be 7.4-fold higher than its activity against the CCRF-CEM line, the presence of the RGD ligand in conjugates **80** and **81** increased this ratio. In particular, the selectivity (*S*) towards CCRF-CEM $\alpha_v\beta_3$ cells increased to 66.9 with *cyclo*[DKP-RGD]-Val-Ala-PTX **80** and to 15.7 with *cyclo*[DKP-RGD]-Phe-Lys-PTX **81**. In order to take into account the remarkable difference in cytotoxic activity shown by the free drug against the two cell lines, we introduced a new parameter, the Targeting Index (T.I.), which provided a direct quantification of the $\alpha_v\beta_3$-targeting potency of the developed SMDCs. These parameters were calculated by correcting the $\alpha_v\beta_3$-selectivity of compounds **80** and **81** with the intrinsic selectivity of PTX (*S* = 7.4), resulting in Targeting Indexes of 9.0 and 2.1, respectively (see Table 3). Finally, the “uncleavable” RGD-PTX conjugate **82** proved completely inactive towards both cell lines CCRF-CEM and CCRF-CEM $\alpha_v\beta_3$ even after the 144 hour-treatment *in continuo*. This

observation is consistent with the outcome of lysosome digestion experiments, and indicates that the linker cleavage is necessary for RGD-PTX conjugates to inhibit cell proliferation.

2.4. Results and Discussion

These results demonstrate that conjugate **80** and, to a lesser extent, SMDC **81** are able to target the $\alpha_v\beta_3$-expressing tumor cells. Moreover, the linker in these anticancer devices turned out to play a fundamental role for both drug activity (i.e. the linker must be "cleavable") as well as for the targeting performances *in vitro* of the whole conjugate (i.e. modifications of the dipeptide linker result in different selectivities). The evaluation of the antiproliferative activity against tumor cell lines expressing the target receptor at different levels is a well-established procedure to screen the targeting properties of both SMDCs and ADCs. This analysis is commonly carried out in parallel with the free drug, whose cytotoxic activity may vary significantly from one tested cancer cell line to the other. In some cases, the selectivity ratios shown by the free payloads are much lower than the ones displayed by the "targeted" analogues against the antigen-positive cells. This is the case of ADCs: as an explanatory example, Table 4A shows the highly selective antiproliferative activity (*S* = 4633.3) of the PSMA-targeted ADC **96** against the PSMA-expressing cancer cell line MDA PCa2b.[164] On the other hand, small ligands are commonly described as weaker binders than mAbs, and this lower binding affinity reflects in the *in vitro* selectivity displayed by the corresponding SMDCs. For instance, the selectivity values of two SMDCs targeting folate (compound **97**, *S* = 813.5)[45] and biotin receptors (compound **98**, *S* = 35.9)[55] are reported in Table 4A and 4B, respectively. Unlike in the ADC technology, the differences between the selectivity of SMDCs and the one displayed by the free payload decrease significantly. For this reason, we introduced the Targeting Index to provide a "clean" quantification of the observed integrin-targeting effect. While the *cyclo*[DKP-RGD]-Val-Ala-PTX (**80**) showed a T.I. = 9.0, the research area of integrin-targeted SMDCs lacks of a "previous best" lead compound. In a recent review, we surveyed the literature in this field, describing the evolution of this technology and, on the other hand, highlighting the *in vitro* evaluation of the antitumor properties of the SMDCs developed so far.[165] It is worth noting that some fundamental data have been reported rarely in these *in vitro* analyses, such as:

- SMDC activity against antigen-negative cells ($\alpha_v\beta_3$ −);
- Activity of the free drug against the $\alpha_v\beta_3$+/$\alpha_v\beta_3$– cellular model.

Nevertheless, Fei and coworkers reported in 2014 the synthesis and biological evaluation of a panel of linear and cyclic RGD peptides, conjugated to a membrane-disrupting cationic peptide $(Lys\text{-}Leu\text{-}Ala\text{-}Lys\text{-}Leu\text{-}Ala)_2$ peptide (KLA).[166]

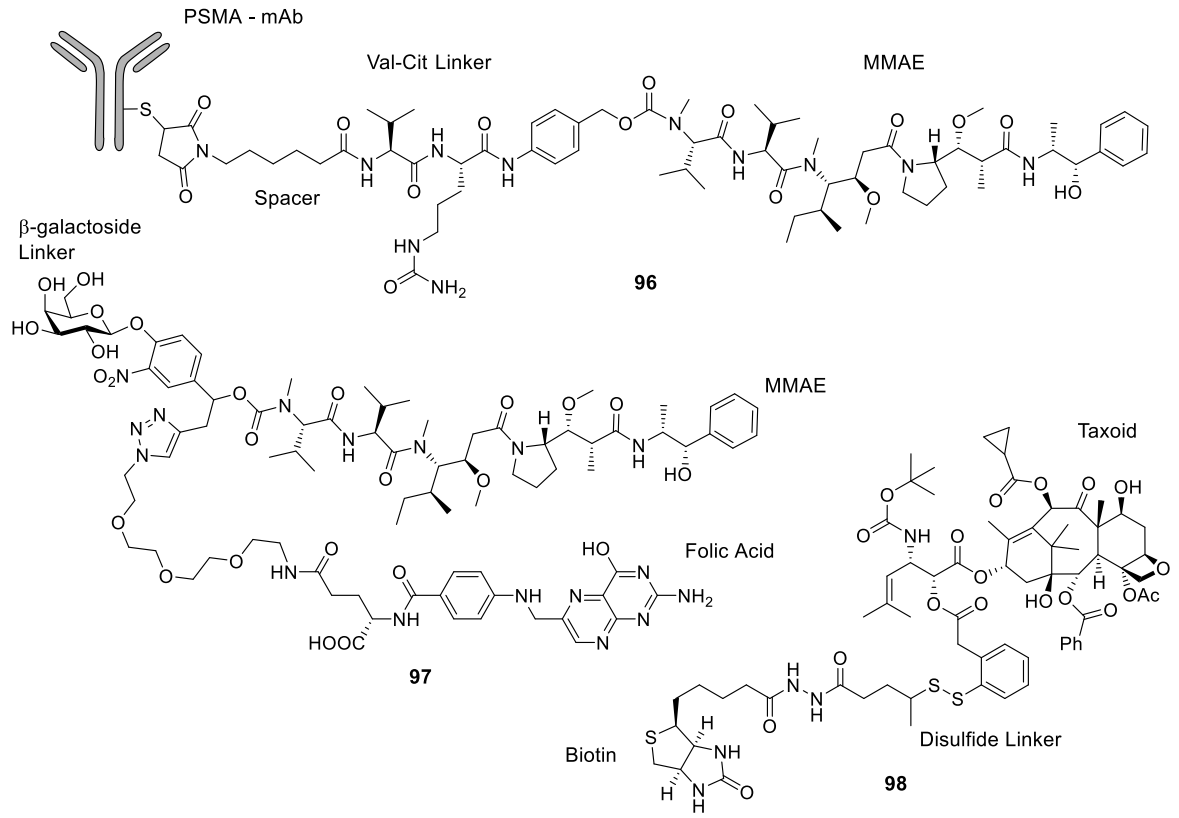

Structure	IC_{50} (nM)		S[a]	T.I.[b]
A	**PC3 (PSMA −)**	**MDA PCa2b (PSMA +)**		
Monomethyl auristatin E (MMAE, **10**)	0.970	0.363	2.7	1
mAb(PSMA)-Val-Cit-MMAE (**96**)	83.4	0.018	4633.3	1716
B	**A549 (FR −)**	**KB (FR +)**		
Monomethyl auristatin E (MMAE, **10**)	0.872	0.240	3.6	1
Folate-MMAE (**97**)	195.2	0.240	813.5	226
C	**L1210 (BR −)**	**L1210FR (BR +)**		
Taxoid	7.05	4.2	1.8	1
Biotin-Taxoid (**98**)	481	13.4	35.9	20

Table 4. Antiproliferative activity of the PSMA-targeted ADC **96** (**A**)[164], folate receptor-targeted SMDC **97** (**B**)[45] and biotin receptor-targeted SMDC **98** (**C**)[55] against cancer cell lines with different expressions of PSMA, FR and BR, respectively. [a] Selectivity (*S*): IC_{50}(receptor −)/IC_{50}(receptor +); [b] Targeting index (T.I.): selectivity/selectivity observed with free drug.

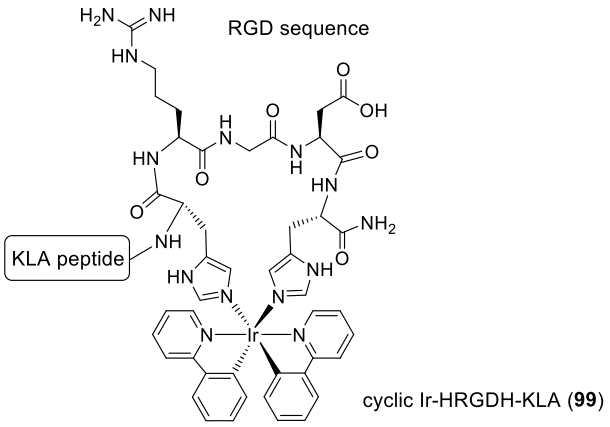

	LC_{50} (μM)			
Structure	**MCFF ($\alpha_v\beta_3$ −)**	**A549 ($\alpha_v\beta_3$ +)**	***S*[a]**	**T.I.[b]**
KLA peptide	> 250	164.8	> 1.5	1
Cyclic Ir-HRGDH-KLA (**99**)	37.7	4.5	8.4	< 5.6

Table 5. Antiproliferative activity of the integrin $\alpha_v\beta_3$-targeted cyclic Ir-HRGDH-KLA (**99**) against MCFF ($\alpha_v\beta_3$ −) and A549 ($\alpha_v\beta_3$ +) cancer cells. [a] Selectivity (*S*): LC_{50}(receptor −)/LC_{50}(receptor +); [b] Targeting index (T.I.): selectivity of **99**/selectivity observed with free KLA peptide.[166]

Although a non-classical cytotoxic agent was used, the group evaluated the cytotoxic activity of the conjugates and the free KLA peptide against MCFF ($\alpha_v\beta_3$ −) and A549 ($\alpha_v\beta_3$ +) cells. The LC_{50} values reported for the KLA peptide and for the most active conjugate in the series (compound **99**) are shown in Table 5: a T.I. < 5.6 can be calculated by taking into account the undefined activity of the free KLA peptide against MCFF cells (LC_{50} > 250 μM).

These literature survey indicates that *cyclo*[DKP-RGD]-Val-Ala-PTX **80** and the experiments performed for its biological evaluation can be considered as a valuable reference in the field of $\alpha_v\beta_3$-targeted chemotherapeutics. The possibility to improve the selectivity for $\alpha_v\beta_3$-expressing cells and the detection of the cell internalization pathways of *cyclo*[DKP-RGD]-drug conjugates represent two fundamental aspects for the validation of the *cyclo*[DKP-RGD] peptidomimetic as a drug-targeting device for cancer therapy.

Third-Generation *cyclo*[DKP-RGD]-PTX Conjugates

3.1. Introduction

The promising results shown by the *cyclo*[DKP-RGD]-Val-Ala-PTX **80** indicated the feasibility of the conjugation of an integrin-binding peptidomimetic to the Val-Ala-PTX linker-drug combination. As discussed in Paragraph 2.4, a quantification of the selectivity of RGD-based SMDCs towards $\alpha_v\beta_3$-expressing cells has been rarely reported in the literature, and the Targeting Index of 9.0 obtained with **80** is significantly lower than the data reported for other anticancer devices, targeting more traditional receptors.

A possible strategy to increase the selectivity of a SMDC is to improve the binding affinity of the ligand module for the receptor. The formation of multivalent interactions between ligand and target protein is the most common approach to increase this binding strength.[122]

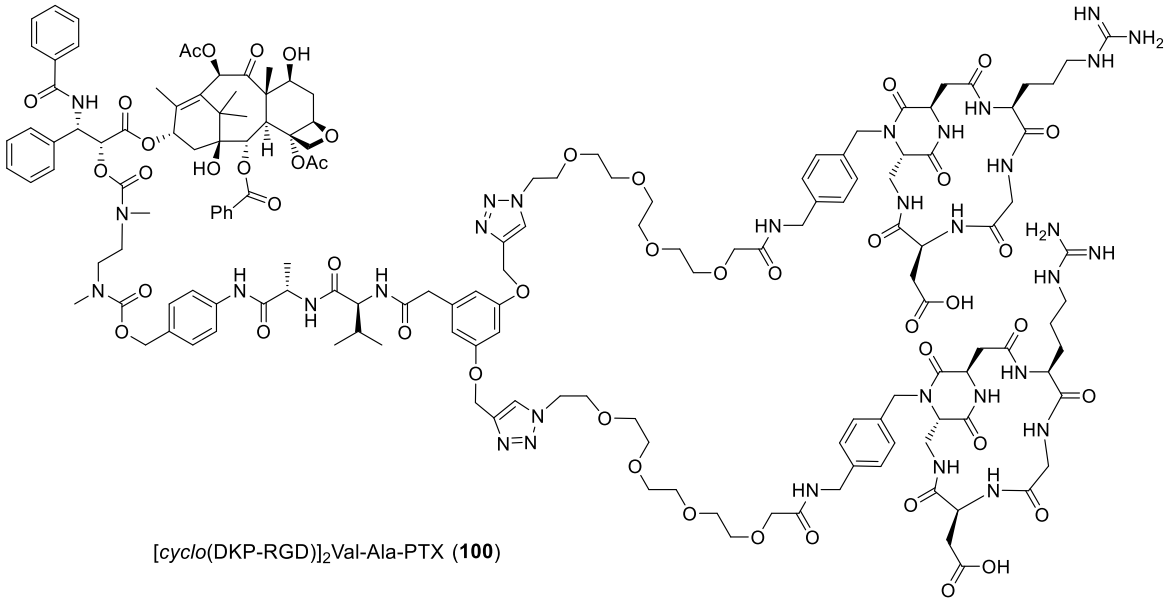

Figure 34. Molecular structures of the dimeric SMDC [*cyclo*(DKP-RGD)]$_2$Val-Ala-PTX **100**.

As discussed in Paragraph 1.5.3, a variety of radiotracers for tumor imaging have been conjugated to dimeric RGD peptides, showing increased tumor uptake and reduced side accumulation to other organs. Besides the applications for tumor imaging *in vivo*, which have

reached the clinic, the advantages of the multimeric ligand presentation have been also demonstrated *in vitro.* In particular, multimeric $\alpha_v\beta_3$-targeting systems exhibit higher binding affinity to the receptor compared to the monomeric analogues, which reflects in a higher cell adhesion and in a more efficient receptor-mediated endocytosis.[167,168] We therefore designed the dimeric [*cyclo*(DKP-RGD)]$_2$Val-Ala-PTX (compound **100** in Fig. 34), aiming at improving the selectivity towards $\alpha_v\beta_3$-expressing cells shown by the monomeric analogue **80**. In order to allow an easy and general synthetic preparation, a symmetric, alkyne-bearing aromatic scaffold was connected to the N-terminus of the Val-Ala linker. The two terminal alkyne moieties of the paclitaxel prodrug (compound **101**, Scheme 7) were used as anchoring point for the double installation of the *cyclo*[DKP-RGD] integrin ligand, through Cu-catalyzed azide-alkyne cycloaddition (CuAAC). A derivative of the RGD peptidomimetic bearing an azido-tetraethylene glycol spacer (compound **102**) was developed to be coupled to **101** in the final conjugation reaction. This flexible layout was chosen to help the SMDC to adapt to the target $\alpha_v\beta_3$ integrin.[169] Moreover, besides improving solubility in aqueous media to the SMDC, short PEG spacers are known to minimize the formation of bulky loops, that can interfere with the ligand binding to the receptor.[142]

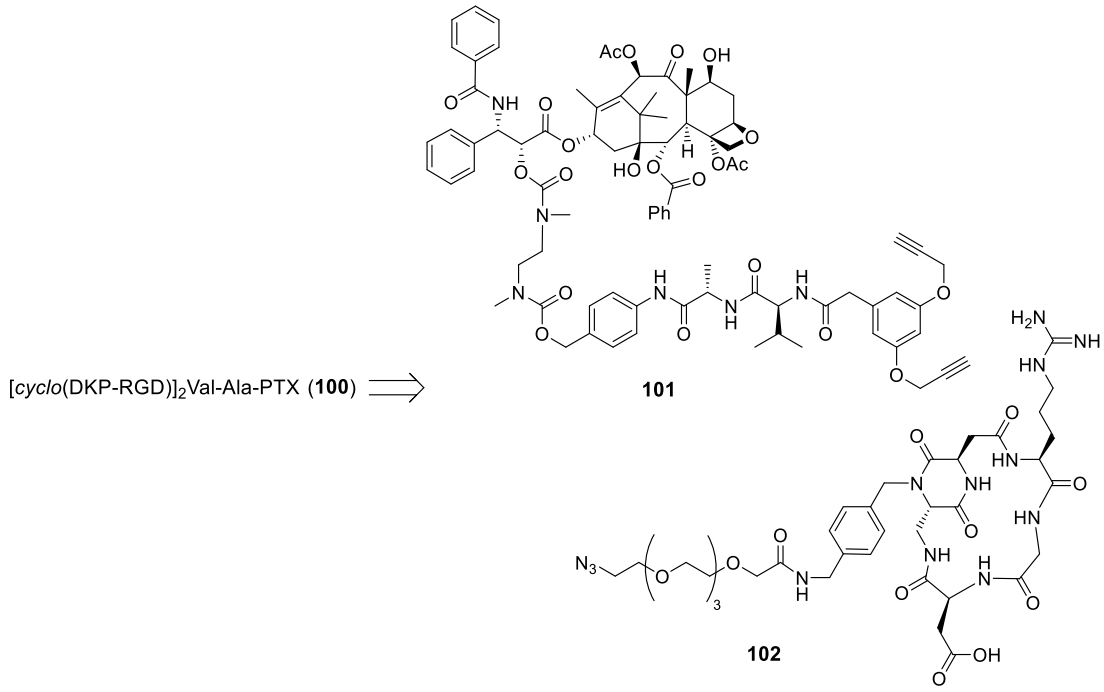

Scheme 7. Retrosynthetic analysis of SMDC **100**: fragmentation into bis-alkyne **101** and azide **102**.

3.2. Synthesis of Third-Generation cyclo[DKP-RGD]-PTX Conjugates

According to the retrosynthetic approach depicted in Scheme 7, the synthesis of fragments **101** and **102** converged to the final isolation of dimeric [*cyclo*(DKP-RGD)]$_2$Val-Ala-PTX **100**. The synthesis of paclitaxel derivative **101** is shown in Scheme 8.

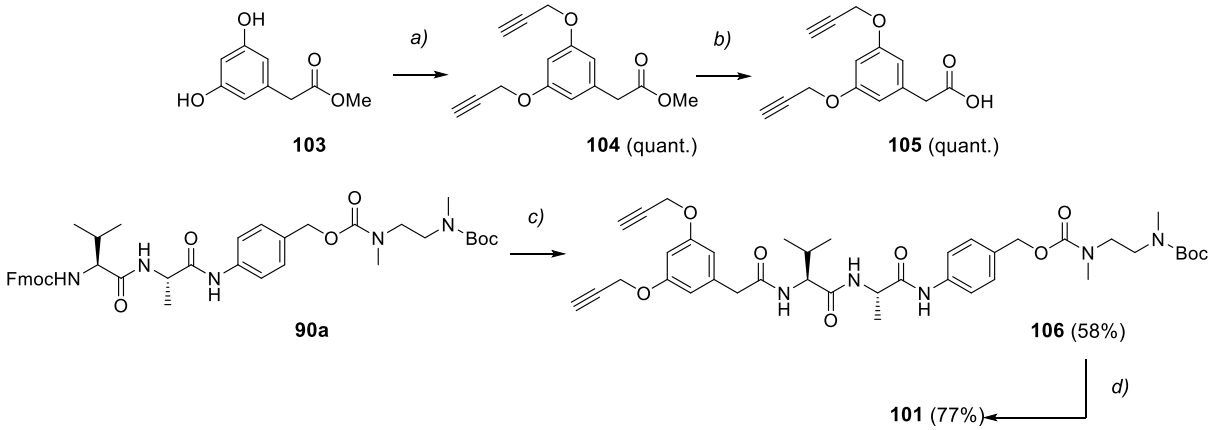

Scheme 8. Synthesis of paclitaxel derivative **101**. Reagents and conditions: *a)* propargyl bromide, K_2CO_3, acetone, RT, 72 h; *b)* LiOH·H_2O, THF/H_2O (2:1), 0 °C, 1.5 h; *c)* [1] piperidine, DMF, RT, 2 h; [2] **105**, HATU, HOAt, *i*Pr_2NEt, DMF, RT, overnight; *d)* [1] TFA/CH_2Cl_2 (1:2), 45 min; [2] 2'-(4-nitrophenoxycarbonyl)paclitaxel (**83**), *i*Pr_2NEt, DMF, 24 h.

The bis-alkyne scaffold was synthesized starting from commercially available methyl 3,5-dihydroxyphenyl acetate (**103**), which was reacted with propargyl bromide and then saponified, affording carboxylic acid **105**. The Val-Ala linker **90a**, whose synthesis is reported in Scheme 5 (pag 45), was deprotected at its N terminus and coupled to acid **105**. The resulting amide **106** was treated with trifluoroacetic acid for Boc removal and reacted with 2'-(4-nitrophenoxycarbonyl)paclitaxel (**83**) under basic conditions, affording carbamate **101**.

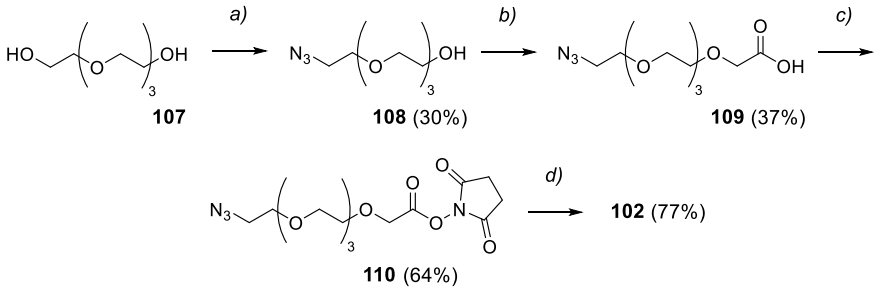

Scheme 9. Synthesis of azide **102**. Reagents and conditions: *a)* [1] Tosyl-Cl, Et_3N, THF, 0 °C to RT overnight; [2] NaN_3, EtOH, reflux, 24 h; *b)* NaH, bromoacetic acid, THF, RT 24 h; *c)* EDC·HCl, NHS, CH_2Cl_2, RT overnight; *d) cyclo*[DKP-RGD]-CH_2NH_2 (**70**), CH_3CN/PBS (1:1; pH 7.5), RT, overnight.

The synthesis of the integrin ligand functionalized with the azido-tetraethylene glycol spacer (**102**) is reported in Scheme 9. Azido-acid **109** was synthesized according to a previously reported methodology,[170] starting from commercially available tetraethylene glycol (**107**). Azido-acid **109** was transformed into the corresponding *N*-hydroxysuccinimidyl ester (**110**),

which was purified by flash chromatography. The pure electrophile **110** was then reacted with the *cyclo*[DKP-RGD]-CH_2NH_2 ligand (**70**), affording the final azide **102** in 77% yields.

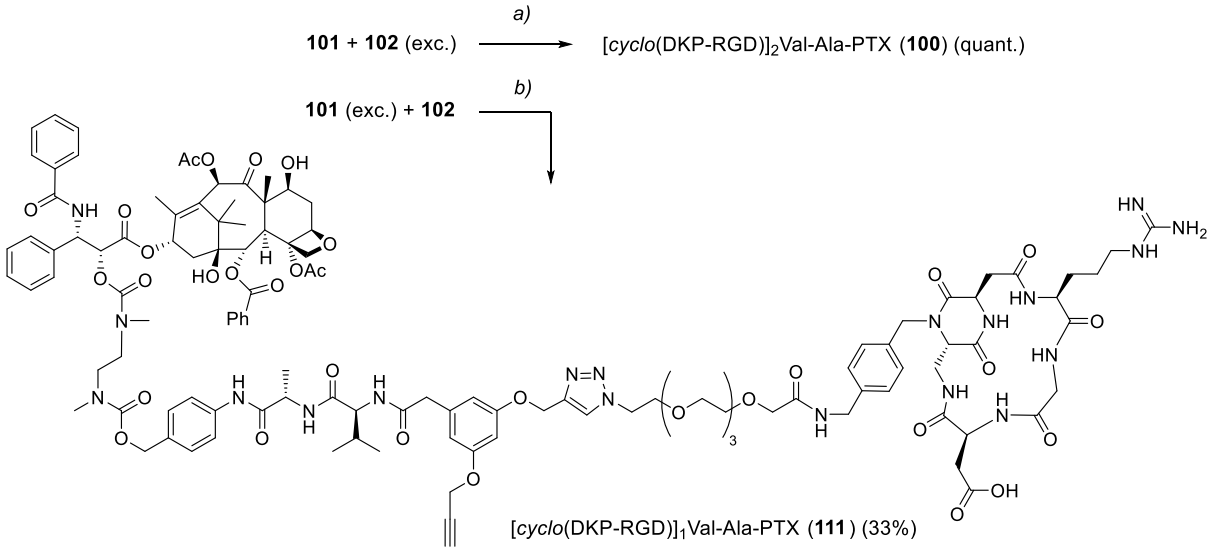

Scheme 10. Copper(I)-catalyzed azide-alkyne cycloaddition for the synthesis of dimeric SMDC [*cyclo*(DKP-RGD)]$_2$Val-Ala-PTX (**100**) and monomeric [*cyclo*(DKP-RGD)]$_1$Val-Ala-PTX (**111**). Reagents and conditions: *a)* **101** (1 eq), **102** (3 eq), $CuSO_4 \cdot 5H_2O$ (0.5 eq), sodium ascorbate (0.6 eq), DMF/H_2O (1:1) RT, overnight; b) **101** (4 eq), **102** (1 eq), $CuSO_4 \cdot 5H_2O$ (1 eq), sodium ascorbate (1.2 eq), DMF/H_2O (1:1) RT, overnight.

Two copper(I)-catalyzed azide-alkyne cycloaddition were performed by varying the relative stoichiometric amounts of bis-alkyne **101** and azide **102** (Scheme 10): the [*cyclo*(DKP-RGD)]$_2$Val-Ala-PTX (**100**) was obtained by reacting **101** with an excess of **102**, whereas the use of the latter as limiting agent led to the monomeric [*cyclo*(DKP-RGD)]$_1$Val-Ala-PTX **111**. This SMDC was prepared to compare the $\alpha_v\beta_3$-targeting properties of the dimeric [*cyclo*(DKP-RGD)]$_2$Val-Ala-PTX (**100**) over a monomeric analogue. As reported in Scheme 10, while the dimeric compound **100** was obtained quantitatively after HPLC purification, SMDC **111** was obtained in lower yields (33%, non-optimized), due to the poor solubility of bis-alkyne **101** in aqueous buffer solution.

3.3. In vitro Biological Evaluation

Analogously to previous *cyclo*[DKP-RGD]-PTX conjugates, the newly synthesized dimeric [*cyclo*(DKP-RGD)]$_2$Val-Ala-PTX **100** and monomeric [*cyclo*(DKP-RGD)]$_1$Val-Ala-PTX **111** were evaluated *in vitro* for their ability to compete with biotinylated vitronectin for the binding to the purified $\alpha_v\beta_3$ integrin. The IC_{50} values obtained are listed in Table 6. As expected, the dimeric compound **100** showed higher binding affinity than the monomeric analogues **80** and **111**. In particular, the IC_{50} obtained for dimeric SMDC **100** was identical to the one reported for the free ligand **64** (i.e. 4.0 and 4.5 nM, respectively). On the other hand, the monomeric [*cyclo*(DKP-RGD)]$_1$Val-Ala-PTX conjugate **111** showed a 10-fold decrease in binding affinity,

as compared to the reference compound *cyclo*(DKP-RGD)-Val-Ala-PTX **80** (i.e. 189 and 13.3 nM, respectively).

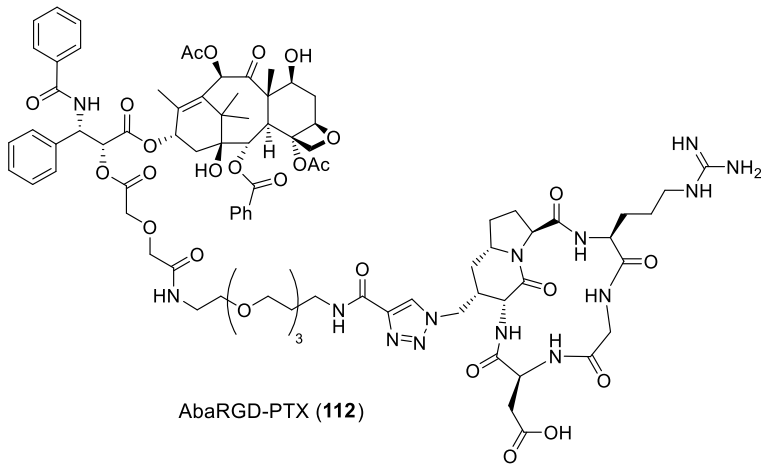

AbaRGD-PTX (**112**)

Structure	**IC_{50} (nM) $\alpha_v\beta_3$**
[*cyclo*(DKP-RGD)]$_2$Val-Ala-PTX (**100**)	4.0 ± 0.1
[*cyclo*(DKP-RGD)]$_1$Val-Ala-PTX (**111**)	189 ± 12
cyclo[DKP-RGD]-Val-Ala-PTX (**80**)[162]	13.3 ± 3.6
cyclo[DKP-RGD] (**64**)[151]	4.5 ± 1.1
AbaRGD-PTX (**112**)[136]	220.0 ± 13.2

Table 6. Inhibition of biotinylated vitronectin binding to purified integrin $\alpha_v\beta_3$. The molecular structure of the Aba-RGD-PTX conjugate **112**, developed by Manzoni and coworkers,[136] is reported above.

This unusual behavior has been recently reported for a similar compound (i.e. the AbaRGD-PTX conjugate **112**), bearing a short polyethylene glycol spacer and an ester linker.[136] Notably, a similar conjugate developed by our group (i.e. SMDC **113**, introduced in Paragraph 4.2.1), bearing a PEG spacer and a different cytotoxic payload (daunorubicin, DNR), showed low-nanomolar IC_{50} values. Therefore, the poor binding potency shown by SMDCs **111** and **112** seems ascribable to specific interactions between paclitaxel and the PEG spacer taking place in the RGD-PTX monomeric presentation, which eventually affect the SMDC binding to the receptor.

This preliminary evaluation of third-generation *cyclo*[DKP-RGD]-PTX conjugates clearly indicates that the dimeric ligand presentation in this class of SMDCs confers enhanced binding strength towards $\alpha_v\beta_3$ integrin. Importantly, SMDC **100** shows a good water solubility, which represents an important improvement of the solubility profile shown by previous *cyclo*[DKP-RGD]-PTX conjugates. Moreover, the Val-Ala linker in SMDC **100** showed the same properties described for compound **80** in Paragraph 2.3.2 (i.e. high stability under different pH conditions drug release in the presence of lysosome extract).

Cell antiproliferative assays are now in progress, aimed at evaluating the effects of the dimeric ligand presentation on the selective anticancer activity of **100** against $\alpha_v\beta_3$-expressing tumor cell lines.

Theranostic *cyclo*[DKP-RGD]-Drug Conjugates

4.1. Introduction

The focus of our group on $\alpha_v\beta_3$-targeted paclitaxel prodrugs has consisted in the development of *cyclo*[DKP-RGD]-PTX conjugates, showing interesting results in terms of synthetic accessibility, affinity for $\alpha_v\beta_3$ integrin, stability and solubility properties. However, the biological evaluation of the *cyclo*[DKP-RGD]-Val-Ala-PTX (**80**) highlighted some important weaknesses of this compound. As discussed in Chapter 3, the relatively low Targeting Index (T.I. = 9.0, Table 3 on page 49) observed in comparative antiproliferative assays against $\alpha_v\beta_3$+/$\alpha_v\beta_3$− cells, prompted the development of the dimeric [*cyclo*(DKP-RGD)]$_2$Val-Ala-PTX (**100**). Although the cell-antiproliferative properties of SMDC **100** are still under investigation, the integrin-mediated endocytosis of these classes of RGD-PTX conjugates can only be inferred from the particular experimental conditions adopted for this assay (i.e. cell washout after incubation with the SMDCs for 6 h, see page 49). Indeed, further evidences of the internalization of these compounds into cancer cells are still missing. Moreover, the analysis of protease activity in the presence of cathepsin inhibitors (Fig. 32 on page 47) showed that the Val-Ala linker is recognized and cleaved by a variety of proteases. The partial expression of these proteolytic enzymes in the extracellular environment could explain the significant cytotoxic activity of compound **80** against CCRF-CEM ($\alpha_v\beta_3$−) cells, which resulted in a decrease of the Targeting Index.

For these reasons, the design of new *cyclo*[DKP-RGD]-drug conjugates was aimed at both the specific drug release in the intracellular environment and the cellular localization of the conjugate. While the intracellular release of the payload results from the installation of a proper linker, the SMDC localization in a specific cellular compartment (e.g. membrane, lysosomes, endoplasmic reticulum, etc.) is made possible by the installation of a fluorescent probe, which is analyzed by fluorescence microscopy. Installation of a variety of imaging dyes onto drugs or therapeutic delivery vehicles (i.e. the so-called theranostic devices), aiming at merging therapeutic and diagnostic applications in a single administration, has been gaining popularity among researchers.[171] In addition to the use of payloads featuring

florescent properties (i.e. anthracyclines), we also investigated this approach through the installation of specific probes in the SMDC, according to other theranostic RGD-drug conjugates already reported in the literature.

4.2. Cyclo[DKP-RGD]-Daunorubicin Conjugate

4.2.1. Synthesis of the cyclo[DKP-RGD]-Val-Cit-DNR Conjugate

The *cyclo*[DKP-RGD] peptidomimetic was linked to the DNA-intercalating agent daunorubicin (DNR), leading to SMDC **113** (Fig. 35). The fluorescence properties of this anthracycline drug were exploited to provide an in-depth analysis of the conjugate's mechanism of action. Moreover, in order to minimize the drug release in the extracellular environment, the valine-citrulline (Val-Cit) dipeptide was selected as linker. This well-known sequence is a specific substrate of cathepsin B, a cysteine protease expressed in the lysosomes.[172]

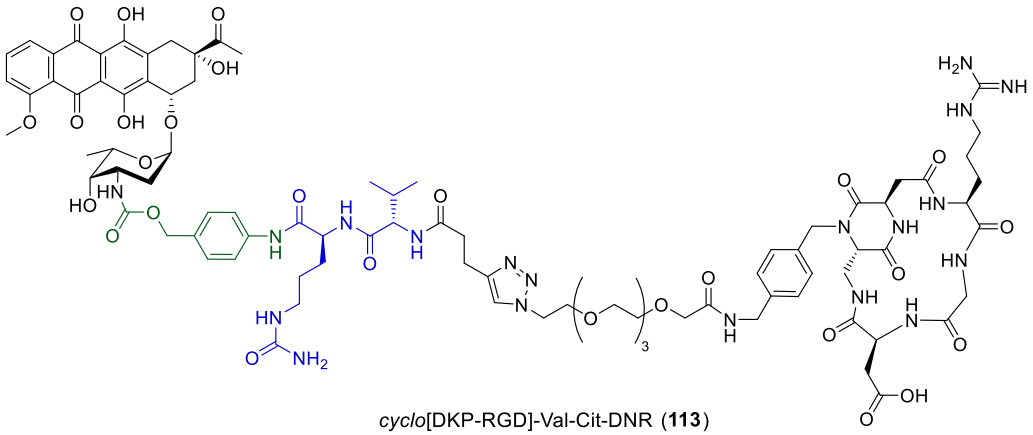

cyclo[DKP-RGD]-Val-Cit-DNR (**113**)

Figure 35. Molecular structures of the SMDC *cyclo*[DKP-RGD]-Val-Cit-DNR **113**.

The daunosamine moiety of the anthracycline drug was used as anchoring point for the linker: this choice resulted in the formation of a stable carbamate bond between the drug and a *p*-aminobenzyl alcohol self-immolative spacer (green moiety in Fig. 35). Unlike the PTX conjugates described in the previous Chapters, this layout allows the release of DNR upon a single and fast 1,6-elimination step (the detailed mechanism is depicted in Scheme 1 on Page 15). To overcome the low water solubility of the Val-Cit dipeptide, the *cyclo*[DKP-RGD] ligand was connected to the linker's N terminus through a tetraethylene glycol spacer. Similarly to the dimeric RGD-PTX conjugate described in Chapter 3, the formation of a triazole ring between the linker-drug module and the ligand was chosen as the last conjugation step: in general, this versatile methodology does not require specific protecting groups at the amino acid side chains and it is adaptable to several linker-drug combinations. The synthesis of the *cyclo*[DKP-RGD]-Val-Cit-DNR **113** is shown in Scheme 11. Similarly to what described in Chapter 2 for SMDCs **80** and **81**, the Val-Cit dipeptide was coupled to *p*-

aminobenzyl alcohol and then activated as 4-nitrophenyl carbonate (Scheme 11, compound **117**). Daunorubicin hydrochloride was attached to the linker by reaction of its daunosamine moiety with electrophile **117**, leading to carbamate **118**. A fast deprotection of the valine residue followed by coupling with 4-pentynoic acid afforded the terminal alkyne-functionalized compound **119**. The final compound was obtained after copper-catalyzed azide-alkyne cycloaddition (CuAAC) between alkyne **119** and *cyclo*[DKP-RGD]-azide **102**, whose synthesis is described in Chapter 3 (Scheme 9 on page 55). The final SMDC **113** was then purified by semi-preparative HPLC and lyophilized before being subjected to biological assays.

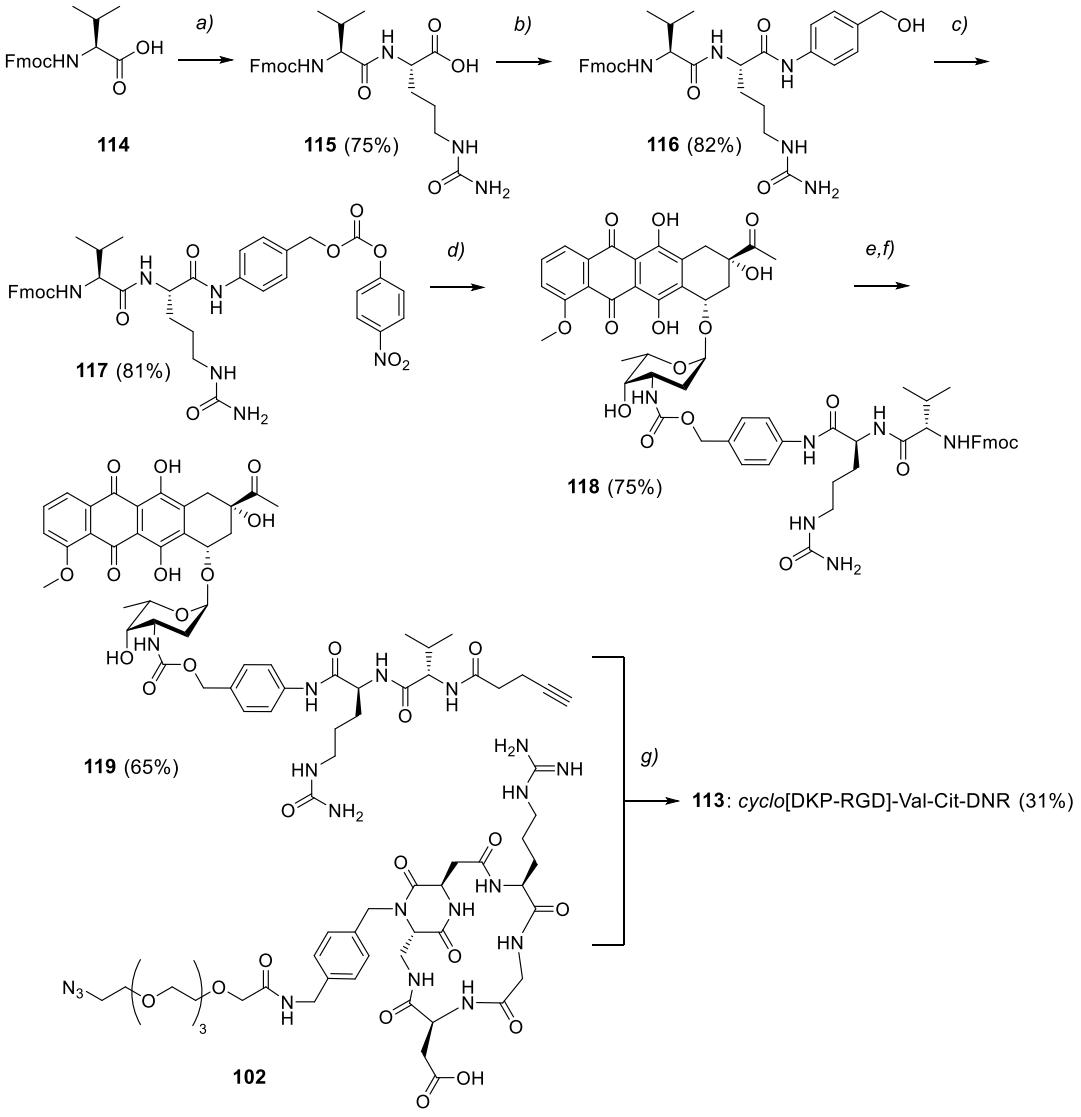

Scheme 11. Synthesis of RGD-DNR conjugate **113**. Reagents and conditions: *a)* [1] DCC, NHS, THF, overnight; [2] *L*-Citrulline, $NaHCO_3$, H_2O/DME/THF 2:2:1, 24 h; *b)* 4-aminobenzyl alcohol, EEDQ, CH_2Cl_2/MeOH 2:1, overnight; *c)* Bis(4-nitrophenyl) carbonate, *i*Pr_2NEt, DMF, 0 °C, 1 h; *d)* Daunorubicin hydrochloride, *i*Pr_2NEt, DMF overnight; *e)* 20% piperidine in DMF, 0° C, 3'; *f)* 4-pentynoic acid, HATU, HOAt, *i*Pr_2NEt, DMF, 0 °C to RT overnight; *g)* $CuSO_4 \cdot 5H_2O$, sodium ascorbate, H_2O/*t*BuOH/DMF, overnight.

4.2.2. In vitro Biological Evaluation of cyclo[DKP-RGD]-Val-Cit-DNR Conjugate

Analogously to all the SMDCs described so far, the newly synthesized *cyclo*[DKP-RGD]-Val-Cit-DNR **113** was evaluated with biotinylated vitronectin in competitive assays for the binding to the purified $\alpha_v\beta_3$ and $\alpha_v\beta_5$ integrins. The IC_{50} values obtained are shown in Table 7. The micromolar IC_{50} value relative the $\alpha_v\beta_5$ receptor further confirms the low affinity of *cyclo*[DKP-RGD] conjugates for this specific integrin. Remarkably, the high observed affinity towards the $\alpha_v\beta_3$ receptor (IC_{50} = 6.9 nM), demonstrates that the use of a tetraethylene glycol spacer in the presence of the daunorubicin payload does not impair the binding to the integrin receptor, unlike what observed with paclitaxel conjugates **111** and **112** featuring this kind of spacer (see Table 6 in Paragraph 3.3).

	IC_{50} (nM)[a]	
Structure	**$\alpha_v\beta_3$**	**$\alpha_v\beta_5$**
cyclo[DKP-RGD]-Val-Cit-DNR (**113**)	6.9 ± 0.7	1270 ± 70
cyclo[DKP-RGD]-Val-Ala-PTX (**80**)[162]	13.3 ± 3.6	924 ± 290
cyclo[DKP-RGD] (**64**)[151]	4.5 ± 1.1	149 ± 25

Table 7. Inhibition of biotinylated vitronectin binding to isolated $\alpha_v\beta_3$ and $\alpha_v\beta_5$ receptors.

Dissolution of SMDC **113** in neutral (pH = 7.4) and acidic (pH = 5.5) buffers and subsequent HPLC-MS analysis after 4 h exposure revealed the high stability of the compound at the tested pH values, as demonstrated with the *cyclo*[DKP-RGD]-PTX family.

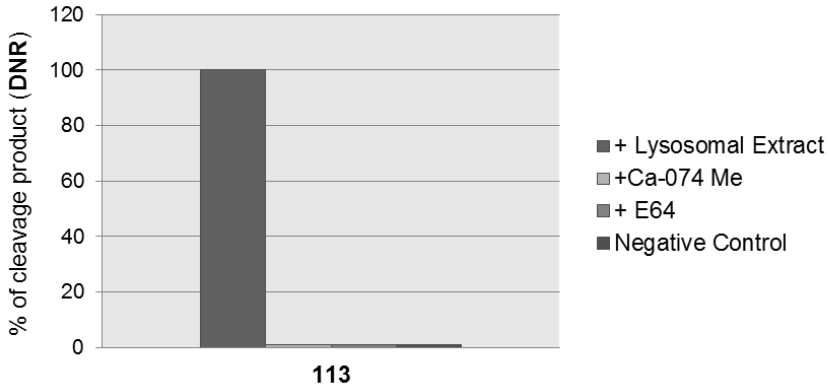

Figure 36. Analysis of lysosomal extract digestion of *cyclo*[DKP-RGD]-Val-Cit-DNR conjugate **113** in the presence of cathepsin B specific inhibitor (CA-074-Me), cysteine proteases inhibitor (E-64) and inactivated lysosomal extract (negative control). Signal detected for *m/z* 528.1 (attributed to free daunorubicin) expressed in percentage relative to that obtained with lysosomal extract (set to 100%).

Lysosomal digestion of the *cyclo*[DKP-RGD]-Val-Cit-DNR conjugate confirmed the high enzyme specificity of the Val-Cit linker. In particular, the release of daunorubicin from the conjugate was completely abolished by both cathepsin B inhibitor CA-074-Me and broader-

scope cysteine proteases inhibitor E-64 (see Fig. 36). Unlike what observed with the Val-Ala and Phe-Lys linkers (Fig. 32 on page 47), this result indicates that the cleavage of the Val-Cit sequence is mainly due to the enzymatic activity of the cysteine protease cathepsin B.

4.2.3. Cell Antiproliferative Assays and Fluorescence Microscopy Analysis

The *cyclo*[DKP-RGD]-Val-Cit-DNR conjugate **113** was tested *in vitro* for its ability to inhibit the proliferation of human leukemia cell lines CCRF-CEM $\alpha_v\beta_3$ ($\alpha_v\beta_3$ +) and CCRF-CEM ($\alpha_v\beta_3$ −), in order to evaluate the impact of the cathepsin B-specific linker on the selectivity towards $\alpha_v\beta_3$ integrin. As described for compounds **80**-**82** in Chapter 2, these antiproliferative assays were carried out under two experimental conditions (i.e. cells incubation with **113** for 144 hours *in continuo* and incubation for 6 hours, followed by cell washout and cell incubation in fresh medium for 138 hours).

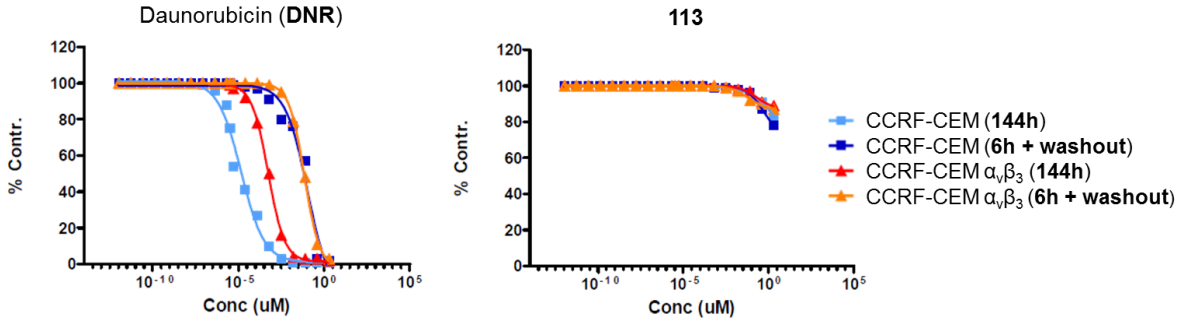

Figure 37. Dose-response curves corresponding to antiproliferative activities of free DNR and SMDC **113** against CCRF-CEM and CCRF-CEM $\alpha_v\beta_3$ under two experimental conditions: 144 h *in continuo* and 6 h incubation + cell washout and cell incubation for 138 h with fresh medium.

As shown by dose-response curves in Figure 37, the free daunorubicin was found to be significantly more efficient against CCRF-CEM ($\alpha_v\beta_3$ −) over the 144 hour-period (IC_{50} = 0.015 nM and 0.55 nM against $\alpha_v\beta_3$– and $\alpha_v\beta_3$+, respectively), whereas it showed comparable activity under the 6 hours + washout conditions (IC_{50} = 108.7 nM and 70.8 nM against $\alpha_v\beta_3$– and $\alpha_v\beta_3$+, respectively). On the other hand, SMDC **113** did not show any cytotoxic activity against the two cell lines (IC_{50} > 2000 nM) under both experimental conditions. In order to investigate this result, the interactions of compound **113** with CCRF-CEM $\alpha_v\beta_3$ and CCRF-CEM cells were evaluated by fluorescence microscopy analysis (Fig. 38). Daunorubicin incubation with the two cell lines over a 24-hour period resulted in a strong intracellular fluorescence. On the other hand, cancer cells incubation with **113** followed by cell washout did not reveal the presence of the SMDC in the intracellular environment, nor on the cell surface. This result indicated not only that the SMDC was not internalized by the cancer cells, but also that **113** was not able to significantly adhere to the cell membrane.

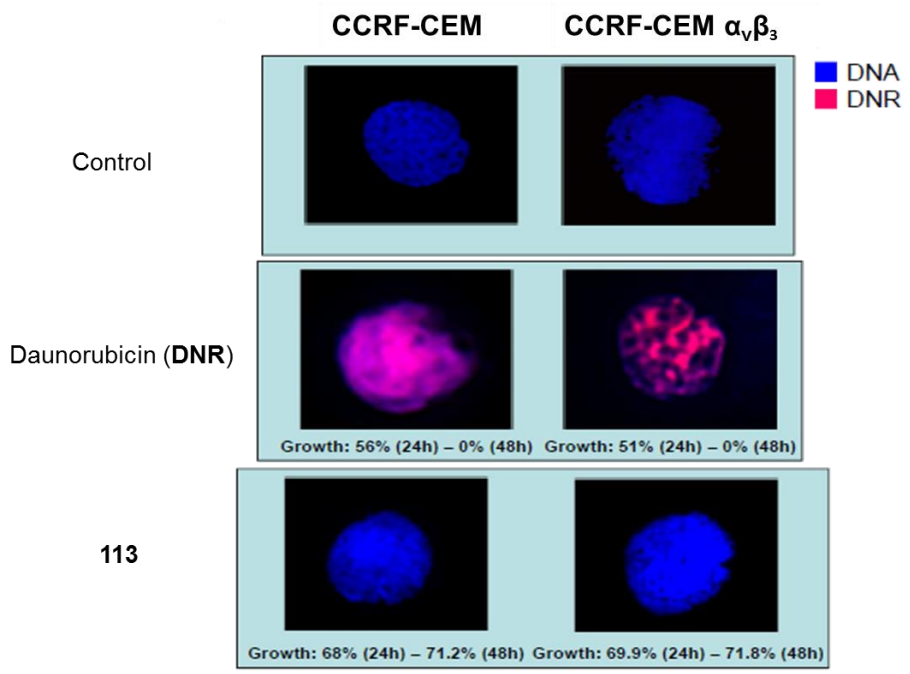

Figure 38. Fluorescence microscopy 100X analysis of 5 μM solutions of daunorubicin and *cyclo*[DKP-RGD]-Val-Cit-DNR conjugate **113**, over 24 h treatment and 2 medium replacements.

Taken together, these data indicated that although compound **113** is able to inhibit the vitronectin binding to the purified $\alpha_v\beta_3$ receptor at low nanomolar concentrations, it does not efficiently bind to the cell-expressed integrin, and the lack of receptor-mediated internalization prevents the cleavage of the Val-Cit linker by means of the intracellular protease cathepsin B. For these reasons, whereas the lack of cytotoxic activity was in agreement with the absence of the SMDC in the intracellular milieu, the competitive binding assay against the purified integrin receptor did not give the whole picture of the compound's behaviors in the presence of integrin-expressing cells.

4.3. Cyclo[DKP-RGD]-Camptotecin Conjugates

4.3.1. Theranostic RGD-CPT Conjugates: A Case Study

The *cyclo*[DKP-RGD]-Val-Cit-DNR conjugate **113** demonstrated that the cellular internalization of RGD-drug conjugates through receptor-mediated endocytosis should not be assumed as a generally-occurring mechanism. However, as discussed in Paragraph 1.5.3, a variety of analyses have been carried out in this field to demonstrate the endocytic pathways of different compounds of this class. The synthesis and biological evaluation of one of these previously reported theranostic compounds was devised, in order to evaluate the discrepancy between our *cyclo*[DKP-RGD]-drug conjugates and the available literature data. In particular, we focused on a camptothecin prodrug (compound **120**, Scheme 12A) developed by Kim and coworkers, featuring a disulfide trigger (blue moiety in Scheme 12)

and a fluorescent naphtalimide dye (red structure).[144] Prodrug **120** treatment with glutathione (GSH) was found to result in CPT release and in a strong, red-shifted fluorescence signal of the naphthalimide moiety (i.e. the emission band at 473 nm of carbamate **120** shifts to 535 nm in amine **125**, as described in Scheme 12B).

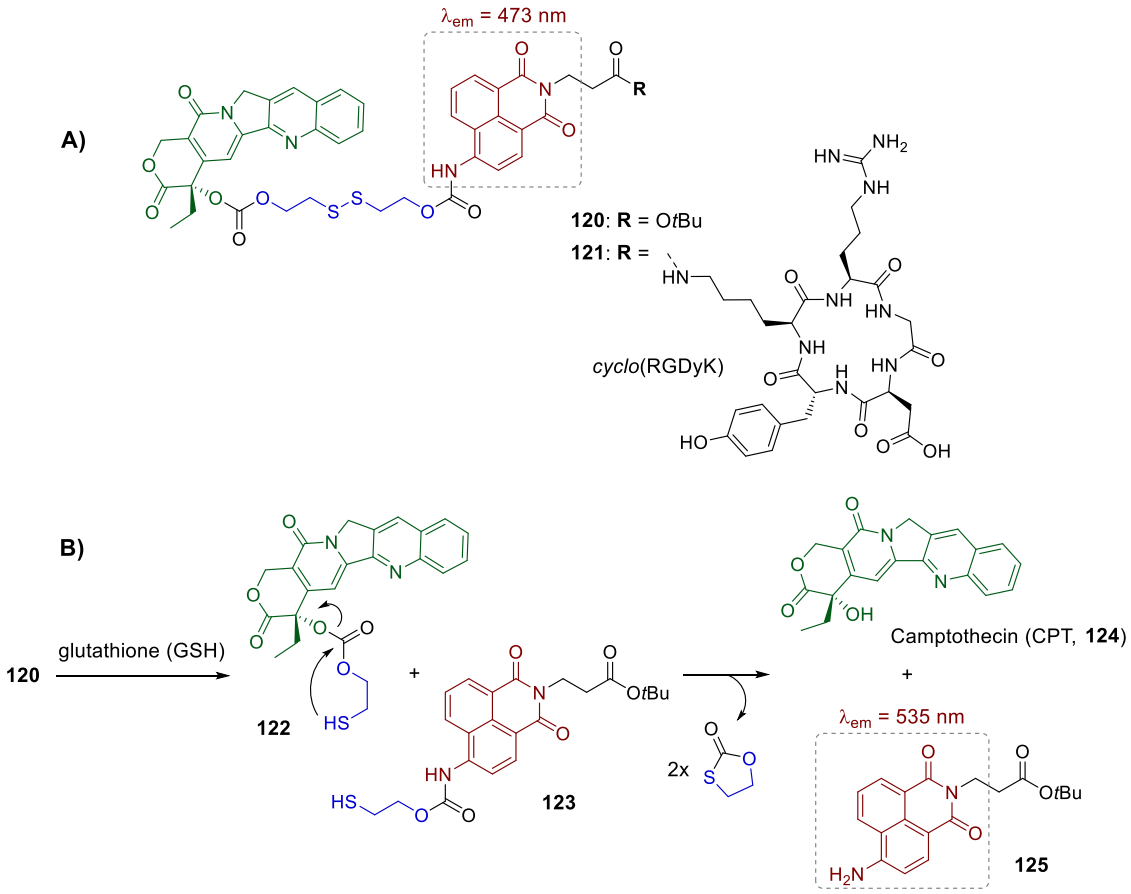

Scheme 12. A) Molecular structures of the fluorescent camptothecin prodrug bearing a disulfide linker (**120**) and the analogue integrin-targeted SMDC **121**; **B**) Mechanism of drug release from prodrug **120** and correlated fluorescence emission variation upon treatment with glutathione.[144]

After the assessment of the outcomes of this reductive cleavage, prodrug **120** was linked to the integrin ligand *cyclo*(RGDyK), resulting in the SMDC **121** (Scheme 12). The Authors designed this compound to provide a real-time monitoring of the SMDC internalization and intracellular drug release. Indeed, as discussed in Paragraph 1.4.1, disulfide linkers have been extensively used to exploit the high expression of antioxidants in the intracellular environment. The change in fluorescent emission of the naphtalimide moiety in SMDC **121** was thus correlated to the amount of CPT released after disulfide bond cleavage. A variety of suitable *in vitro* control experiments were performed, confirming the hypothesized biological activity of the synthesized compound. In particular, the Authors tested SMDC **121** for its ability to penetrate into two cancer cell lines with different $\alpha_v\beta_3$ expression: U87 (human glioblastoma, $\alpha_v\beta_3$+) and C6 (rat glioma, $\alpha_v\beta_3$−). This compound was found to efficiently

recognize $\alpha_v\beta_3$-expressing cell lines: a strong increase in the fluorescence intensity at 535 nm (ascribable to the cleaved linker and thus to the CPT released) was observed in the case of the U87 cells, whereas in the case of the C6 cells only a weak fluorescence signal was revealed (see Figure 39A).

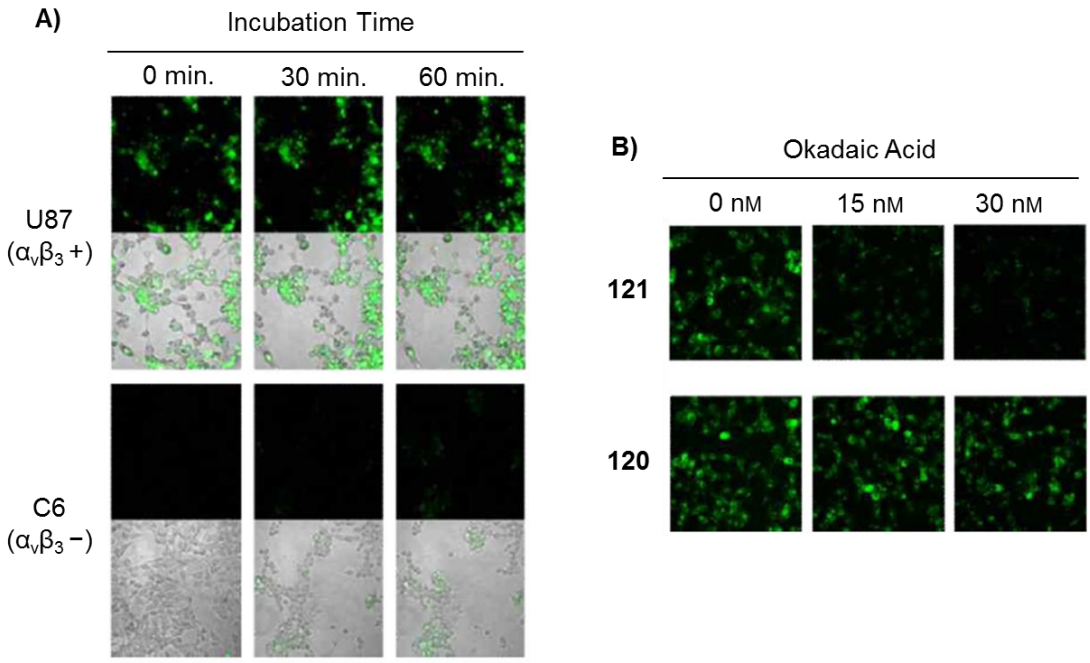

Figure 39. A) Confocal microscopy images of U87 and C6 cancer cells, incubated with SMDC **121**; **B**) Confocal microscopy images of U87 cells, incubated with SMDC **121** and prodrug **120**, in the presence of different concentrations of endocytosis inhibitor okadaic acid.

To provide further evidence for the endocytic process in U87 cells, the cellular uptake of compound **121** was found to be inhibited by the presence of an endocytosis inhibitor, such as okadaic acid. Moreover, the cellular uptake of prodrug **120** resulted not dependent on okadaic acid, indicating different mechanisms of cell penetration displayed by the two compounds. The different biological activities of compounds **120** and **121** were further analyzed by co-localization studies and cell viability assays against U87 cells: the presence or absence of the RGD ligand was found to result in a different intracellular transition of the compound (i.e. **120** was localized in the mitochondria, whereas SMDC **121** showed a transition through the endoplasmic reticulum) as well as in a different dose-response profile in cell viability. Overall, these sets of control experiments demonstrated that RGD-CPT conjugate **121** selectively penetrated into $\alpha_v\beta_3$-expressing tumor cells through integrin-mediated endocytosis. This internalization was followed by cleavage of the disulfide linker in the endoplasmic reticulum upon exposure to intracellular antioxidants, resulting in a fluorescence on-off signal response. However, although the recognition of $\alpha_v\beta_3$-expressing cells was extensively investigated through fluorescence analyses, the antiproliferative activity of compound **121** against the two cell lines ($\alpha_v\beta_3$+/$\alpha_v\beta_3$−) was not evaluated.

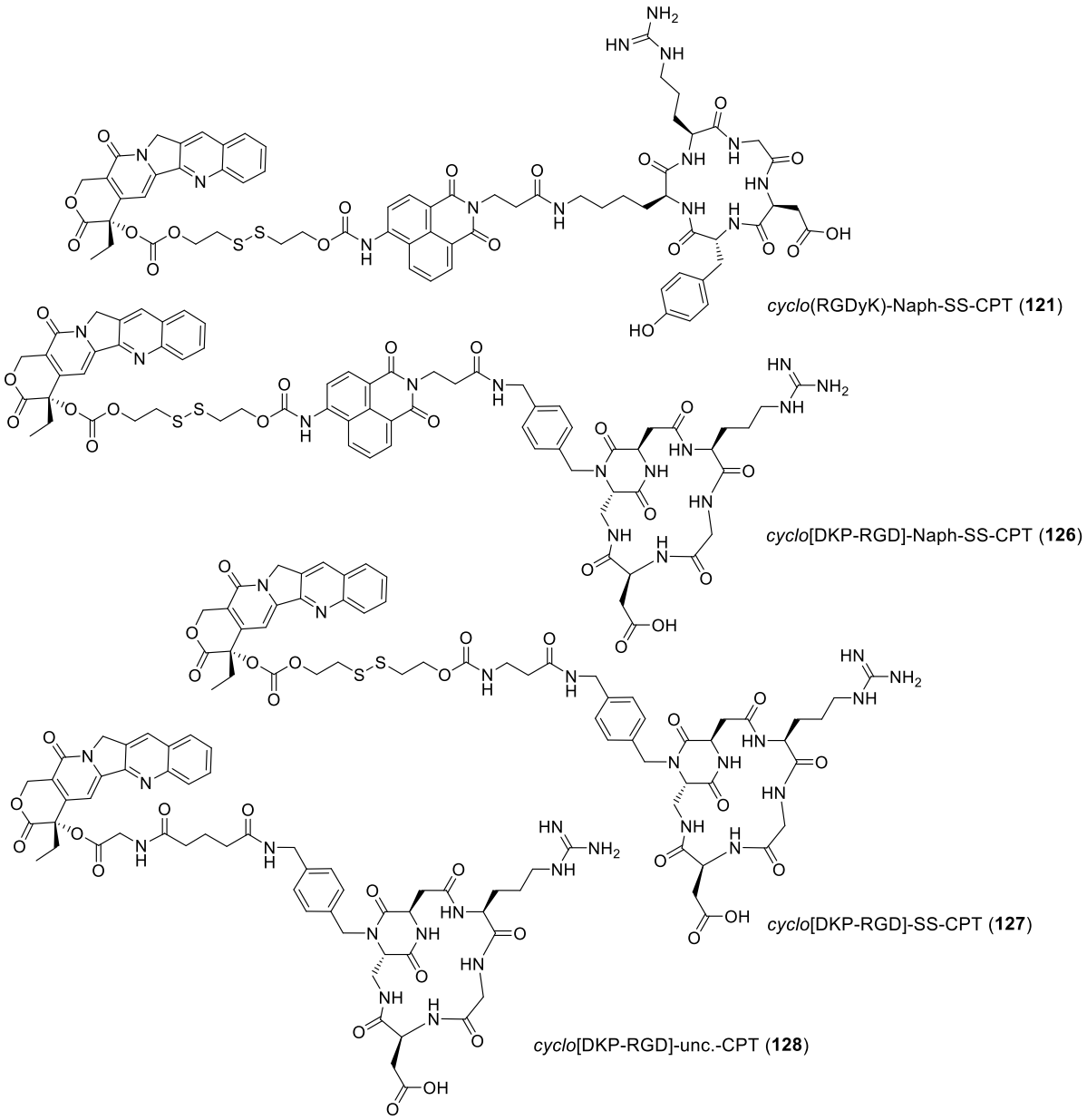

Figure 40. Molecular structures of the four synthesized SMDCs: the *cyclo*(RGDyK)-Naph-SS-CPT **121**, developed by Kim and coworkers,[144] the analogue *cyclo*[DKP-RGD]-Naph-SS-CPT **126**, the naphtalimide-free *cyclo*[DKP-RGD]-SS-CPT **127** and the "uncleavable" *cyclo*[DKP-RGD]-unc.-CPT **128**.

As discussed in the previous chapters, the quantification of the cell-dependent cytotoxic activity of SMDCs was indicated by our group as one of the key requirements for the calculation of the Targeting Index. Therefore, in addition to reference compound **121**, we synthesized new *cyclo*[DKP-RGD]-CPT conjugates, in order to reproduce the biological activity reported by Kim and coworkers as well as to investigate the application of the disulfide linker-camptothecin modules to our integrin ligand.

4.3.2. Synthesis of cyclo[DKP-RGD]-CPT Conjugates

This project consisted in the synthesis of four RGD-CPT conjugates, shown in Fig. 40. Besides the reference compound **121** and the analogue *cyclo*[DKP-RGD]-Naph-SS-CPT (compound **126**), which differed from the first for the integrin ligand, two new naphtalimide-free conjugates were prepared. Compound **127** was endowed with the same disulfide linker of the previous two SMDCs, resulting in a "traditional" small molecule-drug conjugate. On the other hand, a fourth compound (SMDC **128**), in which the tertiary alcohol is linked to the RGD ligand through a stable ester bond, was synthesized as an "uncleavable" compound. This SMDC was designed to be less prone to either enzymatic or reductive cleavage, even though undesired hydrolysis of the tertiary ester should not be excluded. SMDCs **121**, **126**-**128** have been thus synthesized as a comprehensive panel of compounds, in order to perform a SAR analysis of the targeting features of RGD-CPT conjugates.

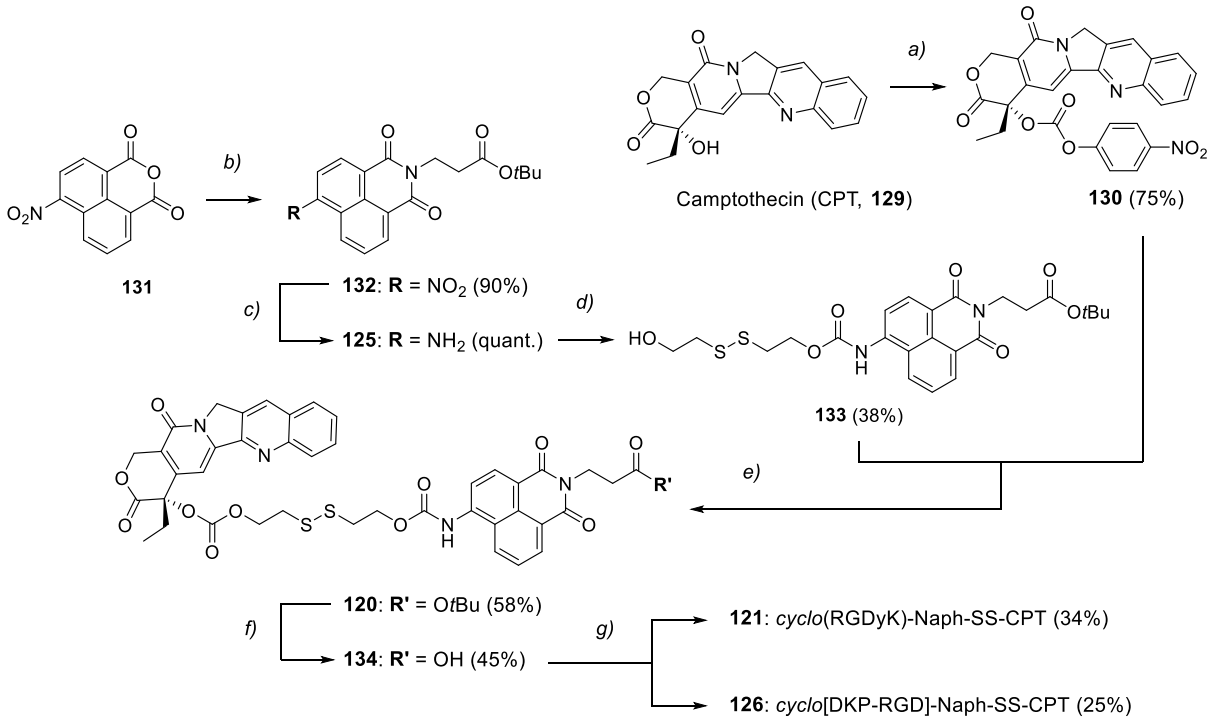

Scheme 13. Synthesis of RGD-CPT conjugates **121** and **126**. Reagent and conditions: *a) p*-nitrophenyl chloroformate, DMAP, CH_2Cl_2, 0 °C, 4h; *b)* β-Alanine *tert*-butyl ester hydrochloride, Et_3N, EtOH reflux, 3h; *c)* $SnCl_2$, EtOH, RT, 1h; *d)* [1] triphosgene, iPr_2NEt, toluene, RT, 2h; [2] 2,2'-dithiodiethanol, THF/CH_2Cl_2 1:1, RT, overnight; *e)* DMAP, CH_2Cl_2, RT, overnight; *f)* TFA/CH_2Cl_2 (1:2), RT, 45 min; *g)* [1] DIC, NHS, DMF, overnight; [2] *cyclo*(RGDyK), CH_3CN/PBS/DMF (1:1:0.5; pH 7.5), overnight (**121**); *cyclo*[DKP-RGD]-CH_2NH_2 (**70**), CH_3CN/PBS/DMF (1:1:0.5; pH 7.5), overnight (**126**).

The two compounds were obtained through the synthetic strategy shown in Scheme 13. The original synthetic route of SMDC **121** was optimized, and all the intermediates were fully characterized by NMR spectroscopy. While the free camptothecin **129** was transformed into the corresponding 4-nitrophenyl carbonate (compound **130**) according to a previously reported procedure,[173] commercially available 4-nitro-1,8-naphthalic anhydride **131** was

reacted with β-alanine *tert*-butyl ester under basic conditions, affording naphtalimide **132**. At this stage, Kim and coworkers reported the reduction of the nitro group by catalytic hydrogenation:[144,174] all our attempts to follow the reported methodology led to a significant formation of byproducts. Reduction with iron powder was also unsuccessful. Finally, the use of an excess of tin(II) chloride afforded clean amine **125** quantitatively, after filtration over silica gel. The amine was transformed into carbamate **133** by treatment with triphosgene and subsequent reaction with an excess of 2,2'-dithiodiethanol. The reaction with CPT derivative **130** yielded prodrug **120**. The *tert*-butyl ester protecting group was then removed and the free carboxylic acid was finally coupled with both *cyclo*(RGDyK) and *cyclo*[DKP-RGD]-CH_2NH_2 (**70**), affording SMDCs **121** and **126**, respectively. We ascribed the low yields of these last conjugation steps (non-optimized) to the poor solubility of carboxylic acid **134** in the aqueous solvent mixture, which was slightly improved by the addition of DMF.

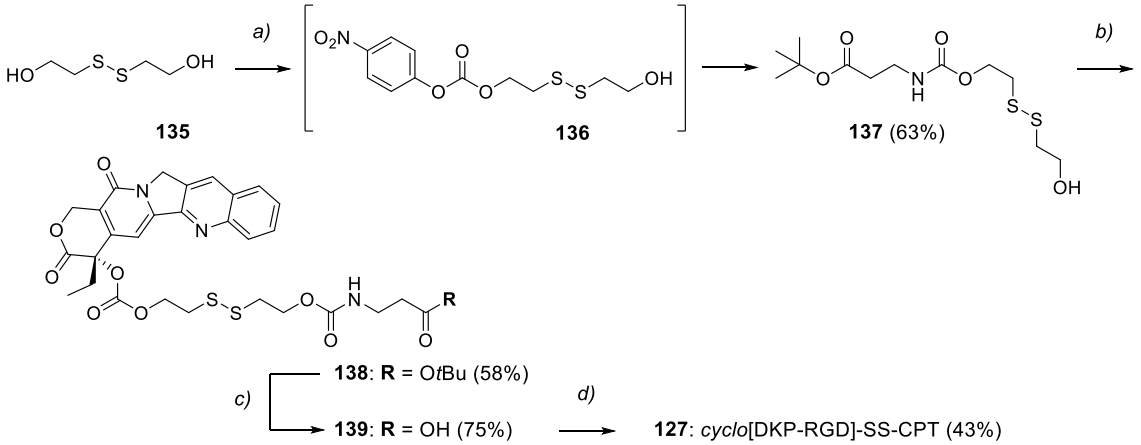

Scheme 14. Synthesis of *cyclo*[DKP-RGD]-SS-CPT conjugate **127**. Reagent and conditions: *a)* [1] *p*-nitrophenyl chloroformate, *i*Pr_2NEt, CH_2Cl_2, RT, overnight; [2] β-alanine *tert*-butyl ester hydrochloride, *i*Pr_2NEt, CH_2Cl_2, RT, overnight; *b)* **130**, DMAP, CH_2Cl_2, RT, overnight; *c)* TFA/CH_2Cl_2 (1:2), RT, 45 min; *d)* [1] DIC, NHS, DMF, overnight; [2] *cyclo*[DKP-RGD]-CH_2NH_2 (**70**), DMF/PBS (1:1; pH 7.5), overnight.

The synthesis of *cyclo*[DKP-RGD]-SS-CPT conjugate (**127**) is reported in Scheme 14. 2,2'-dithiodiethanol (compound **135**) was reacted with a sub-stoichiometric amount of *p*-nitrophenyl chloroformate. β-Alanine *tert*-butyl ester was subsequently added to the reaction mixture, avoiding the isolation of carbonate **136** and yielding carbamate **137**. The latter was reacted with (4-nitrophenoxycarbonyl)-camptothecin (compound **130**), affording carbonate **138** after flash chromatography. The *tert*-butyl ester protecting group was then removed and the free carboxylic acid **139** was coupled to the *cyclo*[DKP-RGD]-CH_2NH_2 peptidomimetic (**70**). Finally, the synthesis of the RGD-CPT conjugate bearing the "uncleavable" linker (**128**) is reported in Scheme 15. The hemiglutarate derivative of camptothecin **140** was prepared according to a previously reported methodology, consisting in the elongation of a CPT-glycinate with glutaric anhidride.[175] The corresponding *N*-hydroxysuccinimidyl ester **141** was

isolated and reacted with the integrin ligand *cyclo*[DKP-RGD]-CH_2NH_2 (**70**), affording the final compound **128** in 85% yield.

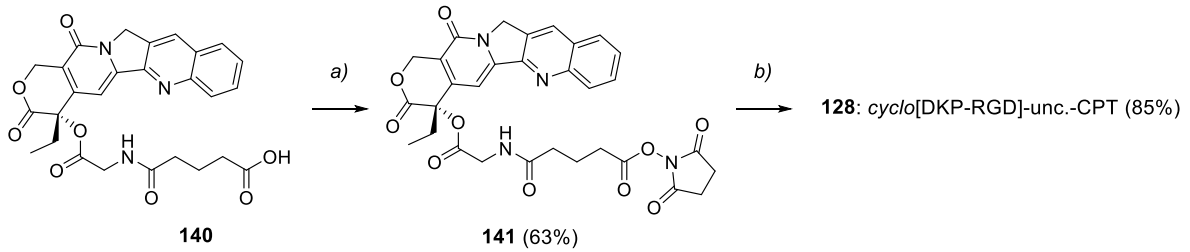

Scheme 15. Synthesis of *cyclo*[DKP-RGD]-unc.-CPT conjugate **128**. Reagent and conditions: *a)* DIC, NHS, 5:1 THF/CH_3CN, RT, overnight; *b) cyclo*[DKP-RGD]-CH_2NH_2 (**70**), CH_3CN/PBS (1:1; pH 7.5), overnight.

The RGD-CPT conjugates **121**, **126**-**128** were all purified by semipreparative HPLC and lyophilized before being subjected to biological assays.

4.3.2. In vitro Biological Evaluation

As described for the previous *cyclo*[DKP-RGD]-drug conjugates, the affinity of compounds **121**, **126**-**128** to the purified $\alpha_v\beta_3$ integrin was evaluated in competitive assays *in vitro*, by measuring the displacement of biotinylated vitronectin from the $\alpha_v\beta_3$ binding site. The obtained IC_{50} values are listed in Table 8.

Structure	**IC_{50} (nM) $\alpha_v\beta_3$**
cyclo(RGDyK)-Naph-SS-CPT (**121**)	5.3 ± 0.5
cyclo[DKP-RGD]-Naph-SS-CPT (**126**)	21.4 ± 2.3
cyclo[DKP-RGD]-SS-CPT (**127**)	15.4 ± 0.8
cyclo[DKP-RGD]-unc.-CPT (**128**)	7.4 ± 1.1
cyclo[DKP-RGD]-Val-Ala-PTX (**80**)[162]	13.3 ± 3.6
cyclo[DKP-RGD] (**64**)[151]	4.5 ± 1.1

Table 8. Inhibition of biotinylated vitronectin binding to purified integrin $\alpha_v\beta_3$.

As indicated by the low-nanomolar IC_{50} values, all tested compounds exhibited high binding affinity for the integrin receptor. In particular, the *cyclo*(RGDyK) ligand (i.e. the RGD ciclopeptide in SMDC **121**) was found to be a slightly better integrin binder than the *cyclo*[DKP-RGD] peptidomimetic. Indeed, while the conjugation of prodrug **120** to the *cyclo*(RGDyK) ligand resulted in the SMDC **121**, showing the lowest IC_{50} value of the series (IC_{50} = 5.3 nM), the analogous conjugate **126** showed the highest IC_{50} value of the group (IC_{50} = 21.4 nM).

The stability of the disulfide linker was evaluated: a 10 mM solution of prodrug **120** in DMSO was treated with dithiothreitol (DTT) at 30 °C. Complete disulfide cleavage was observed over a 10-minute period and the release of free camptothecin (**124**) and amine **125** (see Scheme 12B, on page 65) was observed by analytical HPLC. Moreover, prodrug **120** was found to be stable in cell medium (RPMI + 10% PBS, 1% DMSO at 4 °C), indicating that free camptothecin should be only released in the presence of cancer cells, presumably upon endocytosis.

Fluorescence microscopy assays are currently in progress, aimed at evaluating the selective accumulation and internalization of theranostic SMDCs **121** and **126** in $\alpha_v\beta_3$-expressing cells, with respect to antigen-negative cancer cell lines. This experiment will give an immediate feedback about the different activity of the two RGD ligands *cyclo*(RGDyK) and *cyclo*[DKP-RGD] in terms of cell adhesion and receptor-mediated endocytosis. This qualitative analysis will be supported by cell antiproliferative assays against the $\alpha_v\beta_3$ +/$\alpha_v\beta_3$ − cellular model, as reported in Chapter 2. Compounds **127** and **128** will be also subjected to this assay, in order to validate the use of disulfide linkers in these drug delivery systems.

Conclusions and Perspectives

The research described in this work of thesis highlighted potentialities of the peptidomimetic *cyclo*[DKP-RGD] as targeting moiety, for specific release of cytotoxic agents into integrin-expressing cancer cells. The chemical features of this peptidomimetic allowed its covalent connection to a wide range of chemical compounds and the final products of these conjugation reactions showed better water solubility compared to highly lipophilic anticancer drugs and linkers. The conjugation of *cyclo*[DKP-RGD] to anticancer drugs through peptide linkers, responsible for drug release upon enzymatic cleavage, is a core topic of the present work. In general, attachment of the RGD peptidomimetic to the N termini of these dipeptides does not affect either the affinity of the RGD moiety for the purified $\alpha_v\beta_3$ receptor and the enzymatic cleavage at the linkers' C termini. A significant contribution of the work herein described to the tumor targeting field is the quantification of the ability of *cyclo*[DKP-RGD]-drug conjugates to selectively kill $\alpha_v\beta_3$-expressing cancer cells *in vitro*. We subjected our new compounds to cell viability assays against two isogenic cell lines: human leukemia cancer cells CCRF-CEM were selected as antigen-negative ($\alpha_v\beta_3$ −) model and were transfected with an integrin-coding DNA vector, giving birth to an $\alpha_v\beta_3$-expressing subclone ($\alpha_v\beta_3$ +), namely, CCRF-CEM $\alpha_v\beta_3$. The actual difference in $\alpha_v\beta_3$ expression is evaluated through cell incubation with a fluorescein-labeled anti-$\alpha_v\beta_3$ monoclonal antibody and subsequent flow cytometry or immunofluorescence analysis. Among our new compounds, the *cyclo*[DKP-RGD]-Val-Ala-PTX conjugate (**80**) showed a 66.9-fold higher cytotoxic activity against ($\alpha_v\beta_3$ +) cells, compared to antigen-negative cells. Unexpectedly, the remarkable selectivity of the free PTX against the two isogenic cell lines (*S*: 7.4) prompted us to introduce Targeting Index (T.I. = 9.0 shown by **80**) as a parameter to evaluate the real gain in selectivity provided by the RGD targeting moiety. Although we indicated compound **80** as one of the most selective $\alpha_v\beta_3$-targeting SMDCs ever reported, the selectivity observed is far from the targeting skills shown by other compounds of this class, targeting different and more established transmembrane receptors (e.g. folate and biotin receptors, PSMA, etc.). In general, different factors can contribute to the shrink of selectivity displayed *in vitro* by a ligand-drug conjugate, such as little differences in receptor expression between the two cell lines, SMDC endocytosis through receptor-independent pathways or extracellular linker cleavage. Although our studies on RGD-paclitaxel conjugates highlighted the effects of linker variation

on the observed *in vitro* selectivity, the $\alpha_v\beta_3$-mediated endocytosis of these compounds was only inferred. Our next efforts focused on the development of dimeric RGD-PTX conjugates and theranostic SMDCs. The first project was devised to evaluate whether multimeric RGD presentation would strengthen the SMDC interactions with $\alpha_v\beta_3$ receptors on cancer cells, possibly resulting in a better selectivity for $\alpha_v\beta_3$-overexpressing cell lines. Furthermore, RGD-drug conjugates featuring fluorescence properties were designed and synthesized, in order to unambiguously evaluate the compounds' interactions with cancer cells and the subsequent $\alpha_v\beta_3$-mediated endocytosis. Although the biological evaluation of these latter compounds is still in progress, some interesting aspects emerged from the *in vitro* investigation of *cyclo*[DKP-RGD]-DNR conjugate **113**. Lysosome digestion experiments showed that, unlike Val-Ala and Phe-Lys dipeptides, the Val-Cit linker is selectively cleaved by intracellular cysteine protease cathepsin B. Importantly, compound **113** did not show any cytotoxic activity against the two cell lines, indicating that the Val-Cit linker remains intact under the test conditions. A rationale was provided by fluorescence microscopy analysis, which indicated that the lack of cytotoxic activity is due to an inefficient SMDC internalization into cancer cells. The contrast between the low-nanomolar affinity of SMDC **113** for purified $\alpha_v\beta_3$ receptor and its weak adhesion to $\alpha_v\beta_3$-expressing cancer cells also emerged as an important aspect, to be taken into account for future developments. The reproduction of literature cases of intracellular fluorescence activity or the screening of different *cyclo*[DKP-RGD]-dye conjugates or "theranostic" SMDCs would provide an extensive SAR analysis of the compounds' interactions with both $\alpha_v\beta_3$-positive and $\alpha_v\beta_3$-negative cancer cells. Moreover, the understanding of the effects of multimeric ligand presentations on both cell adhesion and integrin-mediated endocytosis would definitely validate the *cyclo*[DKP-RGD] peptidomimetic as powerful tool in tumor targeting. This analysis, together with an exhaustive linker screening, would hopefully lead to a significant increase of the Targeting Index. Finally, following the new trends in both ADC and SMDC technology, the conjugation of the *cyclo*[DKP-RGD] integrin ligand to picomolar cytotoxic agents will represent an important upgrade for future *in vivo* evaluations.

Experimental Section

General Remarks and Procedures

Materials and Methods

All manipulations requiring anhydrous conditions were carried out in flame-dried glassware, with magnetic stirring and under a nitrogen atmosphere. All commercially available reagents were used as received. Anhydrous solvents were purchased from commercial sources and withdrawn from the container by syringe, under a slight positive pressure of nitrogen. *cyclo*[DKP-RGD]-CH_2NH_2 (**70**),[154] *N*-(Boc)-*N*,*N'*-dimethylethylenediamine (**86**),[163] Fmoc-Val-Ala-*N*-[4-(hydroxymethyl)-phenyl] (**88a**),[161] azido-tetraethylene glycol-acid (**109**),[170] (4-Nitrophenoxycarbonyl)camptothecin (**130**)[173] and (hemiglutarate)glycino-camptothecin (**140**)[175] were prepared according to literature procedures, and their analytical data were in agreement with those already published. Reactions were monitored by analytical thin-layer chromatography (TLC) using silica gel 60 F254 pre-coated glass plates (0.25 mm thickness). Visualization was accomplished by irradiation with a UV lamp and/or staining with a potassium permanganate alkaline solution or ninhydrin. Flash column chromatography was performed according to the method of Still and co-workers[176] using Chromagel 60 ACC (40-63 μm) silica gel. Automated chromatography was performed with Grace Reveleris instrument. Proton chemical shifts are reported in ppm (δ) with the solvent reference relative to tetramethylsilane (TMS) employed as the internal standard ($CDCl_3$ δ = 7.26 ppm; CD_2Cl_2, δ = 5.32 ppm; CD_3OD, δ = 3.31 ppm, D_2O, δ = 4.79 ppm; DMSO-d_6, δ = 2.50 ppm; THF-d_8, δ = 3.58 ppm, 1.72 ppm).[177] The following abbreviations are used to describe spin multiplicity: s = singlet, d = doublet, t = triplet, q = quartet, m = multiplet, bs = broad signal, dd = doublet of doublet, ddd = doublet of doublet of doublet, ddt = doublet of doublet of triplet. Carbon NMR spectra were recorded on a spectrometer operating at 100.63 MHz, with complete proton decoupling. Carbon chemical shifts are reported in ppm (δ) relative to TMS with the respective solvent resonance as the internal standard ($CDCl_3$, δ = 77.16 ppm; CD_2Cl_2, δ = 54.00 ppm; DMSO-d_6, δ = 39.51 ppm; CD_3OD, δ = 49.05 ppm; THF-d_8 δ = 67.57 ppm, 25.37 ppm). HPLC purifications and HPLC traces of final products were performed on Dionex Ultimate 3000 equipped with Dionex RS Variable Wavelenght Detector (column: Atlantis

Prep T3 OBDTM 5 µm 19 × 100 mm; flow 15 mL min^{-1} unless stated otherwise). High resolution mass spectra (HRMS) were recorded on Waters LCT Premier XE instrument. Low resolution mass spectra (MS) were recorded on Thermo Finnigan LCQ Advantage (ESI source), Micro Waters Q-Tof(ESI source) and Bruker Daltonics Microflex LT (MALDI source) instruments.

General Procedures

GENERAL PROCEDURE FOR Boc DEPROTECTION REACTIONS:

GP1: To a 0.03 M CH_2Cl_2 solution of the *N*-Boc-protected compound half volume of TFA was added, and the reaction was stirred at r.t. for 1 h. The solvent was evaporated and then for two times CH_2Cl_2 was added to the residue followed by evaporation under vacuum, to afford the amine TFA salt.

GENERAL PROCEDURE FOR Fmoc DEPROTECTION REACTIONS:

GP2: A 0.01 M solution of the *N*-Fmoc-protected compound (1 eq) in DMF was cooled to 0 °C under nitrogen atmosphere. Piperidine (5 eq) was added and the reaction was stirred at room temperature for 2 h. The mixture was diluted with AcOEt (20 × volume of DMF) and washed twice with a saturated aqueous solution of $NaHCO_3$. The organic phase was dried over Na_2SO_4 and concentrated at rotavapor. CH_2Cl_2 was added to the residue and evaporated to afford a yellow solid. The crude was left under vacuum for 2 h and then used as starting material for the subsequent step.

Biological Assays

SOLID-PHASE RECEPTOR BINDING ASSAY:

Purified $\alpha_v\beta_3$ and $\alpha_v\beta_5$ receptors (Chemicon International, Inc., Temecula, CA) were diluted to 0.5 µg mL^{-1} in coating buffer containing 20 mmol L^{-1} tris(hydroxymethyl) amino methane–HCl (Tris-HCl; pH 7.4), 150 mmol L^{-1} NaCl, 1 mmol L^{-1} $MnCl_2$, 2 mmol L^{-1} $CaCl_2$, and 1 mmol L^{-1} $MgCl_2$. An aliquot of diluted receptors (100 mL $well^{-1}$) was added to 96-well microtiter plates (NUNC MW 96F MEDISORP STRAIGHT) and incubated overnight at 4 °C. The plates were then incubated with blocking solution (coating buffer plus 1% bovine serum albumin) for additional 2 h at room temperature to block nonspecific binding; this was followed by a 3 h incubation at room temperature with various concentrations (10^{-12} − 10^{-12} M) of test compounds in the presence of 1 µg mL^{-1} vitronectin biotinylated by using an EZ-Link Sulfo-NHS-Biotinylation kit (Pierce, Rockford, IL). After being washed, the plates were incubated for 1 h at room temperature with streptavidin biotinylated peroxidase complex (Amersham Biosciences, Uppsala, Sweden) and then for 30 min with Substrate Reagent Solution (100 mL; R&D Systems, Minneapolis, MN), before the reaction was stopped by addition of 2 N

H_2SO_4 (50 mL). The absorbance at 415 nm was read in a Synergy HT Multi-Detection Microplate Reader (BioTek Instruments, Inc.). Each data point is the result of the average of triplicate wells and was analyzed by nonlinear regression analysis with the Prism GraphPad program. Each experiment was repeated in triplicate.

STABILITY TEST:

The stability of compounds **80**, **81**, **82** and **113** was determined by ultraperformance liquid chromatography (UPLC) on a Waters Acquity UPLC BEH C18 column (2.1 × 50 mm, 1.7 µm) by using a Waters Acquity UPLC system equipped with a 2996 Aquity photodiode array detector and a Micromass ZQ 2000 single-quadrupole mass spectrometer, equipped with an electrospray ion source (ESI). Mobile phase A was composed of 0.05% TFA in water, and mobile phase B was 0.05% TFA in CH_3CN. The following conditions were used: a gradient from 20% to 100% B in 3.5 min and held at 100% B for 1 min; spectral analysis from 210–400 nm; a flow rate of 0.6 mL min^{-1}; an injection volume of 10 mL; full scan, mass range from 200-2000 amu. In a control analysis, compounds **80**, **81**, **82** and **113** were diluted at 0.2 mM in 0.05% TFA aqueous solution containing 20% CH_3CN (compound **80**) or in 0.05% TFA aqueous solution (compounds **81** and **82**). Compounds **80**, **81**, **82** and **113** (0.2 mM each) were incubated under neutral or acidic conditions for 4 h at 25 °C. The neutral buffer was composed of 100 mM Tris-HCl (pH 7.4), whereas the acidic buffer was composed of 200 mM sodium acetate (pH 5.5)/1 mM ethylenediaminetetraacetate (EDTA); for compound **80**, the buffers were supplemented with 20% CH_3CN and for compound **113** buffers were supplemented with 20% EtOH.

Compound **120** was subjected to stability assay in RPMI cellular medium containing 10% fetal bovine serum, 1% DMSO, incubated 16 h at 4 °C. As a positive control for the cleavage, 2 pmol of **120** were incubated with 10 mM DTT for 10 min at 30 °C. 2 pmol of the compound from each condition were then analyzed by HPLC Waters Alliance 2695 with XTerra 3.5 mm 5 cm C18 column with 2475 Multy l Fluorescence Detector. **120** was detected by measuring the fluorescence intensity with excitation wavelength set at 370 nm and emission wavelength set at 454 nm. Cleavage product was detected at excitation wavelength 430nm and emission wavelength set at 535 nm.

DIGESTION WITH LYSOSOMAL ENRICHED EXTRACT

0.2 mM solutions of the compounds of interest were digested in 200 mM sodium acetate (pH 5.5)/1 mM EDTA containing 1 mM cysteine at 37 °C for 2 h with 0.5 mg mL^{-1} of lysosomal enriched extract (prepared from a rat liver as previously described in the literature) in the presence or absence of 20 µm CA-074 Me or E-64 protease inhibitors (Enzo Life Sciences). Control samples were prepared by diluting the compounds in the same reaction mixture

acidified with TFA to inactivate the lysosomal enzymes. All samples were analyzed by ESI-LC/MS on a PLRP-S column (Agilent Technologies; 2.1 × 150 mm, 8 µm, 1000 Å) with an Agilent 1100 HPLC system equipped with a diode array detectorwith an electrospray ion source. Mobile phaseA was composed of 0.05% TFA in water, and mobile phase B was 0.05% TFA in CH_3CN. Samples (45 µm) were eluted at 0.25 mL min^{-1} by using a gradient from 20 to 50% B in 22 min, raised to 80% B and held at 80% B for 5 min; the UV signal was recorded at 220 and 280 nm, and MS detection was set in full-scan mode from 300–2000 amu.

EVALUATION OF $\alpha_v\beta_3$ EXPRESSION BY FLOW CYTOMETRY:

Cells were collected, washed with PBS and counted. For each sample, 5 × 105 cells were resuspended in 100 µl of 1% BSA-PBS containing (or not in the case of the negative control) the anti-$\alpha_v\beta_3$ antibody (clone LM609-Millipore MAB 1976) at 1:50 dilution. After incubation for 30 min at 4 °C, samples were washed with PBS and incubated with the secondary antibody (CF488A-goat anti-mouse IgG, Biotium 20011) diluted 1:300 for 30 min at 4 °C. After washing, samples were acquired by a Facscalibur (Becton Dickinson) cytometer and analyzed by CellQuest software (Fig. 33A).

EVALUATION OF $\alpha_v\beta_3$ EXPRESSION BY IMMUNOFLUORESCENCE:

Cells were cytospinned (1000 rpm for 5 min) on glass slides and fixed for 20 min with formaldehyde 3.7% (v/v) solution. After washing with PBS, cells were saturated for 30 min with a blocking solution containing 1% (w/v) BSA and 0.3% (v/v) Triton X-100 in PBS and incubated with the primary anti-$\alpha_v\beta_3$ antibody (clone LM609-Millipore MAB 1976) diluted 1:50 in blocking solution. The primary antibody was removed and cells washed with PBS, followed by immunostaining with the secondary antibody diluted 1:500 (CF488A-goat anti-mouse IgG, Biotium 20011) and counterstaining with Hoechst (Sigma-Aldrich), according to manufacturer's protocols. Samples were washed with PBS and mounted with Mowiol and cover slips. Cell photomicrographs (Fig. 33B) were acquired the blue channel (Hoechst) and in the green channel (anti-$\alpha_v\beta_3$) using a Zeiss fluorescence microscope.

CELL PROLIFERATION ASSAY:

Cells were seeded in 96-well plates with the appropriate complete medium (RPMI 1640 medium with 2 mM L-glutamine, 10% fetal calf serum, 10 mM 2-[4-(2-hydroxyethyl)-1-piperazinyl]ethanesulfonic acid, and 1 mM sodium pyruvate). 48 h after seeding, the medium was replaced with medium containing serial dilutions of the test compounds. [CELL WASHOUT EXPERIMENT = The cells were incubated for 6 h at 37 °C, then washed and reincubated in fresh medium for additional 138 h at 37 °C]. Cell viability was assessed with the CellTiter-Glo luciferase-based ATP detection assay (Promega) by following

manufacturer's instructions. Growth inhibitory activity was evaluated at the end of incubation by using GraphPad Prism software. Experimental data were normalized versus untreated control samples and interpolated by nonlinear regression analysis with GraphPad Prism software to generate dose-response curves. IC_{50} values were calculated by using sigmoidal interpolation curve fitting.

Synthesis of cyclo[DKP-RGD]-Drug Conjugates

cyclo[DKP-RGD]-Val-Ala-PTX (**80**)

2'-(4-Nitrophenoxycarbonyl)paclitaxel (83)

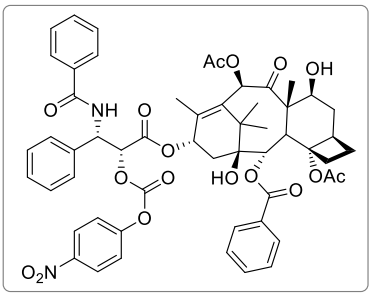

$C_{55}H_{56}N_2O_{17}$
MW: 1017,05

Paclitaxel (200 mg, 0.23 mmol, 1 eq) was dissolved in dry CH_2Cl_2 (2.5 mL) under a nitrogen atmosphere. Pyridine (55 mL, 0.70 mmol, 3 eq) was added dropwise, and the mixture was cooled to −50 °C. A solution of 4-nitrophenylchloroformate (71 mg, 0.35 mmol, 1.5 eq) in dry CH_2Cl_2 (1 mL) was then added under a nitrogen atmosphere. The mixture was warmed to −20 °C and stirred until no unreacted paclitaxel was observable by TLC (approximately 4 h; eluent: 4:6 hexane/AcOEt). The mixture was then diluted with AcOEt (100 mL) and washed with a 1M aqueous solution of $KHSO_4$ (10 mL) and brine (10 mL). The organic phase was dried over Na_2SO_4 and concentrated. The crude residue was purified by a Grace Reveleris system (column: Reveleris Silica 12 g; dry load; flow rate: 36 mL min^{-1}; ramp: from 100% hexane to 100% AcOEt in 15 min) to afford 2'-(4-nitrophenoxycarbonyl)paclitaxel (**83**) as a white foam (165 mg, 69% yield).

R_f=0.26 (4:6 hexane/AcOEt); ^{1}H NMR (400 MHz, CD_2Cl_2): δ = 8.25 (d, J = 9.2 Hz, 2H), 8.16 (d, J = 7.1 Hz, 2H), 7.76 (d, J = 7.1 Hz, 2H), 7.63 (m, 1H), 7.57-7.51 (m, 3H), 7.51-7.46 (m, 4H), 7.47-7.40 (m, 3H), 7.36 (d, J = 9.2 Hz, 2H), 6.98 (d, J = 9.3 Hz, 1H), 6.31 (m, 1H), 6.27 (s, 1H), 6.09 (dd, J = 9.3, 2.8 Hz, 1H), 5.67 (d, J = 7.1 Hz, 1H), 5.56 (d, J = 2.8 Hz, 1H), 4.97 (dd, J = 14.7, 7.0 Hz, 1H), 4.42 (ddd, J = 10.9, 6.5, 4.4 Hz, 1H), 4.30 (d, J = 8.3 Hz, 1H), 4.17 (d, J = 8.3 Hz, 1H), 3.81 (d, J = 7.1 Hz, 1H), 2.53 (m, 1H), 2.49 (s, 3H), 2.44 (m, 1H), 2.24 (dd, J = 15.5, 8.9 Hz, 1H), 2.20 (s, 3H), 1.94 (s, 1H), 1.91 (s, 3H), 1.81 (m, 1H), 1.70 (s, 1H), 1.64 (s, 3H), 1.24 (s, J = 4.6 Hz, 3H), 1.13 ppm (s, 3H); ^{13}C NMR (101 MHz, CD_2Cl_2): δ =

204.1, 171.7, 170.4, 167.9, 167.5, 167.2, 155.4, 152.2, 146.2, 142.7, 136.8, 134.1, 134.0, 133.5, 132.5, 130.6, 129.8, 129.6, 129.1, 127.5, 127.1, 125.8, 122.1, 84.7, 81.4, 79.5, 78.4, 76.7, 75.9, 75.5, 73.0, 72.5, 58.8, 53.2, 46.1, 43.6, 36.1, 36.0, 27.0, 23.1, 22.4, 21.0, 15.0, 9.8 ppm; MS (ESI): *m/z* calcd for $[C_{54}H_{54}N_2O_{18}Na]^+$: 1041.33 $[M+Na]^+$; found: 1042.0; *m/z* calcd for $[C_{54}H_{54}N_2O_{18}K]^+$: 1057.30 $[M+K]^+$; found: 1057.8.

Fmoc-Val-Ala-*N*-[4-[[[(4-nitrophenoxy)carbonyl]oxy]methyl]phenyl] (89a)

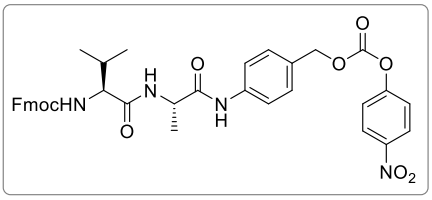

$C_{37}H_{36}N_4O_9$
MW: 680,71

Compound **88a** (285 mg, 0.552 mmol, 1 eq) was dissolved in dry THF (15 mL) under nitrogen atmosphere. Pyridine (111 µL, 1.382 mmol, 2.5 eq) was added, and the solution was cooled at 0 °C. 4-Nitrophenyl chloroformate (222 mg, 1.105 mmol, 2 eq) was added and the stirred reaction was allowed to reach room temperature. The reaction was monitored by TLC (eluent: 4:6 hexane/AcOEt). After 1.5 h the mixture was diluted with AcOEt (100 mL), washed with a 1 M aqueous solution of $KHSO_4$ (2 × 20 mL) and brine (2 × 20 mL). The organic phase was dried over Na_2SO_4 and concentrated. The crude was purified by a Grace Reveleris system (column: Reveleris Silica 4 g, dry load, flow rate: 22 mL min^{-1}, ramp from 100% hexane to 100% AcOEt in 20 min) to afford **89a** (330 mg, 88% yield).

R_f = 0.42 (Hex/AcOEt, 4:6); ^{1}H NMR (400 MHz, THF-d_8) δ 9.36 (s, 1H), 8.26 (d, *J* = 8.9 Hz, 2H), 7.82 (d, *J* = 7.2 Hz, 1H), 7.76 (d, *J* = 7.5 Hz, 2H), 7.71-7.61 (m, 4H), 7.45 (d, *J* = 8.9 Hz, 2H), 7.40-7.30 (m, 4H), 7.25 (t, *J* = 7.4 Hz, 2H), 6.82 (d, *J* = 8.6 Hz, 1H), 5.21 (s, 2H), 4.57 (dq, $J^1 = J^2$ = 6.5 Hz, 1H), 4.40 (dd, *J* = 10.2, 7.3 Hz, 1H), 4.29 (m, 1H), 4.20 (t, *J* = 6.8 Hz, 1H), 4.03 (t, *J* = 7.5 Hz, 1H), 2.05 (dq, *J* = 13.3, 6.6 Hz, 1H), 1.36 (d, *J* = 7.0 Hz, 3H), 0.94 (d, *J* = 6.2 Hz, 3H), 0.92 ppm (d, *J* = 6.2 Hz, 3H); ^{13}C NMR (101 MHz, THF-d_8) δ 172.1, 171.4, 157.2, 156.7, 153.1, 146.3, 145.1, 142.1, 140.7, 130.5, 130.0, 128.1, 127.5, 125.8, 125.7, 122.6, 120.4, 119.8, 71.0, 67.1 (overlapped with solvent signal), 61.1, 50.0, 48.1, 32.0, 19.5, 18.4, 17.9 ppm.

Fmoc-Val-Ala-*N*-[4-[[[(*N*-(Boc)-*N*,*N*'-dimethylethylenediamine)carbonyl]oxy]methyl]phenyl] (90a)

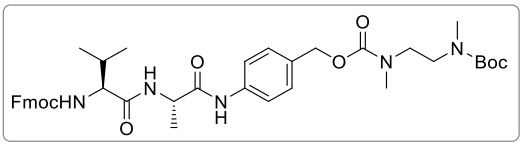

$C_{40}H_{51}N_5O_8$
MW: 729,88

A solution of *N*-(Boc)-*N*,*N'*-dimethylethylenediamine (**86**) (130 mg, 0.53 mmol, 2 eq) in dry THF (1 mL) and *i*Pr_2NEt (113 µL, 0.66 mmol, 2.5 eq) were added under nitrogen atmosphere to a solution of **89a** (180 mg, 0.26 mmol, 1 eq) in dry THF (11 mL) kept at 0 °C. The mixture was allowed to reach r.t. and stirred overnight, then the solvent was removed at rotavapor. AcOEt (70 mL) was added and the solution was washed with a 1 M aqueous solution of $KHSO_4$ (2 × 15 mL) and a saturated aqueous solution of $NaHCO_3$ (3 × 15 mL). The organic phase was dried over Na_2SO_4 and concentrated. The crude was purified over a pad of silica (gradient: 100% CH_2Cl_2 to 4% MeOH / 96% CH_2Cl_2), affording **90a** (212 mg, 91% yield).
R_f = 0.25 (3:7 hexane/AcOEt); ^{1}H NMR (400 MHz, CD_3OD) δ 7.78 (d, *J* = 7.5 Hz, 2H), 7.65 (dd, *J* = 7.1, 4.4 Hz, 2H), 7.58 (dd, *J* = 6.8, 4.1 Hz, 2H), 7.41-7.34 (m, 2H), 7.34-7.26 (m, 4H), 5.04 (s, 2H), 4.50 (q, *J* = 7.0 Hz, 1H), 4.44-4.32 (m, 2H), 4.21 (t, *J* = 6.8 Hz, 1H), 3.95 (d, *J* = 6.9 Hz, 1H), 3.47-3.32 (m, 4H), 2.93 (s, rotamer A + B, 3H), 2.84 (s, rotamer A, 3H), 2.72 (s, rotamer B, 3H), 2.08 (dq, *J* = 13.4, 6.6 Hz, 1H), 1.43 (d, *J* = 7.5 Hz, 3H), 1.41 (s, 9H), 0.98 (d, *J* = 6.7 Hz, 3H), 0.95 ppm (d, *J* = 7.2 Hz, 3H); ^{13}C NMR (101 MHz, CD_3OD) δ 174.1, 172.9, 158.9, 158.0 (rotamer A), 157.5 (rotamer B), 145.3, 145.2, 142.6, 139.7 (rotamer A), 139.6 (rotamer B), 133.8 (rotamer A), 133.6 (rotamer B), 130.0 (rotamer A), 129.7 (rotamer B), 128.8, 128.2, 126.2, 121.2, 120.9, 81.2 (rotamer A), 80.9 (rotamer B), 68.2, 68.0, 62.3, 51.0, 48.4, 48.0, 47.6, 35.6 (rotamer A), 35.2 (rotamer B), 35.1 (rotamer A), 34.6 (rotamer B), 31.9, 28.7, 19.7, 18.7, 18.0 ppm.

(Hemiglutarate)-Val-Ala-*N*-[4-[[[(*N*-(Boc)-*N*,*N*'-dimethylethylenediamine)carbonyl]oxy]methyl]phenyl] (91a)

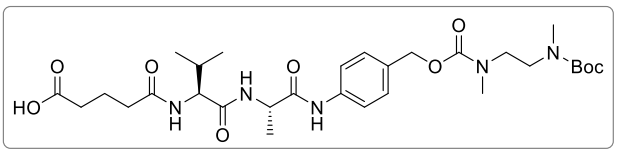

$C_{30}H_{47}N_5O_9$
MW: 621,73

Compound **90a** (167 mg, 0.23 mmol, 1 eq) was deprotected following General Procedure GP2. The crude free amine was dissolved in dry DMF (3 mL) and cooled at 0 °C under nitrogen atmosphere. Glutaric anhydride (65 mg, 0.57 mmol, 2.5 eq), DMAP (7 mg, 0.12 mmol, 0.25 eq) and *i*Pr_2NEt (147 µL, 0.86 mmol, 3.75 eq) were added. The mixture was allowed to reach room temperature and stirred overnight. Half of the DMF volume was

removed under high vacuum, then the mixture was diluted with AcOEt (70 mL), washed with a 1 M aqueous solution of $KHSO_4$ (2 × 10 mL) and brine (1 × 10 mL). The organic phase was dried and concentrated, then the crude was purified by flash chromatography [gradient: 1% (MeOH + 0.1% CH_3COOH) / 99% (CH_2Cl_2 + 0.1% CH_3COOH) to 10% (MeOH + 0.1% CH_3COOH) / 90% (CH_2Cl_2 + 0.1% CH_3COOH)] affording **91a** (109 mg, 77% yield).
^{1}H NMR (400 MHz, CD_3OD) *δ* 7.59 (dd, *J* = 7.5, 4.6 Hz, 2H), 7.31 (d, *J* = 8.2 Hz, 2H), 5.05 (s, 2H), 4.49 (q, *J* = 7.1 Hz, 1H), 4.21 (d, *J* = 7.1 Hz, 1H), 3.49-3.33 (m, 4H), 2.93 (bs, rotamer A + B, 3H), 2.85 (s, rotamer A, 3H), 2.74 (s, rotamer B, 3H), 2.40-2.28 (m, 4H), 2.09 (dq, *J* = 13.7, 6.8 Hz, 6H), 1.96-1.84 (m, 2H), 1.47-1.39 (m, 12H), 0.98 (d, *J* = 6.7 Hz, 3H), 0.96 ppm (d, *J* = 6.7 Hz, 3H); ^{13}C NMR (101 MHz, CD_3OD) *δ* 177.2, 175.7, 173.7, 173.0, 158.0, 157.4, 139.7 (rotamer A), 139.5 (rotamer B), 133.8 (rotamer A), 133.6 (rotamer B), 130.0 (rotamer A), 129.6 (rotamer B), 121.1, 81.2 (rotamer A), 80.9 (rotamer B), 68.2 (rotamer A), 67.9 (rotamer B), 60.3, 51.1, 47.9, 47.6, 35.8, 35.6 (rotamer A), 35.3 (rotamer B), 35.2 (rotamer A), 34.6 (rotamer B), 34.4, 31.8, 28.7, 22.3, 19.7, 18.7, 18.0 ppm.

***cyclo*[DKP-RGD]-Val-Ala-*N*-[4-[[[(*N*-(Boc)-*N*,*N*'-dimethylethylenediamine)carbonyl]oxy]methyl]phenyl] (Boc-92a)**

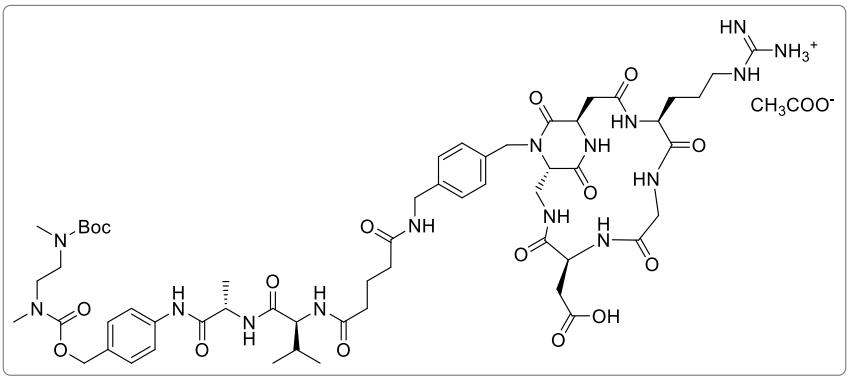

$C_{57}H_{83}N_{15}O_{16}$
MW: 1234,38 + AcOH

DIC (7.7 µL, 4.9 × 10^{-2} mmol, 2.2 eq) and NHS (3 mg, 2.6 × 10^{-2} mmol, 1.4 eq) were added to a solution of **90a** (28 mg, 4.5 × 10^{-2} mmol, 2 eq) in dry DMF (1 mL). The resulting solution was stirred overnight under nitrogen. Volatiles were then removed *in vacuo* to give an off-white solid, which was re-dissolved in CH_3CN (1 mL) and cooled at 0 °C. A solution of **70** (19 mg, 2.3 × 10^{-2} mmol, 1 eq) in pH 7.5 phosphate buffer (1 mL) was then added to the CH_3CN solution, and the pH was adjusted to 7.3-7.6 with NaOH (0.2 M). The resulting solution was warmed to room temperature and stirred overnight. During the first 5 hours the pH value was kept near 7.3 adding 0.2 M aqueous NaOH when necessary. The solution was concentrated and the crude was purified by semipreparative-HPLC [Waters Atlantis 21 mm × 10 cm column, gradient: 90% (H_2O + 0.1% CH_3COOH) / 10% (CH_3CN + 0.1% CH_3COOH) to 47% (H_2O + 0.1% CH_3COOH) / 53% (CH_3CN + 0.1% CH_3COOH) in 9 min; t_R (product): 8.5 min].

The purified product was then freeze-dried to give **Boc-92a** as a white solid (14 mg, 48% yield over two steps).

^{1}H NMR (400 MHz, CD_3OD) δ 7.58 (dd, J = 7.9, 4.8 Hz, 2H), 7.31 (d, J = 7.9 Hz, 2H), 7.26 (d, J = 8.3 Hz, 2H), 7.22 (d, J = 8.3 Hz, 2H), 5.13 (d, J = 15.0 Hz, 1H), 5.05 (s, 2H), 4.95 (dd, J = 8.7, 5.8 Hz, 1H), 4.58 (dd, J = 9.9, 3.7 Hz, 1H), 4.47 (q, J = 7.0 Hz, 1H), 4.44 (d, J = 17.8 Hz, 1H), 4.36 (d, J = 15.2 Hz, 1H), 4.31 (d, J = 15.2 Hz, 1H), 4.17 (d, J = 6.9 Hz, 1H), 3.97 (dd, J = 14.8, 4.9 Hz, 1H), 3.96 (d, J = 15.0 Hz, 1H), 3.93-3.86 (m, 2H), 3.52 (d, J = 17.8 Hz, 1H), 3.50 (dd, J = 14.8, 7.8 Hz, 1H), 3.45-3.35 (m, 4H), 3.22 (t, J = 7.1 Hz, 2H), 2.97 (m, 1H), 2.94 (bs, rotamer A + B, 3H), 2.77 (m, 1H), 2.85 (rotamer A, 3H), 2.74 (rotamer B, 3H) 2.56 (dd, J = 16.9, 5.8 Hz, 1H), 2.51 (dd, J = 12.9, 3.7 Hz, 1H), 2.33 (t, J = 7.3 Hz, 2H), 2.27 (t, J = 7.3 Hz, 2H), 2.21-2.05 (m, 3H), 1.94 (m, 1H), 1.75-1.56 (m, 2H), 1.43 (d, J = 7.0 Hz, 3H), 1.42 (s, 9H), 0.99 (d, J = 6.8 Hz, 3H), 0.96 ppm (d, J = 6.9 Hz, 3H); ^{13}C NMR (101 MHz, CD_3OD) δ 175.8, 175.3, 173.8, 173.8, 173.5, 173.1, 172.1, 171.6, 171.0, 158.6, 158.0, 157.5 (rotamer A), 157.4 (rotamer B), 140.2, 139.6 (rotamer A), 139.5 (rotamer B), 135.8, 133.9 (rotamer A), 133.7 (rotamer B), 130.0 (rotamer A), 129.7 (rotamer B), 129.4, 129.2, 121.2, 81.2 (rotamer A), 81.1 (rotamer B), 68.2 (rotamer A), 67.9 (rotamer B) , 60.5, 60.2, 56.0, 53.1, 51.1, 50.2, 48.2, 47.6, 47.6, 43.7, 43.6, 42.2, 39.7, 38.6, 36.09, 35.8, 35.6, 35.3, 34.7, 31.7, 28.7, 27.4, 27.1, 23.1, 19.7, 18.7, 18.0 ppm. MS (ESI) *m/z* calcd. for $[C_{57}H_{84}N_{15}O_{16}]^+$: 1234.62 $[M+H]^+$, found: 1234.64.

***cyclo*[DKP-RGD]-Val-Ala-PTX (80)**

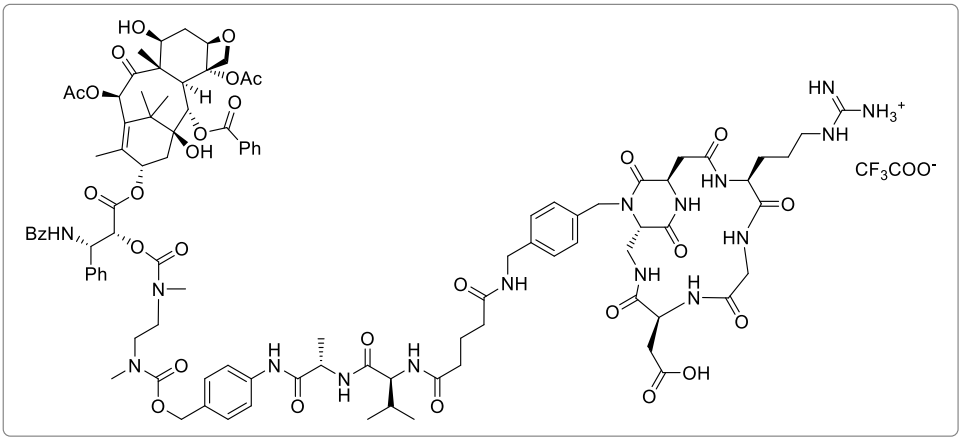

$C_{100}H_{124}N_{16}O_{29}$
MW: 2014,18 + TFA

Boc-92a (14 mg) was deprotected following General Procedure GP1 and lyophilized overnight. The corresponding trifluoroacetate salt (**92a**, 12 mg, 8.8×10^{-3} mmol, 1 eq) was dissolved in dry DMF (100 µL) under nitrogen atmosphere and cooled at 0 °C. Compound **83** (27 mg, 26.5×10^{-3} mmol, 3 eq) was dissolved in dry DMF (900 µL) and added to the substrate solution, followed by iPr$_2$NEt (8 µL, 44.1×10^{-3} mmol, 5 eq). The mixture was allowed to reach room temperature and stirred overnight. The solvent was removed under

vacuum and the crude was purified by semipreparative-HPLC [Waters Atlantis 21 mm × 10 cm column, gradient: 90% (H_2O + 0.1% CF_3COOH) / 10% (CH_3CN + 0.1% CF_3COOH) to 100% (CH_3CN + 0.1% CF_3COOH) in 11 min; t_R (product): 7.1 min]. The purified product was then freeze-dried to give the desired compound **80** as a white solid (14 mg, 78% yield over two steps).

^{1}H NMR (400 MHz, CD_3OD) δ 8.27-8.02 (m, 2H), 7.81 (d, *J* = 7.6 Hz, 2H), 7.67 (m, 1H), 7.63-7.33 (m, 10H), 7.33-7.26 (m, 3H), 7.26 (d, *J* = 8.0 Hz, 2H), 7.22 (d, *J* = 8.2 Hz, 2H), 7.15 (d, *J* = 8.3 Hz, 1H), 6.46 (d, *J* = 4.6 Hz, 1H), 6.11 (m, 1H), 5.99 (d, *J* = 4.6 Hz, 1H), 5.81 (d, *J* = 6.2 Hz, 1H), 5.64 (m, 1H), 5.46 (d, *J* = 4.7 Hz, 1H), 5.33 (m, 1H), 5.12 (d, *J* = 14.9 Hz, 1H), 5.06-4.93 (m, 2H), 4.98-4.83 (m, 2H), 4.82-4.71 (m, 2H), 4.57 (dd, *J* = 9.9, 3.6 Hz, 1H), 4.50-4.40 (m, 2H), 4.39-4.28 (m, 3H), 4.23-4.14 (m, 2H), 4.16 (d, *J* = 6.7 Hz, 1H), 3.97 (m, 1H), 3.90 (d, *J* = 6.5 Hz, 1H), 3.88-3.79 (m, 2H), 3.69 (m, 1H), 3.61-3.42 (m, 3H), 3.22 (t, *J* = 6.9 Hz, 2H), 3.31-3.17 (m, 2H), 2.97 (dd, *J* = 15.6, 7.4 Hz, 1H), 2.93-2.77 (NMe rotamers, 6H), 2.76 (m, 1H), 2.55 (dd, *J* = 16.8, 5.6 Hz, 1H), 2.52 (m, 1H), 2.49 (s, rotamer A, 3H), 2.38 (s, rotamer B, 3H), 2.37-2.30 (m, 2H), 2.26 (t, *J* = 7.4 Hz, 2H), 2.15 (s, rotamer A, 3H), 2.11 (s, rotamer B, 3H), 2.19-2.07 (m, 2H), 2.02-1.89 (m, 6H), 1.81 (m, 1H), 1.66 (s, rotamer A, 3H), 1.73-1.59 (m, 2H), 1.64 (s, rotamer B, 3H), 1.43 (d, *J* = 7.1 Hz, 3H), 1.13 (bs, 6H), 1.01-0.92 ppm (m, 6H); ^{13}C NMR (101 MHz, CD_3OD) δ 205.3, 175.9, 175.3, 173.8, 173.7, 173.5, 173.4, 173.0, 172.1, 171.6, 171.6, 171.1, 170.9, 167.7, 167.7, 158.6, 157.9, 156.6, 140.2, 139.5, 138.4, 135.8, 134.9, 134.0, 133.8, 132.9, 131.4, 131.2, 130.1, 130.1, 130.0, 129.7, 129.6, 129.5, 129.4, 129.2, 128.9, 128.8, 128.6, 128.2, 121.3, 121.2, 85.9, 82.2, 79.1, 77.5, 77.0, 76.9, 76.3, 72.9, 72.4, 68.2, 67.0, 60.6, 60.2, 59.2, 56.0, 55.1, 53.1, 51.1, 50.2, 48.2, 47.9, 44.6, 43.7, 43.6, 39.6, 38.6, 37.5, 36.1, 35.7, 35.6, 35.4, 35.1, 31.6, 27.4, 27.1, 27.0, 23.3, 23.1, 22.5, 20.8, 19.7, 18.7, 18.0, 15.2, 10.5 ppm. MS (ESI) *m/z* calcd. for $[C_{100}H_{126}N_{16}O_{29}]^{2+}$: 1007.45 $[M+2H]^{2+}$, found: 1007.57; MS (ESI) *m/z* calcd. for $[C_{100}H_{125}N_{16}O_{29}Na]^{2+}$: 1018.44 $[M+H+Na]^{2+}$, found: 1018.56; MS (MALDI) *m/z* calcd. for $[C_{100}H_{125}N_{16}O_{29}]^{+}$: 2015.14 a.m.u. $[M+H]^{+}$; found: 2014.4 (HCCA matrix), 2015.7 (SIN matrix). HRMS (ESI+): *m/z* calcd. for $[C_{100}H_{125}N_{16}O_{29}]^{+}$: 2013.8793 $[M+H]^{+}$; found: 2013.8818; HRMS (ESI+): *m/z* calcd. for $[C_{100}H_{126}N_{16}O_{29}]^{2+}$: 1007.4433 $[M+2H]^{2+}$; found: 1007.4435.

cyclo[DKP-RGD]-Phe-Lys-PTX (**81**)

Fmoc-Phe-Lys(Alloc)-OH (87b)

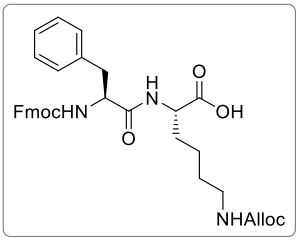

$C_{34}H_{37}N_3O_7$
MW: 599,68

Fmoc-Phe-OH (500 g, 1.29 mmol, 1.5 eq) was dissolved in dry THF (7.5 mL) under nitrogen atmosphere. NHS (163 mg, 1.42 mmol, 1.7 eq) and DCC (103 mg, 1.42 mmol, 1.7 eq) were added, and the mixture was stirred overnight at room temperature. The solution was filtered through cotton and concentrated to afford Fmoc-Phe-OSu as a white foam. H-Lys(Alloc)-OH (200 mg, 0.858 mmol, 1 eq) was dissolved in H_2O (7 mL) and $NaHCO_3$ (144 mg, 1.716 mmol, 2 eq) was added. Fmoc-Phe-OSu (623 mg, 1.287 mmol, 1.5 eq) was dissolved in THF (7 mL) and added to the stirred solution of H-Lys(Alloc)-OH. The mixture was stirred for 24 h at room temperature, followed by addition of a 1 M aqueous solution of $KHSO_4$ (40 mL). The suspension was extracted with CH_2Cl_2 (4 × 20 mL), then the collected organic phases were dried and concentrated. The crude was purified by flash chromatography [eluent: 5:5:1 AcOEt/Hex/MeOH + 0,1% AcOH] affording **87b** (440 mg, 86% yield).

^{1}H NMR (400 MHz, DMSO-d_6) δ 8.20 (d, J = 7.6 Hz, 1H), 7.87 (d, J = 7.5 Hz, 2H), 7.69-7.54 (m, 3H), 7.40 (td, J = 7.4, 2.7 Hz, 2H), 7.36-7.22 (m, 5H), 7.20-7.15 (m, 2H), 5.87 (ddt, J = 17.2, 10.5, 5.3 Hz, 1H), 5.24 (dd, J = 17.2, 1.6 Hz, 1H), 5.13 (dd, J = 10.5, 1.6 Hz, 1H), 4.43 (d, J = 5.3 Hz, 2H), 4.31 (m, 1H), 4.23-4.05 (m, 4H), 3.03 (dd, J = 13.7, 3.1 Hz, 1H), 2.99-2.93 (m, 2H), 2.78 (dd, J = 13.7, 11.3 Hz, 1H), 1.75 (m, 1H), 1.60 (m, 1H), 1.49-1.26 ppm (m, 5H); ^{13}C NMR (101 MHz, DMSO-d_6) δ 173.6, 171.6, 155.9, 155.8, 143.8, 143.7, 140.7, 138.2, 133.9, 129.3, 128.0, 127.6, 127.0, 126.2, 125.3, 120.1, 116.8, 65.7, 64.1, 56.0, 52.1, 46.6, 39.1, 37.5, 30.9, 29.1, 25.2, 22.7 ppm.

Fmoc-Phe-Lys(Alloc)-*N*-[4-(hydroxymethyl)phenyl] (88b)

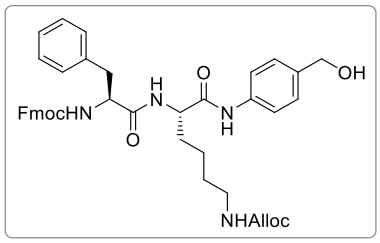

$C_{41}H_{44}N_4O_7$
MW: 704,82

Compound **87b** (415 mg, 0.69 mmol, 1 eq) was dissolved in dry THF. *N*-Methylmorpholine (152 µL, 1.38 mmol, 2 eq) was added and the mixture was cooled at 0 °C. After the addition of EDC hydrochloride (146 mg, 0.76 mmol, 1.1 eq), HOAt (113 mg, 0.83 mmol, 1.2 eq) and 4-aminobenzyl alcohol (170 mg, 1.38 mmol, 2 eq), the mixture was allowed to reach room temperature and stirred 4 h under nitrogen atmosphere. The mixture was diluted with a 1 M $KHSO_4$ aqueous solution (100 mL) and extracted with CH_2Cl_2 (3 × 20 mL). The combined organic phases were dried and concentrated to afford a red solid. The crude was treated with a 2:1 mixture of Et_2O/CH_2Cl_2, sonicated and filtered over Büchner funnel. The solid was purified by flash chromatography [gradient: from 1% MeOH / 99% CH_2Cl_2 to 10% MeOH / 90% CH_2Cl_2] to afford **88b** as a solid (350 mg, 71% yield).

R_f = 0.44 (9:1 CH_2Cl_2/MeOH); ^{1}H NMR (400 MHz, DMSO-d_6) δ 9.99 (s, 1H), 8.20 (d, *J* = 7.8 Hz, 1H), 7.87 (d, *J* = 7.5 Hz, 2H), 7.68-7.51 (m, 5H), 7.40 (t, *J* = 7.5 Hz, 2H), 7.35-7.20 (m, 8H), 7.20-7.13 (m, 2H), 5.86 (ddt, *J* = 17.2, 10.5, 5.3 Hz, 1H), 5.23 (dd, *J* = 17.2, 1.4 Hz, 1H), 5.18-5.04 (m, 2H), 4.51-4.37 (m, 4H), 4.33 (m, 1H), 4.25-4.08 (m, 4H), 3.04 (dd, *J* = 13.5, 3.5 Hz, 1H), 2.97 (dd, *J* = 12.6, 6.4 Hz, 2H), 2.79 (dd, *J* = 13.5, 10.9 Hz, 1H), 1.73 (m, 1H), 1.65 (m, 1H), 1.49-1.21 ppm (m, 4H); ^{13}C NMR (101 MHz, DMSO-d_6) δ 171.6, 170.4, 155.9, 155.8, 143.7, 140.7, 138.1, 137.5, 137.5, 133.8, 129.2, 128.0, 127.6, 127.0, 126.9, 126.2, 125.2, 120.1, 119.0, 116.8, 65.6, 64.1, 62.6, 56.0, 53.4, 46.6, 40.2 (overlapped with solvent signal), 37.4, 32.0, 29.2, 22.7 ppm.

Fmoc-Phe-Lys(Alloc)-*N*-[4-[[[(4-nitrophenoxy)carbonyl]oxy]methyl]phenyl] (89b)

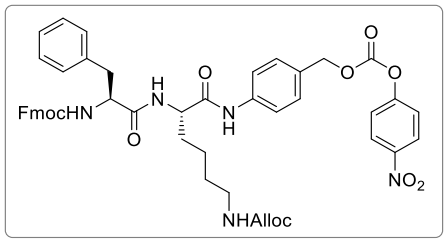

$C_{48}H_{47}N_5O_{11}$
MW: 869,93

A solution of compound **88b** (170 mg, 0.24 mmol, 1 eq) in a mixture of dry THF (13 mL) and dry DMF (1 mL) under nitrogen atmosphere was cooled to 0 °C. Pyridine (50 µL, 0.60 mmol, 2.5 eq) and 4-nitrophenylchloroformate (97 mg, 0.48 mmol, 2 eq) were added, then the

mixture was allowed to reach room temperature and stirred for 2 h. AcOEt (140 mL) was added and the solution was washed with a 1 M aqueous solution of $KHSO_4$ (3 × 20 mL) and brine (20 mL). The organic phase was dried and concentrated, then the crude was purified by a Grace Reveleris system (column: Reveleris Silica 4 g, dry load, flow rate: 36 mL min^{-1}, ramp from 100% CH_2Cl_2 to 100% AcOEt in 18 min) to afford **89b** as a solid (185 mg, 88% yield).

R_f = 0.78 (93:7 CH_2Cl_2/MeOH); ^{1}H NMR (400 MHz, THF-d_8) δ 9.31 (s, 1H), 8.27 (d, J = 9.1 Hz, 2H), 8.27 (m, 1H), 7.77 (d, J = 7.5 Hz, 2H), 7.68 (d, J = 8.3 Hz, 2H), 7.60 (t, J = 8.2 Hz, 2H), 7.46 (d, J = 9.1 Hz, 2H), 7.42-7.30 (m, 4H), 7.26 (t, J = 7.4 Hz, 2H), 7.21-7.02 (m, 5H), 6.86 (m, 1H), 6.31 (s, 1H), 5.86 (ddt, J = 22.0, 10.6, 5.5 Hz, 1H), 5.24 (s, 2H), 5.21 (bd, J = 22.0 Hz, 1H), 5.06 (bd, J = 10.6 Hz, 1H), 4.43 (d, J = 5.5 Hz, 2H), 4.53-4.34 (m, 3H), 4.24 (dd, J = 9.9, 7.4 Hz, 1H), 4.17 (t, J = 7.4 Hz, 1H), 3.16-3.01 (m, 3H), 2.91 (dd, J = 13.8, 7.6 Hz, 1H), 1.90 (m, 1H), 1.63 (m, 1H), 1.53-1.43 (m, 2H), 1.43-1.33 ppm (m, 2H); ^{13}C NMR (101 MHz, THF-d_8) δ 171.9, 170.7, 156.8, 156.7, 153.1, 145.1, 142.1, 140.6, 138.3, 134.8, 130.6, 130.0, 128.7, 128.1, 127.6, 126.9, 125.9, 125.8, 125.7, 122.6, 120.4, 120.0, 116.4, 71.1, 67.0 (overlapped with solvent signal), 56.9, 54.3, 48.1, 41.1, 38.9, 32.5, 30.5, 23.6 ppm. MS (ESI) *m/z* calcd. for $[C_{48}H_{47}N_5NaO_{11}]^+$: 892.32 $[M+Na]^+$, found: 892.50.

Fmoc-Phe-Lys(Alloc)-*N*-[4-[[[(*N*-(Boc)-*N*,*N*'-dimethylethylenediamine)carbonyl]oxy]methyl]phenyl] (90b)

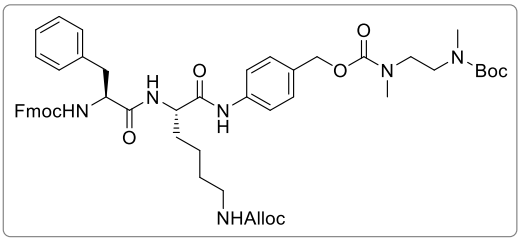

$C_{51}H_{62}N_6O_{10}$
MW: 919,09

A solution of *N*-(Boc)-*N*,*N'*-dimethylethylenediamine **86** (97 mg, 0.52 mmol, 2.5 eq) in dry THF (1 mL) and *i*Pr_2NEt (106 µL, 0.76 mmol, 3 eq) were added under nitrogen atmosphere to a solution of **89b** (180 mg, 0.21 mmol, 1 eq) in dry THF (9 mL) kept at 0 °C. The mixture was stirred overnight at room temperature, then the solvent was removed at rotavapor. AcOEt (100 mL) was added and the solution was washed with a 1 M aqueous solution of $KHSO_4$ (3 × 20 mL), a saturated aqueous solution of $NaHCO_3$ (2 × 20 mL) and brine (20 mL). The organic phase was dried and concentrated. The crude was purified over a pad of silica (gradient: 100% CH_2Cl_2 to 5% MeOH / 95% CH_2Cl_2), affording **90b** (140 mg, 75% yield).

R_f = 0.34 (95:5 CH_2Cl_2/MeOH); ^{1}H NMR (400 MHz, CD_2Cl_2) δ 8.61 (s, 1H), 7.76 (d, J = 7.5 Hz, 2H), 7.53 (dd, J = 14.8, 7.6 Hz, 4H), 7.39 (t, J = 7.5 Hz, 2H), 7.33-7.24 (m, 4H), 7.18 (d, J = 8.5 Hz, 5H), 6.90 (s, 1H), 5.86 (ddt, J = 17.0, 10.3, 5.8 Hz, 1H), 5.64 (s, 1H), 5.24 (d, J =

17.0 Hz, 1H), 5.14 (d, *J* = 10.3 Hz, 1H), 5.12-5.07 (m, *J* = 5.9 Hz, 1H), 5.04 (s, 2H), 4.58-4.46 (m, 4H), 4.42 (dd, *J* = 10.4, 6.8 Hz, 1H), 4.32 (dd, *J* = 10.4, 4.9 Hz, 1H), 4.16 (dd, $J_1 = J_2$ = 6.8 Hz, 1H), 3.43-3.26 (m, 4H), 3.20-3.07 (m, 3H), 3.02 (m, 1H), 2.91 (s, rotamer A + B, 3H), 2.84 (s, rotamer A, 3H), 2.74 (s, rotamer B, 3H), 1.93 (m, 1H), 1.68 (m, 1H), 1.53-1.44 (m, 2H), 1.42 (s, 9H), 1.39-1.29 ppm (m, 2H); ^{13}C NMR (101 MHz, CD_2Cl_2) *δ* 172.1, 169.9, 157.0, 156.9, 156.7, 156.3 (rotamer A), 155.7 (rotamer B), 144.2 (rotamer A), 144.1 (rotamer B), 141.7, 138.2, 136.6, 133.6, 133.3, 129.6, 129.1, 128.9, 128.1, 127.5, 125.4, 125.3, 120.3, 120.2, 117.4, 79.6 (rotamer A + B), 67.5, 67.0 (rotamer A), 66.7 (rotamer B), 65.8, 56.9, 54.3, 47.5, 47.0 (rotamer A + B), 46.8 (rotamer A + B), 40.49, 38.44, 35.5 (rotamer A + B), 35.1 (rotamer A), 34.7 (rotamer B), 31.2, 29.8, 28.5, 22.8 ppm. MS (ESI) *m/z* calcd. for $[C_{51}H_{62}N_6NaO_{10}]^+$: 941.44 $[M+Na]^+$, found: 941.70.

(Hemiglutarate)-Phe-Lys(Alloc)-*N*-[4-[[[(*N*-(Boc)-*N*,*N′*-dimethylethylenediamine)carbonyl]oxy]methyl]phenyl] (91b)

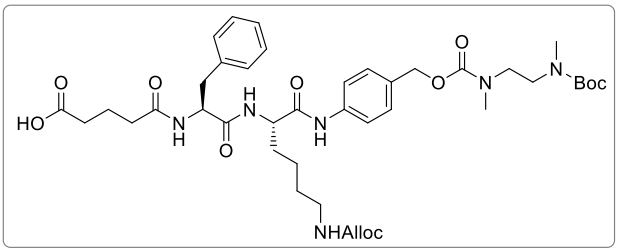

$C_{41}H_{58}N_6O_{11}$
MW: 810,95

Compound **90b** (135 mg, 0.15 mmol, 1 eq) was deprotected following the General Procedure GP2. The crude free amine was dissolved in dry DMF (2 mL) and cooled at 0 °C under nitrogen atmosphere. Glutaric anhydride (42 mg, 0.36 mmol, 2.5 eq), DMAP (5 mg, 0.04 mmol, 0.25 eq) and *i*Pr_2NEt (95 µL, 0.55 mmol, 3.75 eq) were added. The mixture was allowed to reach room temperature and stirred overnight. The solution was diluted with AcOEt (70 mL), washed with a 1 M aqueous solution of $KHSO_4$ (3 × 8 mL) and then with brine (8 mL). The organic phase was dried and concentrated, then the crude was purified by flash chromatography [gradient: 3% (MeOH + 0.2% CH_3COOH) / 97% (CH_2Cl_2 + 0.2% CH_3COOH) to 7% (MeOH + 0.2% CH_3COOH) / 93% (CH_2Cl_2 + 0.2% CH_3COOH)] affording **91b** (120 mg, quantitative yield).

^{1}H NMR (400 MHz, CD_3OD) *δ* 7.64-7.57 (m, 2H), 7.36 (d, *J* = 8.3 Hz, 2H), 7.30-7.19 (m, 4H), 7.15 (t, *J* = 6.9 Hz, 1H), 6.96 (t, *J* = 5.2 Hz, 1H), 5.92 (ddt, *J* = 17.3., 10.4, 5.3 Hz, 1H), 5.29 (dd, J = 17.3, 1.5 Hz, 1H), 5.17 (d, *J* = 10.4 Hz, 1H), 5.09 (s, 2H), 4.67 (dd, *J* = 9.2, 5.6 Hz, 1H), 4.51 (d, *J* = 5.3 Hz, 2H), 4.45 (dd, *J* = 8.7, 5.4 Hz, 1H), 3.48-3.37 (m, 4H), 3.18 (dd, *J* = 14.0, 5.6 Hz, 1H), 3.16-3.10 (m, 2H), 2.97 (s, rotamer A, 3H), 2.96 (s, rotamer B, 3H), 2.93 (dd, *J* = 14.0, 9.2 Hz, 1H), 2.88 (s, rotamer A, 3H), 2.78 (s, rotamer B, 3H), 2.26 (t, *J* = 7.2 Hz, 2H), 2.21 (t, *J* = 7.4 Hz, 2H), 1.93-1.74 (m, 2H), 1.86-1.77 (m, 2H), 1.60-1.50 (m, 2H),

1.45 (s, 9H), 1.48-1.41 ppm (m, 2H); ^{13}C NMR (101 MHz, CD_3OD) δ 176.8, 175.2, 173.6, 172.1, 158.6, 158.0 (rotamer A), 157.8 (rotamer B), 157.4 (rotamer A), 157.3 (rotamer B), 139.4 (rotamer A), 139.2 (rotamer B), 138.1, 134.3, 133.7, 133.6, 130.2, 129.9, 129.6, 129.3, 127.7, 121.2, 117.4, 81.1 (rotamer A), 80.9 (rotamer B), 68.1 (rotamer A), 67.9 (rotamer B), 66.2, 55.9, 55.2, 47.9 (rotamer A), 47.5 (rotamer B), 47.3 (rotamer A), 46.8 (rotamer B), 41.3, 38.7, 35.7 (rotamer A), 35.4 (rotamer B), 34.9 (rotamer A), 34.7 (rotamer B), 34.0, 32.7, 30.3, 28.7, 23.9, 22.0 ppm.

(*N*-hydroxysuccinimidylglutarate)-Phe-Lys(Alloc)-*N*-[4-[[[(*N*-(Boc)-*N*,*N'*-dimethylethylenediamine)carbonyl]oxy]methyl]phenyl] (91b-OSu)

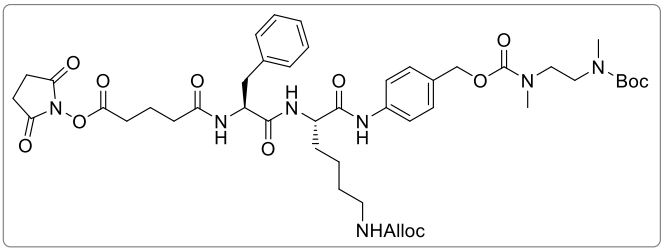

$C_{45}H_{61}N_7O_{13}$
MW: 908,02

A stock solution of NHS (solution A, 25 mg in 1 mL dry DMF) and one of EDC·HCl (solution B, 25 mg in 1 mL dry DMF) were prepared under nitrogen atmosphere. Compound **91b** (25 mg, 3.1×10^{-2} mmol, 1 eq) was dissolved in dry DMF (508 µL) and cooled at 0 °C under nitrogen atmosphere. Solution A (184 µL, 1.3 eq) and solution B (308 µL, 1.3 eq) were added to the substrate solution. The mixture was allowed to reach room temperature and stirred overnight. The solution was diluted with AcOEt (70 mL) and washed with water (3×10 mL). The organic phase was dried and concentrated, then the crude was purified by flash chromatography (eluent: 100% AcOEt), affording **91b-OSu** (26 mg, 93% yield).

R_f = 0.67 (9:1 CH_2Cl_2/MeOH); MS (ESI) *m/z* calcd. for $[C_{45}H_{61}N_7NaO_{13}]^+$: 930.42 $[M+Na]^+$, found: 930.51.

cyclo[DKP-RGD]-Phe-Lys(Alloc)-_N_-[4-[[[(_N_,_N_′-dimethylethylenediamine)carbonyl]oxy]methyl]phenyl] (92b)

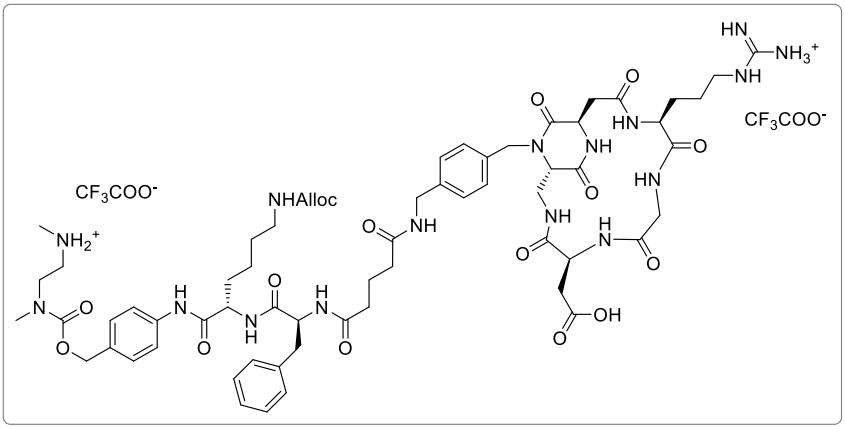

$C_{63}H_{86}N_{16}O_{16}$
MW: 1323,48 + 2TFA

cyclo[DKP-RGD]-CH_2NH_2 **70** (17 mg, 2.1 × 10^{-2} mmol, 1 eq) was dissolved in pH 7.5 phosphate buffer solution (1,5 mL). The pH was adjusted to 7.5 with a 0.2 M NaOH solution (a few drops) and the solution was then cooled to 0 °C. Compound **91b-OSu** (23 mg, 2.1 × 10^{-2} mmol, 1.2 eq) was dissolved in CH_3CN (2 mL) and added to the substrate solution. The mixture was warmed to room temperature and stirred overnight. During the first 3 h the pH value was kept near 7.3 adding 0.2 M aqueous NaOH when necessary. After 4 h a white precipitate was observed. The solvent was removed, then the crude was treated with H_2O + 0.1% CH_3COOH and centrifuged. This procedure was repeated three times, in order to remove the hydrophilic fraction from the crude. The Boc protecting group was then removed following General Procedure GP1 and the crude was purified by semipreparative-HPLC [Waters Atlantis 21 mm × 10 cm column, gradient: 100% (H_2O + 0.1% CF_3COOH) to 50% (H_2O + 0.1% CF_3COOH) / 50% (CH_3CN + 0.1% CF_3COOH) in 8 min; t_R (product): 6.3 min]. The purified product was then freeze dried to give the desired compound **92b** as a white solid (18 mg, 55% yield over two steps).

^{1}H NMR (400 MHz, CD_3OD) δ 7.58 (d, J = 8.5 Hz, 2H), 7.35 (d, J = 8.4 Hz, 2H), 7.30-7.16 (m, 7H), 7.16-7.10 (m, 2H), 5.89 (ddt, J = 22.4, 10.6, 5.4 Hz, 1H), 5.26 (d, J = 17.3 Hz, 1H), 5.19-5.11 (m, 2H), 5.11 (s, 2H), 4.93 (m, 1H), 4.63 (dd, J = 9.3, 5.5 Hz, 1H), 4.59 (dd, J = 9.7, 3.8 Hz, 1H), 4.48 (d, J = 5.2 Hz, 2H), 4.45-4.41 (m, 2H), 4.34 (d, J = 15.2 Hz, 1H), 4.29 (d, J = 15.2 Hz, 1H), 3.97 (d, J = 14.3 Hz, 1H), 3.96 (d, J = 14.9 Hz, 1H), 3.93-3.87 (m, 2H), 3.62 (t, J = 5.8 Hz, 2H), 3.52 (d, J = 17.2 Hz, 1H), 3.49 (dd, J = 15.6, 6.0 Hz, 1H), 3.26-3.13 (m, 5H), 3.09 (t, J = 6.7 Hz, 2H), 2.97 (s, 3H), 2.96 (dd, J = 16.9, 10.4 Hz, 1H), 2.91 (m, 1H), 2.82-2.65 (m, 4H), 2.57 (dd, J = 16.9, 5.8 Hz, 1H), 2.51 (dd, J = 13.5, 3.8 Hz, 1H), 2.22 (t, J = 6.8 Hz, 2H), 2.16 (t, J = 7.4 Hz, 2H), 2.12 (m, 1H), 1.97 (m, 1H), 1.89-1.80 (m, 3H), 1.80-1.58 (m, 3H), 1.56-1.47 (m, 2H), 1.45-1.32 ppm (m, 2H); ^{13}C NMR (101 MHz, CD_3OD) δ 175.5, 175.3, 173.9, 173.5, 172.4, 172.0, 171.6, 170.9, 161.3, 158.8, 158.7, 140.2, 138.4, 135.8,

134.6, 133.7, 130.3, 129.8, 129.5, 129.2, 127.8, 121.4, 117.4, 68.5, 66.3, 60.3, 56.3, 56.0, 55.4, 53.2, 50.3, 48.7 (overlapped with solvent signal), 48.2, 46.8, 43.7, 43.6, 42.2, 41.5, 39.7, 38.9, 38.6, 36.0, 35.8, 35.6, 34.9, 34.0, 32.8, 30.5, 27.4, 27.1, 24.1, 23.0 ppm. MS (ESI) *m/z* calcd. for $[C_{63}H_{87}N_{15}O_{16}]^+$: 1323.65 $[M+H]^+$, found: 1324.7, MS (ESI) *m/z* calcd. for $[C_{63}H_{88}N_{15}O_{16}]^{2+}$: 662.33 $[M+2H]^{2+}$, found: 662.6.

***cyclo*[DKP-RGD]-Phe-Lys(Alloc)-PTX (93)**

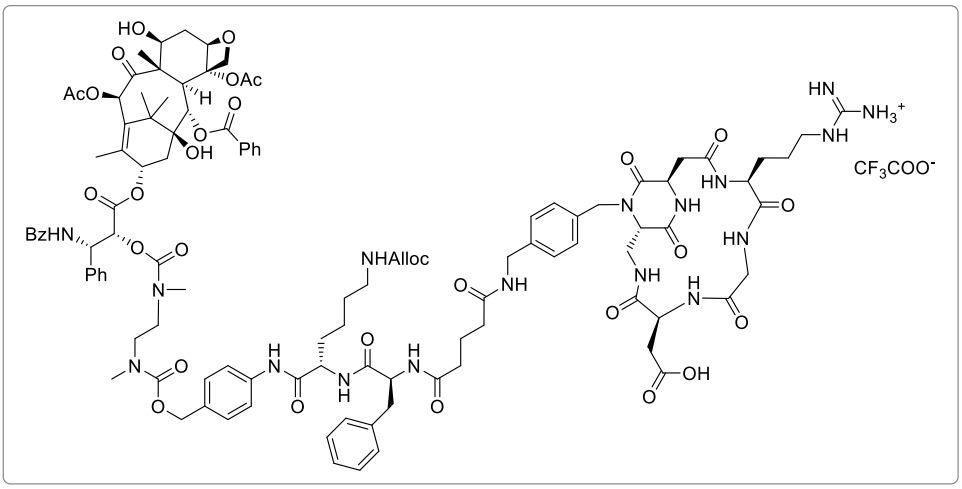

$C_{111}H_{135}N_{17}O_{31}$
MW: 2203,39 + TFA

Compound **92b** (10 mg, 6.5 × 10^{-3} mmol, 1 eq) was dissolved in dry DMF (100 µl) under nitrogen atmosphere the obtained solution was cooled to 0 °C. 2'-(4-nitrophenoxycarbonyl)-paclitaxel **83** (20 mg, 19.4 × 10^{-3} mmol, 3 eq) was dissolved in dry DMF (900 µL) and added to the substrate solution, followed by *i*Pr_2NEt (6 µL, 32.1 × 10^{-3} mmol, 5 eq). The mixture was allowed to reach room temperature and stirred overnight. The solution was diluted with Et_2O and the obtained white solid was recovered by centrifugation. This procedure was repeated three times, then the crude was purified by semipreparative-HPLC [Waters Atlantis 21 mm × 10 cm column, gradient: 90% (H_2O + 0.1% CF_3COOH) / 10% (CH_3CN + 0.1% CF_3COOH) to 100% (CH_3CN + 0.1% CF_3COOH) in 11 min; t_R (product): 7 min]. The purified product was then freeze dried to give the desired compound **93** as a white solid (12 mg, 80% yield).

^{1}H NMR (400 MHz, CD_3OD) δ 8.15 (dt, *J* = 15.2, 8.4 Hz, 2H), 7.88-7.77 (m, 2H), 7.66 (m, 1H), 7.62-7.47 (m, 6H), 7.39 (ddd, *J* = 24.1, 15.4, 7.8 Hz, 6H), 7.29-7.07 (m, 11H), 6.46 (d, *J* = 2.8 Hz, 1H), 6.11 (m, 1H), 5.99 (d, *J* = 4.7 Hz, 1H), 5.88 (ddt, *J* = 22.4, 10.6, 5.3 Hz, 1H), 5.81 (d, *J* = 6.7 Hz, 1H), 5.64 (m, 1H), 5.46 (d, *J* = 4.8 Hz, 1H), 5.34 (m, 1H), 5.25 (d, *J* = 17.1 Hz, 1H), 5.18-5.09 (m, 2H), 5.07-4.96 (m, 3H), 4.95 (dd, *J* = 8.7, 5.7 Hz, 1H), 4.80 (d, *J* = 13.0 Hz, 1H), 4.76 (d, *J* = 12.7 Hz, 1H), 4.64 (dd, *J* = 8.6, 5.7 Hz, 1H), 4.58 (dd, *J* = 9.9, 3.5 Hz, 1H), 4.52-4.39 (m, 4H), 4.33 (m, 1H), 4.20 (s, rotamer A, 2H), 4.18 (s, rotamer B, 2H), 4.06-3.84 (m, 4H), 3.83 (dd, *J* = 17.6, 7.6 Hz, 1H), 3.71 (m, 1H), 3.57-3.44 (m, 2H), 3.21 (t, *J* = 7.0 Hz, 2H), 3.16 (dd, *J* = 13.8, 4.9 Hz, 1H), 3.12 (m, 1H), 3.08 (t, *J* = 5.8 Hz, 2H), 2.98 (m,

1H), 2.98-2.79 (NMe rotamers, 6H), 2.88-2.72 (m, 2H), 2.61-2.52 (m, 3H), 2.49 (s, rotamer A, 3H), 2.38 (s, rotamer B, 3H), 2.24-2.08 (m, 8H), 2.02-1.93 (m, 4H), 1.88-1.76 (m, 4H), 1.74-1.67 (m, 3H), 1.65 (d, J = 6.8 Hz, 3H), 1.55-1.45 (m, 2H), 1.43-1.31 (m, 2H), 1.29 (bs, J = 9.0 Hz, 2H), 1.13 ppm (bs, 6H); ^{13}C NMR (101 MHz, CD_3OD) δ 205.3, 175.5, 175.2, 173.9, 173.5, 172.3, 172.1, 171.6, 171.4, 171.0, 170.8, 167.7, 161.5, 161.2, 158.6, 158.3, 157.9, 156.6, 142.9, 142.5, 140.2, 139.3, 138.4, 135.8, 134.6, 132.9, 131.4, 131.2, 130.3, 130.1, 129.7, 129.6, 129.5, 129.3, 128.9, 128.8, 128.6, 128.2, 127.8, 121.3, 117.4, 85.9, 82.2, 79.1, 77.5, 77.0, 76.8, 76.3, 72.9, 72.4, 66.3, 60.2, 59.2, 56.2, 56.0, 55.3, 53.1, 50.2, 48.2 (overlapped with solvent signal), 47.7, 44.6, 43.7, 43.6, 42.2, 41.5, 39.6, 38.7, 38.6, 37.5, 36.0, 35.8, 35.6, 35.4, 34.9, 34.8, 32.9, 30.7, 30.5, 27.4, 27.1, 27.0, 24.1, 23.3, 23.0, 22.4, 20.9, 15.2, 10.5 ppm. MS (ESI) *m/z* calcd. for $[C_{111}H_{137}N_{17}O_{31}]^{2+}$: 1101.99 $[M+2H]^{2+}$, found: 1102.05; MS (ESI) *m/z* calcd. for $[C_{111}H_{136}N_{17}NaO_{31}]^{2+}$: 1112.95 $[M+H+Na]^{2+}$, found: 1113.04.

***cyclo*[DKP-RGD]-Phe-Lys-PTX (81)**

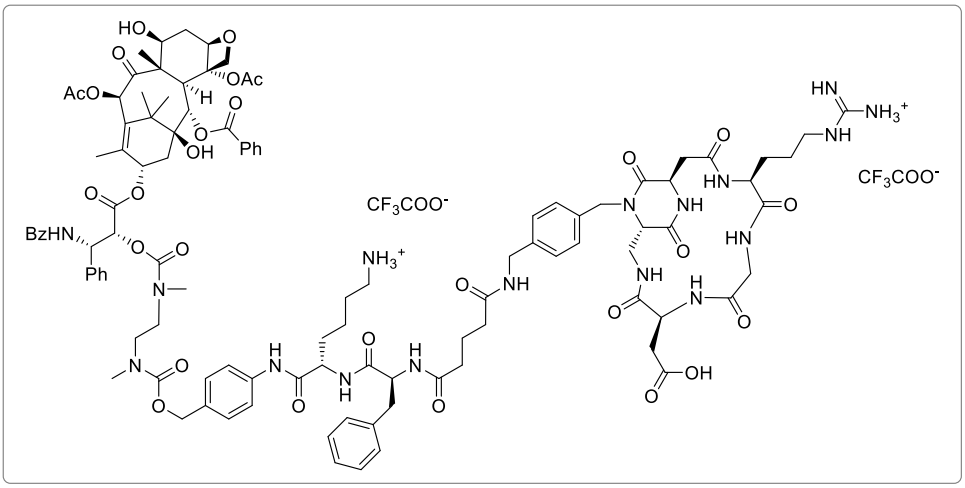

$C_{107}H_{131}N_{17}O_{29}$
MW: 2119,32 + 2TFA

A cleavage cocktail composed by Bu_3SnH (88 µl) and CH_3COOH (44 µL) in dry DMF (5 mL) was prepared in a flame-dried flask, equipped with 4 Å molecular sieves. Compound **93** (5 mg, 2.2×10^{-3} mmol, 1 eq) was dissolved with 500 µL of the cleavage cocktail under nitrogen atmosphere, then $Pd(PPh_3)_4$ (0.5 mg, 4.3×10^{-4} mmol, 0.2 eq) was added. The mixture was stirred overnight at room temperature, then it was diluted with Et_2O (5 mL), and the white solid was recovered by centrifugation. This procedure was repeated three times, then the obtained white solid was purified by semipreparative-HPLC [multistep gradient: from 0 min to 1 min 90% (H_2O + 0.1% CF_3COOH) / 10% (CH_3CN + 0.1% CF_3COOH); ramp to 100% (CH_3CN + 0.1% CF_3COOH) in 10 min; t_R (product): 6.7 min]. The purified product was then freeze-dried to give the desired compound **81** as a white solid (4,4 mg, 87% yield).
MS (ESI) *m/z* calcd. for $[C_{107}H_{133}N_{17}O_{29}]^{2+}$: 1059.97 $[M+2H]^{2+}$; found: 1060.18; MS (ESI) *m/z* calcd. $[C_{107}H_{132}N_{17}NaO_{29}]^{2+}$: 1070.97 $[M+H+Na]^{2+}$; found: 1071.20; MS (MALDI) *m/z* calcd for

$[C_{107}H_{132}N_{17}O_{29}]^+$: 2120.29 a.m.u. $[M+H]^+$; found: 2120.2 (HCCA matrix), 2120.2 (SIN matrix). HRMS (ESI+): *m/z* calcd. for $[C_{107}H_{132}N_{17}O_{29}]^+$: 2118.9371 $[M+H]^+$; found: 2118.9368; *m/z* calcd. for $[C_{107}H_{133}N_{17}O_{29}]^{2+}$: 1059.9722 $[M+H]^+$; found: 1059.9729.

"uncleavable" cyclo[DKP-RGD]-PTX (**82**)

***N*-(Boc)-*N'*-(glutaryl)-*N*,*N'*-dimethylethylenediamine (Boc-94)**

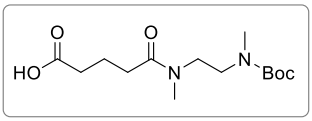

$C_{14}H_{26}N_2O_5$
MW: 302,37

A solution of glutaric anhydride (80 mg, 0.70 mmol, 1 eq) in DMF (2 mL) was cooled to 0 °C, then a solution of *N*-(Boc)-*N,N'*-dimethylethylenediamine (**86**, 198 mg, 1.05 mmol, 1.5 eq) in DMF (1 mL) and *i*Pr_2NEt (240 µL, 1.40 mmol, 2 eq) were added. The mixture was allowed to reach room temperature and stirred for 6 h. The mixture was diluted with AcOEt (70 mL), washed with a 1 M aqueous solution of $KHSO_4$ (4 × 10 mL) and brine (10 mL). The organic phase was dried and concentrated under vacuum affording **Boc-94** as a pale-yellow oil (207 mg, quantitative yield).

^{1}H NMR (400 MHz, CD_3OD) *δ* 3.53 (t, *J* = 5.8 Hz, 2H), 3.44-3.35 (m, 2H), 3.06 (s, NMe^1 rotamer A, 3H), 2.94 (s, NMe^1 rotamer B 3H), 2.87 (bs, NMe^2 3H), 2.43 (t, *J* = 7.4 Hz, 2H), 2.36 (dt, *J* = 7.2, 2.5 Hz, 2H), 1.94-1.83 (m, 2H), 1.46 ppm (s, 9H); ^{13}C NMR (101 MHz, CD_3OD) *δ* 176.9, 175.0 (rotamer A), 174.8 (rotamer B), 157.5 (rotamer A), 157.3 (rotamer B), 81.2 (rotamer A), 80.9 (rotamer B), 48.8 (overlapped with solvent signal), 48.5 (overlapped with solvent signal), 48.2, 47.8, 47.3, 46.8, 46.7, 46.25 (8 CH_2 rotamers), 36.9, 36.6, 36.3, 35.9, 35.1, 34.8, 34.6, 34.3 (8 NMe rotamers), 34.1 (rotamer A), 34.0 (rotamer B), 33.5 (rotamer A), 32.6 (rotamer B), 28.7, 21.8 (rotamer A), 21.5 ppm (rotamer B).

***N*-[carbonyl(2'-paclitaxel)]-*N'*-(glutaryl)-*N*,*N'*-dimethylethylenediamine (95)**

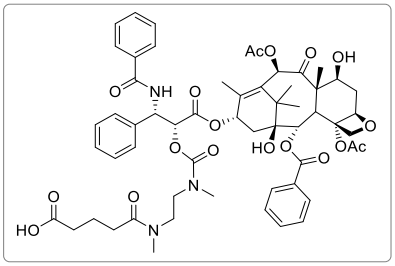

$C_{57}H_{67}N_3O_{18}$
MW: 1082,17

Compound **Boc-94** (75 mg, 0.25 mmol, 3 eq) was deprotected following the General Procedure GP1. The obtained oily product was dissolved in dry DMF (1 mL) and added dropwise under nitrogen atmosphere to a solution of 2'-(4-nitrophenoxycarbonyl)-paclitaxel (**83**, 84 mg, 0.08 mmol, 1 eq) in dry DMF (2 mL), previously cooled to 0 °C. The mixture was

allowed to reach room temperature and it was stirred overnight under nitrogen atmosphere. The solution was diluted with AcOEt (100 mL), washed with a 1 M aqueous solution of $KHSO_4$ (2 × 10 mL) and brine (10 mL). The organic phase was dried and concentrated. The crude was purified by flash chromatography (eluent: CH_2Cl_2/MeOH, 94:6 + 0,1% formic acid) affording compound **95** as a white foam (73 mg, 82% yield).

^{1}H NMR (400 MHz, CD_2Cl_2) δ 8.90 (d, J = 9.7 Hz, 1H), 8.17 (d, J = 7.2 Hz, rotamer A, 2H), 8.11 (d, J = 7.2 Hz, rotamer B, 2H), 7.82 (d, J = 7.4 Hz, rotamer A, 2H), 7.76 (d, J = 7.4 Hz, rotamer B, 2H), 7.62 (m, 1H), 7.52 (m, 4H), 7.46-7.35 (m, 3H), 7.33-7.25 (m, 3H), 6.28 (s, 1H), 6.24 (m, 1H), 6.16 (dd, J = 9.7, 2.9 Hz, 1H), 5.66 (d, J = 7.1 Hz, 1H), 5.40 (d, J = 2.9 Hz, 1H), 5.00 (m, 1H), 4.45 (dd, J = 10.9, 6.7 Hz, 1H), 4.29 (d, J = 8.3 Hz, 1H), 4.20 (d, J = 8.3 Hz, 1H), 3.94 (m, 1H), 3.82 (d, J = 7.1 Hz, 1H), 3.52 (m, 1H), 3.38 (m, 1H), 3.01 (m, 1H), 2.95 (s, rotamer A 3H), 2.92 (s, rotamer B, 3H), 2.89 (s, rotamer B, 1H), 2.88 (s, rotamer A, 3H), 2.58 (s, 3H), 2.49 (m, 1H), 2.35-2.12 (m, 6H), 2.20 (s, 3H), 1.94 (s, J = 10.5 Hz, 3H), 1.90-1.74 (m, 2H), 1.64 (s, 3H), 1.63 (m, 1H), 1.64 (s, rotamer A, 3H), 1.62 (s, rotamer B, 3H), 1.21 (s, 3H), 1.11 ppm (s, 3H); ^{13}C NMR (101 MHz, CD_2Cl_2) δ 204.4, 176.6, 173.0, 171.8, 170.5, 169.4, 169.0, 167.1, 155.3, 143.6, 138.1, 134.7, 133.9, 133.0, 131.7, 130.6, 130.0, 129.1, 129.0, 128.4, 128.3, 127.3, 84.7, 81.3, 79.3, 76.7, 76.1, 76.1, 75.6, 72.6, 71.8, 58.8, 53.2, 46.8, 46.1, 46.1, 43.6, 36.9 (rotamer A), 36.7 (rotamer B), 36.1, 36.0, 35.8 (rotamer A), 34.8 (rotamer B), 33.1, 32.6, 27.0, 23.1, 22.5, 21.1, 20.3, 14.9, 9.9 ppm.

cyclo[DKP-RGD]-unc.-PTX (82)

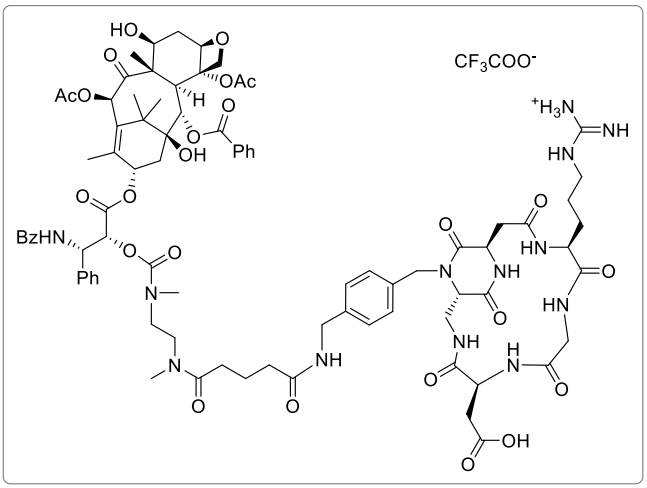

$C_{84}H_{103}N_{13}O_{25}$
MW: 1694,81 + TFA

DIC (3.8 µl, 2.4 × 10^{-2} mmol, 1.3 eq) and NHS (3 mg, 2.6 × 10^{-2} mmol, 1.4 eq) were added to a solution of compound **95** (24 mg, 2.2 × 10^{-2} mmol, 1.2 eq) in dry DMF (1 mL). The resulting mixture was stirred overnight under nitrogen. Volatiles were removed *in vacuo* to give an off-white solid, which was re-dissolved in acetonitrile (1 mL) and cooled to 0 °C. A solution of *cyclo*[DKP-RGD]-CH_2NH_2 **70** (16 mg, 1.9 × 10^{-2} mmol, 1 eq) in pH 7.5 PBS (1 mL) was then

added to the acetonitrile solution. The resulting solution was warmed to room temperature and stirred overnight. During the first 5 hours the pH value was kept within the range 7.3-7.6 adding 0.2 M aqueous NaOH, when necessary. The solution was concentrated and the crude was purified by semipreparative-HPLC [Waters Atlantis 21 mm × 10 cm column, gradient: 90% (H_2O + 0.1% CF_3COOH) / 10% (CH_3CN + 0.1% CF_3COOH) to 25% (H_2O + 0.1% CF_3COOH) / 75% (CH_3CN + 0.1% CF_3COOH) in 12 min; t_R (product): 8.8 min]. The purified product was then freeze dried to give the desired compound **82** as a white solid (17 mg, 50% yield).

^{1}H NMR (400 MHz, CD_3OD) δ 8.18-8.07 (m, 2H), 7.83 (d, *J* = 7.2 Hz, 1H), 7.78 (d, *J* = 7.5 Hz, 1H), 7.67 (m, 1H), 7.64-7.36 (m, 9H), 7.35-7.20 (m, 5H), 6.44 (d, *J* = 8.7 Hz, 1H), 6.08 (m, 1H), 5.94 (d, *J* = 5.5 Hz, 1H), 5.80 (t, *J* = 7.7 Hz, 1H), 5.64 (m, 1H), 5.42 (d, *J* = 5.6 Hz, 1H), 5.31 (d, *J* = 7.2 Hz, 1H), 5.13 (dd, J = 15.0, 8.1 Hz, 1H), 5.00 (t, *J* = 9.3 Hz, 1H), 4.92 (m, 1H), 4.57 (d, *J* = 9.6 Hz, 1H), 4.48-4.29 (m, 3H), 4.24-4.12 (m, 3H), 4.01-3.86 (m, 4H), 3.81 (dd, *J* = 18.2, 7.4 Hz, 1H), 3.74-3.63 (m, 2H), 3.66 (s, 2H), 3.62-3.42 (m, 6H), 3.22 (t, *J* = 7.0 Hz, 2H), 3.01-2.84 (m, 6H), 2.72 (m, 1H), 2.56 (dd, *J* = 17.2, 5.7 Hz, 1H), 2.53-2.44 (m, 2H), 2.46 (s, rotamer A, 3H), 2.36 (s, rotamer A, 3H), 2.34-2.17 (m, 4H), 2.16 (s, rotamer A, 3H), 2.14 (s, rotamer B, 3H), 2.14 (m, 1H), 1.98 (m, 1H), 1.96 (s, rotamer A, 3H), 1.94 (s, rotamer B, 3H), 1.89-1.68 (m, 6H), 1.66 (s, rotamer A, 3H), 1.65 (s, rotamer B, 3H), 1.13 (s, rotamer A, 3H), 1.11 ppm (s, rotamer B, 3H); ^{13}C NMR (101 MHz, CD_3OD) δ 205.3, 175.4, 175.3, 174.9, 173.9, 173.8, 173.4, 172.0, 171.6, 171.6, 171.4, 171.0, 167.7, 158.7, 156.7, 156.4, 142.6, 140.4, 138.5, 135.8, 134.8, 134.8, 134.6, 132.9, 131.4, 131.2, 130.1, 129.7, 129.6, 129.5, 129.3, 128.9, 128.8, 128.6, 128.4, 85.9, 82.2, 79.1, 77.5, 77.1, 76.9, 76.3, 72.9, 72.8, 72.4, 60.2, 56.0, 53.1, 50.2, 48.2, 47.9, 47.0, 44.6, 43.7, 43.6, 42.2, 39.6, 38.6, 37.6, 36.7, 36.2, 35.7, 35.6, 34.8, 33.4, 27.5, 27.1, 27.0, 23.3, 22.5, 22.4, 20.8, 15.2, 15.0, 10.5 ppm. MS (ESI) *m/z* calcd. for $[C_{84}H_{104}N_{13}O_{25}]^+$: 1694.73 $[M+H]^+$; found: 1695.48; MS (ESI) *m/z* calcd. for $[C_{84}H_{105}N_{13}O_{25}]^{2+}$: 847.87 $[M+2H]^{2+}$; found: 848.23. HRMS (ESI+): *m/z* calcd. for $[C_{84}H_{104}N_{13}O_{25}]^+$: 1694.7261 $[M+H]^+$; found: 1694.7302; *m/z* calcd. for $[C_{84}H_{105}N_{13}O_{25}]^{2+}$: 847.8667 $[M+2H]^{2+}$; found: 847.8676.

[cyclo(DKP-RGD)]$_2$Val-Ala-PTX (**100**)

methyl 3,5-bis(propynyloxy)phenyl acetate (104)

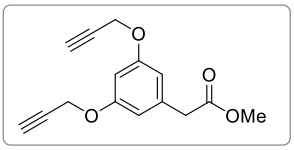

$C_{15}H_{14}O_4$
MW: 258,27

Methyl 3,5-hydroxyphenyl acetate (250 mg, 1.37 mmol, 1 eq) was dissolved in dry acetone (11 mL) under nitrogen atmosphere. The solution was cooled in an ice bath. Propargyl bromide (945 µL, 11.0 mmol, 8 eq) and K_2CO_3 (1.5 g, 11.0 mmol, 8 eq) were added, and the mixture was stirred at room temperature 72 h. The mixture was concentrated, then the crude was dissolved in AcOEt (70 mL) and washed with water (3 × 10 mL). The organic phase was dried over Na_2SO_4 and concentrated. The crude residue was purified by a Grace Reveleris system (column: Reveleris Silica 12 g; dry load; flow rate: 30 mL min^{-1}; ramp: from 100% hexane to 100% AcOEt in 18 min) to afford **104** as a white solid (356 mg, yield: quantitative).
R_f = 0.58 (1:1 hexane/AcOEt); ^{1}H NMR (400 MHz, $CDCl_3$) δ 6.53 (bs, 3H), 4.65 (d, J = 2.4 Hz, 4H), 3.68 (s, 3H), 3.56 (s, 2H), 2.53 ppm (t, J = 2.4 Hz, 2H); ^{13}C NMR (101 MHz, $CDCl_3$) δ 171.6, 158.7, 136.2, 109.1, 101.0, 78.4, 75.8, 55.9, 52.2, 41.4 ppm.

3,5-bis(propynyloxy)phenyl acetic acid (105)

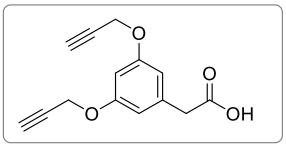

$C_{14}H_{12}O_4$
MW: 244,25

Compound **104** (165 mg, 0.64 mmol, 1 eq) was dissolved in THF (20 mL) under a nitrogen atmosphere. The solution was cooled to 0 °C, then a solution of $LiOH{\cdot}H_2O$ (67 mg, 1.6 mmol, 2.5 eq) in H_2O (10 mL) was added. The mixture was stirred 1,5 h at 0 °C. The mixture was acidified to ca. pH = 2 with a 1 M $KHSO_4$ aqueous solution and extracted with CH_2Cl_2 (4 × 20 mL). The organic phase was dried over Na_2SO_4 and concentrated, affording **105** as a white solid (158 mg, quantitative yield).
R_f = 0.36 (1:1 hexane/AcOEt); ^{1}H NMR (400 MHz, MeOD) δ 6.59-6.51 (m, 3H), 4.70 (d, J = 2.4 Hz, 4H), 3.54 (s, 2H), 2.92 ppm (t, J = 2.4 Hz, 2H).

[3,5-bis(propynyloxy)phenylacetyl]-Val–Ala-*N*-[4-[[[(N-(Boc)-*N*,*N*'-dimethylethylenediamine) carbonyl]oxy]methyl]phenyl] (106)

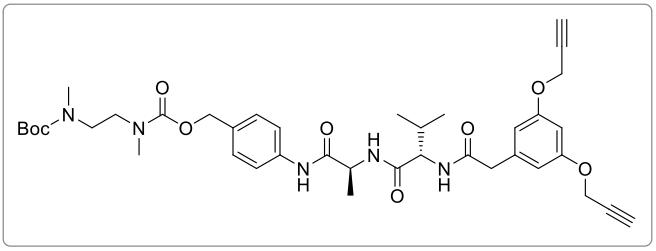

$C_{39}H_{51}N_5O_9$
MW: 733,86

N-Fmoc-protected compound **90a** (160 mg, 0.219 mmol, 1 eq) was dissolved in DMF under a nitrogen atmosphere. The solution was cooled to 0 °C and piperidine (108 µL, 1.1 mmol, 5 eq) was added. The reaction was stirred at room temperature for 2 h. The mixture was diluted with AcOEt (20 × volume of DMF) and washed twice with a saturated aqueous solution of $NaHCO_3$. The organic phase was dried over Na_2SO_4 and concentrated at rotavapor. CH_2Cl_2 was added to the residue and evaporated to afford a yellow solid. The crude was filtered over silica gel [gradient: from 1:1 AcOEt/hexane to 9:1 CH_2Cl_2/MeOH; R_f = 0.2 (9:1 CH_2Cl_2/MeOH)] affording **90a-NH** as a solid. A solution of acid **105** (68 mg, 0.28 mmol, 1.5 eq) in dry DMF (2.3 mL) was cooled to 0 °C under a nitrogen atmosphere. HATU (114 mg, 0.3 mmol, 1.6 eq), HOAT (41 mg, 0.3 mmol, 1.6 eq) and *i*Pr_2NEt (100 µL, 0.57 mmol, 3 eq) were added and the mixture was stirred for 20 min at 0 °C. A solution of **90a-NH** (96 mg, 0.19 mmol, 1 eq) in dry DMF (2.3 mL) was added to the stirred mixture. The reaction was allowed to slowly reach room temperature and stirred overnight. The mixture was diluted with a 4:1 AcOEt/CH_2Cl_2 mixture (100 mL) and washed with 1 M aqueous solution of $KHSO_4$ (2 × 15 mL), a saturated aqueous solution of $NaHCO_3$ (1 × 15 mL) and brine (1 × 20 mL). The organic phase was dried over Na_2SO_4 and concentrated. The solid was suspended in Et_2O. The product was collected by centrifugation and purified by flash chromatography [gradient: from 99:1 CH_2Cl_2/MeOH to 97:3 CH_2Cl_2/MeOH] to afford amide **106** as a white solid (101 mg, 58% o.t.s.).

R_f = 0.3 (100 % AcOEt); ^{1}H NMR (400 MHz, MeOD + DMSO-d_6) δ 7.57 (m, 2H), 7.32 (m, 2H), 6.60 (d, J = 2.2 Hz, 2H), 6.53 (t, J = 2.2 Hz, 1H), 5.06 (s, 2H), 4.70 (d, J = 2.4 Hz, 4H), 4.46 (q, J = 7.1 Hz, 1H), 4.20 (d, J = 7.2 Hz, 1H), 3.56 (s, 1H), 3.41 (m, 4H), 3.03 (t, J = 2.4 Hz, 2H), 2.95 (m, rotamer A+B, 3H), 2.85 (bs, rotamer A, 3H), 2.75 (bs, rotamer B, 3H), 2.11 (m, 1H), 1.42 (m, 12H), 0.99 (d, J = 7.0 Hz, 3H), 0.96 ppm (d, J = 6.9 Hz, 3H); ^{13}C NMR (101 MHz, MeOD + DMSO-d_6) δ 173.6, 173.3, 172.9, 160.2, 139.3, 130.0, 129.7, 121.0, 110.0, 101.8, 79.9, 77.2, 68.1, 67.9, 60.4, 56.7, 51.0, 43.6, 35.6, 35.3, 34.7, 31.9, 28.8, 19.8, 18.7, 18.1 ppm.

[3,5-bis(propynyloxy)phenylacetyl]-Val-Ala-PTX (101)

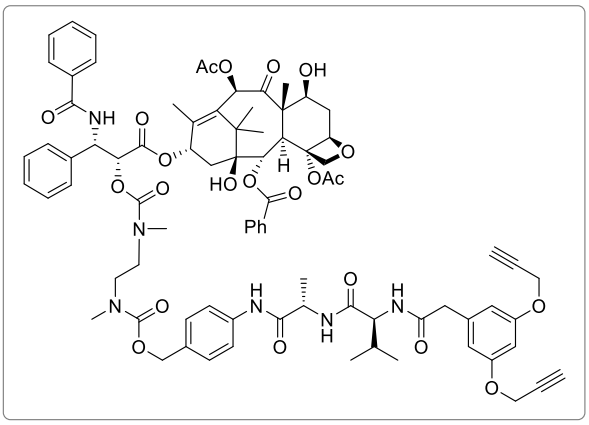

$C_{82}H_{92}N_6O_{22}$
MW: 1513,66

Compound **106** (75 mg, 0.1 mmol, 1 eq) was deprotected following the General Procedure GP1. The corresponding trifluoroacetate salt was dissolved in dry DMF (2 mL) and *i*Pr_2NEt (52 µL, 0.3 mmol, 3 eq). The resulting solution was added at 0 °C to a stirred solution of **83** (204 mg, 0.2 mmol, 2 eq) in dry DMF (1 mL), under a nitrogen atmosphere. The reaction was then allowed to reach room temperature and stirred overnight. AcOEt (100 mL) was added and the solution was washed with a 1 M aqueous solution of $KHSO_4$ (2 × 10 mL) and brine (1 × 15 mL). The organic phase was dried over Na_2SO_4 and concentrated, then the crude was purified by a Grace Reveleris system (column: Reveleris Silica HP 12 g, dry load, flow rate: 25 mL min^{-1}, ramp from 0% to 15% of MeOH in CH_2Cl_2 in 15 min) to afford carbamate **101** as a white solid (116 mg, 77% yield).

R_f = 0.22 (100 % AcOEt); ^{1}H NMR (500 MHz, DMSO-d_6) δ 9.94 (s, 1H), 9.20 (d, J = 8.8 Hz, rotamer A, 1H), 9.13 (d, J = 8.7 Hz, rotamer B, 1H), 8.23 (d, J = 6.7 Hz, 1H), 8.07 (d, J = 8.7 Hz, 1H), 7.98 (m, 2H), 7.84 (d, J = 7.6 Hz, 2H), 7.78 – 7.69 (m, 1H), 7.65 (m, 2H), 7.60 – 7.52 (m, 3H), 7.52 – 7.40 (m, 6H), 7.29 – 7.15 (m, 3H), 6.54 (d, J = 2.2 Hz, 2H), 6.49 (t, J = 2.2 Hz, 1H), 6.31 (s, 1H), 5.86 (m, rotamer A, 1H), 5.61 (m, rotamer B, 1H), 5.42 (d, J = 6.9 Hz, 1H), 5.27 (m, rotamer A, 1H), 5.17 (m, rotamer B,1H), 5.02 – 4.81 (m, 4H), 4.73 (d, J = 2.3 Hz, 4H), 4.60 (m, 1H), 4.40 (m, 1H), 4.21 (m, 1H), 4.11 (m, 1H), 4.07 – 3.97 (m, 2H), 3.59 (d, J = 4.3 Hz, 1H), 3.54 (t, J = 2.3 Hz, 1H), 3.45 (dd, J = 40.6, 13.8 Hz, 3H), 3.19 (m, 1H), 2.77 (m, 6H), 2.38 – 2.21 (m, 4H), 2.14 – 2.02 (m, 3H), 1.98 (dq, J = 13.5, 6.8 Hz, 1H), 1.89 – 1.77 (m, 4H), 1.63 (t, J = 11.7 Hz, 1H), 1.50 (s, 4H), 1.30 (d, J = 7.0 Hz, 3H), 1.24 (s, 1H), 1.08 – 0.98 (m, 6H), 0.85 ppm (dd, J = 15.8, 6.7 Hz, 6H); ^{13}C NMR (101 MHz, DMSO-d_6) δ 202.3, 171.0, 170.8, 169.8, 169.5, 168.7, 166.5, 166.3, 165.2, 158.1, 155.5, 155.2, 154.6, 154.6, 139.9, 139.7, 138.8, 138.6, 137.3, 134.4, 134.2, 133.4, 133.2, 133.1, 131.5, 131.4, 130.0, 129.7, 129.5, 128.6, 128.2, 128.1, 127.7, 127.3, 119.0, 108.7, 99.9, 83.6, 80.2, 79.1, 78.1, 76.8, 76.7, 75.5, 75.2, 74.7, 74.5, 70.5, 70.3, 66.0, 57.5, 57.3, 55.4, 54.0, 49.0, 46.3, 46.0, 42.9, 42.2, 36.5, 35.4, 34.8, 34.4, 33.9, 33.8, 30.6, 26.3, 22.4, 21.4, 20.6, 19.1, 18.1,

17.8, 13.8, 9.7 ppm; MS (ESI+) m/z calcd for $[C_{82}H_{92}N_6NaO_{22}]^+$: 1535.62 $(M+Na)^+$; found: 1535.89.

azido-tetraethylene glycol-*N*-hydroxysuccinimidyl ester (110):

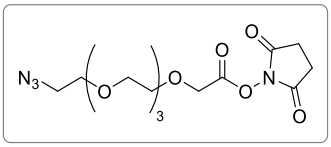

$C_{14}H_{22}N_4O_8$
MW: 374,35

Carboxylic acid **109** (77 mg, 0.28 mmol, 1 eq) was dissolved in dry THF and cooled to 0 °C under a nitrogen atmosphere. EDC·HCl (69 mg, 0.36 mmol, 1.3 eq) and NHS (41 mg, 0.36 mmol, 1.3 eq) were added and the mixture was allowed to reach room temperature and stirred overnight. The solvent was removed and the crude was purified over a pad of silica [eluent: 8:2 AcOEt/hexane] affording NHS-ester **110** (67 mg, 64% yield).
R_f = 0.43 (9:1 CH_2Cl_2/MeOH). MS (ESI+): *m/z* calcd for $[C_{14}H_{22}N_4NaO_8]^+$: 397.13, $[M+Na]^+$; found 397.19.

***cyclo*[DKP-RGD]-tetraethylene glycol-azide (102):**

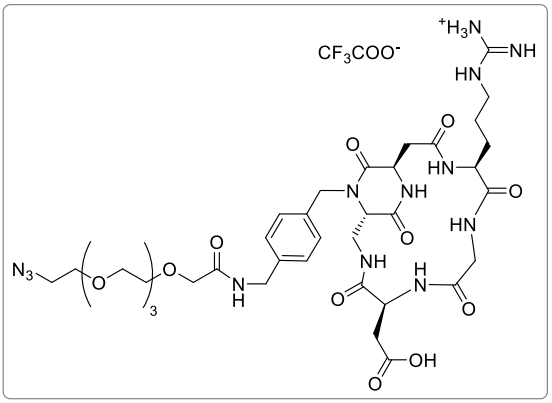

$C_{37}H_{55}N_{13}O_{13}$
MW: 889,93 + TFA

Ester **110** (17 mg, 4.5×10^{-2} mmol, 1.3 eq) was dissolved in acetonitrile (2 mL) under a nitrogen atmosphere and cooled to 0 °C. A solution of **70** (30 mg, 3.5×10^{-2} mmol, 1 eq) in PBS (1.5 mL; pH 7.5) was added to the acetonitrile solution, and the pH value was adjusted to 7.3-7.6 with NaOH (0.2 M). The resulting solution was warmed to room temperature and stirred overnight. During the first 5 h, the pH value was kept near to 7.3 by adding 0.2 M aqueous NaOH if necessary. The solution was concentrated, and the crude residue was purified by semipreparative HPLC [Waters Atlantis 21 mm × 10 cm column, flow: 9 mL min^{-1}, gradient: 90% (H_2O + 0.1% CF_3COOH) / 10% (CH_3CN + 0.1% CF_3COOH) to 55% (H_2O + 0.1% CF_3COOH) / 45% (CH_3CN + 0.1% CF_3COOH) in 10 min; t_R (product): 8.3 min]. The purified product was then freeze dried to give azide **102** as a white solid (27 mg, 77% yield).

^{1}H NMR (400 MHz, D_2O) δ 7.36 (d, J = 8.1 Hz, 2H), 7.32 (d, J = 8.2 Hz, 2H), 5.12 (d, J = 15.4 Hz, 1H), 4.90 (t, J = 7.1 Hz, 1H), 4.59 (dd, J = 7.9, 5.4 Hz, 1H), 4.48 (s, 2H), 4.34 (d, J = 17.1 Hz, 1H), 4.22 (dd, J = 9.6, 5.2 Hz, 1H), 4.19-4.11 (m, 4H), 4.01 (d, J = 14.6 Hz, 1H), 3.80-3.75 (m, 3H), 3.75-3.69 (m, 3H), 3.69–3.59 (m, 10H), 3.47-3.43 (m, 2H), 3.25 (t, J = 6.8 Hz, 2H), 3.01-2.88 (m, 2H), 2.81 (dd, J = 16.9, 7.1 Hz, 1H), 2.67 (dd, J = 14.0, 5.4 Hz, 1H), 2.08-1.97 (m, 1H), 1.90-1.78 (m, 1H), 1.77-1.60 ppm (m, 2H); ^{13}C NMR (101 MHz, D_2O) δ 174.1, 173.9, 173.1, 172.8, 172.7, 170.9, 170.1, 168.6, 156.8, 137.8, 134.1, 128.1, 127.8, 70.5, 69.5, 69.2, 59.3, 54.0, 52.1, 50.1, 49.4, 47.6, 42.5, 42.2, 40.6, 39.2, 38.0, 34.6, 25.8, 24.7 ppm; MS (ESI+) *m/z* calcd for $[C_{37}H_{56}N_{13}O_{13}]^+$: 890.41 $[M+H]^+$; found: 890.47; *m/z* calcd $[C_{37}H_{55}N_{13}NaO_{13}]^+$: 912.39 $[M+Na]^+$; found: 912.45.

[*cyclo*(DKP-RGD)]$_2$Val-Ala-PTX (100)

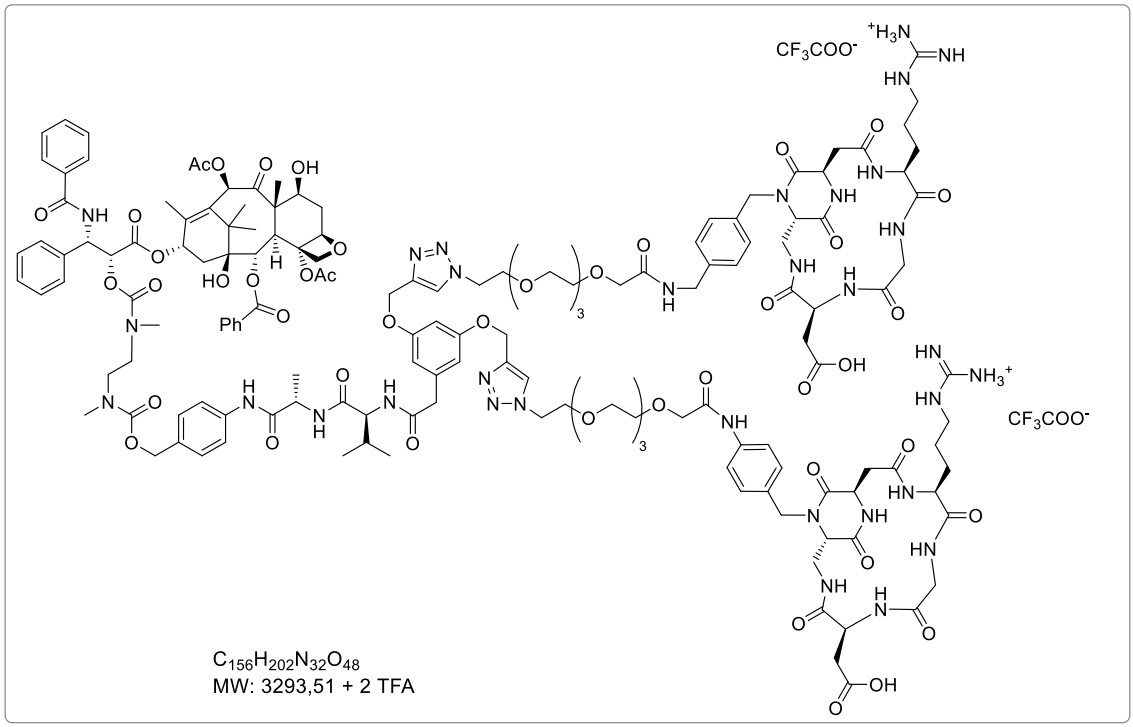

bis-alkyne **101** (5 mg, 33.2 × 10^{-3} mmol, 1 eq) and azide **102** (10 mg, 9.96 × 10^{-3} mmol, 3 eq) were dissolved in a degased 1:1 mixture of H_2O/DMF (400 µL) under a nitrogen atmosphere. Degased aqueous solutions of $CuSO_4 \cdot 5H_2O$ (0.017 M, 96 µL, 0.5 eq) and sodium ascorbate (0.03 M, 96 µL, 0.6 eq) were added in the darkness at room temperature and the mixture was stirred overnight. The solvent was removed under vacuum, and the crude residue was purified by semipreparative HPLC [Waters Atlantis 21 mm × 10 cm column; gradient: 90% (H_2O+0.1% CF_3COOH)/10% (CH_3CN+0.1% CF_3COOH) to 100% (CH_3CN+0.1% CF_3COOH) in 17 min; t_R (product) = 15.8 min]. The purified product was then freeze-dried to give the desired compound **100** as a white solid (11 mg, quantitative yield).

MS (ESI+): *m/z* calcd for $[C_{156}H_{204}N_{32}O_{48}]^{2+}$: 1646.73, $[M+2H]^{2+}$; found 1647.02; MS (ESI+): *m/z* calcd for $[C_{156}H_{203}N_{32}NaO_{48}]^{2+}$: 1657.72, $[M+H+Na]^{2+}$; found 1658.01; MS (MALDI): *m/z* calcd for $[C_{156}H_{203}N_{32}O_{48}]^{+}$: 3294,47 $[M+H]^{+}$; found: 3291 (HCCA matrix), 3294 (SIN matrix); HRMS (ESI+): *m/z* calcd for $[C_{156}H_{204}N_{32}O_{48}]^{2+}$: 1646.7248, $[M+2H]^{2+}$; found 1646.7260; *m/z* calcd for $[C_{156}H_{205}N_{32}O_{48}]^{3+}$ 1098.1523, $[M+3H]^{3+}$ found 1098.1475.

[*cyclo*(DKP-RGD)]$_1$Val-Ala-PTX (111)

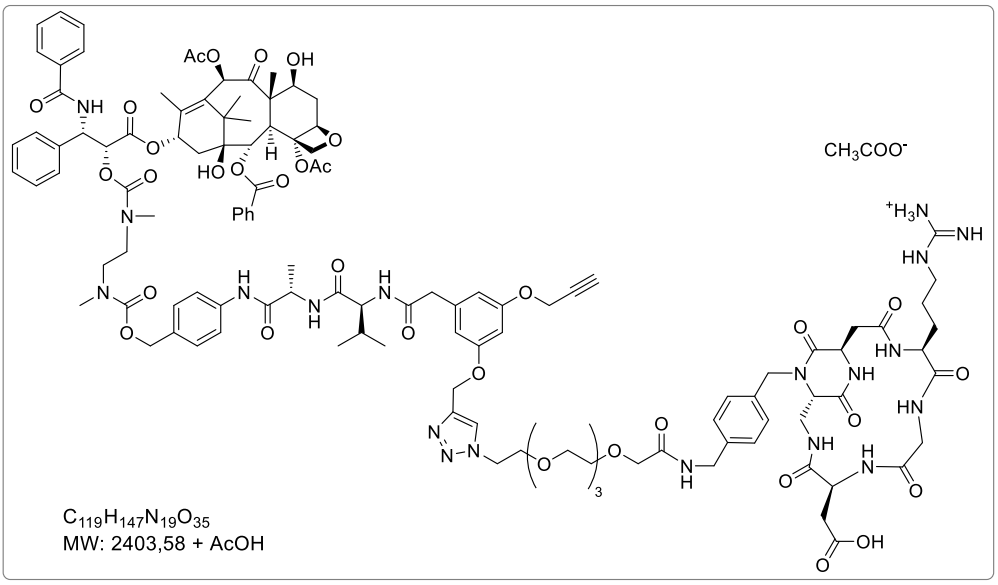

Bis-alkyne **101** (50 mg, 33.0×10^{-3} mmol, 4 eq) and azide **102** (10 mg, 9.9×10^{-3} mmol, 1 eq) were dissolved in a degased 2:1 H_2O/DMF mixture (3 mL) under a nitrogen atmosphere. $CuSO_4 \cdot 5H_2O$ (2.93 mg, 9.96×10^{-3} mmol, 1 eq) and sodium ascorbate (2.37 mg, 11.95×10^{-3} mmol, 1.2 eq) were added in the darkness at room temperature and the mixture was stirred overnight. The solvent was removed under vacuum, and the crude was treated with a 1:1 H_2O/CH_3CN mixture. The white solid residue (excess of alkyne **101**) was removed by centrifugation. The solution was concentrated and the crude was purified by semipreparative HPLC [Waters Atlantis 21 mm × 10 cm column, flow: 10 mL min^{-1}, gradient: 90% (H_2O + 0.1% CH_3COOH)/10% (CH_3CN + 0.1% CH_3COOH) to 100% (CH_3CN + 0.1% CH_3COOH) in 17 min; t_R (product): 11.1 min]. The purified product was then freeze dried to give conjugate **111** as a white solid (8.1 mg, 33% yield).

MS (ESI+) *m/z* calcd for $[C_{119}H_{148}N_{19}NaO_{35}]^{2+}$: 1213.02 $(M+H+Na)^{2+}$; found: 1213.32; *m/z* calcd for $[C_{119}H_{147}N_{19}Na_2O_{35}]^{2+}$: 1224.01 $(M+2Na)^{2+}$; found: 1224.34; MS (MALDI): *m/z* calcd for $[C_{119}H_{148}N_{19}O_{35}]^{+}$: 2404.55 $[M+H]^{+}$; found: 2404.2 (HCCA matrix), 2405.6 (SIN matrix); HRMS (ESI+): *m/z* calcd for $[C_{119}H_{148}N_{19}O_{35}]^{+}$: 2403.0380 $[M+H]^{+}$; found: 2403.0361; *m/z* calcd for $[C_{119}H_{149}N_{19}O_{35}]^{2+}$: 1202.0227 $[M+2H]^{2+}$; found: 1202.0223.

cyclo[DKP-RGD]-Val-Cit-DNR (**113**)

Fmoc-Val-Cit-OH (115)

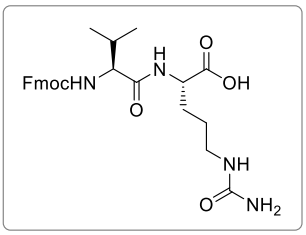

$C_{26}H_{32}N_4O_6$
MW: 496,56

Fmoc-Val-OH (1,5 g, 4.4 mmol 1.1 eq) and NHS (560 mg, 4.9 mmol, 1.1 eq) were dissolved in dry THF (16 mL) under nitrogen atmosphere. The mixture was cooled to 0°C then DCC (3.08 g, 14.9 mmol) was added and the mixture was stirred at room temperature overnight. The solution was filtered over a cotton septum and it was concentrated at rotavapor affording Fmoc-Val-OSu as a white foam. The latter was suspended in DME (13 mL) and added to a 13 mL aqueous solution of H-Cit-OH (850 mg, 4.9 mmol, 1.1 eq) and $NaHCO_3$ (410 mg, 4.9 mmol, 1.1 eq). THF (5 mL) was added and the mixture was stirred at room temperature overnight. The mixture was diluted with 15% aqueous citric acid (20 mL), and the organic layer was extracted with a 10% isopropanol/ethyl acetate (3 × 30 mL) mixture. The combined organic layers were washed with water (3 × 20 mL), and brine (1 × 20 mL). The organic phase was dried and concentrated. The crude was treated with Et_2O (50 mL), filtered over a Büchner funnel and washed with ether, affording compound **115** (1.7 g, 75% yield).
^{1}H NMR (400 MHz, DMSO-d_6) δ 12.52 (s, 1H), 8.16 (d, J = 7.3 Hz, 1H), 7.89 (d, J = 7.5 Hz, 2H), 7.75 (t, J = 7.1 Hz, 2H), 7.49-7.27 (m, 5H), 5.93 (t, J = 5.6 Hz, 1H), 5.37 (s, 2H), 4.36-4.19 (m, 3H), 4.15 (m, 1H), 3.92 (dd, J = 8.9, 7.3 Hz, 1H), 2.95 (m, 2H), 1.99 (m, 1H), 1.69 (m, 1H), 1.57 (m, 1H), 1.40 (m, 2H), 1.52-1.28 (m, 2H), 0.89 (d, J = 6.9 Hz, 3H), 0.86 ppm (d, J = 6.7 Hz, 3H). ^{13}C NMR (101 MHz, DMSO-d_6) δ 173.4, 171.2, 158.7, 156.0, 143.9, 143.8, 140.7, 127.6, 127.0, 125.3, 120.0, 65.6, 59.8, 51.8, 46.7, 38.7 (overlapped with solvent signal), 30.5, 28.4, 26.6, 19.1, 18.1 ppm.

Fmoc-Val-Cit-*N*-[4-(hydroxymethyl)phenyl] (116)

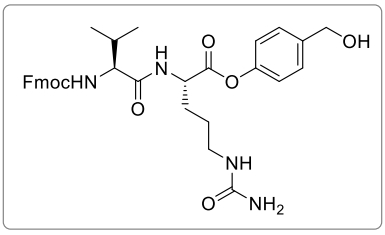

$C_{33}H_{38}N_4O_7$
MW: 602,69

Fmoc-Val-Cit-OH (**115**, 800 mg, 1.6 mmol, 1 eq) was dissolved in a 22 mL of dry CH_2Cl_2 / dry MeOH 2:1 mixture under nitrogen atmosphere. EEDQ (800 mg, 3.2 mmol, 2 eq) and 4-

aminobenzyl alcohol (390 mg, 3.2 mmol, 2 eq) were added and the mixture was stirred overnight at room temperature. After solvent removal, the crude was treated with Et_2O (40 mL), sonicated, filtered over a Büchner funnel and washed with ether, affording compound **116** (800 mg, 82% yield).

^{1}H NMR (400 MHz, DMSO-d_6) δ 9.98 (t, 1H), 8.11 (d, *J* = 7.5 Hz, 1H), 7.89 (d, *J* = 7.5 Hz, 2H), 7.74 (t, *J* = 7.8 Hz, 2H), 7.54 (d, *J* = 8.4 Hz, 2H), 7.50-7.37 (m, 3H), 7.32 (t, *J* = 7.2 Hz, 2H), 7.23 (d, *J* = 8.4 Hz, 2H), 5.97 (t, *J* = 5.5 Hz, 1H), 5.41 (s, 2H), 5.10 (t, *J* = 5.6 Hz, 1H), 4.47-4.37 (m, 3H), 4.36-4.18 (m, 3H), 3.93 (dd, *J* = 8.7, 7.2 Hz, 1H), 3.10-2.87 (m, 2H), 1.99 (m, 1H), 1.71 (m, 1H), 1.59 (m, 1H), 1.52-1.28 (m, 2H), 0.88 (d, *J* = 6.8 Hz, 3H), 0.85 ppm (d, *J* = 6.8 Hz, 3H); ^{13}C NMR (101 MHz, DMSO-d_6) δ 171.3, 170.4, 158.9, 156.1, 143.9, 143.8, 140.7, 137.5, 137.5, 127.7, 127.1, 126.9, 125.4, 120.1, 118.9, 65.7, 62.6, 60.1, 53.1, 46.7, 38.6 (overlapped with solvent signal), 30.5, 29.6, 26.8, 19.2, 18.3 ppm.

Fmoc-Val-Cit-*N*-[4-[[[(4-nitrophenoxy)carbonyl]oxy]methyl]phenyl] (117)

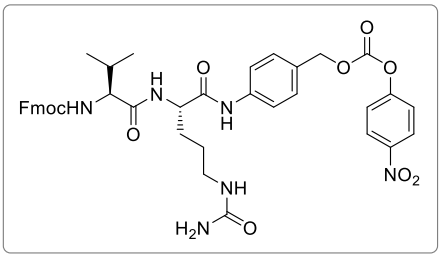

$C_{40}H_{42}N_6O_{10}$
MW: 766,81

A solution of **116** (350 mg, 0.6 mmol, 1 eq) in dry DMF (3 mL) was sonicated and cooled at 0 °C under nitrogen atmosphere. *i*Pr_2NEt (298 µL, 1.7 mmol, 3 eq) and bis(4-nitrophenyl) carbonate (530 mg, 1.7 mmol, 3 eq) were added, then the mixture was allowed to reach r.t. and stirred for 1 hour. The mixture was diluted with Et_2O (70 mL), sonicated and filtered over a Büchner funnel. The solid was re-suspended in Et_2O and the filtration was repeated, affording carbonate **117** (365 mg, 81% yield).

^{1}H NMR (400 MHz, DMSO-d_6) δ 10.14 (s, 2H), 8.31 (d, *J* = 9.2 Hz, 2H), 8.14 (d, *J* = 7.4 Hz, 1H), 7.89 (d, *J* = 7.5 Hz, 3H), 7.74 (t, *J* = 7.7 Hz, 3H), 7.65 (d, *J* = 8.5 Hz, 3H), 7.57 (d, *J* = 9.2 Hz, 2H), 7.42 (t, *J* = 9.5 Hz, 4H), 7.32 (t, *J* = 7.4 Hz, 2H), 5.98 (t, *J* = 5.3 Hz, 1H), 5.41 (s, 2H), 5.24 (s, 2H), 4.42 (m, 1H), 4.35-4.17 (m, 3H), 3.93 (dd, *J* = 8.8, 7.2 Hz, 1H), 3.09-2.88 (m, 2H), 1.99 (m, 1H), 1.79-1.54 (m, 2H), 1.42 (d, *J* = 27.0 Hz, 2H), 0.89 (d, *J* = 6.7 Hz, 3H), 0.86 ppm (d, *J* = 6.8 Hz, 3H); ^{13}C NMR (101 MHz, DMSO-d_6) δ 171.3, 170.8, 158.9, 156.1, 155.3, 152.0, 145.2, 143.9, 143.8, 140.7, 139.4, 129.5, 129.3, 127.7, 127.1, 125.4, 122.6, 120.1, 119.0, 70.3, 65.7, 60.1, 53.1, 46.7, 38.9 (overlapped with solvent signal), 30.5, 29.4, 26.8, 19.2, 18.3 ppm.

Fmoc-Val-Cit-*N*-[4-[[[(daunorubicin)carbonyl]oxy]methyl]phenyl] (118)

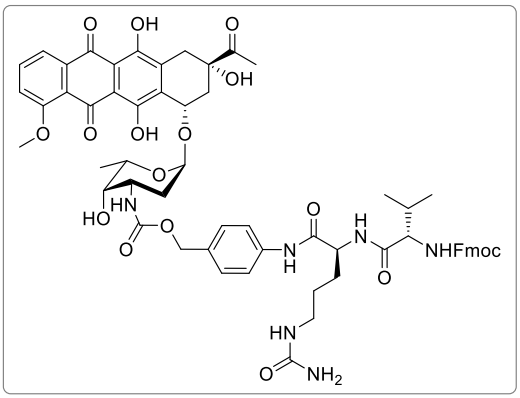

$C_{61}H_{66}N_6O_{17}$
MW: 1155,22

Compound **117** (51 mg, 0.07 mmol, 1,5 eq) was dissolved in dry DMF (1 mL) under nitrogen atmosphere and cooled at 0 °C. A solution of Daunorubicin hydrochloride (25 mg, 0.05 mmol, 1 eq) in dry DMF (1 mL) and *i*Pr_2NEt (15 µL, 0.9 mmol, 2 eq) were added to the cooled solution and the mixture was stirred at r.t. overnight. AcOEt (70 mL) was added, and the solution was washed with a 1 M aqueous solution of $KHSO_4$ (2 × 10 mL), saturated aqueous $NaHCO_3$ (2 × 10 mL) and brine (1 × 10 mL). The organic phase was dried and concentrated. The crude was suspended in a 9:1 mixture of CH_2Cl_2 / MeOH and centrifuged. The liquid fraction was concentrated and purified by flash chromatography (eluents: AcOEt/Hex/MeOH 7:2:1, then CH_2Cl_2/MeOH 9:1), affording compound **118** (39 mg, 75% yield).

R_f = 0.35 (CH_2Cl_2/MeOH, 9:1); ^{1}H NMR (400 MHz, DMSO-d_6) δ 14.02 (s, 1H), 13.27 (s, 1H), 10.03 (s, 1H), 8.10 (d, *J* = 7.4 Hz, 1H), 7.95-7.81 (m, 3H), 7.73 (t, *J* = 7.9 Hz, 2H), 7.69 (m, 1H), 7.54 (d, *J* = 8.4 Hz, 2H), 7.41 (dd, *J* = 14.1, 7.9 Hz, 2H), 7.36-7.27 (m, 2H), 7.24 (d, *J* = 8.4 Hz, 2H), 6.84 (d, *J* = 8.0 Hz, 1H), 5.97 (t, *J* = 5.4 Hz, 1H), 5.54 (s, 1H), 5.40 (s, 2H), 5.22 (m, 1H), 4.94 (m, 1H), 4.89 (s, 2H), 4.71 (d, *J* = 5.7 Hz, 1H), 4.40 (dd, *J* = 13.2, 7.6 Hz, 2H), 4.35-4.13 (m, 4H), 3.97 (s, 3H), 3.91 (dd, *J* = 8.8, 7.1 Hz, 1H), 3.73 (m, 1H), 3.45 (m, 1H), 3.06-2.86 (m, 4H), 2.27 (s, 3H), 2.21 (dd, *J* = 11.9, 2.8 Hz, 1H), 2.09 (dd, *J* = 14.1, 5.4 Hz, 1H), 1.98 (m, 1H), 1.84 (dd, *J* = 12.6, 9.6 Hz, 1H), 1.68 (m, 1H), 1.58 (m, 1H), 1.48 (dd, *J* = 12.4, 3.7 Hz, 1H), 1.44-1.30 (m, 2H), 1.13 (d, *J* = 6.4 Hz, 3H), 0.87 (d, *J* = 6.8 Hz, 3H), 0.84 ppm (d, *J* = 6.7 Hz, 3H); ^{13}C NMR (101 MHz, DMSO-d_6) δ 211.8, 186.5, 171.3, 170.5, 160.8, 158.9, 156.2, 155.3, 154.5, 143.9, 143.8, 140.7, 138.5, 136.2, 135.7, 134.7, 134.5, 131.9, 128.5, 127.6, 127.1, 125.4, 120.1, 119.7, 118.9, 110.8, 110.7, 100.2, 75.2, 70.1, 68.0, 66.7, 65.7, 64.9, 60.1, 56.6, 53.1, 47.2, 46.7, 38.6, 36.2, 31.6, 30.4, 29.9, 29.5, 29.0, 26.8, 24.1, 19.2, 18.3, 17.0 ppm. MS (ESI) *m/z* calcd for $[C_{61}H_{66}N_6NaO_{17}]^+$: 1177.44 $[M+Na]^+$; found: 1177.6; MS (ESI) *m/z* calcd $[C_{61}H_{65}N_6O_{17}]^-$: 1153.44 $[M-H]^-$; found: 1153.8.

4-pentynoic amide-*N*-[4-[[[(daunorubicin)carbonyl]oxy]methyl]phenyl] (119)

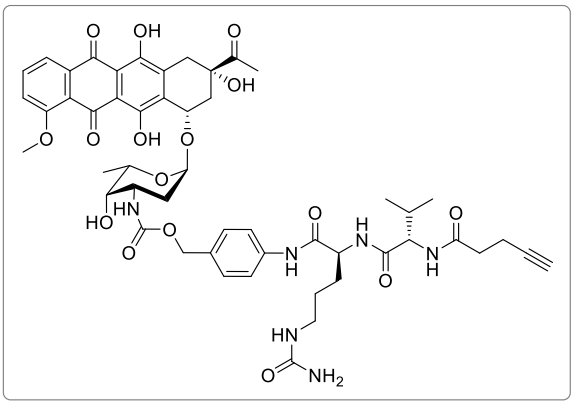

$C_{51}H_{60}N_6O_{16}$
MW: 1013,07

Compound **118** was deprotected following GP2 (reaction time: 3 min) and purified by semipreparative-HPLC [Water's Atlantis 21 mm × 10 cm column, gradient: 90% (H_2O + 0.1% CF_3COOH) / 10% (CH_3CN + 0.1% CF_3COOH) to 100% (CH_3CN + 0.1% CF_3COOH) in 11 min; product peak at 5.7 min]. The corresponding mono-acetate salt (**NH-118**) was freeze dried and used in the following step. 4-pentynoic acid (4 mg, 3.9×10^{-2} mmol, 1.5 eq) was dissolved in dry DMF (500 µL) under nitrogen atmosphere and cooled at 0 °C. HATU (16 mg, 4.2×10^{-2} mmol, 1.6 eq), HOAt (6 mg, 4.2×10^{-2} mmol, 1.6 eq) and *i*Pr_2NEt (13 µL, 7.8×10^{-2} mmol, 3 eq) were added and the mixture was stirred at 0 °C for 15 min. **NH-118** (26 mg, 2.6×10^{-2} mmol, 1 eq) and *i*Pr_2NEt (5 µL, 2.6×10^{-2} mmol, 1 eq) were dissolved in dry DMF (1 mL) and added to the cooled solution. The mixture was stirred overnight at r.t under nitrogen atmosphere. The solvent was removed under high-vacuum and the crude was purified by flash chromatography (gradient from CH_2Cl_2 / MeOH 9:1 to CH_2Cl_2 / MeOH 88:12), affording amide **119** (22 mg, 83% yield).

R_f = 0.76 (CH_2Cl_2/MeOH, 8:2); ^{1}H NMR (400 MHz, DMSO-d_6) δ 14.03 (s, 1H), 13.29 (s, 1H), 9.95 (s, 1H), 8.11 (d, *J* = 7.5 Hz, 1H), 7.96-7.85 (m, 3H), 7.65 (t, *J* = 4.8 Hz, 1H), 7.55 (d, *J* = 8.4 Hz, 2H), 7.24 (d, *J* = 8.4 Hz, 2H), 6.84 (d, *J* = 7.9 Hz, 1H), 5.99 (t, *J* = 5.7 Hz, 1H), 5.54 (bs, 1H), 5.40 (bs, 2H), 5.22 (s, 1H), 4.99-4.91 (m, 1H), 4.91-4.82 (m, 2H), 4.70 (bs, 1H), 4.35 (dd, *J* = 13.4, 7.5 Hz, 1H), 4.26-4.12 (m, 2H), 3.98 (s, 3H), 3.70 (m, 1H), 3.44 (s, 1H), 3.04-2.88 (m, 4H), 2.74 (s, 1H), 2.46-2.31 (m, 4H), 2.26 (s, 3H), 2.20 (m, 1H), 2.10 (dd, *J* = 14.1, 5.5 Hz, 1H), 1.96 (m, 1H), 1.84 (m, 1H), 1.67 (s, 1H), 1.57 (m, 1H), 1.47 (dd, *J* = 12.3, 3.3 Hz, 1H), 1.44-1.29 (m, 2H), 1.12 (d, *J* = 6.9 Hz, 3H), 0.85 (d, *J* = 6.8 Hz, 3H), 0.82 ppm (d, *J* = 6.7 Hz, 3H); ^{13}C NMR (101 MHz, DMSO-d_6) δ 211.9, 186.5, 186.4, 171.2, 170.6, 160.8, 158.9, 156.2, 155.3, 154.5, 138.6, 136.2, 135.7, 134.6, 134.5, 131.8, 128.5, 120.0, 119.7, 118.9, 110.7, 110.6, 100.3, 83.8, 75.2, 71.3, 70.1, 68.0, 66.7, 64.9, 57.6, 56.6, 53.1, 47.2, 41.6, 38.6, 36.2, 34.0, 33.0, 31.6, 30.5, 29.9, 29.2, 29.0, 26.8, 24.1, 19.2, 18.2, 17.0, 14.3, 13.9 ppm.

***cyclo*[DKP-RGD]-Val-Cit-DNR (113)**

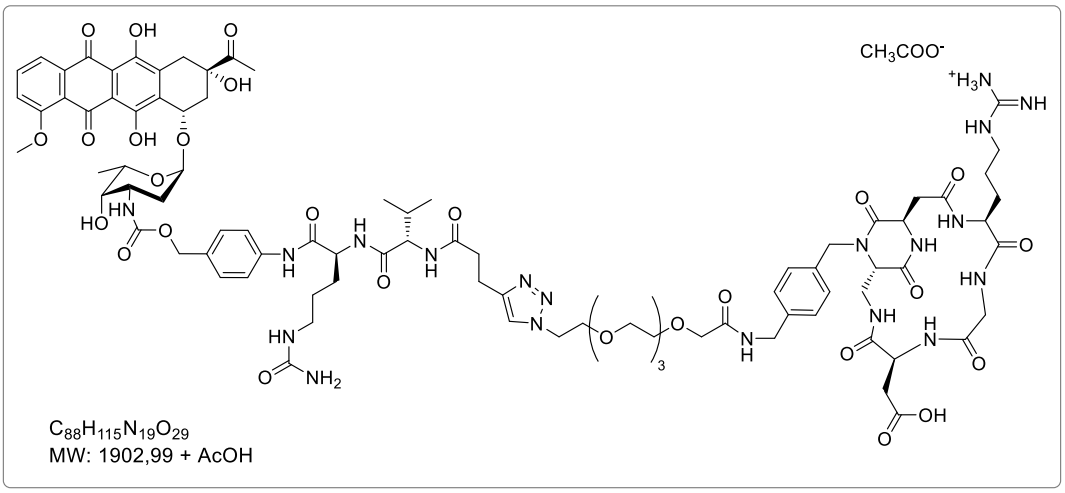

To a suspention of compound **102** (10 mg, 9.9×10^{-3} mmol, 1 eq) and **119** (16 mg, 14.9×10^{-3} mmol, 1.5 eq) in *t*BuOH (200 µL) and H_2O (22 µL) were added a 0.05 M aqueous solution of $CuSO_4$ (120 µL, 0.6 eq) and a 0.05 M aqueous solution of sodium ascorbate (179 µL, 0.8 eq). Dry DMF (50 µL) was added to help the dissolution, then the mixture was sonicated under nitrogen atmosphere for 2 min and stirred at r.t. overnight. The mixture was concentrated and purified by semipreparative-HPLC [Water's Atlantis 21 mm × 10 cm column, gradient: 85% (H_2O + 0.1% CH_3COOH) / 15% (CH_3CN + 0.1% CH_3COOH) to 30% (H_2O + 0.1% CH_3COOH) / 70% (CH_3CN + 0.1% CH_3COOH) in 14 min; product peak at 8.5 min]. The pure fractions were partially concentrated at rotavapor to remove CH_3CN, then the aqueous solution was freeze dried to yield the desired compound **113** as a flurry red solid (6 mg, 31% yield).

MS (ESI) *m/z* calcd for $[C_{88}H_{116}N_{19}O_{29}]^+$: 1902.82 $[M+H]^+$; found: 1902.79; MS (ESI) *m/z* calcd for $[C_{88}H_{117}N_{19}O_{29}]^{2+}$: 951.91 $[M+2H]^{2+}$; found: 951.97; *m/z* calcd $[C_{88}H_{116}N_{19}NaO_{29}]^{2+}$: 962.90 $[M+H+Na]^{2+}$; found: 962.91; MS (MALDI) *m/z* calcd for $[C_{88}H_{116}N_{19}O_{29}]^+$: 1903.97 a.m.u. $[M+H]^+$; found: 1903.7 (HCCA matrix), 1904.5 (SIN matrix). HRMS (ESI+): *m/z* calcd for $[C_{88}H_{116}N_{19}O_{29}]^+$: 1902.8181 $[M+H]^+$; found: 1902.8181; m/z calcd for $[C_{88}H_{117}N_{19}O_{29}]^{2+}$: 951.9127 $[M+2H]^{2+}$; found: 951.9123.

RGD-Naph-SS-CPT (**121**, **126**)

***tert*-butyl 3-(4-nitro-1,8-naphthalimide)propanoate (132)**

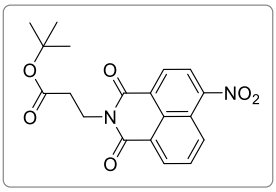

$C_{19}H_{18}N_2O_6$
MW: 370,36

A solution of β-alanine *tert*-butyl ester hydrochloride (217 mg, 1.2 mmol, 1.5 eq), 4-nitro-1,8-naphthalic anhydride (200 mg, 0.8 mmol, 1 eq) and Et_3N (0.176 mL, 1.28 mmol, 1.6 eq) in dry EtOH (4 mL) was heated to reflux and stirred for 3 h under a nitrogen atmosphere. The reaction mixture was diluted with AcOEt (100 mL) and washed with a 1 M aqueous solution of $KHSO_4$ (3 × 20 mL) and brine (1 × 20 mL). The organic phase was dried and concentrated. The crude was purified by flash chromatography on silica gel (0.5% MeOH in CH_2Cl_2) affording imide **132**, as a yellow solid (260 mg, 90% yield).
R_f= 0.33 (0.2% MeOH in CH_2Cl_2); ^{1}H NMR (400 MHz, $CDCl_3$) δ 8.83 (dd, J = 8.8, 1.1 Hz, 1H), 8.73 (dd, J = 7.3, 1.0 Hz, 1H), 8.69 (d, J = 8.0 Hz, 1H), 8.40 (d, J = 8.0 Hz, 1H), 7.98 (dd, J = 8.7, 7.3 Hz, 1H), 4.46 (d, J = 15.0 Hz, 2H), 2.72-2.66 (m, 2H), 1.42 ppm (s, 9H); ^{13}C NMR (101 MHz, $CDCl_3$) δ 170.3, 163.1, 162.3, 149.7, 132.6, 130.0, 129.9, 129.5, 129.1, 126.9, 124.0, 123.7, 122.9, 81.1 ppm.

***tert*-butyl 3-(4-amino-1,8-naphthalimide)propanoate (125)**

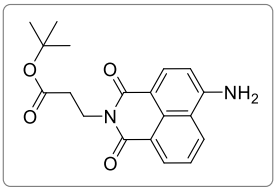

$C_{19}H_{20}N_2O_4$
MW: 340,38

To a suspension of **132** (100 mg, 0.27 mmol, 1 eq) in dry EtOH (3 mL), $SnCl_2$ (213 mg, 1.12 mmol, 4.2 eq) was added portionwise over a period of 1 h under a nitrogen atmosphere at room temperature. The color of the reaction mixture changed from yellow to red and as the reaction progresses and it slowly turned limpid. The solution was diluted with AcOEt (100 mL) and a saturated aqueous solution of $NaHCO_3$ (20 mL) was added. The white precipitate was filtered over cotton, then the two layers were separated. The organic phase was further washed with a saturated aqueous solution of $NaHCO_3$ (2 × 20 mL) and brine (1 × 25 mL). The organic phase was dried and concentrated. The crude was purified over a pad of silica (eluent: 4:6 hexane/AcOEt), affording amine **125**, as a red solid (90 mg, quantitative yield).

R_f= 0.27 (6:4 AcOEt/hexane); ^{1}H NMR (400 MHz, MeOD) δ 8.52 (dd, J = 7.3, 1.0 Hz, 1H), 8.43 (d, J = 8.4 Hz, 1H), 8.32 (dd, J = 8.4, 1.0 Hz, 1H), 7.66 (dd, J = 8.4, 7.3 Hz, 1H), 7.34 (d, J = 8.4 Hz, 1H), 4.38 (t, J = 7.3 Hz, 2H), 2.63 (t, J = 7.3 Hz, 2H), 1.37 ppm (s, 9H); ^{13}C NMR (101 MHz, MeOD) δ 172.6, 165.9, 165.4, 154.5, 135.4, 132.1, 130.5, 129.1, 125.9, 123.3, 120.1, 112.1, 106.6, 82.0, 37.1, 35.1, 28.2 ppm.

tert-butyl 3-[4-(2-hydroxyethyl-SS)-1,8-naphthalimide]propanoate (133)

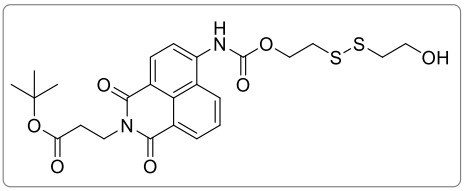

$C_{24}H_{28}N_2O_7S_2$
MW: 520,62

Triphosgene (130 mg, 0.441 mmol, 3 eq) was added to a solution of amine **125** (50 mg, 0.147 mmol, 1 eq) in dry toluene (1 mL) under a nitrogen atmosphere. The reaction mixture was cooled to 0 °C and iPr$_2$NEt (75 µL, 0.441 mmol, 3 eq) was added dropwise. The mixture was allowed to reach room temperature and stirred for 2 h. A solution of 2,2'-dithioethanol (89 µL, 0.735 mmol, 5 eq) in a 1:1 CH_2Cl_2/THF mixture (1 mL) was added and the reaction was stirred overnight at room temperature. AcOEt (100 mL) was added and the solution was washed with a 1 M aqueous solution of $KHSO_4$ (1 × 20 mL). The organic phase was dried and concentrated, then the crude was purified by a Grace Reveleris system (column: Reveleris Silica HP 12 g, dry load, flow rate: 27 mL min^{-1}, ramp from 100% hexane to 70% AcOEt in 15 min) affording carbamate **133**, as a yellow solid (29 mg, 38% yield).

R_f= 0.27 (6:4 AcOEt/hexane); ^{1}H NMR (400 MHz, MeOD) δ 8.44-8.39 (m, 2H), 8.33 (d, J = 8.3 Hz, 1H), 8.12 (d, J = 8.3 Hz, 1H), 7.69 (dd, J = 8.6, 7.3 Hz, 1H), 4.53 (t, J = 6.5 Hz, 2H), 4.32 (t, J = 7.4 Hz, 2H), 3.83 (t, J = 6.4 Hz, 2H), 3.10 (t, J = 6.5 Hz, 2H), 2.91 (t, J = 6.4 Hz, 2H), 2.62 (t, J = 7.4 Hz, 2H), 1.39 ppm (s, 9H); ^{13}C NMR (101 MHz, MeOD) δ 172.5, 165.3, 164.8, 155.6, 142.1, 133.1, 132.2, 129.9, 129.6, 127.5, 125.1, 123.7, 118.9, 118.4, 82.1, 64.8, 61.3, 42.3, 38.4, 37.2, 34.9, 28.2 ppm. MS (ESI): m/z calcd for $[C_{24}H_{28}N_2NaO_7S_2]^+$: 543.12 $[M+Na]^+$; found: 543.2.

Camptothecin-SS-naphthalimide(tert-butyl 3-aminopropanoate) (**120**)

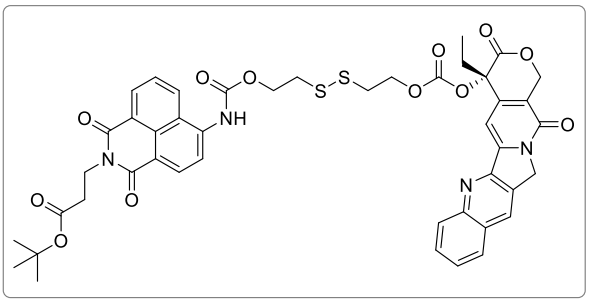

$C_{45}H_{42}N_4O_{12}S_2$
MW: 894,97

A solution of alcohol **133** (33 mg, 0.063 mmol, 1.5 eq) in dry CH_2Cl_2 (3 mL) was cooled to 0 °C under a nitrogen atmosphere, then (4-nitrophenoxycarbonyl)-camptothecin (**130**, 22 mg, 0.042 mmol, 1eq) and DMAP (10 mg, 0.084 mmol, 2 eq) were added. The mixture was allowed to reach room temperature and stirred overnight. The reaction mixture was diluted with AcOEt (70 mL) and washed with a 1 M aqueous solution of $KHSO_4$ (3 × 20 mL) and brine (1 × 20 mL). The organic phase was dried and concentrated, the crude was then purified by a Grace Reveleris system (column: Reveleris Silica HP 12 g, dry load, flow rate: 25 mL min^{-1}, ramp from 100% hexane to 100% AcOEt in 20 min) to afford carbonate **120** as a yellow solid (22 mg, 58% yield).

R_f= 0.32 (9:1 AcOEt/hexane); ^{1}H NMR (400 MHz, CD_2Cl_2) δ 8.51 (d, J = 7.2 Hz, 1H), 8.42 (t, J = 6.3 Hz, 1H), 8.33 (d, J = 14.3 Hz, 1H), 8.29 (d, J = 8.5 Hz, 1H), 8.12 (dd, J = 19.5, 11.9 Hz, 2H), 7.92 (d, J = 8.0 Hz, 1H), 7.80 (t, J = 7.5 Hz, 1H), 7.65 (dt, J = 9.9, 7.7 Hz, 2H), 7.27 (s, 1H), 5.43-5.18 (m, 2H), 5.07 (dd, J = 48.3, 19.0 Hz, 2H)., 4.54 (m, 1H), 4.47-4.23 (m, 5H), 3.02 (dt, J = 17.3, 5.9 Hz, 3H), 2.62 (dd, J = 16.4, 8.9 Hz, 2H), 2.25-2.01 (m, 2H), 1.40 (d, J = 4.4 Hz, 9H), 0.96 ppm (t, J = 7.3 Hz, 3H); ^{13}C NMR (101 MHz, CD_2Cl_2) δ 170.9, 167.7, 164.2, 163.7, 157.4, 154.2, 153.3, 152.7, 149.2, 147.0, 145.9, 139.9, 132.4, 131.6, 131.4, 131.0, 129.8, 129.2, 129.1, 128.7, 128.7, 128.4, 127.2, 126.8, 123.5, 123.4, 120.3, 118.0, 116.8, 96.0, 81.0, 78.8, 67.3, 66.9, 63.6, 50.4, 38.1, 37.2, 36.5, 34.2, 32.0, 30.1, 28.2, 7.8 ppm. MS (ESI): *m/z* calcd for $[C_{45}H_{43}N_4O_{12}S_2]^+$: 895.23 $[M+H]^+$; found: 895.5.

Camptothecin-SS-naphthalimide(3-aminopropionic acid) (134)

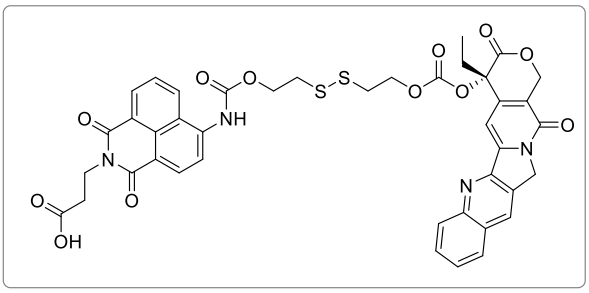

$C_{41}H_{34}N_4O_{12}S_2$
MW: 838,86

A solution of *tert*-butyl ester **120** (35 mg, 0.04 mmol) in dry CH_2Cl_2 (2 mL) was cooled to 0 °C under a nitrogen atmosphere and TFA (1 mL) was added. The mixture was allowed to reach room temperature and stirred for 45 min. The crude was purified by flash chromatography on silica gel (gradient from 1% MeOH to 10% MeOH + 1% HCOOH in CH_2Cl_2) affording carboxylic acid **134**, as a yellow solid (16 mg, 45% yield).

R_f= 0.46 (9:1 CH_2Cl_2/MeOH); ^{1}H NMR (400 MHz, DMSO-d_6) δ 8.59 (t, J = 7.0 Hz, 2H), 8.43 (m, 1H), 8.37 (dd, J = 8.0, 5.9 Hz, 1H), 8.14-8.00 (m, 3H), 7.77 (ddd, J = 34.1, 17.7, 9.5 Hz, 2H), 7.65 (dd, J = 10.0, 5.0 Hz, 1H), 7.07 (m, 1H), 5.74 (t, J = 2.1 Hz, 1H), 5.51 (s, 2H), 5.28-5.13 (m, 2H), 4.46-4.30 (m, 4H), 4.29-4.18 (m, 2H), 3.07 (dd, J = 13.1, 7.1 Hz, 3H), 2.24-2.10 (m, 2H), 0.96-0.87 ppm (m, 3H); ^{13}C NMR (101 MHz, DMSO-d_6) δ 167.1, 163.4, 162.8, 156.5, 153.7, 152.8, 152.1, 147.8, 146.2, 144.8, 140.5, 131.5, 130.8, 130.4, 129.6, 129.3, 129.0, 128.5, 128.2, 128.0, 127.7, 126.2, 123.9, 122.2, 119.2, 118.4, 117.1, 94.5, 78.0, 66.4, 62.8, 50.2, 36.8, 36.4, 33.8, 30.3, 29.0, 7.5 ppm. MS (ESI): *m/z* calcd for $[C_{41}H_{35}N_4O_{12}S_2]^+$: 839.17 $[M+H]^+$; found: 839.3.

***cyclo*[RGDyK]-Naph-SS-CPT (121)**

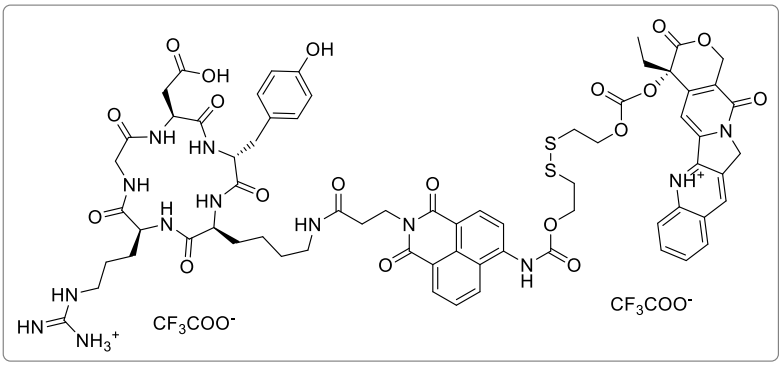

$C_{68}H_{73}N_{13}O_{19}S_2$
1440,52 + 2TFA

To a solution of carboxylic acid **134** (11.3 mg, 13.5 × 10^{-3} mmol, 1.5 eq) in dry DMF (500 µL) under a nitrogen atmosphere, NHS (2.1 mg, 18.0 × 10^{-3} mmol, 2 eq) was added and the reaction mixture was cooled to 0 °C. DIC (2.79 µL, 18.0 × 10^{-3} mmol, 2 eq) was added to the solution and the mixture was then stirred overnight at room temperature. Approximately half of the solvent was removed under high vacuum. CH_3CN (600 µL) and a solution of

cyclo(RGDyK) (FutureChem Co., Ltd., 7.6 mg, 9.0×10^{-3} mmol, 1 eq) in pH 7.5 PBS (600 µL) were then added. The reaction mixture was stirred overnight at room temperature; during the first 3 h the pH value was kept near 7.3-7.5 adding 0.2 M aqueous NaOH when necessary. The crude was then purified by semipreparative-HPLC [Waters Atlantis 21 mm × 10 cm column, gradient: 90% (H_2O + 0.1% CF_3COOH) / 10% (CH_3CN + 0.1% CF_3COOH) to 15% (H_2O + 0.1% CF_3COOH) / 85% (CH_3CN + 0.1% CF_3COOH) in 10 min; t_R (product): 7.25 min]. The purified product was then freeze dried to give **121** as a yellow solid (5 mg, 34% yield).
MS (ESI): *m/z* calcd for $[C_{68}H_{74}N_{13}O_{19}S_2]^+$: 1440.47 $[M+H]^+$; found: 1440.6; MS (MALDI): *m/z* calcd for $[C_{68}H_{74}N_{13}O_{19}S_2]^+$: 1441.52 $[M+H]^+$; found: 1441.1 (HCCA matrix).

cyclo[DKP-RGD]-Naph-SS-CPT (126)

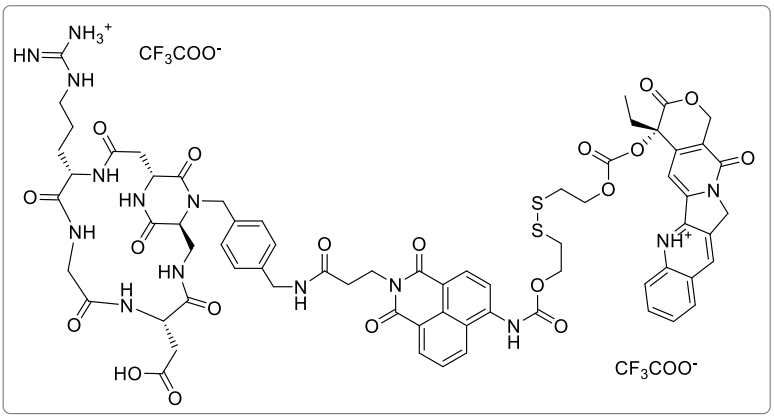

$C_{68}H_{70}N_{14}O_{19}S_2$
MW: 1451,51 + 2 TFA

To a solution of carboxylic acid **134** (10 mg, 11.9×10^{-3} mmol, 1 eq) in dry DMF (600 µL) under a nitrogen atmosphere, NHS (1.8 mg, 15.5×10^{-3} mmol, 1.3 eq) was added and the reaction mixture was cooled to 0 °C. DIC (2.4 µL, 15.5×10^{-3} mmol, 1.3 eq) was added to the solution and the mixture was then stirred overnight at room temperature. Approximately half of the solvent was removed under high vacuum. Then CH_3CN (700 µL) and a solution of *cyclo*[DKP-RGD]-CH_2NH_2 (**70**, 11 mg, 13.1×10^{-3} mmol, 1.1 eq) in pH 7.5 PBS (700 µL) were added. The reaction mixture was stirred overnight at room temperature; during the first 3 h the pH value was kept near 7.3-7.5 adding 0.2 M aqueous NaOH when necessary. The crude was then purified by semipreparative-HPLC [Waters Atlantis 21 mm × 10 cm column, gradient: 90% (H_2O + 0.1% CF_3COOH) / 10% (CH_3CN + 0.1% CF_3COOH) to 15% (H_2O + 0.1% CF_3COOH) / 85% (CH_3CN + 0.1% CF_3COOH) in 10 min; t_R (product): 7.1 min]. The purified product was then freeze dried to give **126** as a yellow solid (5.5 mg, 25% yield).
MS (ESI): *m/z* calcd for $[C_{68}H_{71}N_{14}O_{19}S_2]^+$: 1451.45 $[M+H]^+$; found: 1451.5; MS (MALDI): *m/z* calcd for $[C_{68}H_{71}N_{14}O_{19}S_2]^+$: 1452.50 $[M+H]^+$; found: 1452.2 (HCCA matrix); HRMS (ESI+): *m/z* calcd for $[C_{68}H_{71}N_{14}O_{19}S]^+$: 1451.4456 $[M+H]^+$; found 1451.4458; *m/z* calcd for $[C_{68}H_{72}N_{14}O_{19}S_2]^{2+}$: 726.2265 $[M+2H]^{2+}$; found 726.2243.

cyclo[DKP-RGD]-SS-CPT (**127**)

2-hydroxyethyl-SS-(*tert*-butyl 3-aminopropanoate) (137)

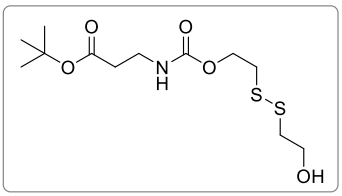

$C_{12}H_{23}NO_5S_2$
MW: 325,44

To a solution of 2,2'-dithioethanol (**135**, 139 mg, 0.9 mmol, 3 eq) in CH_2Cl_2 (15 mL), *i*Pr_2NEt (56 µL, 0.33 mmol, 1.1 eq) was added. 4-nitrophenyl chloroformate (60 mg, 0.3 mmol, 1 eq) was added at 0 °C and the reaction mixture was stirred overnight at room temperature. A solution of β-alanine *tert*-butyl ester hydrochloride (120 mg, 0.66 mmol, 2.2 eq) and *i*Pr_2NEt (133 µL, 0.78 mmol, 2.6 eq) in CH_2Cl_2 (12 mL) was then added and the reaction was stirred overnight at room temperature. AcOEt (100 mL) was added and the solution was washed with a 1 M aqueous solution of $KHSO_4$ (1 × 20 mL). The organic phase was dried over Na_2SO_4 and concentrated. The crude was purified by a Grace Reveleris system (column: Reveleris Silica 12 g, dry load, flow rate: 30 mL min^{-1}; ramp from 100% hexane to 100% AcOEt in 20 min) to afford 2-hydroxyethyl-SS-(tert-buthyl 3-aminopropanoate (**137**) as a pale yellow solid (62 mg, 63% yield).
R_f: 0.29 (6:4 AcOEt/hexane); ^{1}H NMR (400 MHz, MeOD) δ 4.29 (t, J = 6.5 Hz, 2H), 3.80 (t, J = 6.5 Hz, 2H), 3.34 (t, J = 6.8 Hz, 2H), 2.95 (t, J = 6.5 Hz, 2H), 2.87 (t, J = 6.5 Hz, 2H), 2.45 (t, J = 6.8 Hz, 2H), 1.47 ppm (s, 9H); ^{13}C NMR (101 MHz, MeOD) δ 172.8, 158.5, 81.9, 63.9, 61.2, 42.2, 38.6, 37.8, 36.6, 28.4 ppm.

Camptothecin-SS-(*tert*-butyl 3-aminopropanoate) (138)

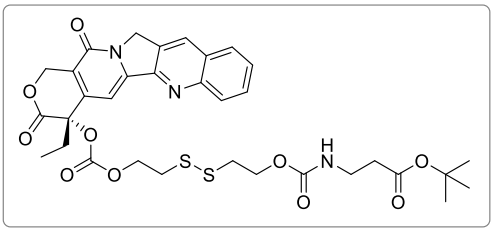

$C_{33}H_{37}N_3O_{10}S_2$
MW: 699,79

To a solution of CPT derivative **130** (56 mg, 0.11 mmol, 1 eq) in dry CH_2Cl_2 (8 mL) under a nitrogen atmosphere, alcohol **137** (81 mg, 0.25 mmol, 2.2 eq) and DMAP (47 mg, 0.385 mmol, 3.5 eq) were added at 0 °C and the mixture was stirred overnight at room temperature. The reaction mixture was diluted with AcOEt (75 mL) and washed with a 1 M aqueous solution of $KHSO_4$ (2 × 20 mL) and brine (1 × 25 mL). The organic phase was dried over Na_2SO_4 and concentrated. The crude was purified by a Grace Reveleris system (column: Reveleris Silica HP 12 g, dry load, flow rate: 25 mL min^{-1}, ramp from 100% hexane

to 100% AcOEt in 20 min) to afford compound carbonate **138** as a pale yellow solid (45 mg, 58% yield).

R_f= 0.31 (100% AcOEt); ^{1}H NMR (400 MHz, CD_2Cl_2) δ 8.42 (s, 1H), 8.19 (d, J = 8.4 Hz, 1H), 7.97 (d, J = 7.5 Hz, 1H), 7.84 (ddd, J = 8.4, 6.9, 1.4 Hz, 1H), 7.68 (ddd, J = 7.5, 6.9, 1.4 Hz, 1H), 7.28 (s, 1H), 5.65 (d, J = 17.1 Hz, 1H), 5.36 (d, J = 17.1 Hz, 1H), 5.28 (bs, 2H), 4.37 (t, J = 6.5 Hz, 2H), 4.18 (dt, J = 6.3 Hz, 2H), 3.32 (dt, J = 6.3 Hz, 2H), 2.94 (t, J = 6.5 Hz, 2H), 2.88 (t, J = 6.3 Hz, 2H), 2.39 (t, J = 6.3 Hz, 2H), 2.25 (dq, J = 15, 7.5 Hz, 1H), 2.15 (dq, J = 15, 7.5 Hz, 1H), 1.42 (s, 9H), 1.00 ppm (t, J = 7.5 Hz, 3H); ^{13}C NMR (101 MHz, CD_2Cl_2) δ 171.8, 167.7, 157.6, 153.8, 152.9, 149.2, 147.0, 145.8, 131.6, 130.9, 129.9, 129.2, 128.7, 128.7, 128.3, 120.4, 95.9, 81.1, 78.5, 67.5, 66.9, 62.8, 50.4, 38.3, 37.2, 37.1, 35.9, 32.1, 30.1, 28.2, 7.8 ppm. MS (ESI): *m/z* calcd for $[C_{33}H_{37}N_3NaO_{10}S_2]^+$: 722.18 $[M+Na]^+$; found: 722.31.

Camptothecin-SS-(3-aminopropanoic acid) (139)

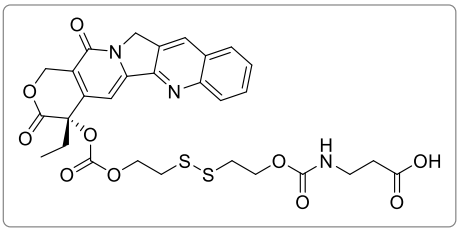

$C_{29}H_{29}N_3O_{10}S_2$
MW: 643,68

A solution of *tert*-butyl ester **138** (45 mg, 0.064 mmol) in dry CH_2Cl_2 (3.5 mL) was cooled to 0 °C under a nitrogen atmosphere and TFA (1.75 mL) was added. The mixture was then allowed to reach room temperature and stirred for 90 min. The crude was purified by flash chromatography on silica gel (gradient from 1% MeOH to 10% MeOH + 1% HCCOH in CH_2Cl_2) affording carboxylic acid **139**, as a pale yellow solid (30 mg, 75% yield).

R_f= 0.40 (9:1 CH_2Cl_2/MeOH). MS (ESI): *m/z* calcd for $[C_{29}H_{29}N_3NaO_{10}S_2]^+$: 666.12 $[M+Na]^+$; found: 666.40; *m/z* calcd for $[C_{29}H_{28}N_3Na_2O_{10}S_2]^+$: 688.10 $[M+Na-H]^+$; found: 688.39.

***cyclo*[DKP-RGD]-SS-CPT (127)**

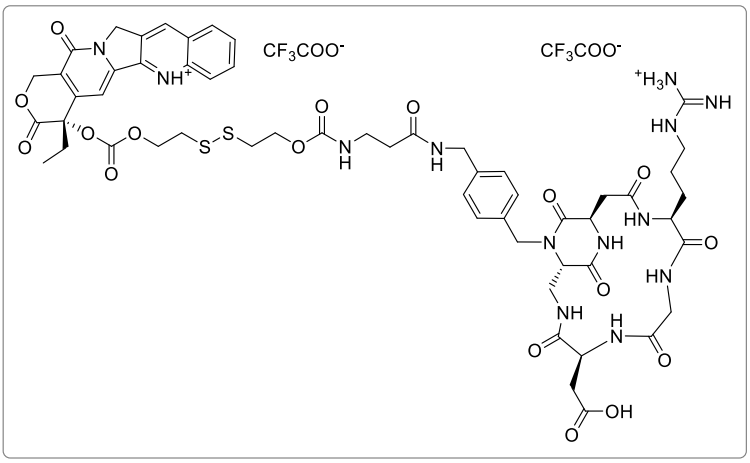

$C_{56}H_{65}N_{13}O_{17}S_2$
MW: 1256,33 + 2TFA

DIC (8 µL, 5.2 × 10^{-2} mmol, 4 eq) and NHS (6 mg, 5.2 × 10^{-2} mmol, 4 eq) were added to a solution of carboxylic acid **139** (30 mg, 4.7 × 10^{-2} mmol, 3.5 eq) in dry DMF (1 mL). The resulting solution was stirred overnight under a nitrogen atmosphere. Approximately half of the solvent was removed under high vacuum. Then acetonitrile (600 µL) was added and the mixture was cooled to 0 °C. A solution of *cyclo*[DKP-RGD]-CH_2NH_2 (**70**, 11 mg, 1.3 × 10^{-2} mmol, 1 eq) in PBS (600 µL; pH 7.5) was then added to the acetonitrile solution, and the pH value was adjusted to 7.3-7.6 with NaOH aq. (0.2 M). The resulting solution was warmed to room temperature and stirred overnight. During the first 5 h, the pH value was kept near to 7.3 by adding 0.2 M aqueous NaOH if necessary. The solution was concentrated, and the crude residue was purified by semipreparative HPLC [Waters Atlantis 21 mm × 10 cm column, gradient: 90% (H_2O + 0.1% CF_3COOH) / 10% (CH_3CN + 0.1% CF_3COOH) to 100% (CH_3CN + 0.1% CF_3COOH) in 13 min; t_R (product): 7.3 min]. The purified product was then freeze dried to give **127** as a yellow solid (7 mg, 43% yield).

^{1}H NMR (500 MHz, DMSO-d_6 + D_2O) δ 8.67 (s, 1H), 8.14 (d, J = 8.7 Hz, 1H), 8.10 (d, J = 7.0 Hz, 1H), 7.86 (ddd, J = 8.7, 7.0, 1.1 Hz, 1H), 7.71 (ddd, J = 8.1, 7.0, 1.1 Hz, 1H), 7.19 (d, J = 8.2 Hz, 2H), 7.15 (d, J = 8.2 Hz, 2H), 7.12 (s, 1H), 5.50 (s, 2H), 5.29 (s, 2H), 4.98 (d, J = 15.1 Hz, 1H), 4.79 (dd, J = 9.2, 5.8 Hz, 1H), 4.37 (m, 1H), 4.34-4.27 (m, 2H), 4.22 (d, J = 17.1 Hz, 1H), 4.20 (s, 2H), 4.12-4.03 (m, 2H), 3.85 (d, J = 15.1 Hz, 1H), 3.80-3.75 (m, 2H), 3.72 (d, J = 13.7 Hz, 1H), 3.47 (dd, J = 14.5, 7.1 Hz, 1H), 3.35 (d, J = 17.1 Hz, 1H), 3.16 (t, J = 7.2 Hz, 2H), 3.10 (dt, J = 6.9, 1.9 Hz, 2H), 2.97 (dt, J = 6.0, 1.9 Hz, 2H), 2.86 (t, J = 6.2 Hz, 2H), 2.79 (dd, J = 16.6, 9.3 Hz, 1H), 2.58 (dd, J = 13.5, 9.9 Hz, 1H), 2.43 (dd, J = 13.5, 3.7 Hz, 1H), 2.35 (dd, J = 16.6, 5.7 Hz, 1H), 2.28 (t, J = 7.2 Hz, 2H), 2.15 (dq, J = 14.7, 7.2 Hz, 1H), 2.15 (dq, J = 14.7, 7.2 Hz, 1H), 1.97 (m, 1H), 1.69 (m, 1H), 1.54-1.39 (m, 2H), 0.90 ppm (t, J = 7.4 Hz, 3H); ^{13}C NMR (126 MHz, DMSO-d_6 + D_2O) δ 171.7, 171.6, 171.3, 171.1, 170.8, 169.6, 169.6, 169.1, 167.5, 157.0, 156.7, 156.1, 153.2, 152.4, 148.2, 146.5, 145.3, 139.1, 134.8,

132.1, 130.9, 130.0, 129.2, 128.9, 128.4, 128.2, 128.1, 128.0, 119.4, 95.1, 78.3, 66.7, 66.6, 62.0, 58.8, 53.9, 51.2, 50.7, 48.4, 46.7, 42.4, 42.0, 40.7, 38.3, 37.6, 37.4, 37.2, 36.6, 35.7, 35.4, 30.6, 26.3, 26.0, 7.8 ppm. MS (ESI): *m/z* calcd for $[C_{56}H_{66}N_{13}O_{17}S_2]^+$: 1256.41 $[M+H]^+$; found: 1256.61; *m/z* calcd for $[C_{56}H_{65}N_{13}NaO_{17}S_2]^+$: 1278.40 $[M+Na]^+$; found: 1278.59; *m/z* calcd for $[C_{56}H_{67}N_{13}O_{17}S_2]^{2+}$: 628.71 $[M+2H]^{2+}$; found: 628.80; HRMS (ESI+): *m/z* calcd for $[C_{56}H_{66}N_{13}O_{17}S_2]^+$: 1256.4136 $[M+H]^+$; found 1256.4139; *m/z* calcd for $[C_{56}H_{67}N_{13}O_{17}S_2]^{2+}$: 628.7105 $[M+2H]^{2+}$; found 628.7082.

"uncleavable" cyclo[DKP-RGD]-CPT (**128**)

(*N*-hydroxysuccinimidyl-glutarate)glycino-Camptothecin (141)

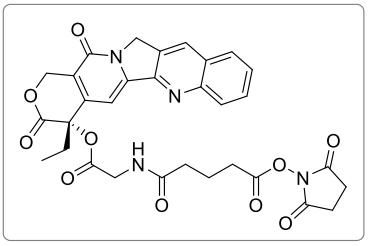

$C_{31}H_{28}N_4O_{10}$
MW: 616,58

DIC (24 µL, 0.154 mmol, 2 eq) and NHS (18 mg, 0.154 mmol, 2 eq) were added to a solution of **140** (40 mg, 0.077 mmol, 1 eq) in a 5:1 mixture dry THF/CH_3CN (1.8 mL). The mixture was stirred overnight at room temperature and the white solid formed was filtered off. Evaporation of the filtrate and crystallization with isopropyl alcohol afforded **141** as a white solid (30 mg, 63% yield).

^{1}H NMR (499.7 MHz, DMSO-d_6) δ 8.71 (s, 1 H), 8.45 (t, *J* = 5.8 Hz, 1 H), 8.18 (d, *J* = 8.4 Hz, 1 H), 8.14 (d, *J* = 8.4 Hz, 1 H), 7.87 (m, 1 H), 7.73 (m, 1 H), 7.17 (s, 1 H), 5.50 (s, 2 H), 5.29-5.32 (m, 2 H), 4.16 (dd, *J* = 18.0, 6.0 Hz, 1 H), 2.78 (m, 4H), 2.66-2.70 (m, 2H), 2.21-2.28 (m, 2H), 2.08-2.18 (m, 2H), 1.80-1.88 (m, 2H), 0.91 ppm (t, *J* = 7.3 Hz, 3H). HRMS (ESI): *m/z* calcd for $[C_{31}H_{29}N_4O_{10}]^+$: 617.1878 $[M+H]^+$; found: 617.1879.

***cyclo*[DKP-RGD]-unc.-CPT (128)**

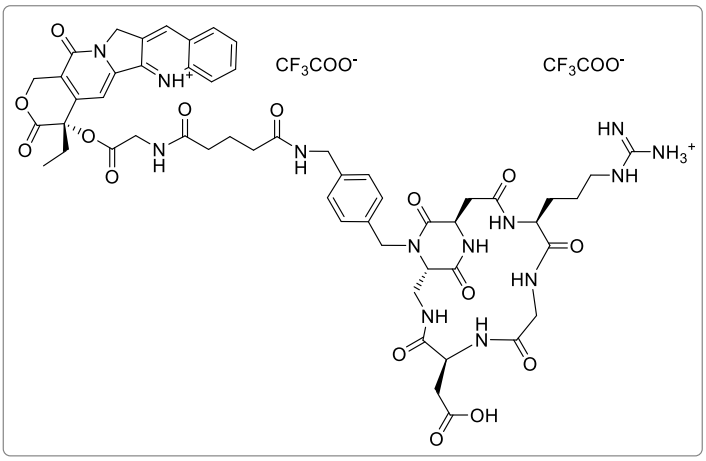

$C_{54}H_{61}N_{13}O_{15}$
MW: 1132,16 + 2TFA

Compound **141** (8.6 mg, 14.0 × 10^{-2} mmol, 1.2 eq) was dissolved in CH_3CN (1 mL) and a solution of *cyclo*[DKP-RGD]-CH_2NH_2 (**70**, 20 mg, 11.7 × 10^{-2} mmol, 1 eq) in pH 7.5 PBS (1 mL) was added. The reaction mixture was stirred overnight at room temperature; during the first 3 h the pH value was kept near 7.3-7.5 adding 0.2 M aqueous NaOH when necessary. The crude was then purified by semipreparative-HPLC [Waters Atlantis 21 mm × 10 cm column, multistep gradient: from 0 min to 1 min 80% (H_2O + 0.1% CF_3COOH) / 20% (CH_3CN + 0.1% CF_3COOH); ramp to 29% (H_2O + 0.1% CF_3COOH) / 71% (CH_3CN + 0.1% CF_3COOH) in 6.5 min; t_R (product): 7.2 min]. The purified product was then freeze dried to give the desired compound **128** as a yellow solid (13 mg, 85% yield).

^{1}H NMR (400 MHz, D_2O + CD_3CN) δ 8.35 (s, 1H), 8.06 (d, J = 8.0 Hz, 1H), 7.90-7.76 (m, 2H), 7.60 (m, 1H), 7.44 (s, 1H), 7.23 (d, J = 7.9 Hz, 2H), 7.19 (d, J = 7.9 Hz, 2H), 5.83 (d, J = 16.4 Hz, 1H), 5.66 (d, J = 16.4 Hz, 1H), 5.13 (d, J = 15.1 Hz, 1H), 5.04 (t, J = 7.0 Hz, 1H), 4.69 (dd, J = 8.4, 5.2 Hz, 2H), 4.62 (d, J = 18.2 Hz, 1H), 4.51 (d, J = 14.7 Hz, 1H), 4.47 (d, J = 15.6 Hz, 1H), 4.32 (dd, J = 9.7, 4.9 Hz, 1H), 4.27 (s, 2H), 4.16-4.06 (m, 3H), 3.79 (d, J = 17.1 Hz, 1H), 3.67 (dd, J = 14.0, 5.4 Hz, 1H), 3.40 (t, J = 6.8 Hz, 2H), 3.15-2.89 (m, 4H), 2.79 (dd, J = 14.0, 4.7 Hz, 1H), 2.59-2.51 (m, 2H), 2.45 (d, J = 0.9 Hz, 3H), 2.44-2.34 (m, 2H), 2.19 (m, 1H), 2.14-2.04 (m, 2H), 2.00 (m, 1H), 1.90-1.76 (m, 2H), 1.24 ppm (t, J = 7.3 Hz, 3H); ^{13}C NMR (101 MHz, D_2O + CD_3CN) δ 174.9, 174.0, 172.9, 172.6, 172.0, 171.7, 169.9, 169.3, 169.2, 168.5, 167.8, 156.6, 155.9, 149.8, 146.1, 144.6, 137.2, 133.1, 131.6, 130.2, 127.6, 127.4, 127.1, 126.8, 96.6, 76.6, 65.8, 58.3, 53.2, 51.1, 49.3, 48.4, 48.1, 46.4, 41.7, 41.5, 40.2, 39.9, 38.2, 37.1, 34.0, 33.8, 33.7, 29.9, 25.0, 24.0, 21.0, 6.4 ppm. MS (ESI): *m/z* calcd for $[C_{54}H_{62}N_{13}O_{15}]^+$: 1132.45 $[M+H]^+$; found: 1132.70; MS (MALDI): *m/z* calcd for $[C_{54}H_{62}N_{13}O_{15}]^+$: 1133.15 $[M+H]^+$; found: 1133.7 (HCCA matrix).

HPLC Traces of the Final Products

***cyclo*[DKP-RGD]-Val-Ala-PTX (80)**

Waters Atlantis 21 mm × 10 cm column, gradient from 90% (H_2O + 0.1% CF_3COOH) / 10% (CH_3CN + 0.1% CF_3COOH) to 100% (CH_3CN + 0.1% CF_3COOH) in 11 min.

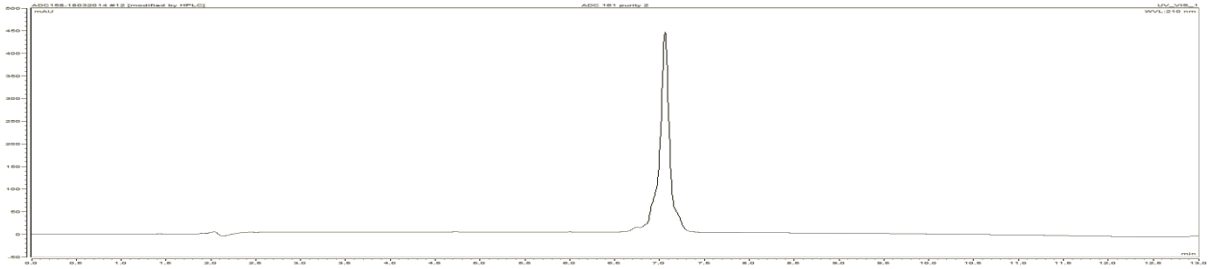

***cyclo*[DKP-RGD]-Phe-Lys-PTX (81)**

Waters Atlantis 21 mm × 10 cm column, multistep gradient: from 0 min to 1 min 90% (H_2O + 0.1% CF_3COOH) / 10% (CH_3CN + 0.1% CF_3COOH); ramp to 100% (CH_3CN + 0.1% CF_3COOH) in 10 min.

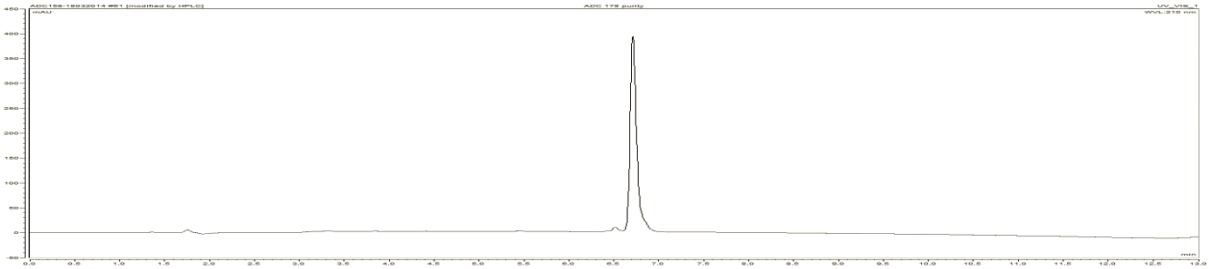

***cyclo*[DKP-RGD]-unc.-PTX (82)**

Waters Atlantis 21 mm × 10 cm column, gradient: 90% (H_2O + 0.1% CF_3COOH) / 10% (CH_3CN + 0.1% CF_3COOH) to 25% (H_2O + 0.1% CF_3COOH) / 75% (CH_3CN + 0.1% CF_3COOH) in 12 min.

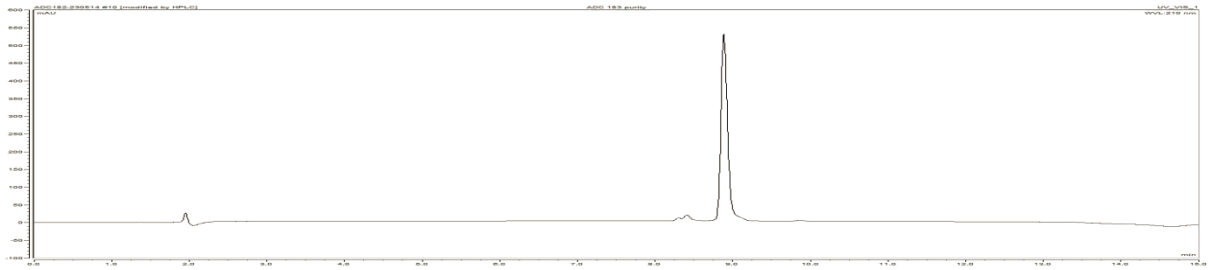

[*cyclo*(DKP-RGD)]$_2$Val-Ala-PTX (100)

Waters Atlantis 21 mm × 10 cm column; gradient: 90% (H_2O+0.1% CF_3COOH)/10% (CH_3CN+0.1% CF_3COOH) to 100% (CH_3CN+0.1% CF_3COOH) in 17 min.

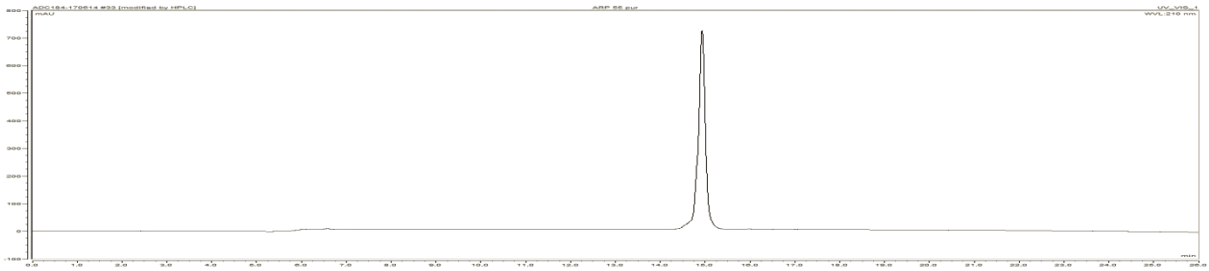

[*cyclo*(DKP-RGD)]$_1$Val-Ala-PTX (111)

Waters Atlantis 21 mm × 10 cm column, gradient: 90% (H_2O + 0.1% CH_3COOH)/10% (CH_3CN + 0.1% CH_3COOH) to 100% (CH_3CN + 0.1% CH_3COOH) in 17 min.

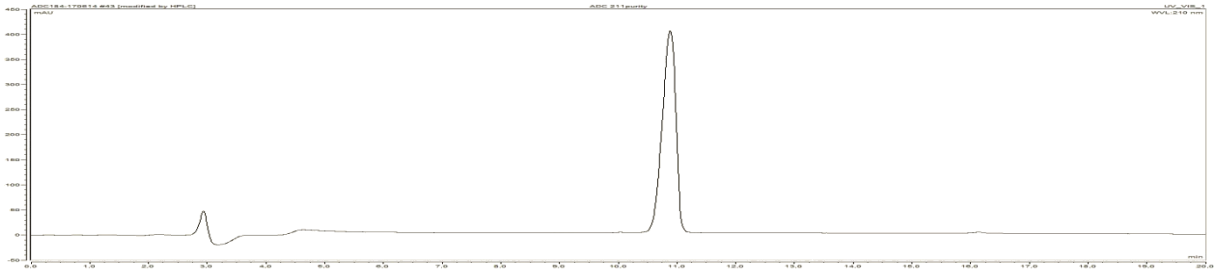

cyclo[DKP-RGD]-Val-Cit-DNR (113)

Water's Atlantis 21 mm × 10 cm column, gradient: 85% (H_2O + 0.1% CH_3COOH) / 15% (CH_3CN + 0.1% CH_3COOH) to 30% (H_2O + 0.1% CH_3COOH) / 70% (CH_3CN + 0.1% CH_3COOH) in 14 min.

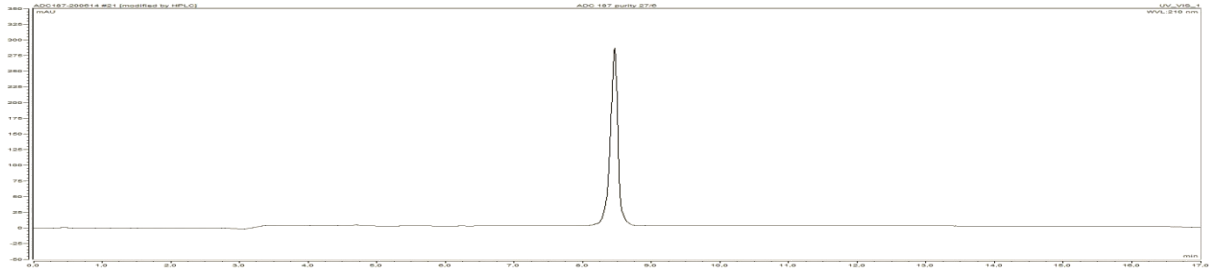

cyclo[RGDyK]-Naph-SS-CPT (121)

Waters Atlantis 21 mm × 10 cm column, gradient: 90% (H_2O + 0.1% CF_3COOH) / 10% (CH_3CN + 0.1% CF_3COOH) to 15% (H_2O + 0.1% CF_3COOH) / 85% (CH_3CN + 0.1% CF_3COOH) in 10 min.

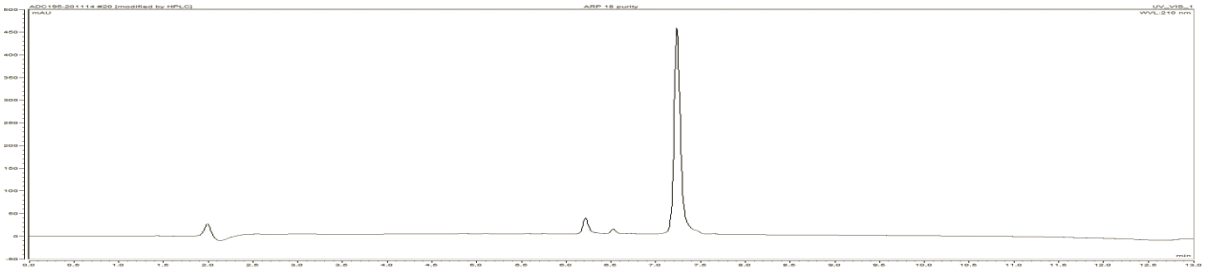

cyclo[DKP-RGD]-Naph-SS-CPT (126)

Waters Atlantis 21 mm × 10 cm column, gradient: 90% (H_2O + 0.1% CF_3COOH) / 10% (CH_3CN + 0.1% CF_3COOH) to 15% (H_2O + 0.1% CF_3COOH) / 85% (CH_3CN + 0.1% CF_3COOH) in 10 min.

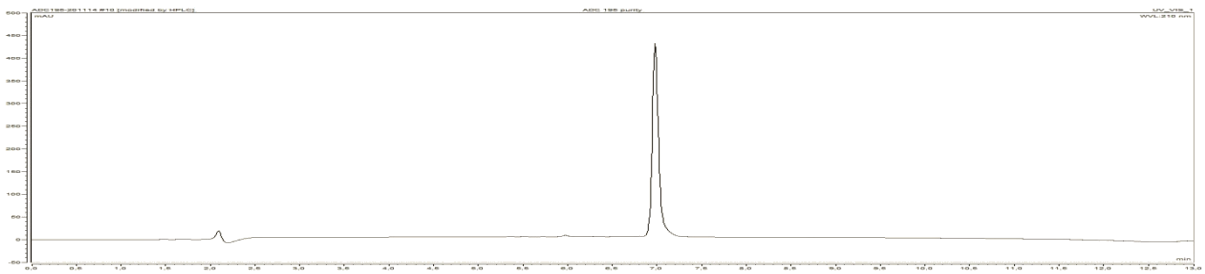

cyclo[DKP-RGD]-SS-CPT (127)

Waters Atlantis 21 mm × 10 cm column, gradient: 90% (H_2O + 0.1% CF_3COOH) / 10% (CH_3CN + 0.1% CF_3COOH) to 100% (CH_3CN + 0.1% CF_3COOH) in 13 min.

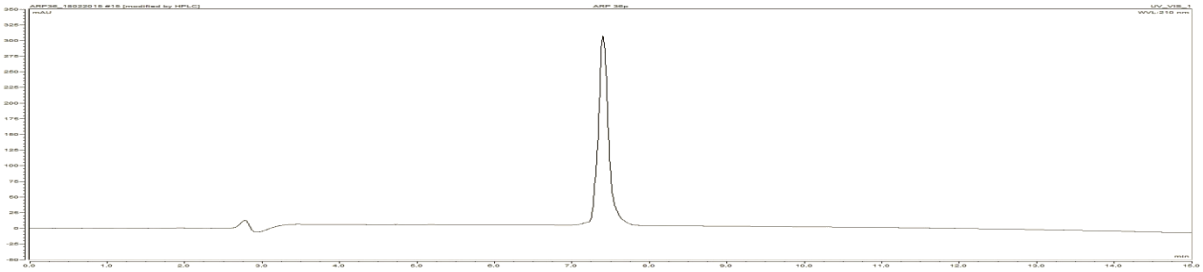

cyclo[DKP-RGD]-unc.-CPT (128)

Waters Atlantis 21 mm × 10 cm column, multistep gradient: from 0 min to 1 min 80% (H_2O + 0.1% CF_3COOH) / 20% (CH_3CN + 0.1% CF_3COOH); ramp to 29% (H_2O + 0.1% CF_3COOH) / 71% (CH_3CN + 0.1% CF_3COOH) in 6.5 min.

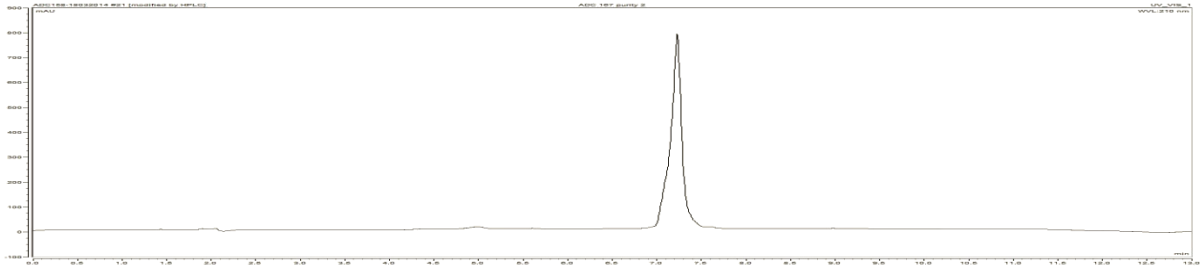

Appendix of NMR data

Compound 80

^{1}H NMR (400 MHz, CD_3OD)

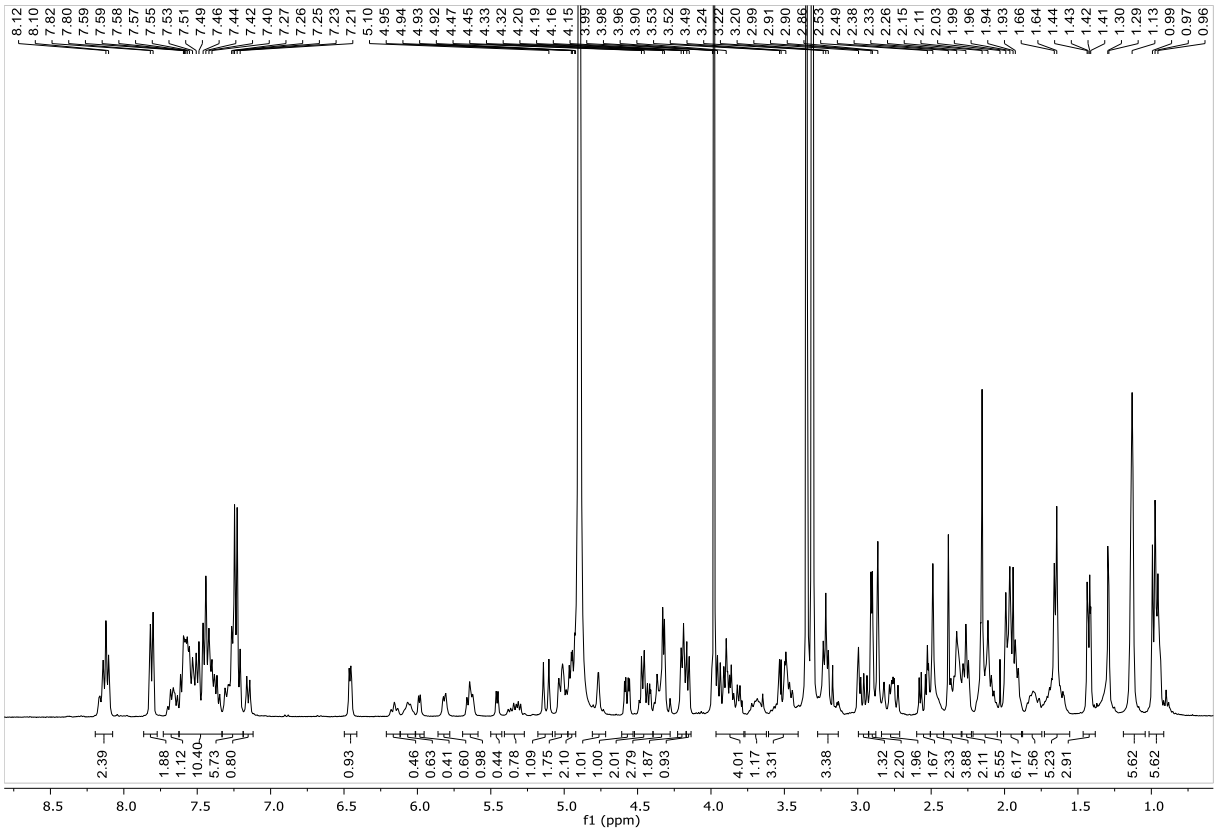

^{13}C NMR (101 MHz, CD_3OD)

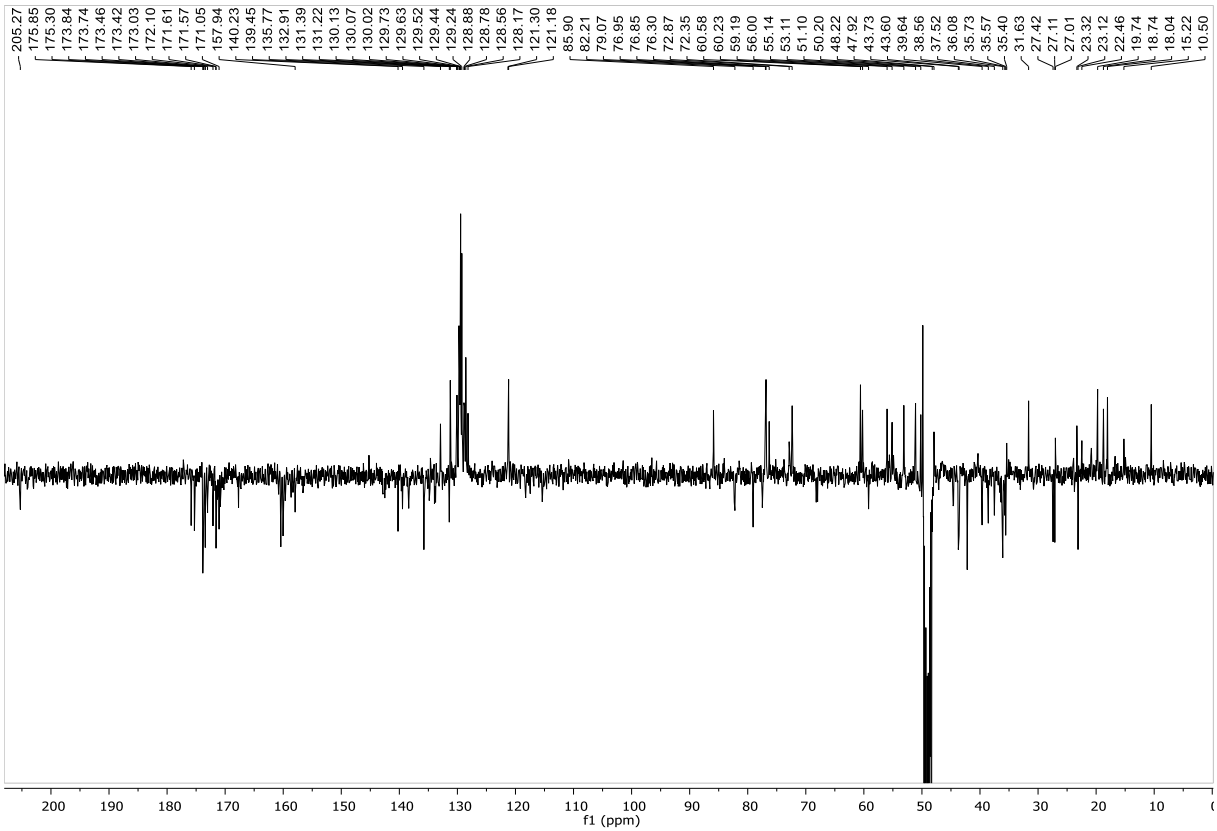

Compound 82

^{1}H NMR (400 MHz, CD_3OD)

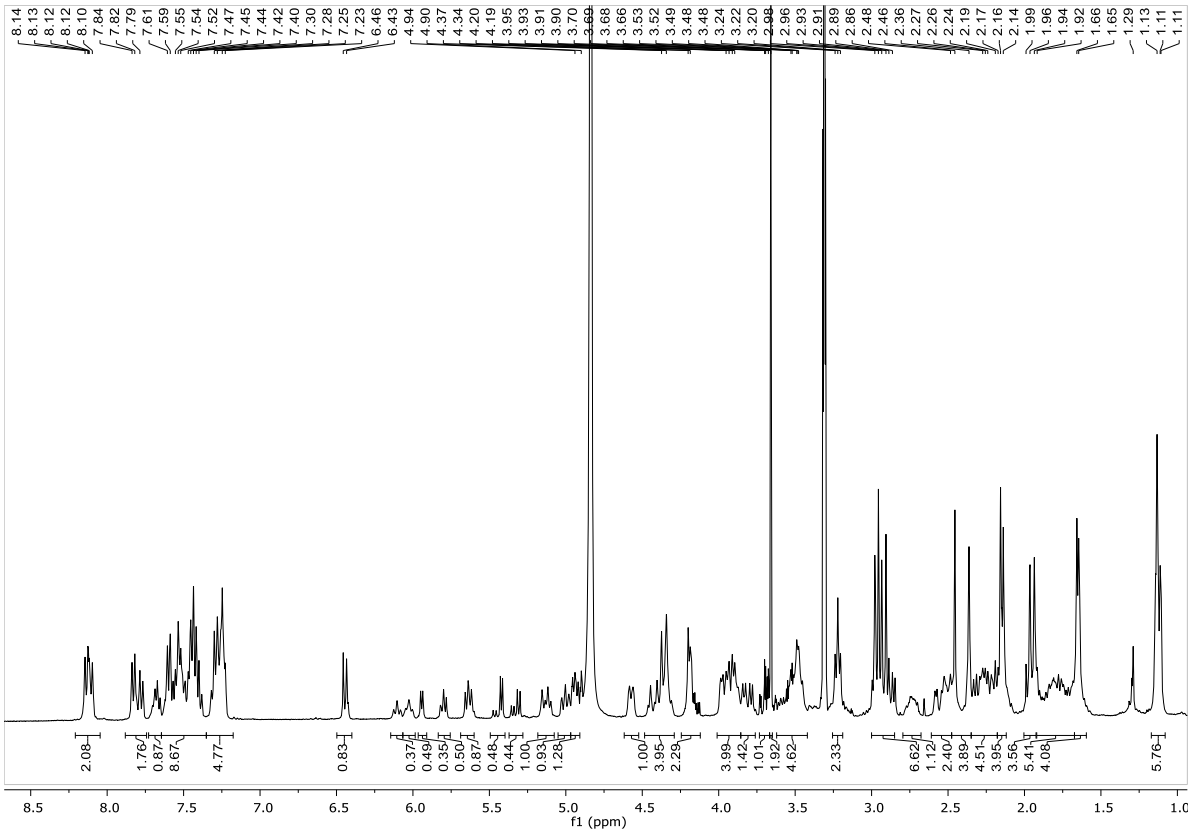

^{13}C NMR (101 MHz, CD_3OD)

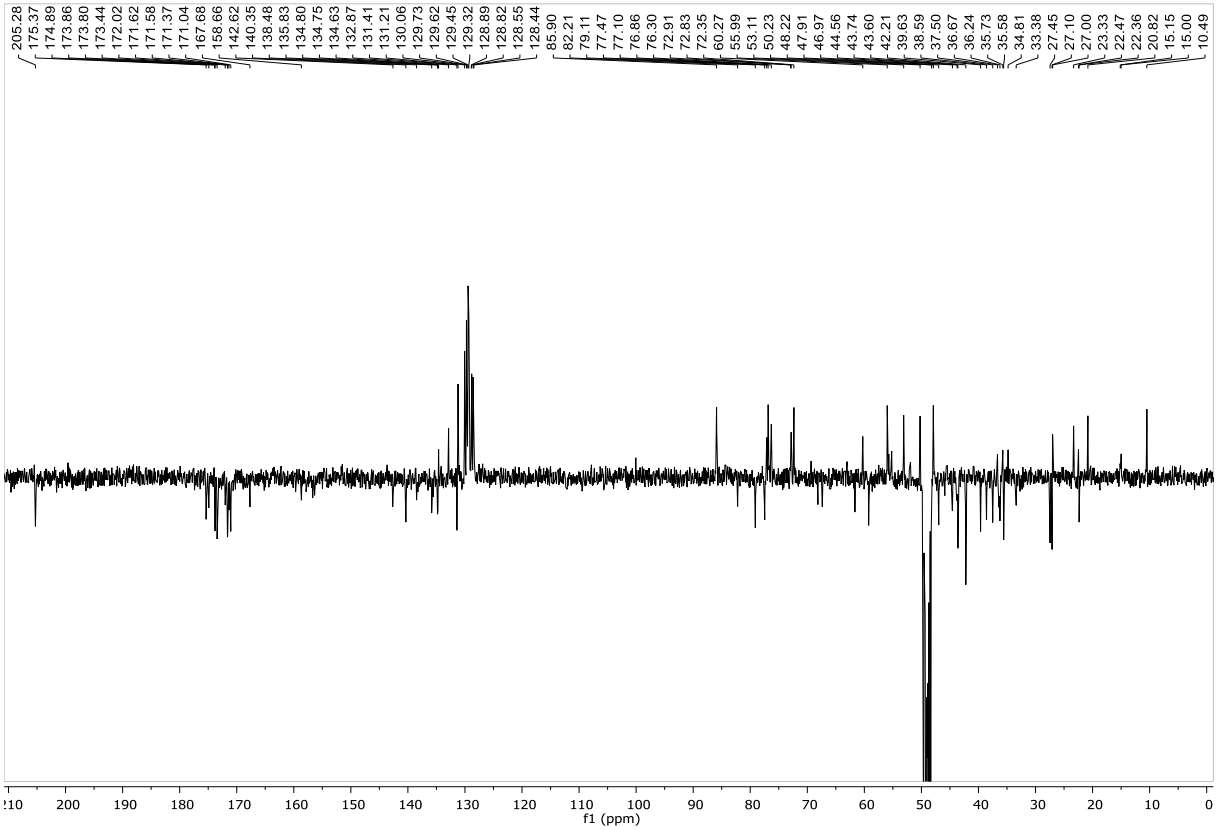

Compound 83

^{1}H NMR (400 MHz, CD_2Cl_2)

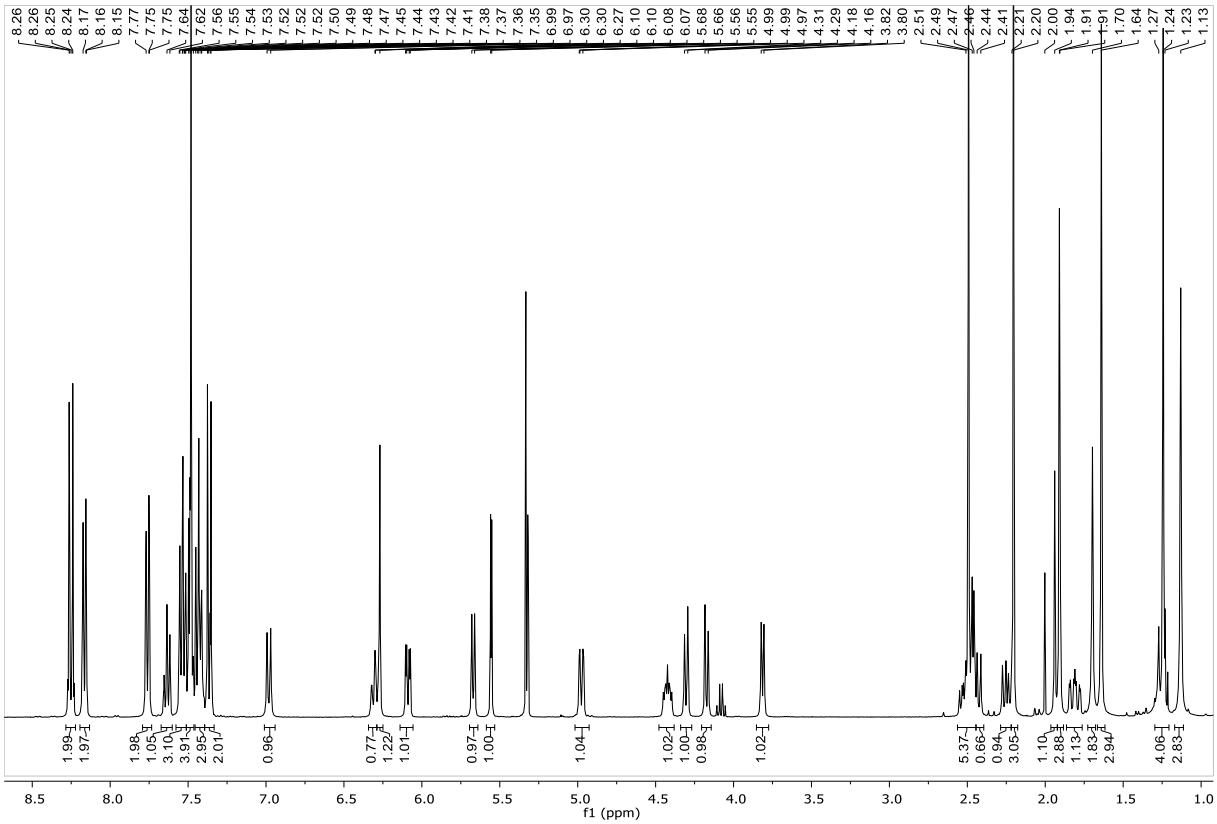

^{13}C NMR (101 MHz, CD_2Cl_2)

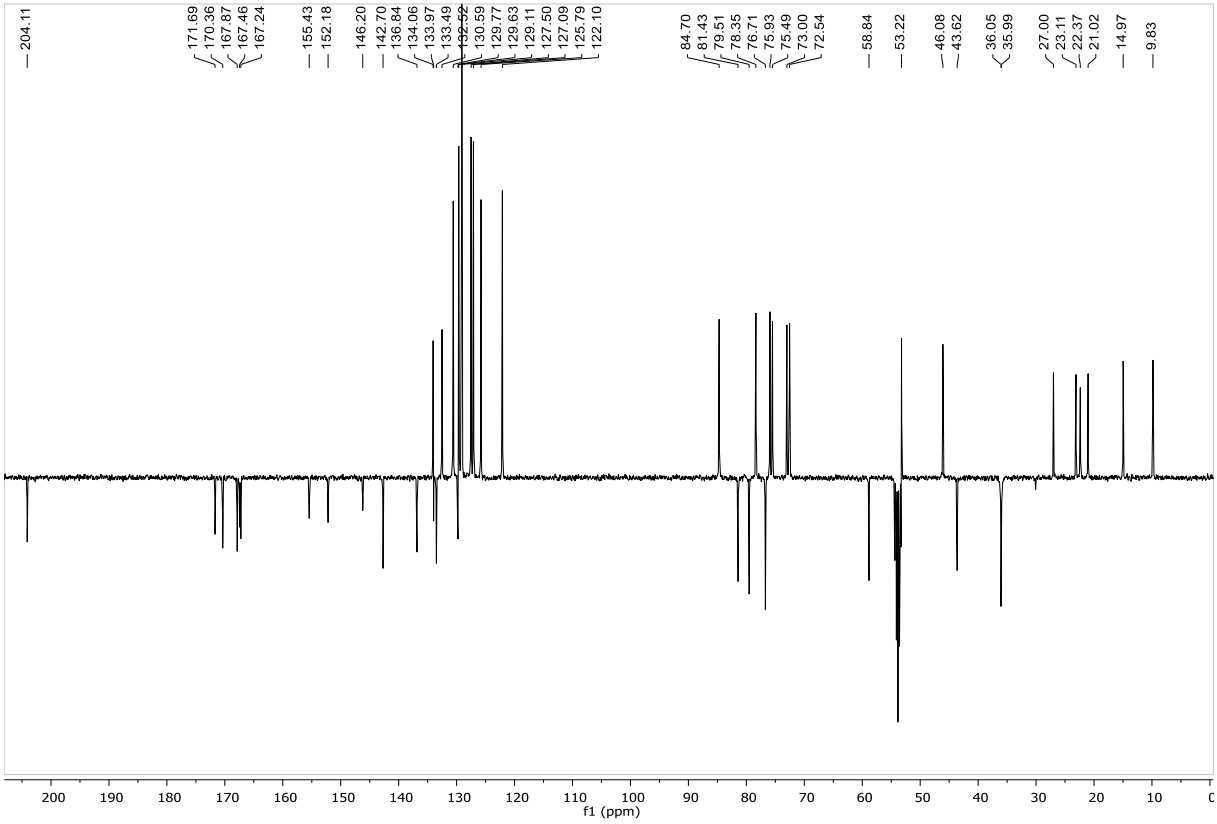

Compound 87b

^{1}H NMR (400 MHz, DMSO-d_6)

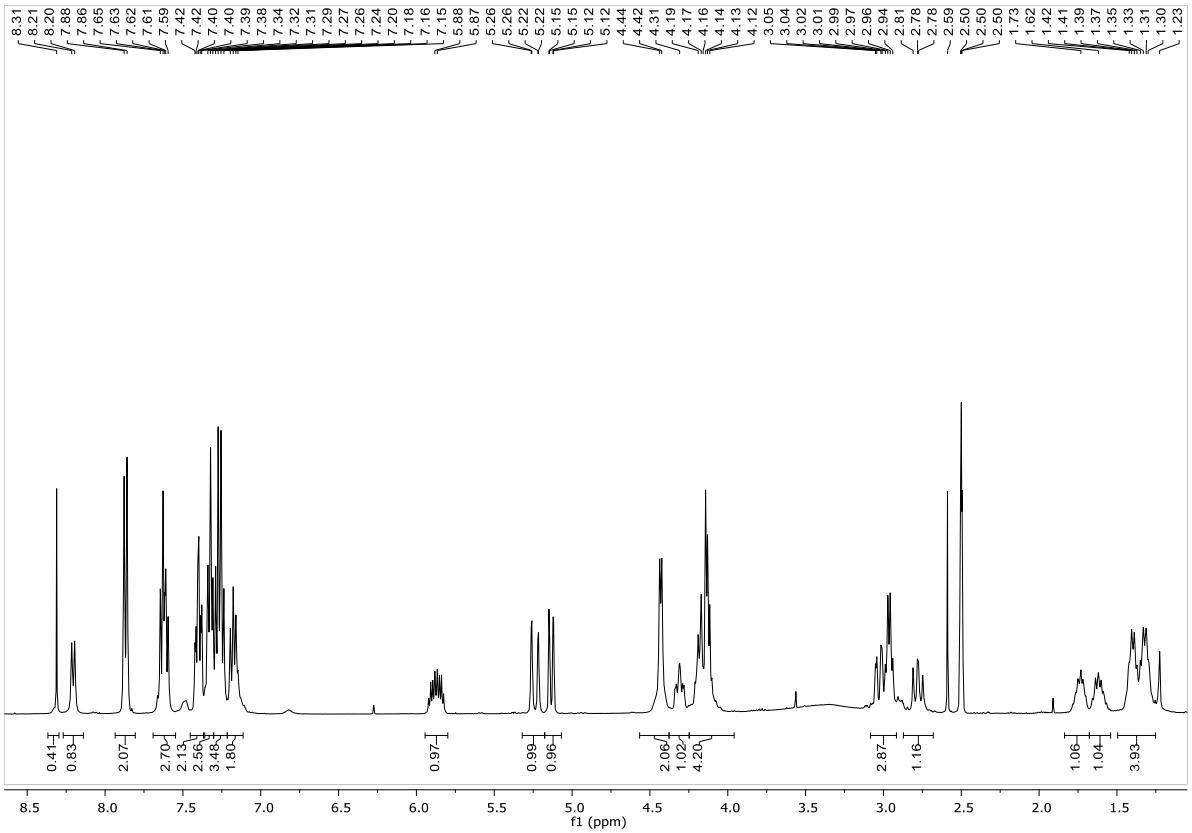

^{13}C NMR (101 MHz, DMSO-d_6)

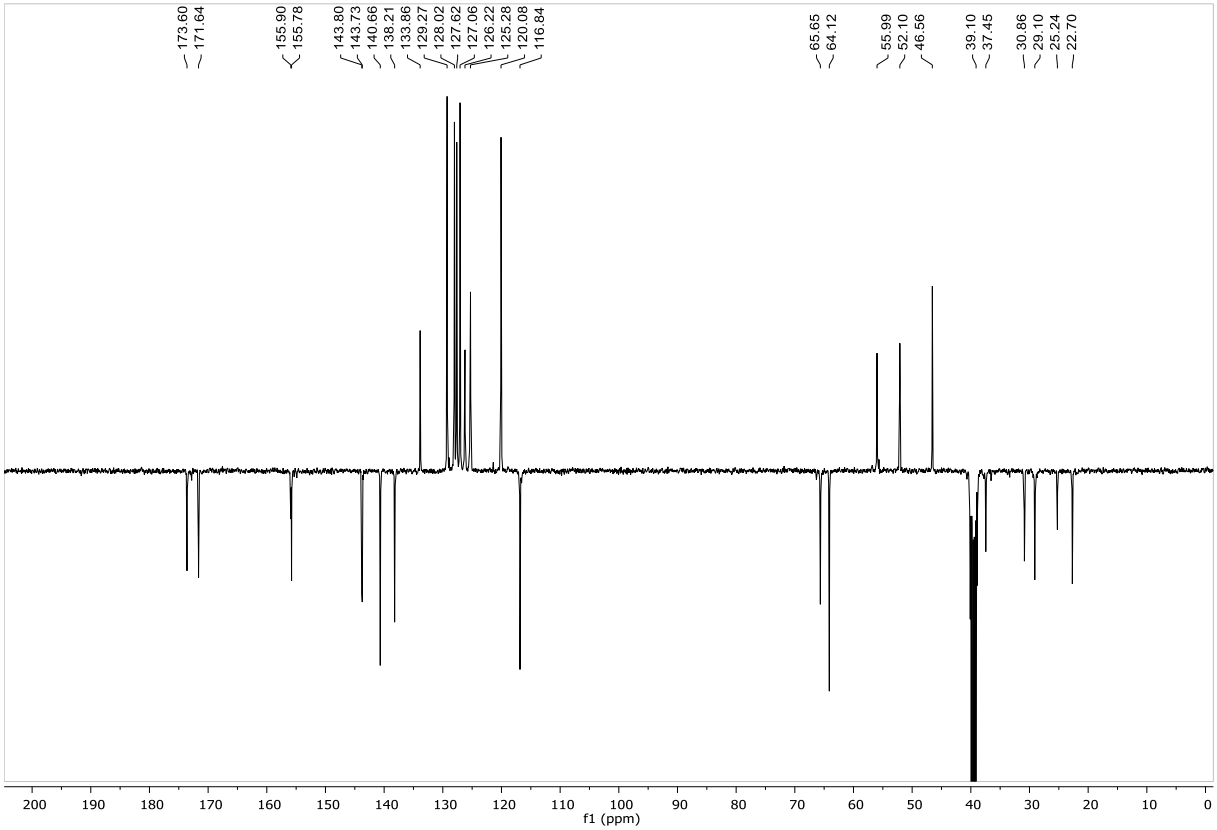

Compound 88b

^{1}H NMR (400 MHz, DMSO-d_6)

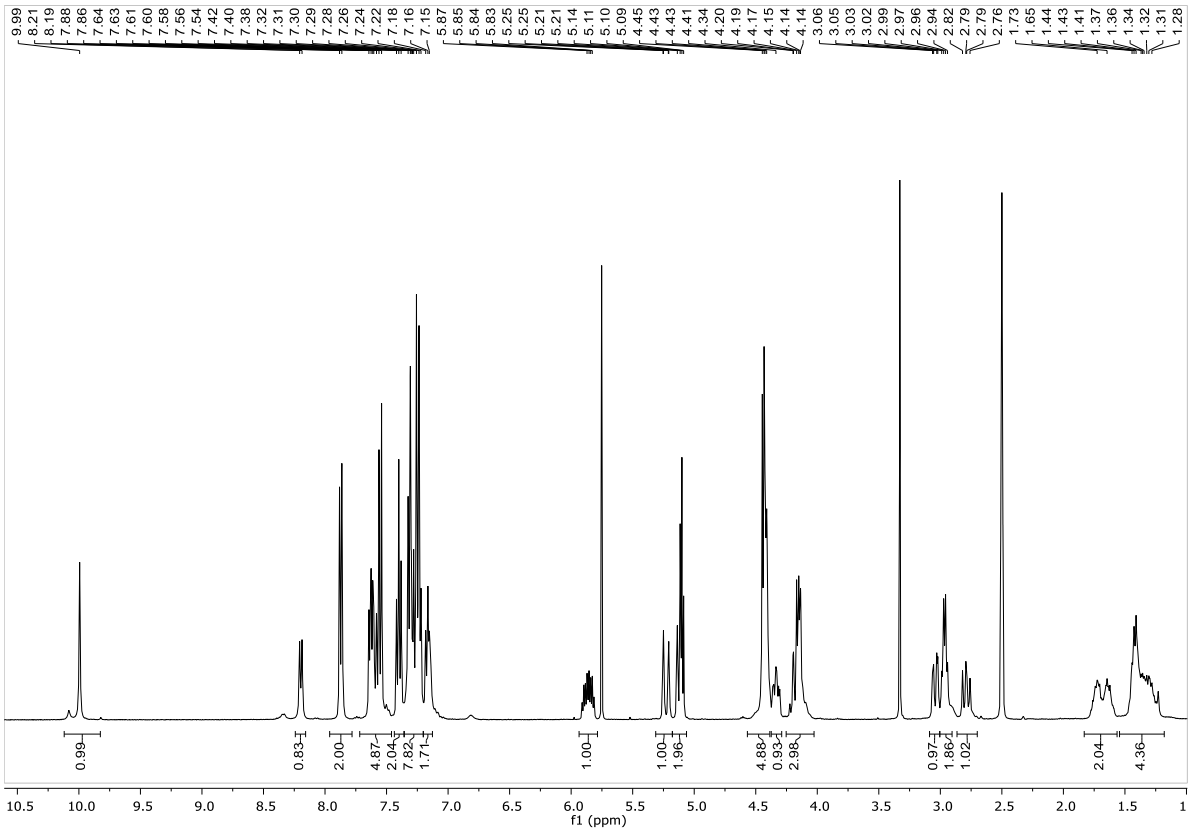

^{13}C NMR (101 MHz, DMSO-d_6)

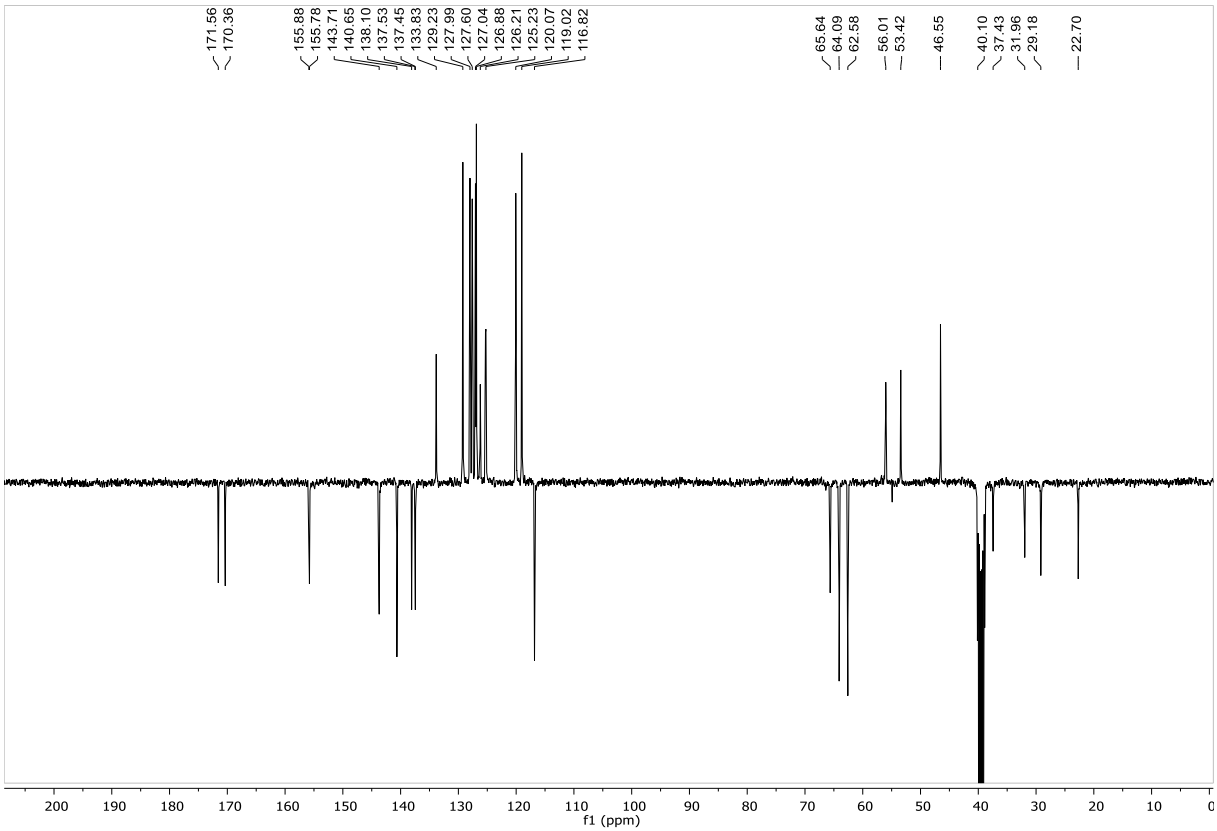

Compound 89a

^{1}H NMR (400 MHz, THF-d_8)

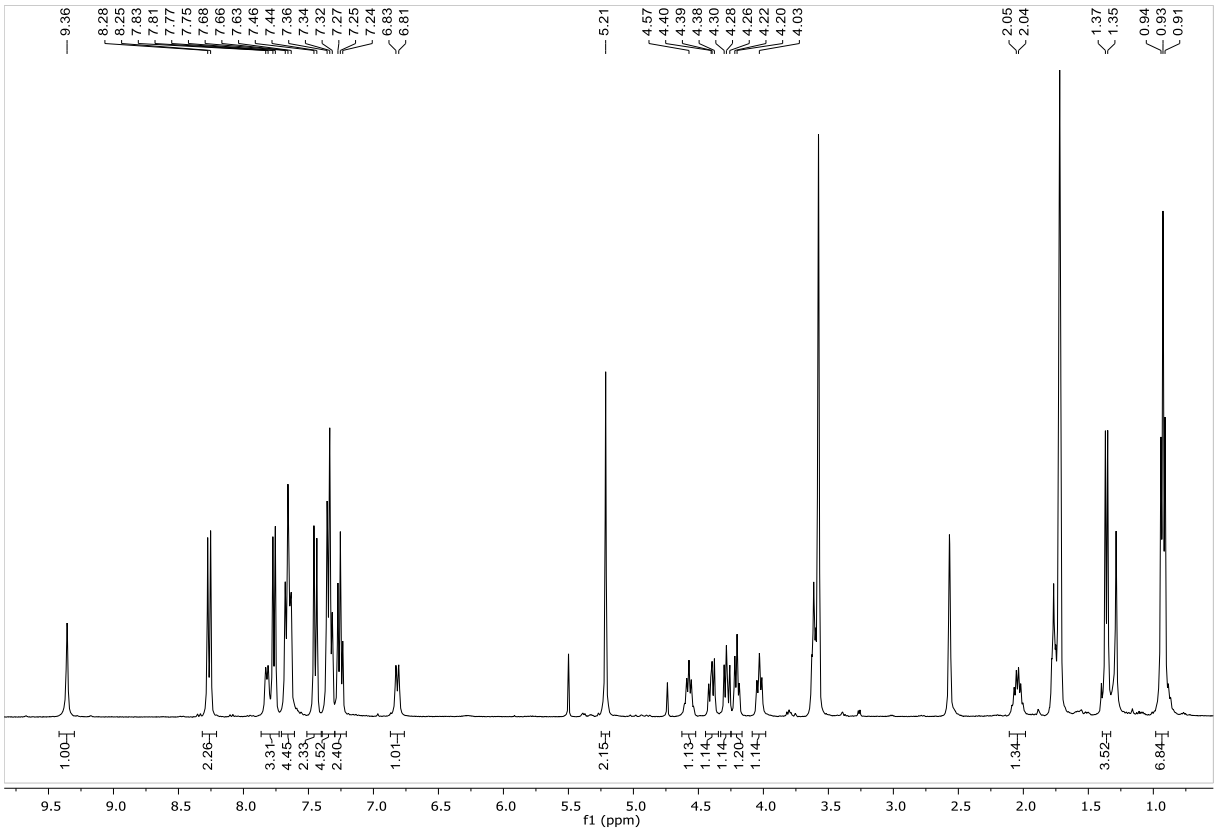

^{13}C NMR (101 MHz, THF-d_8)

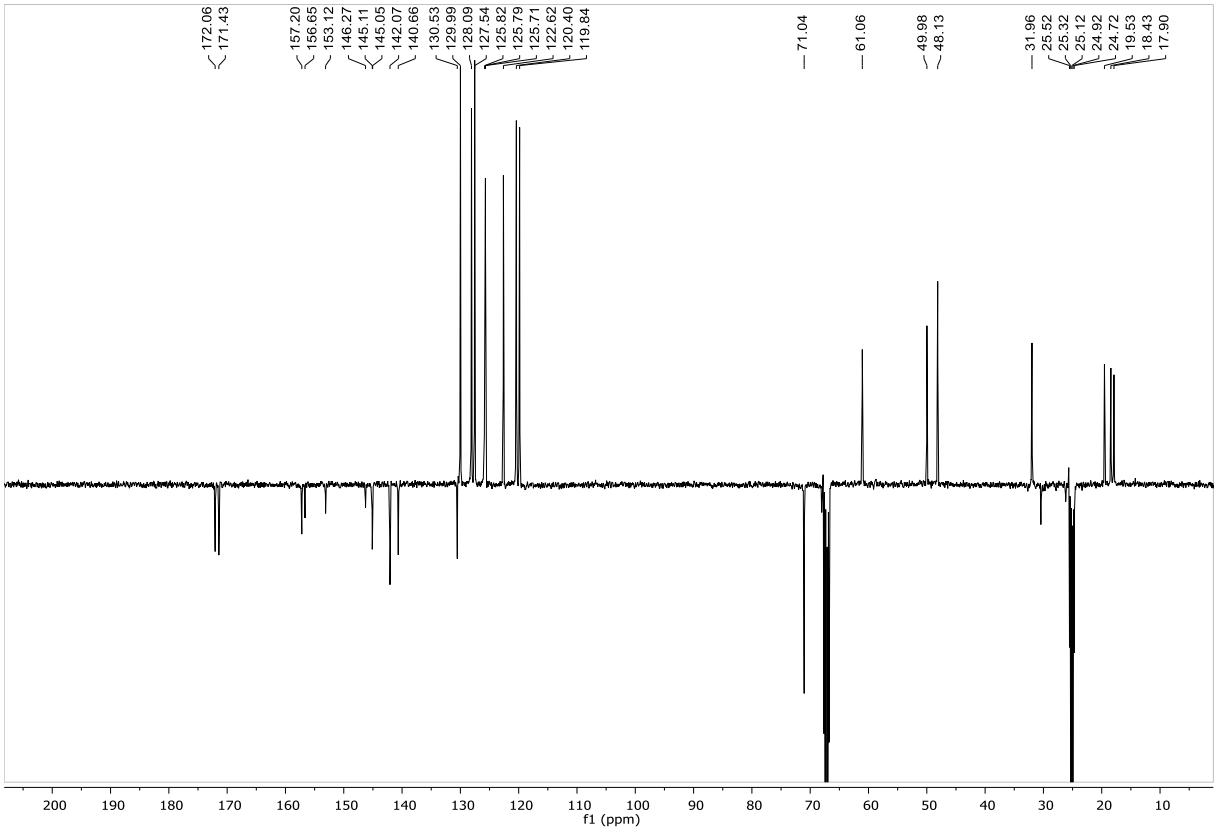

Compound 89b

^{1}H NMR (400 MHz, THF-d_8)

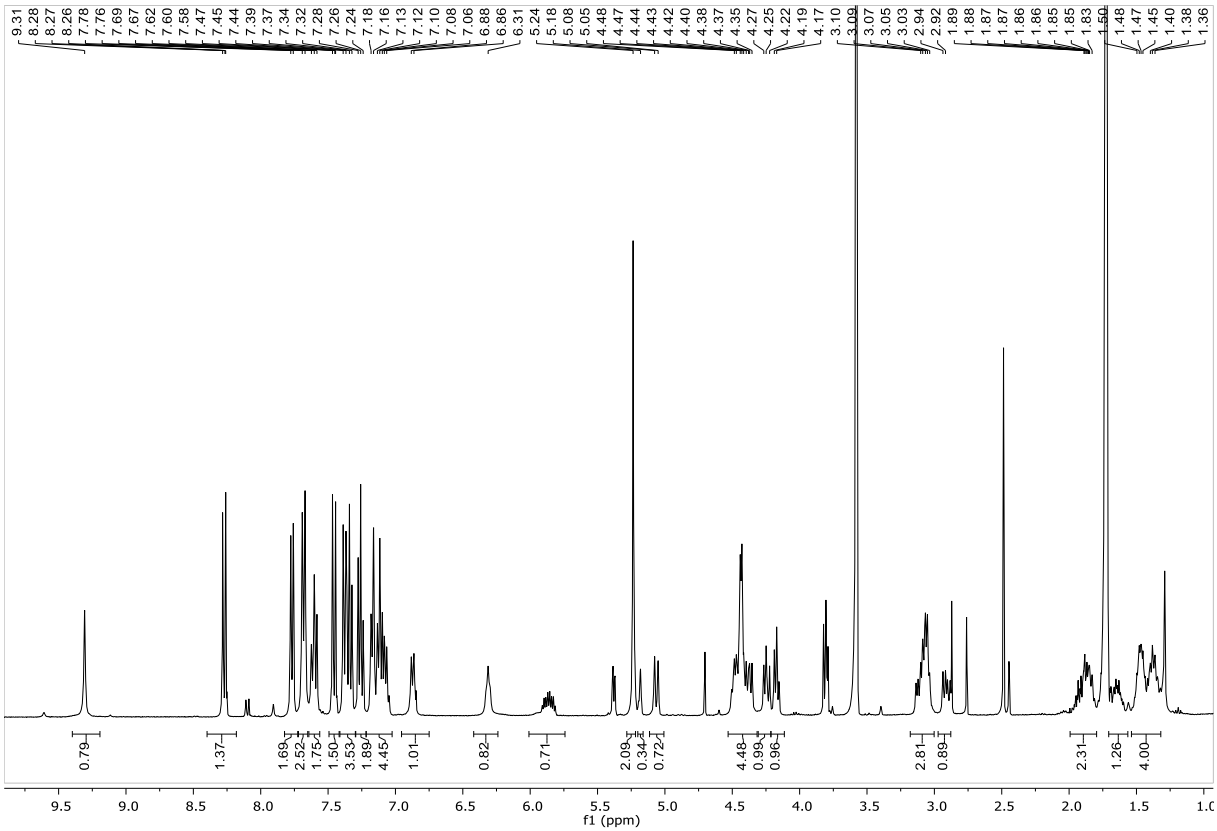

^{13}C NMR (101 MHz, THF-d_8)

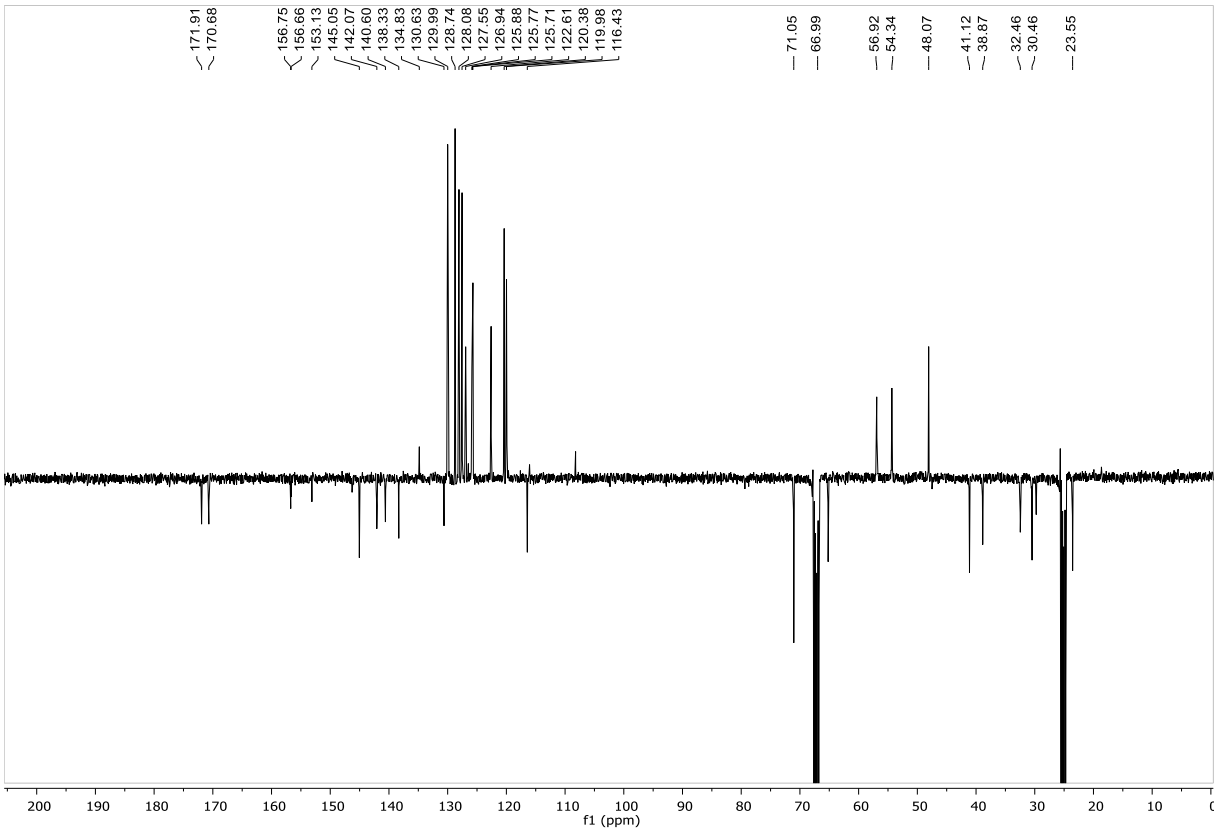

Compound 90a

^{1}H NMR (400 MHz, CD_3OD)

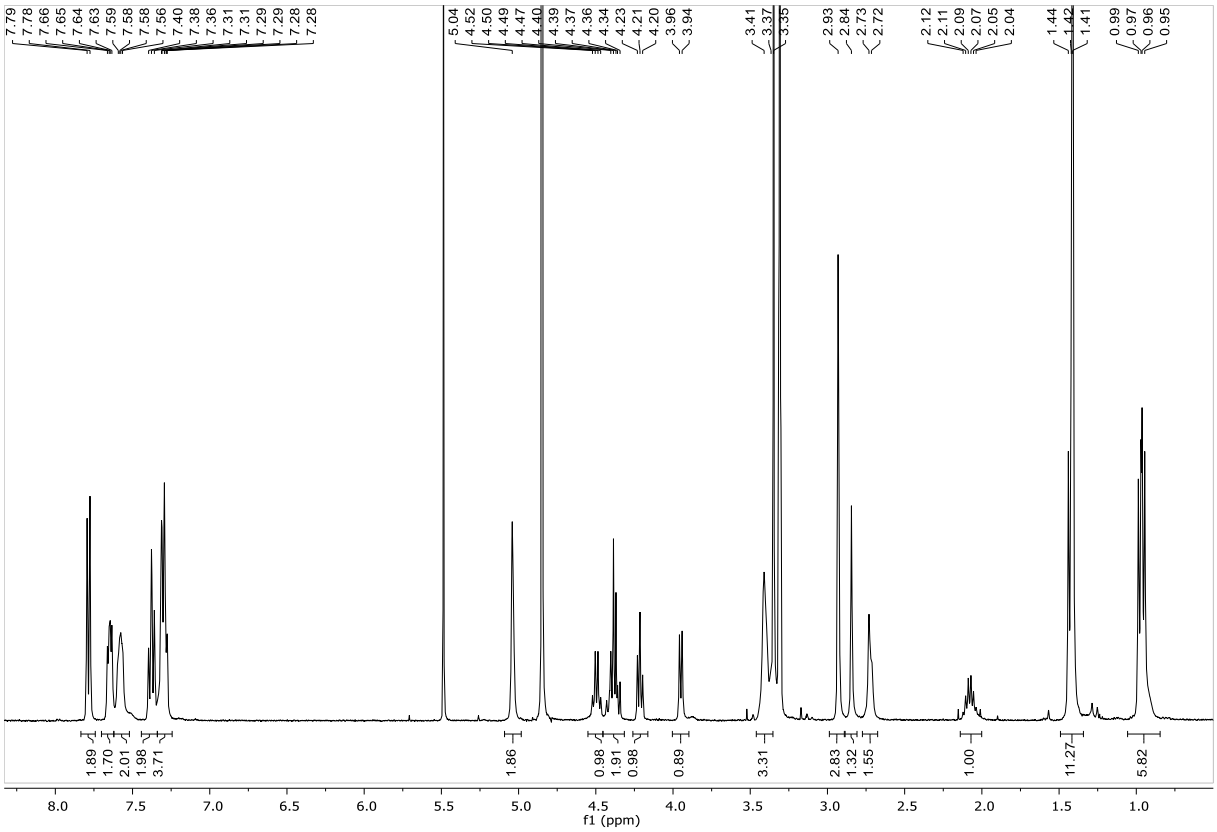

^{13}C NMR (101 MHz, CD_3OD)

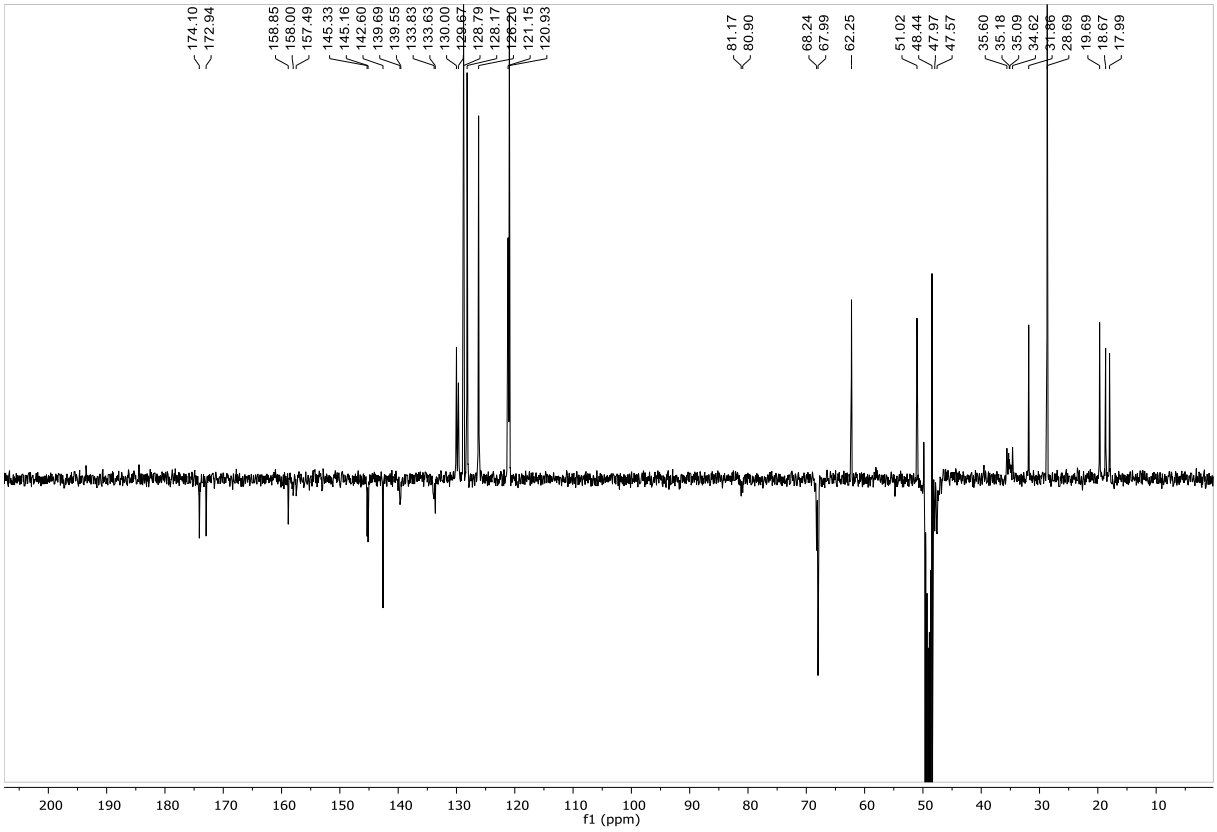

Compound 90b

^{1}H NMR (400 MHz, CD_2Cl_2)

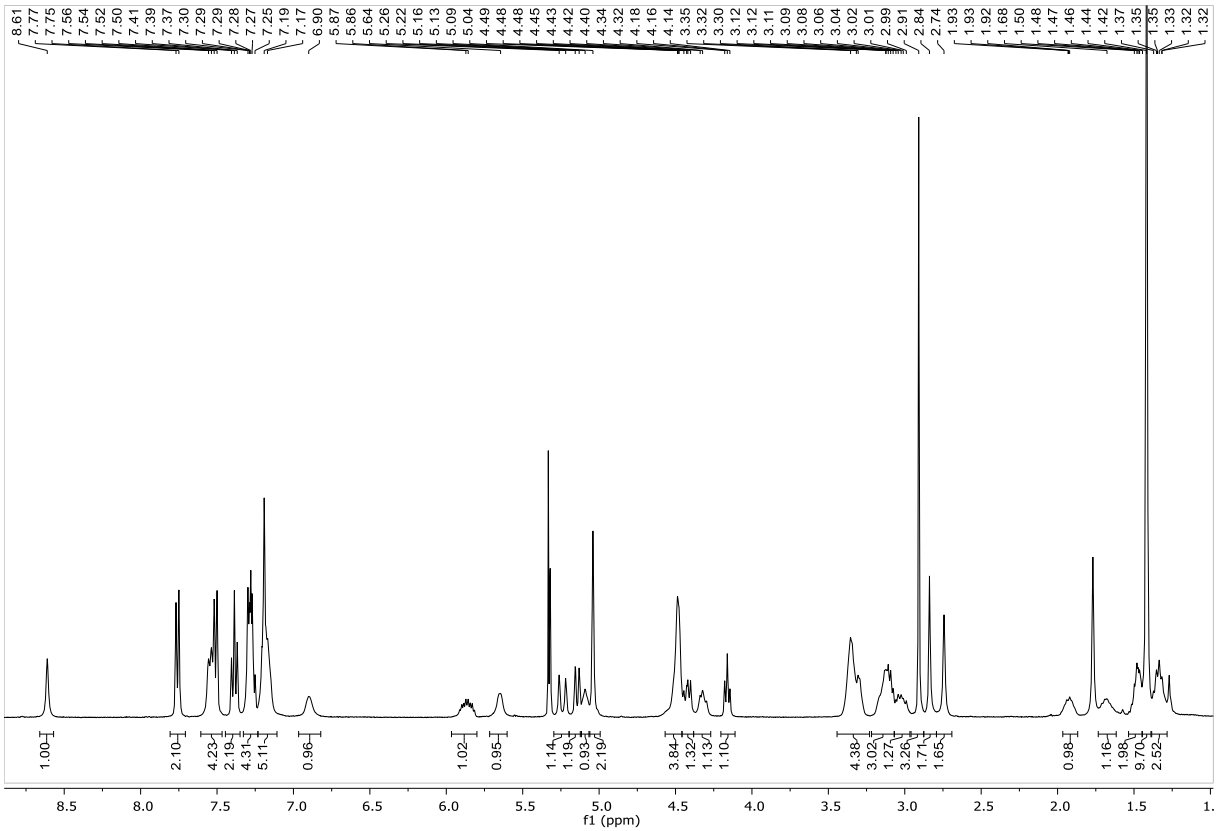

^{13}C NMR (101 MHz, CD_2Cl_2)

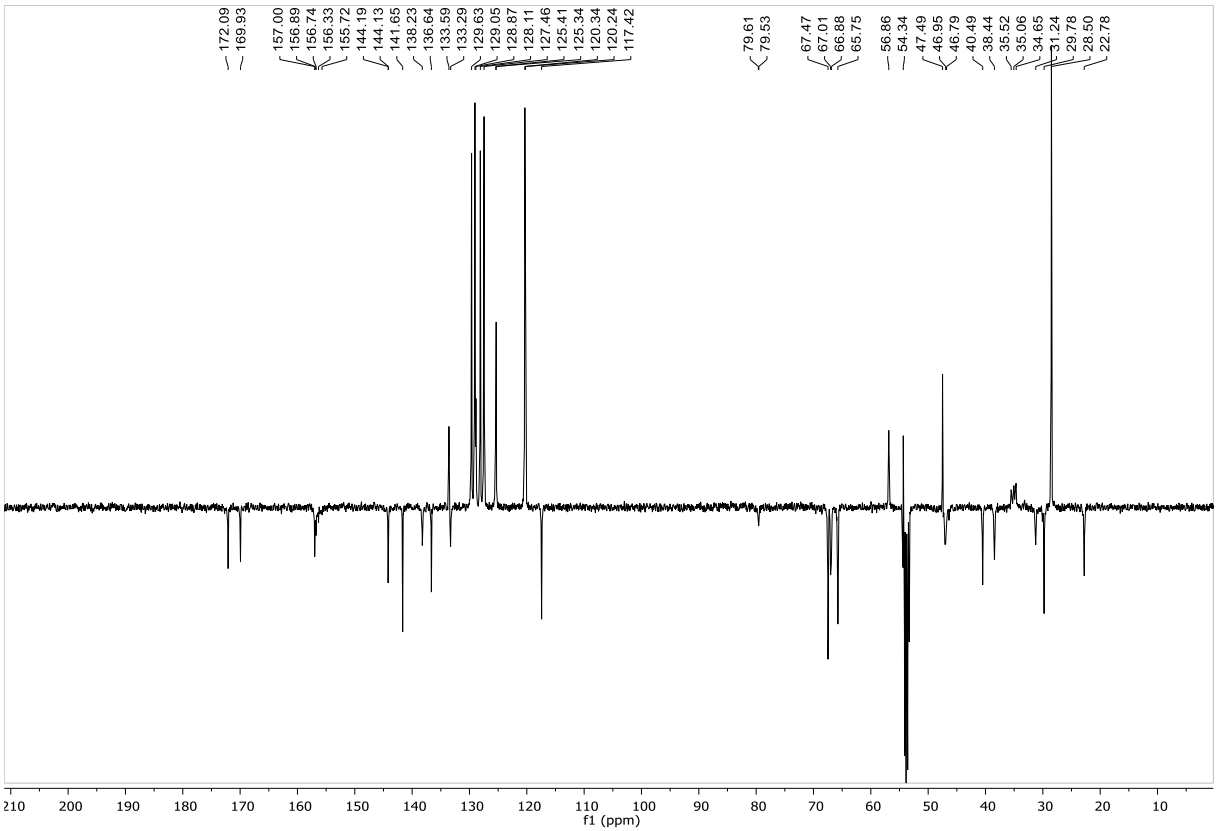

Compound 91a

^{1}H NMR (400 MHz, CD_3OD)

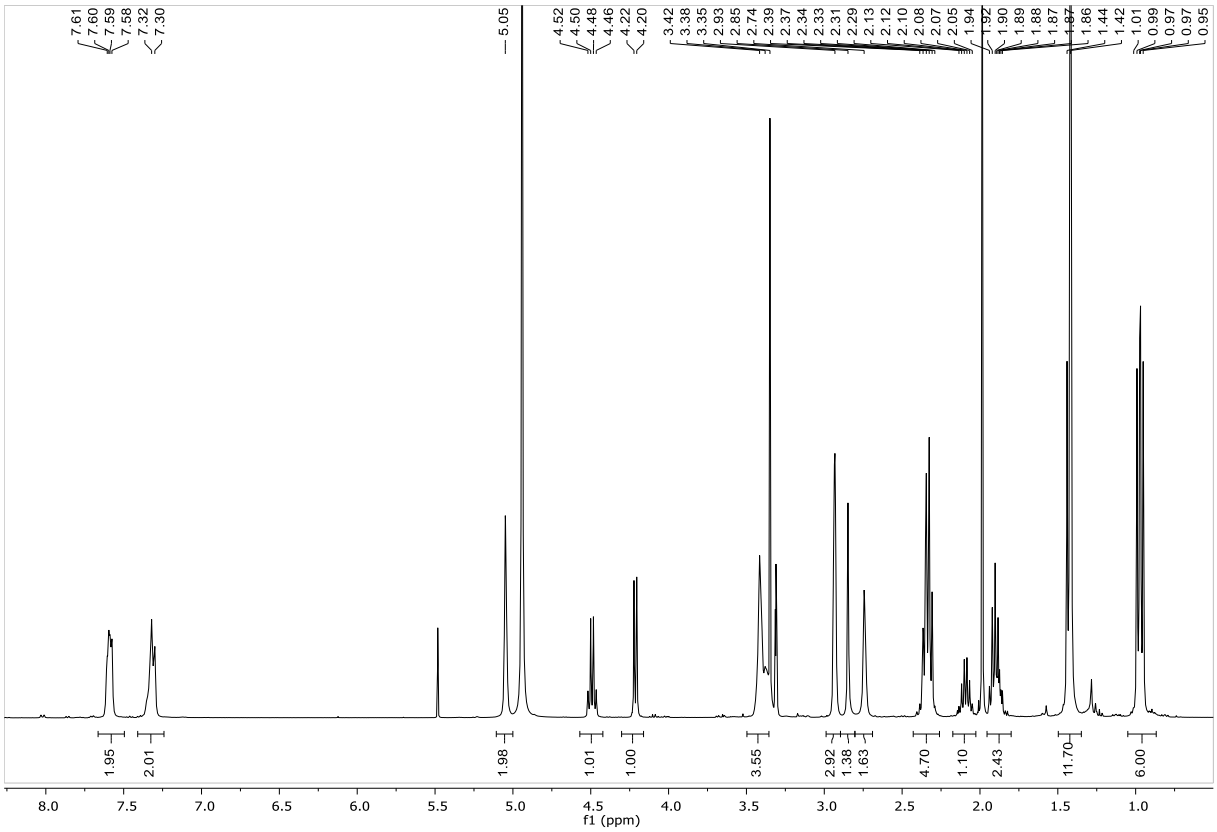

^{13}C NMR (101 MHz, CD_3OD)

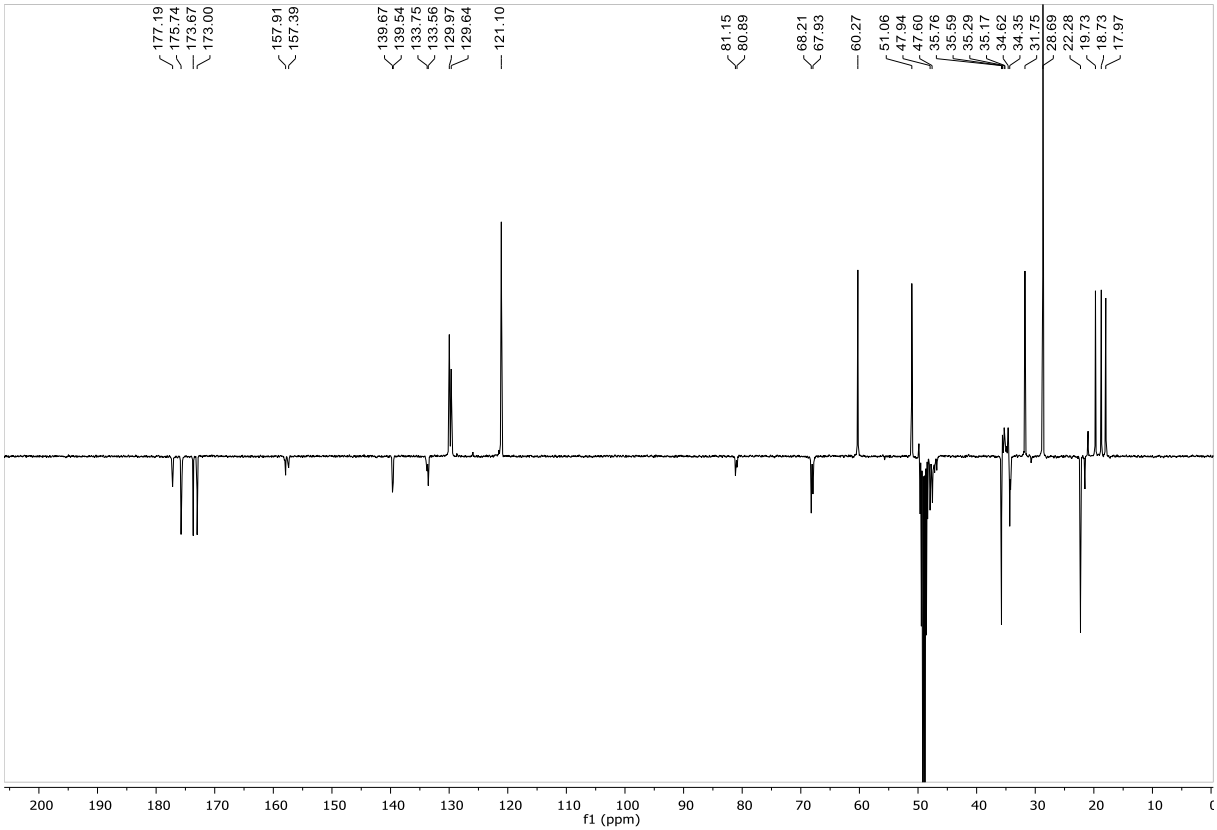

Compound 91b

^{1}H NMR (400 MHz, CD_3OD)

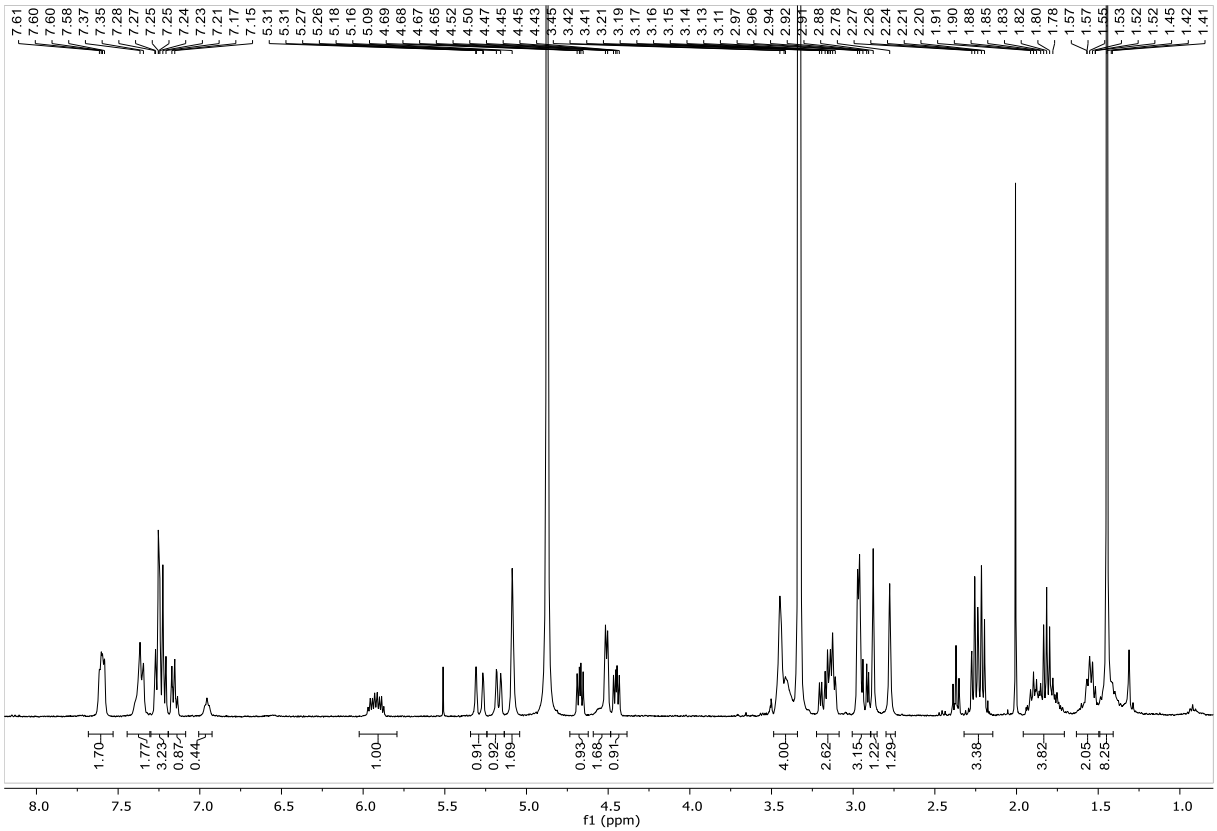

^{13}C NMR (101 MHz, CD_3OD)

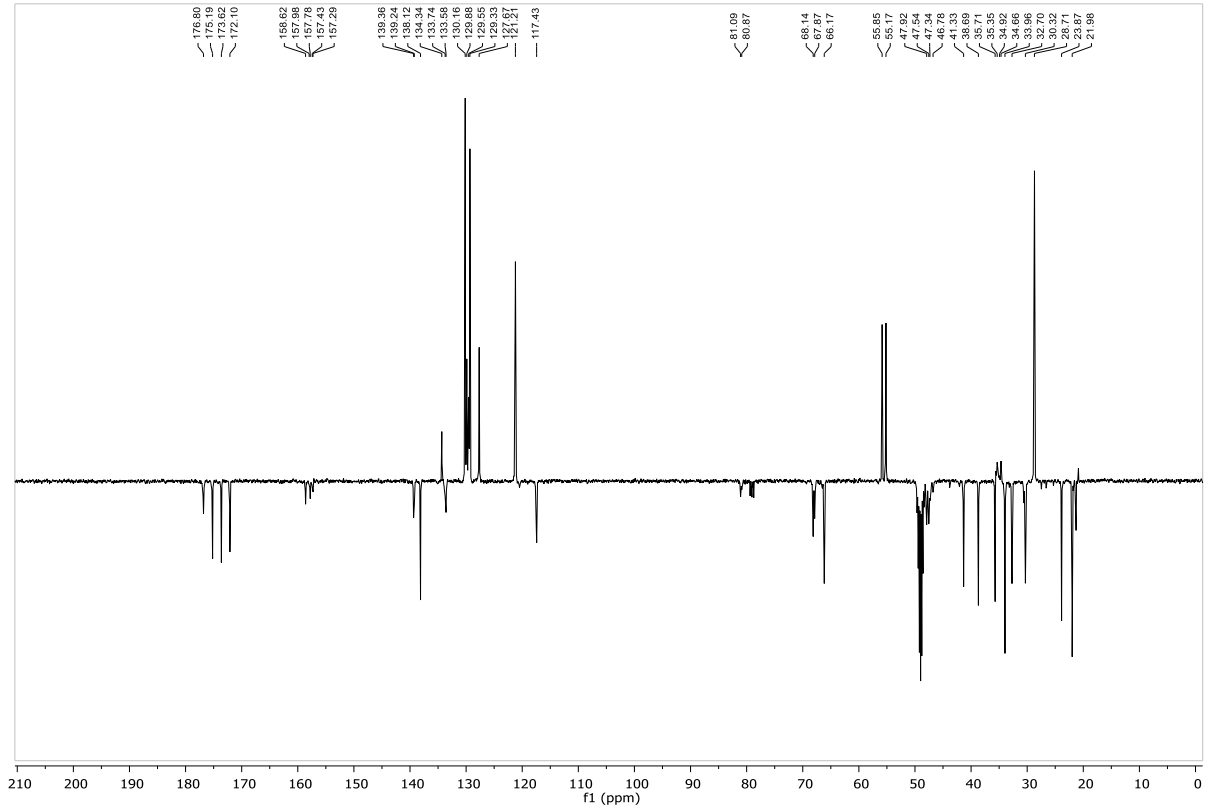

Compound Boc-92a

^{1}H NMR (400 MHz, CD_3OD)

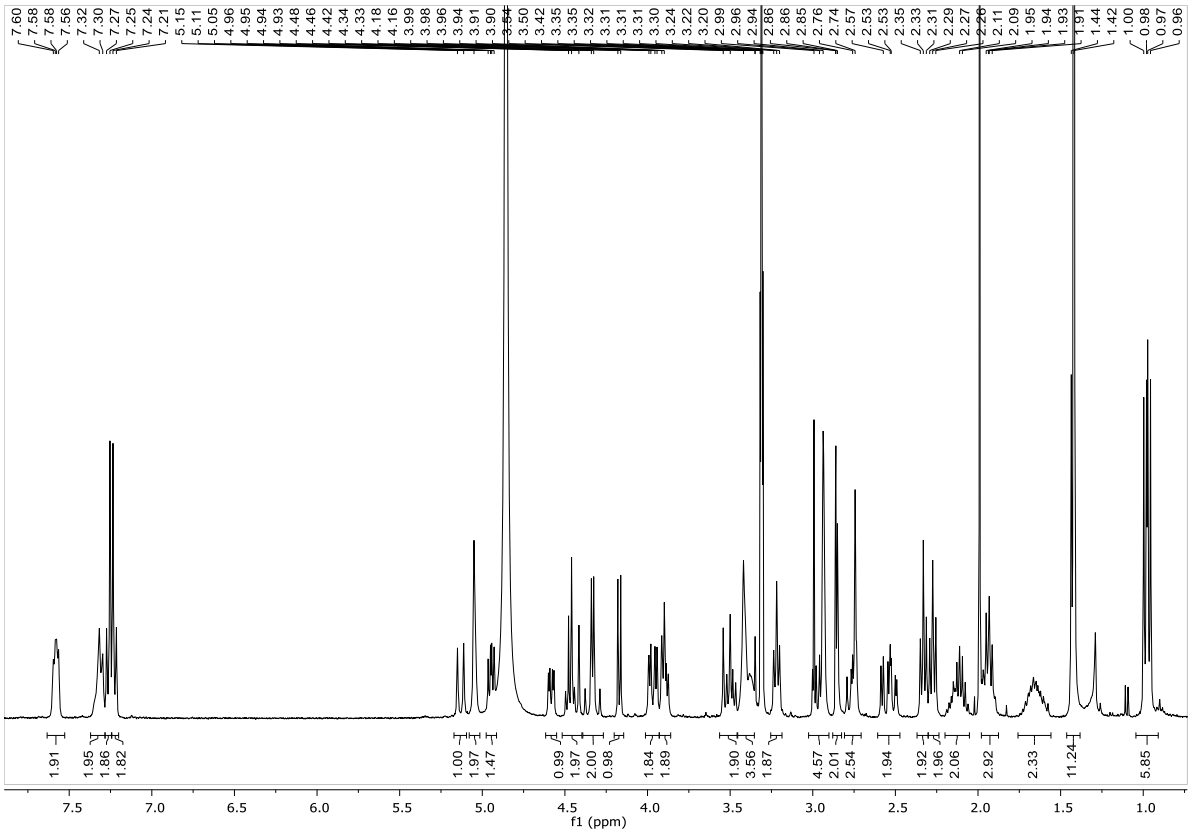

^{13}C NMR (101 MHz, CD_3OD)

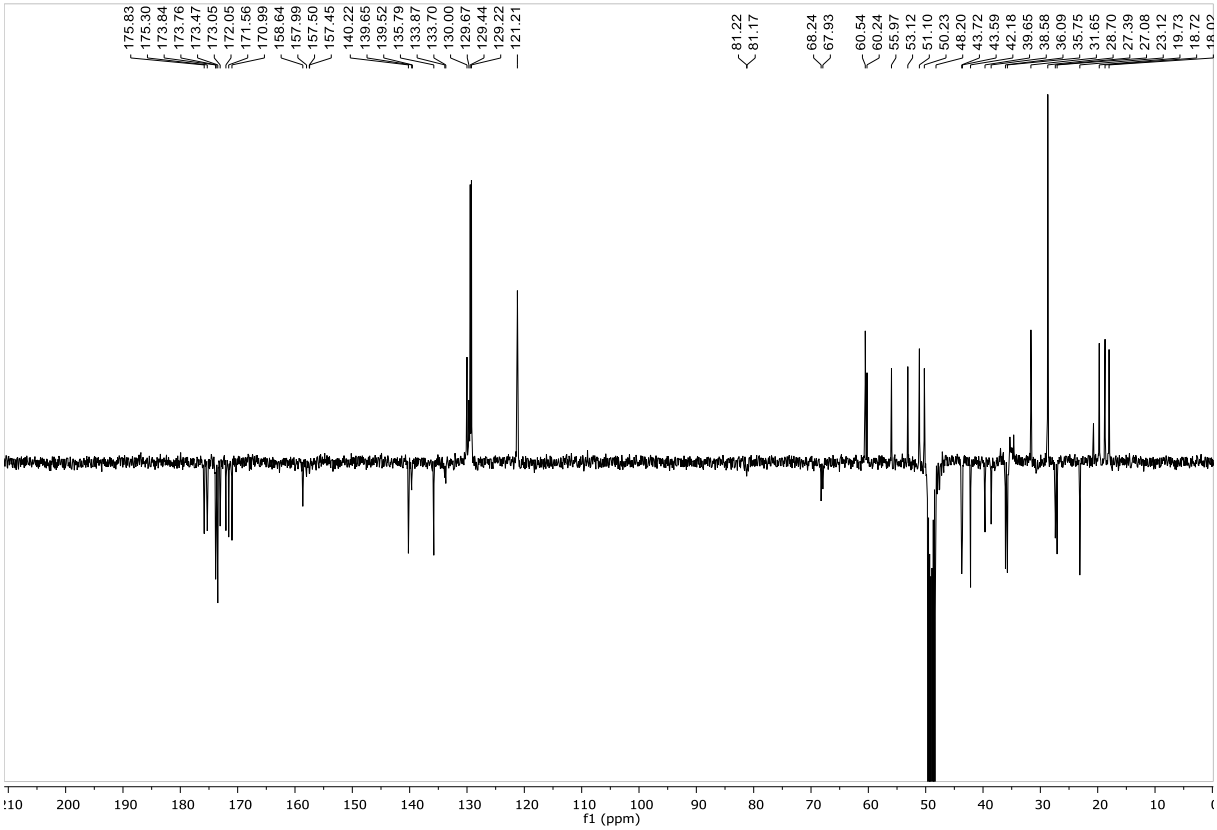

Compound 92b

^{1}H NMR (400 MHz, CD_3OD)

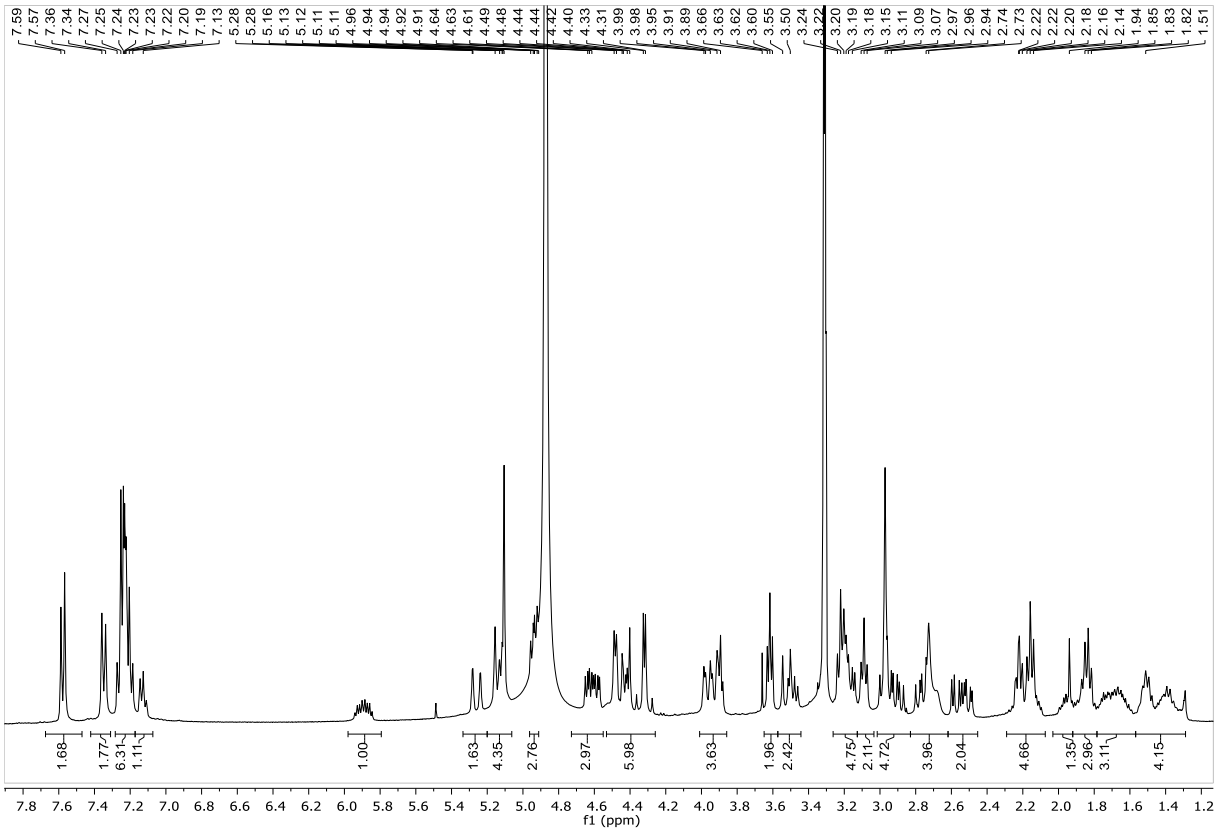

^{13}C NMR (101 MHz, CD_3OD)

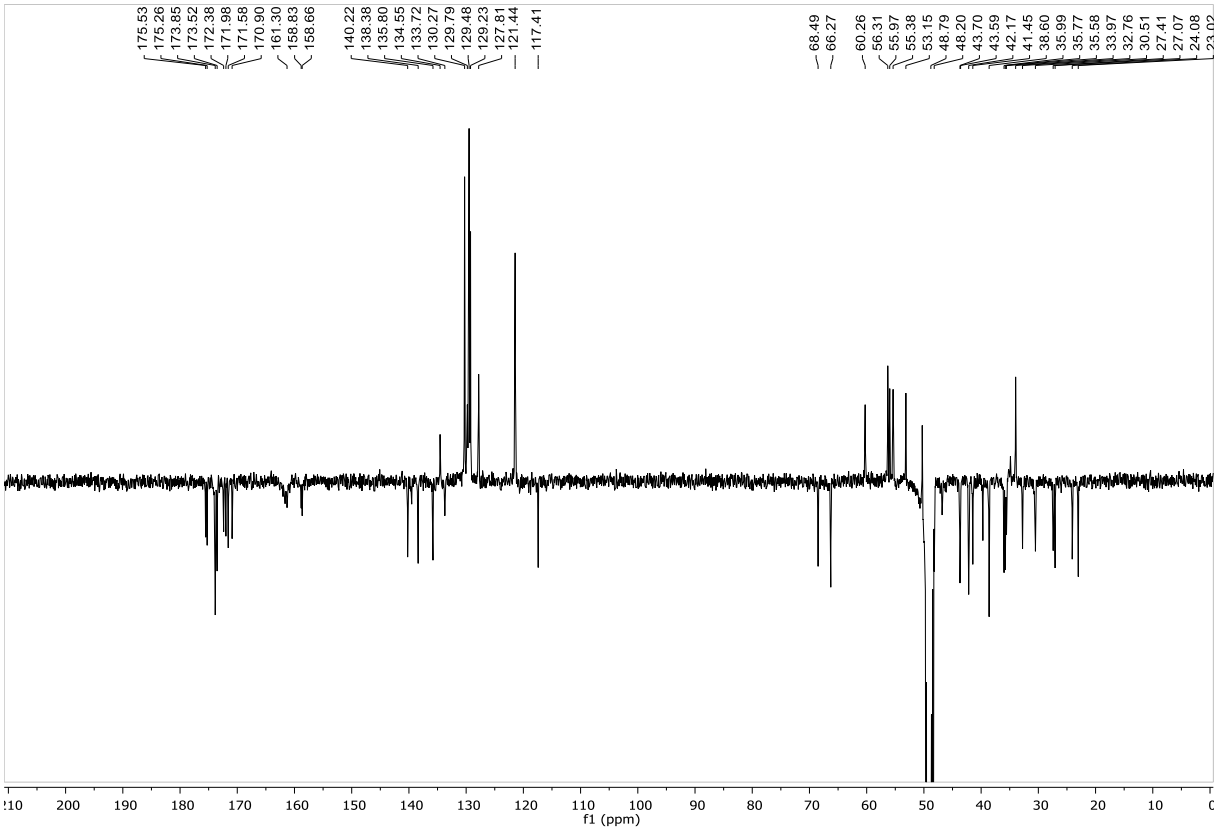

Compound 93

^{1}H NMR (400 MHz, CD_3OD)

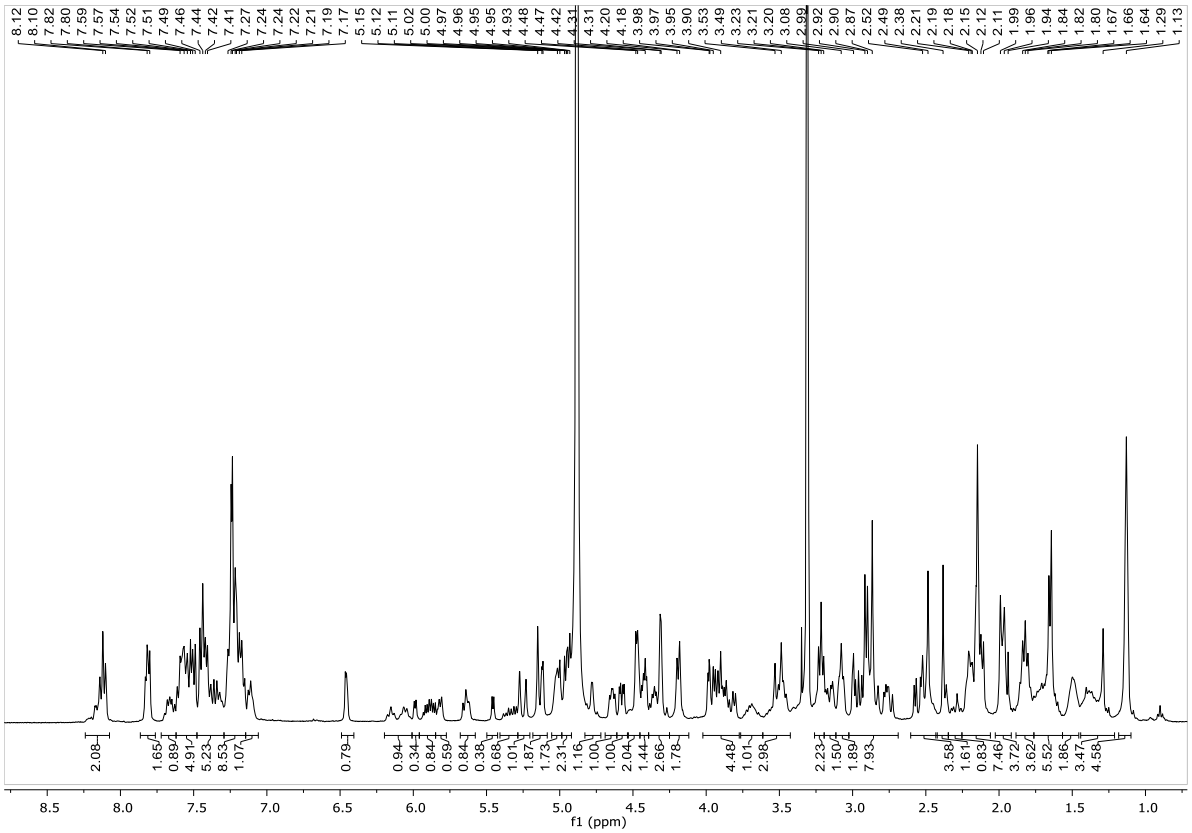

^{13}C NMR (101 MHz, CD_3OD)

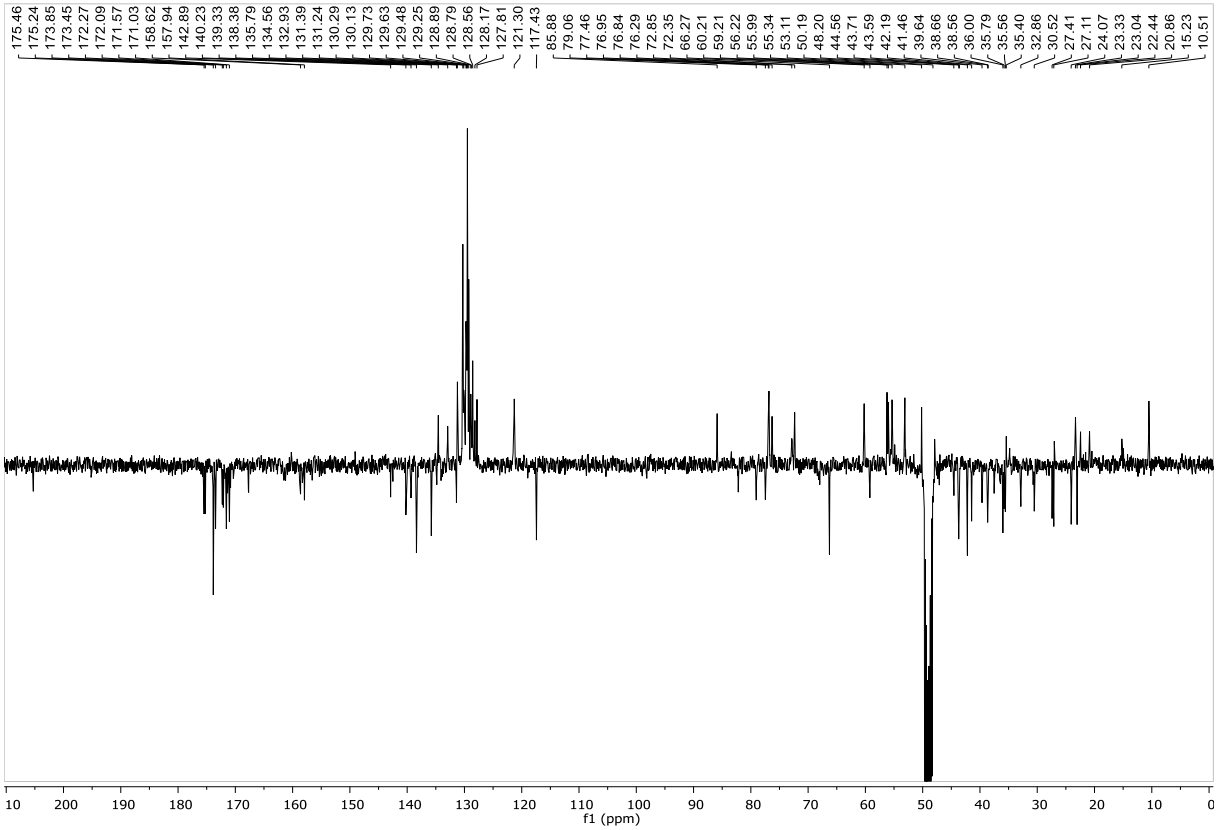

Compound Boc-94

^{1}H NMR (400 MHz, CD_3OD)

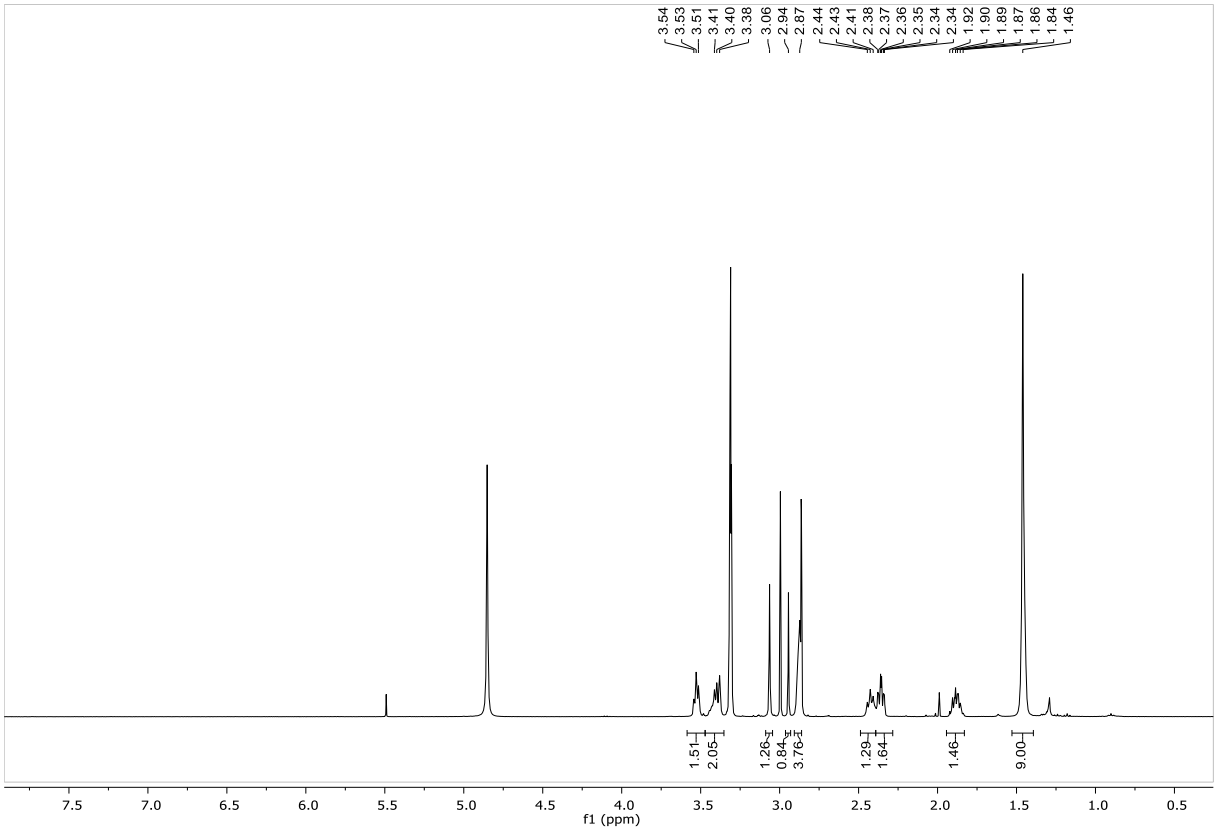

^{13}C NMR (101 MHz, CD_3OD)

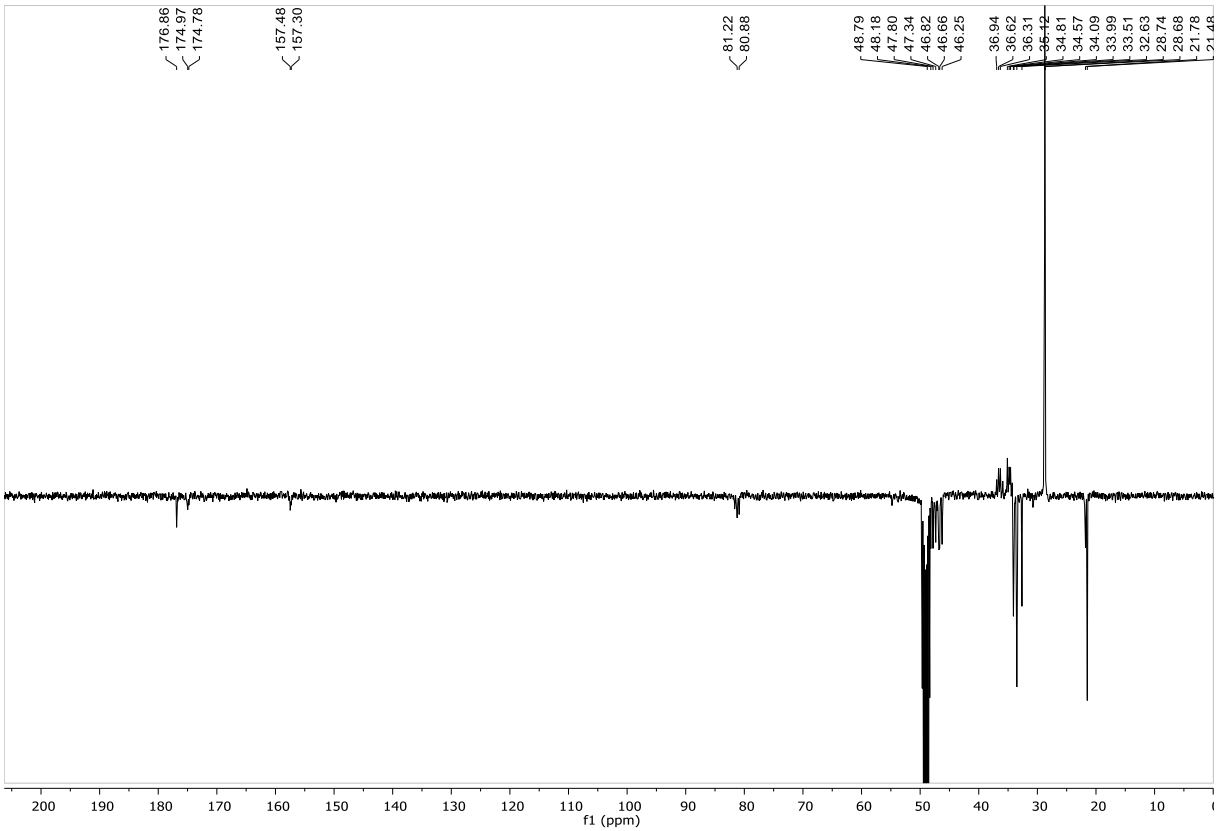

Compound 95

^{1}H NMR (400 MHz, CD_2Cl_2)

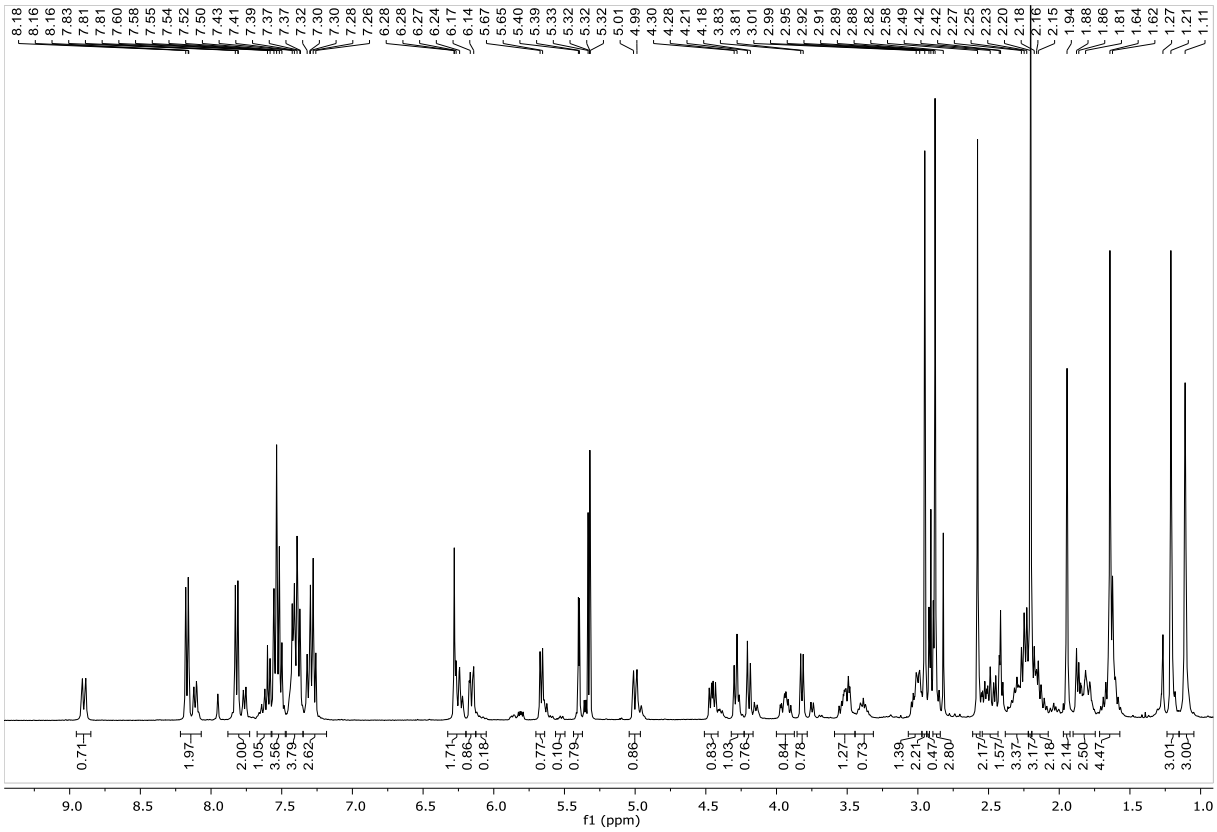

^{13}C NMR (101 MHz, CD_2Cl_2)

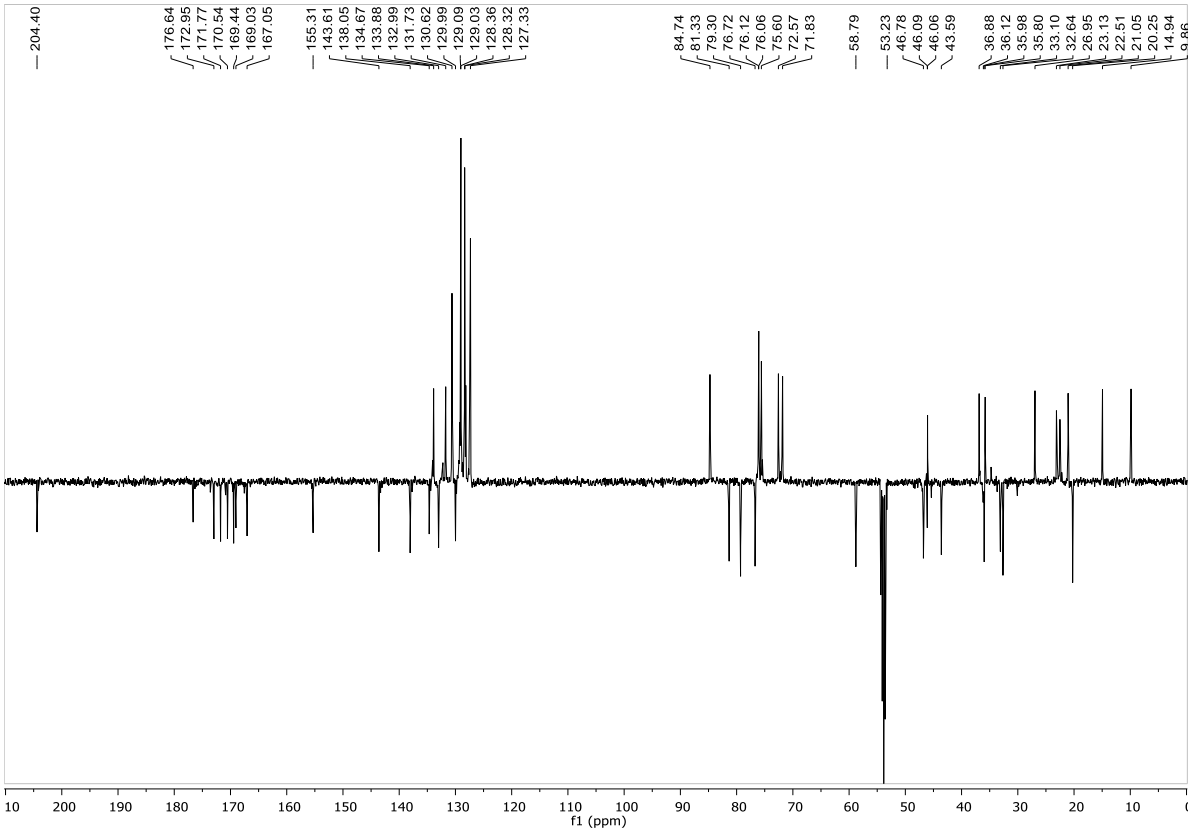

Compound 101

^{1}H NMR (500 MHz, DMSO-d_6)

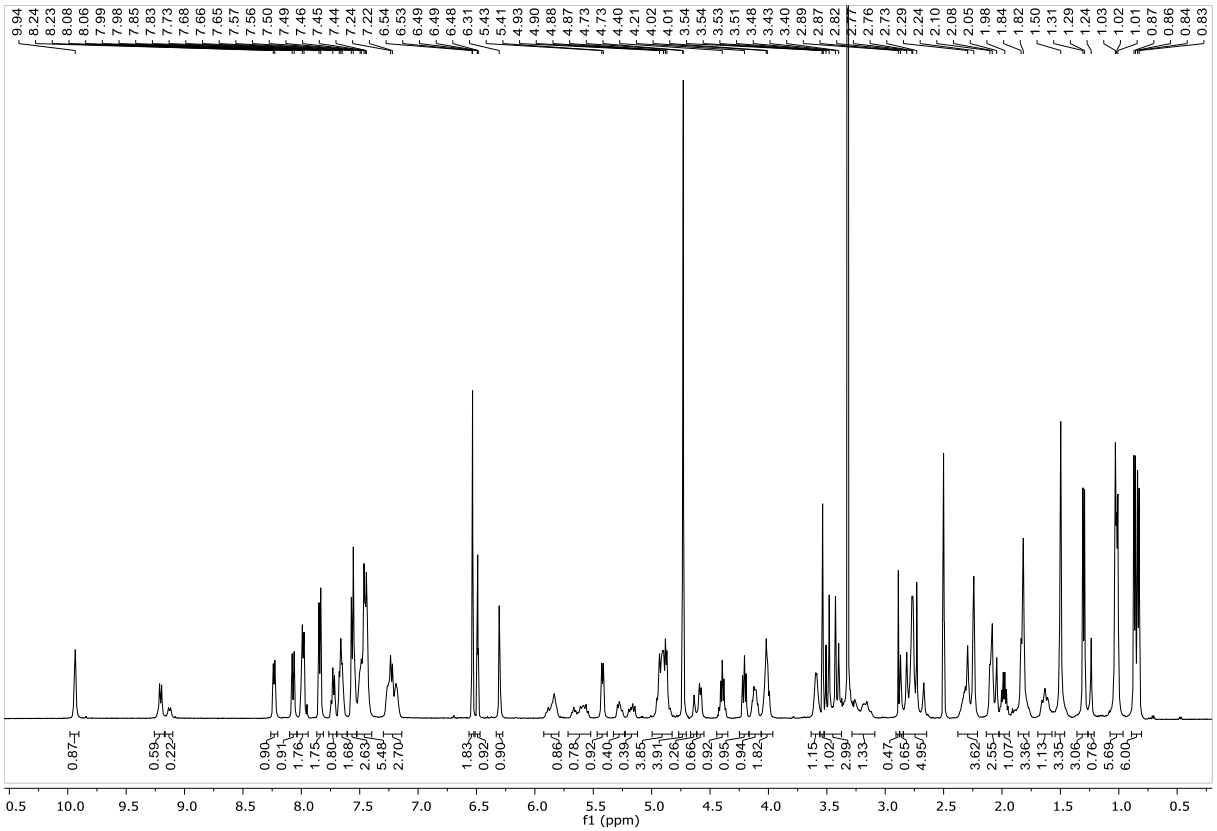

^{13}C NMR (101 MHz, DMSO-d_6)

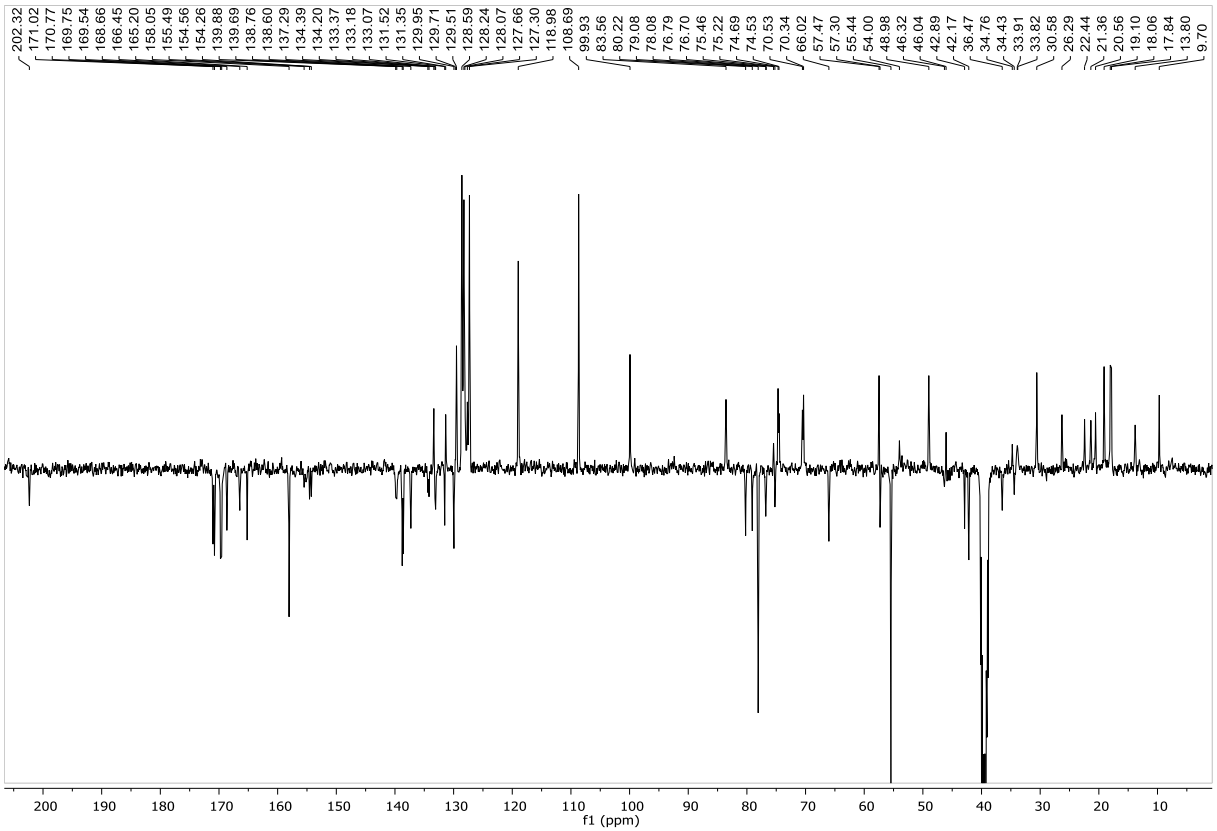

Compound 102

^{1}H NMR (400 MHz, D_2O)

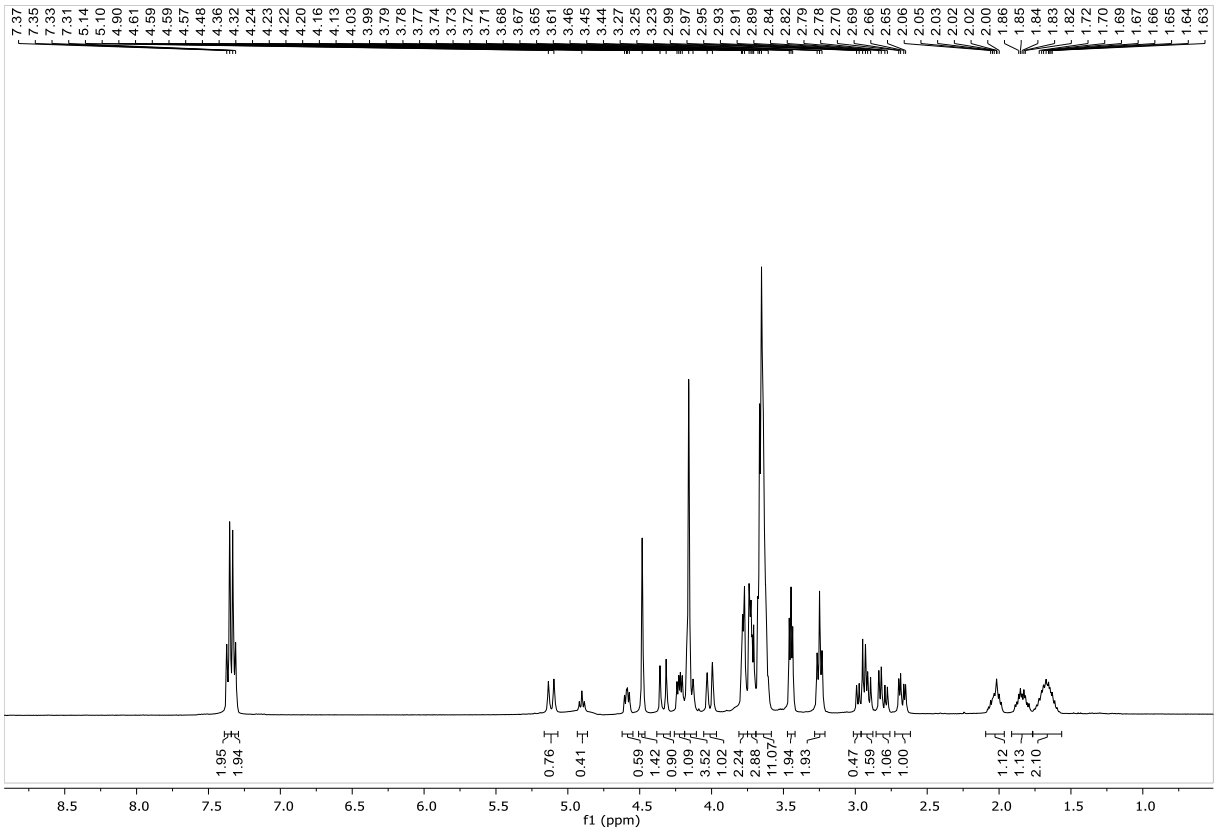

^{13}C NMR (101 MHz, D_2O)

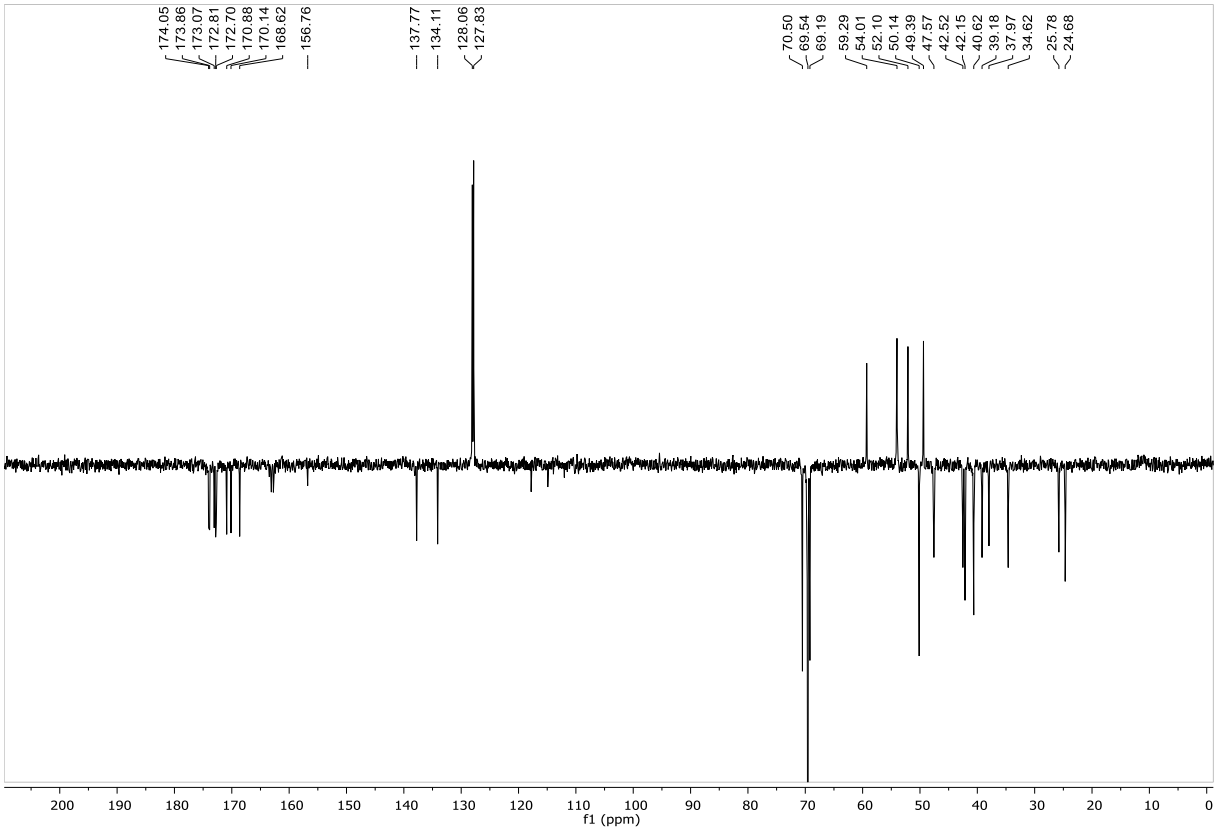

Compound 104

^{1}H NMR (400 MHz, $CDCl_3$)

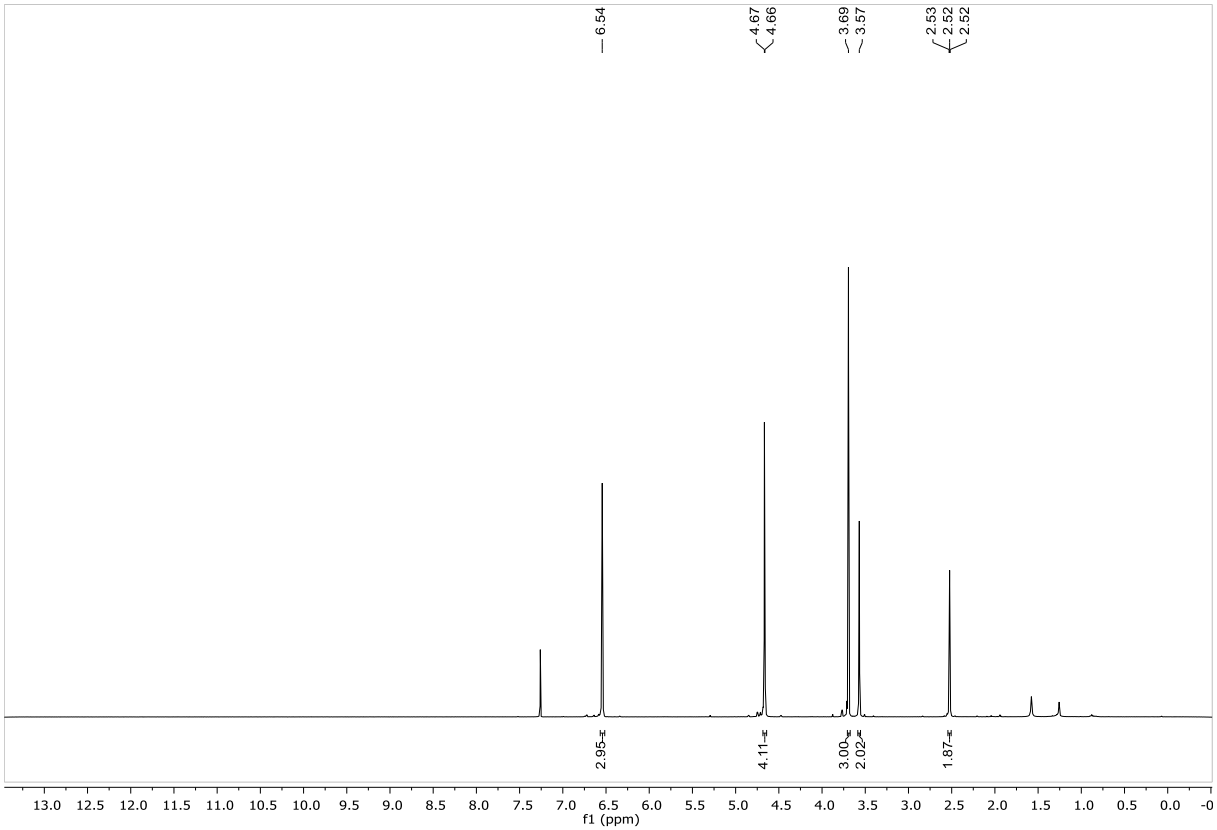

^{13}C NMR (101 MHz, $CDCl_3$)

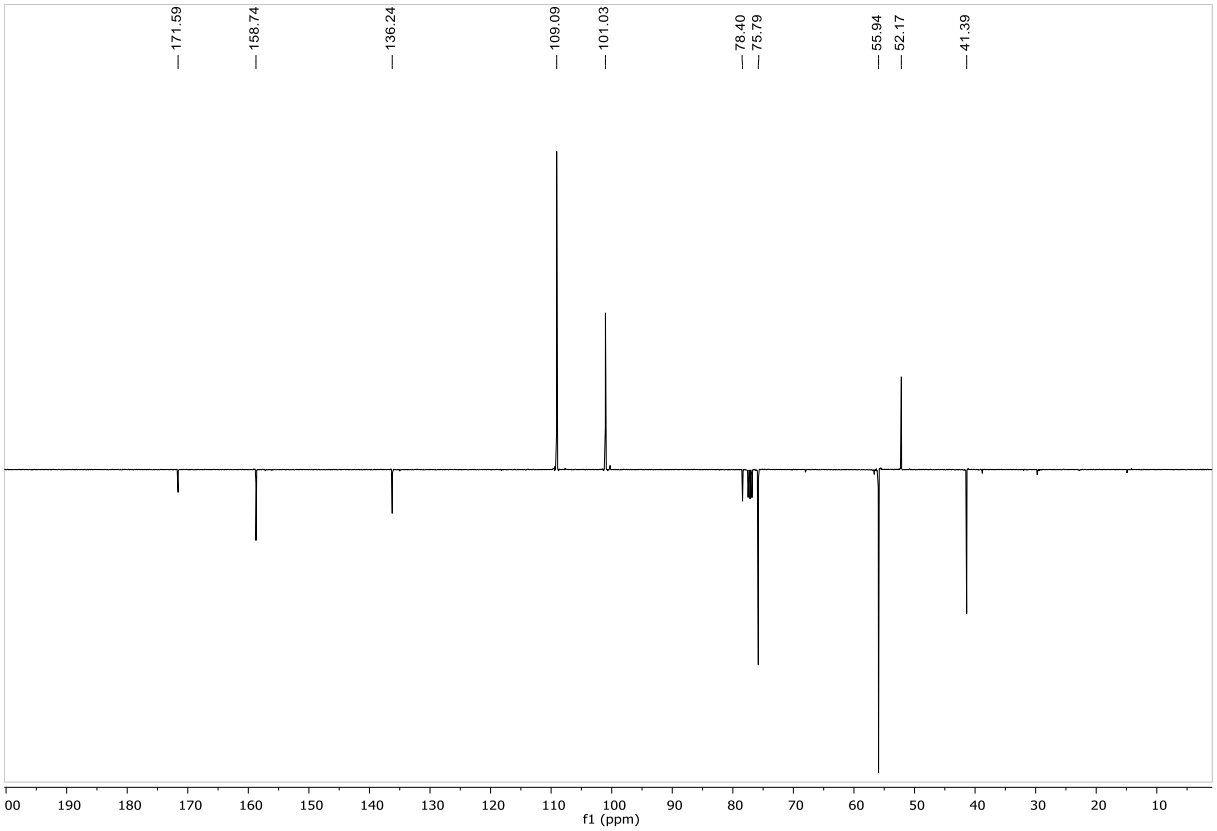

Compound 106

^{1}H NMR (400 MHz, MeOD + DMSO-d_6)

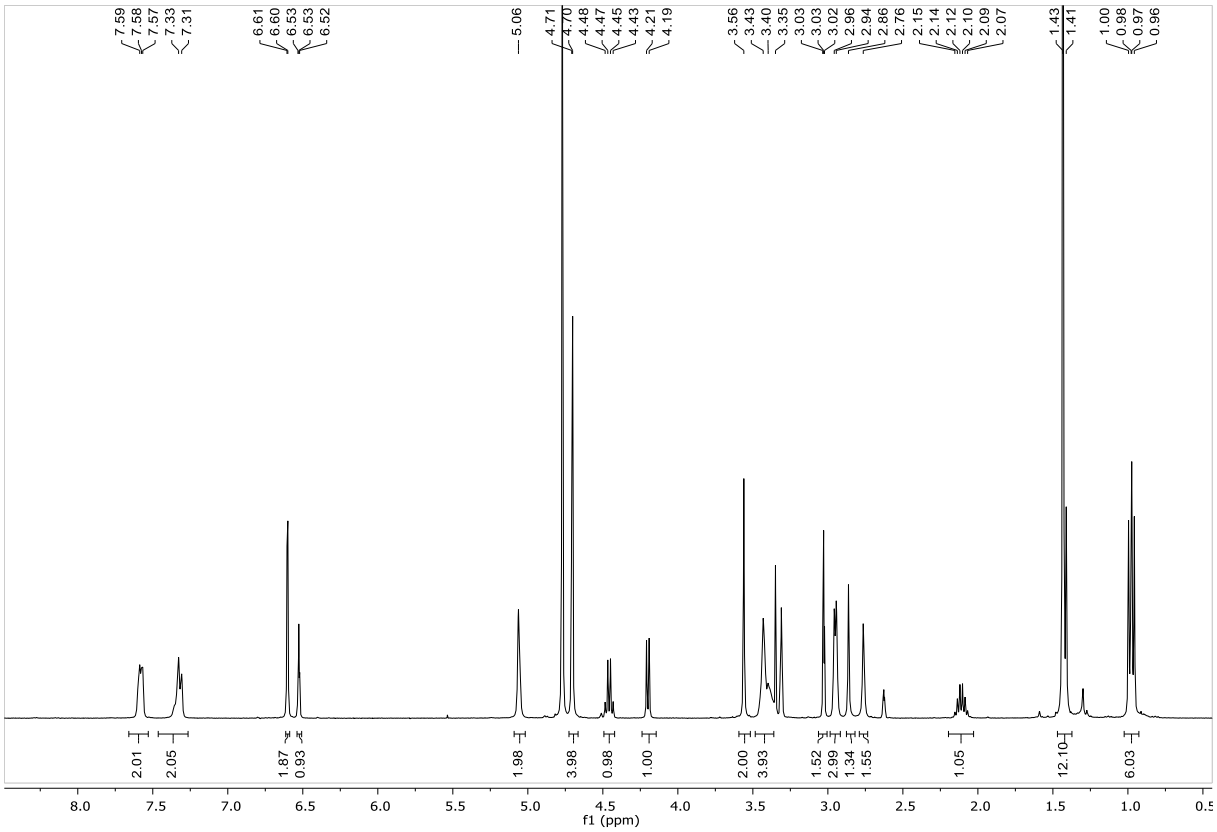

^{13}C NMR (101 MHz, MeOD + DMSO-d_6)

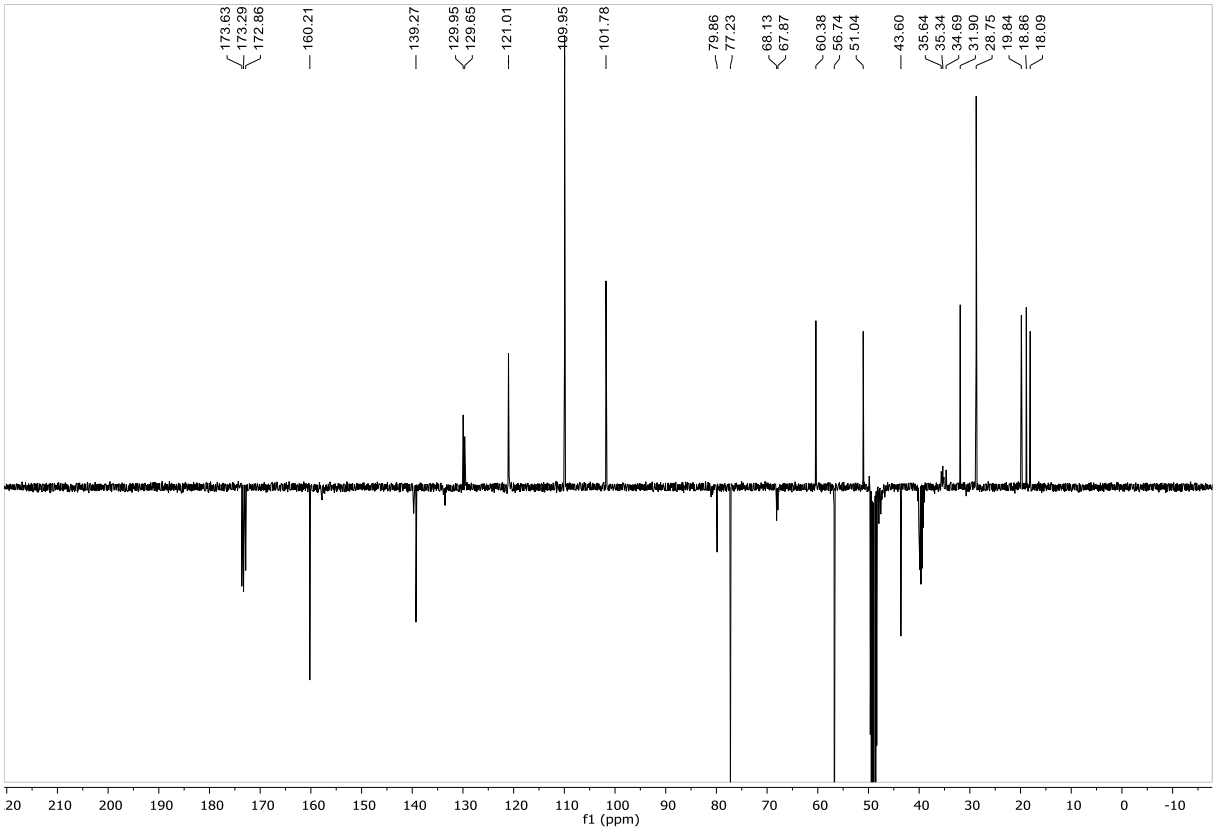

Compound 115

^{1}H NMR (400 MHz, DMSO-d_6)

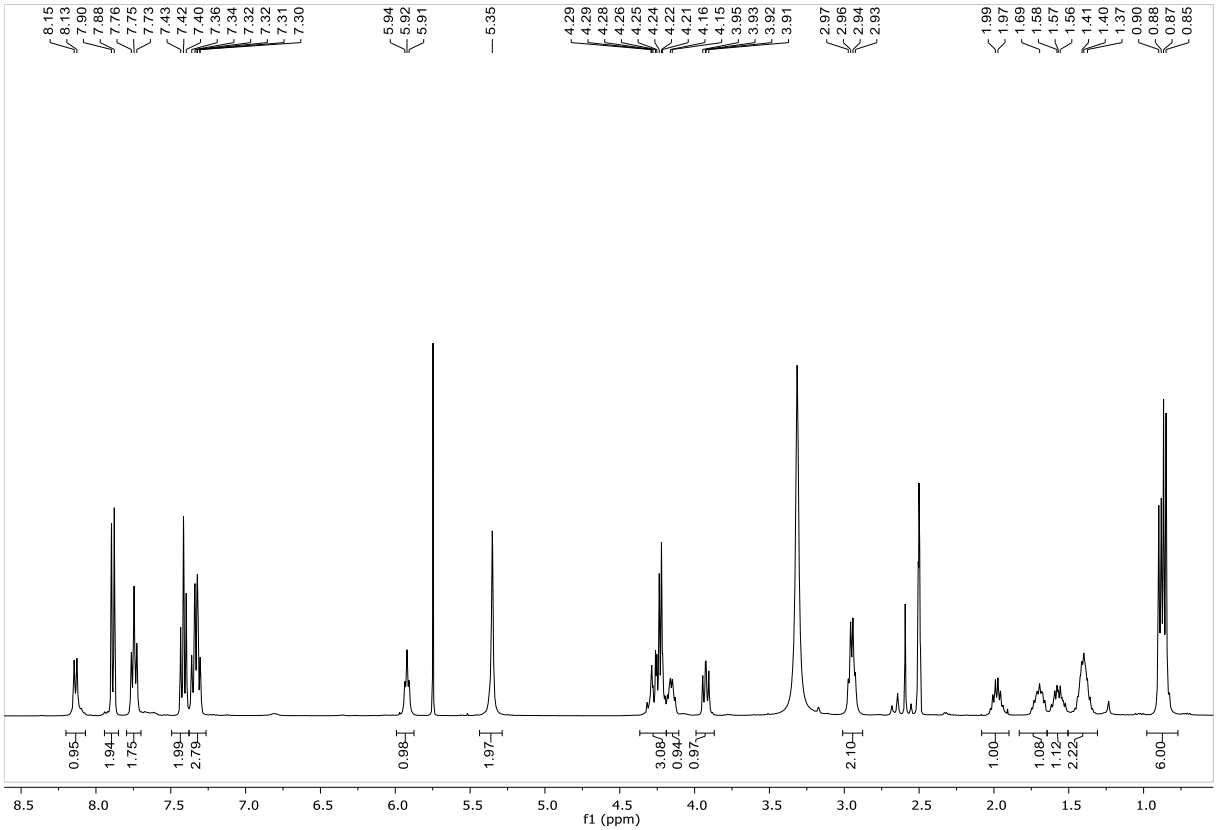

^{13}C NMR (101 MHz, DMSO-d_6)

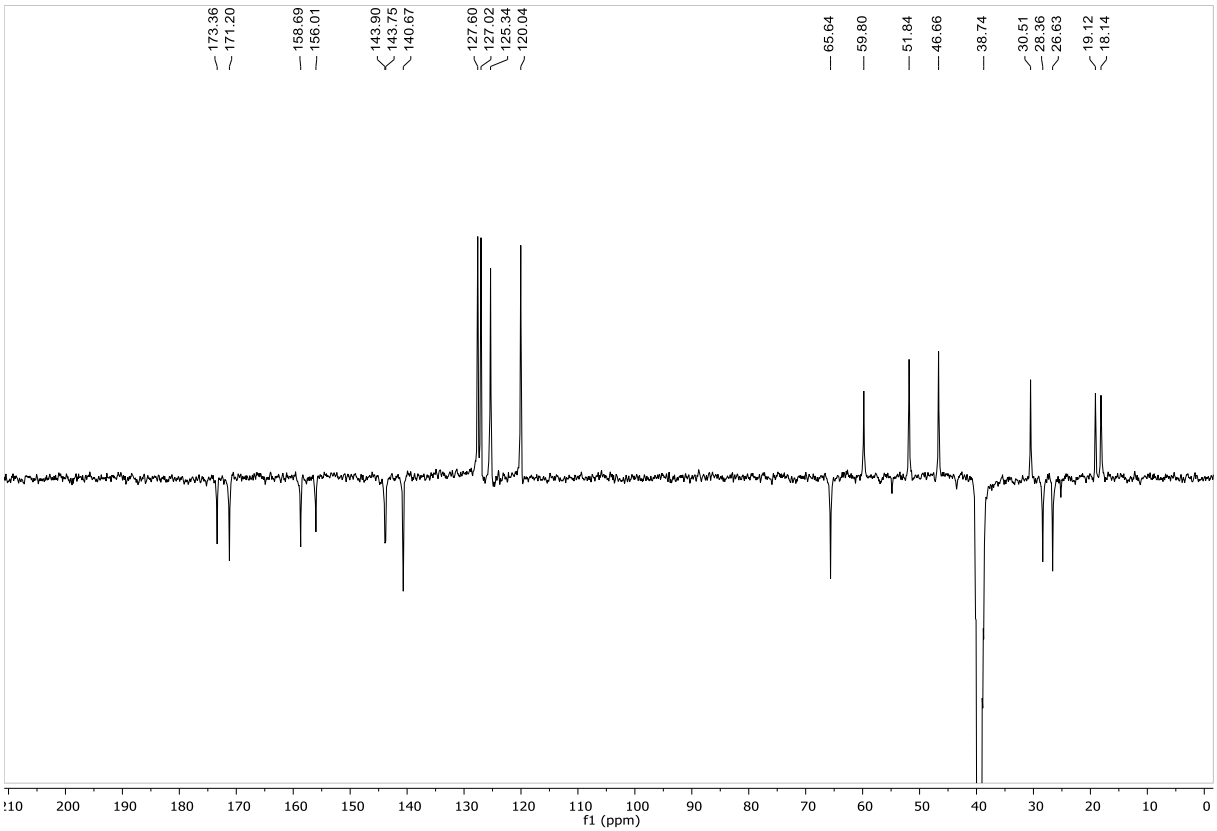

Compound 116

^{1}H NMR (400 MHz, DMSO-d_6)

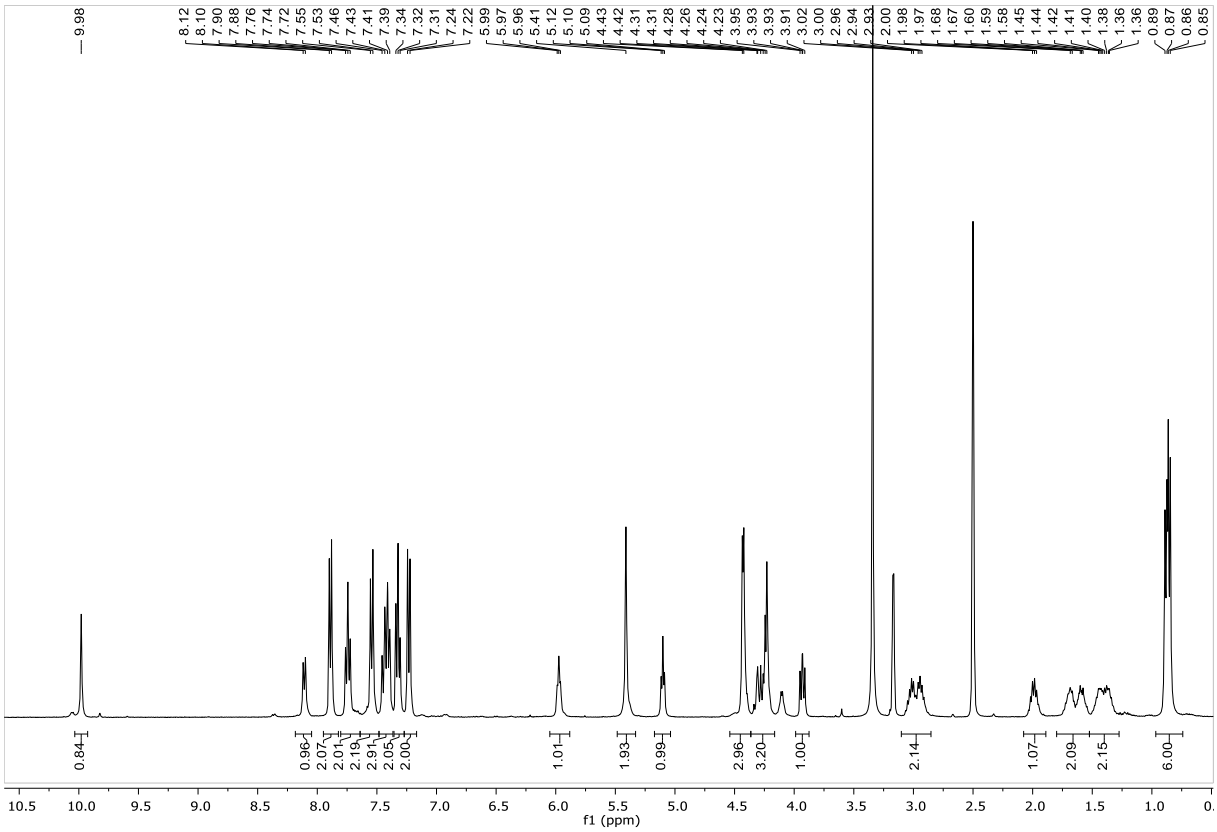

^{13}C NMR (101 MHz, DMSO-d_6)

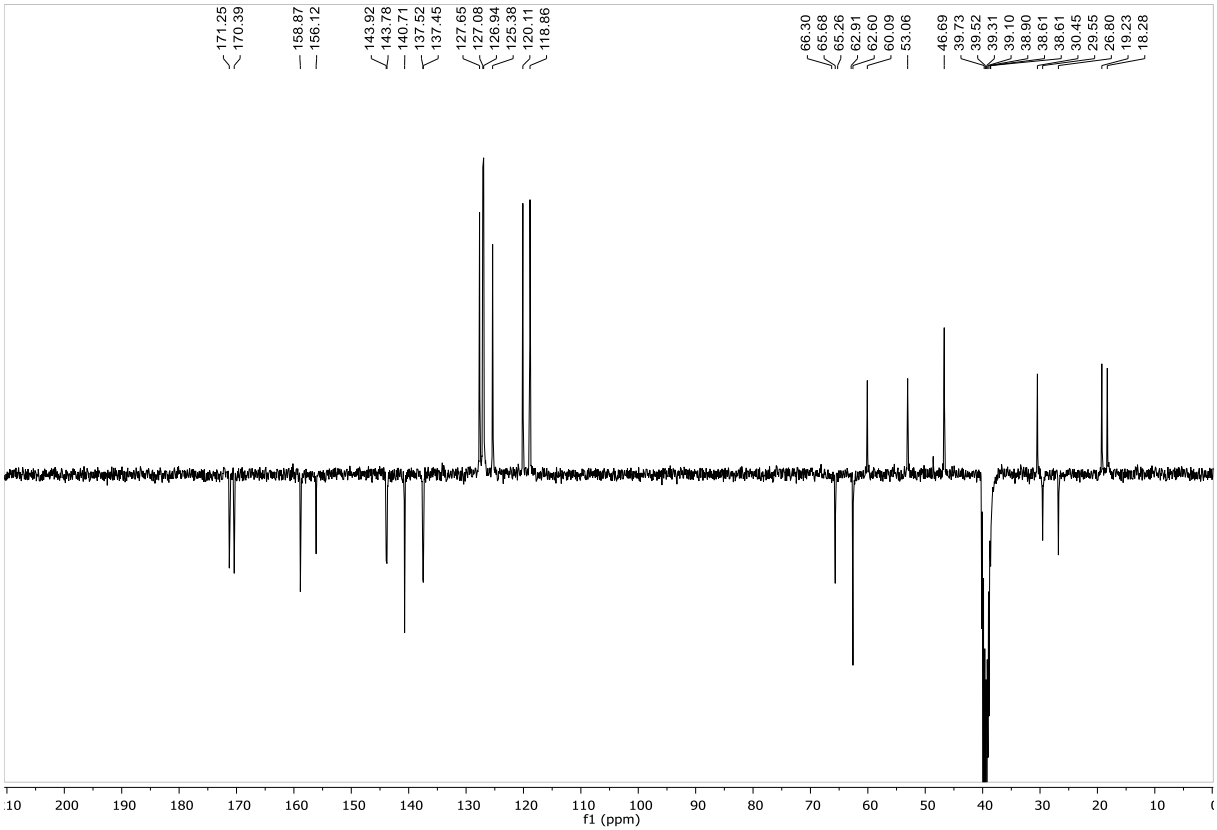

Compound 117

^{1}H NMR (400 MHz, DMSO-d_6)

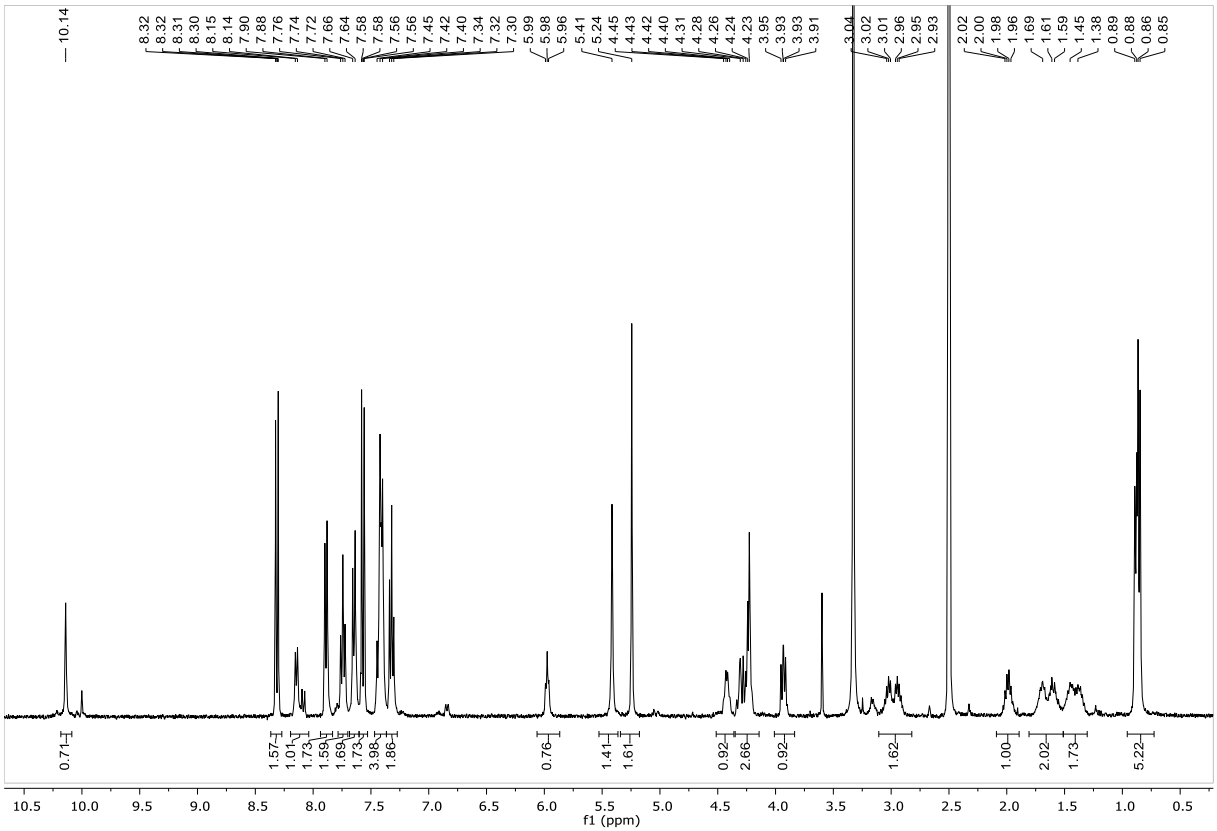

^{13}C NMR (101 MHz, DMSO-d_6)

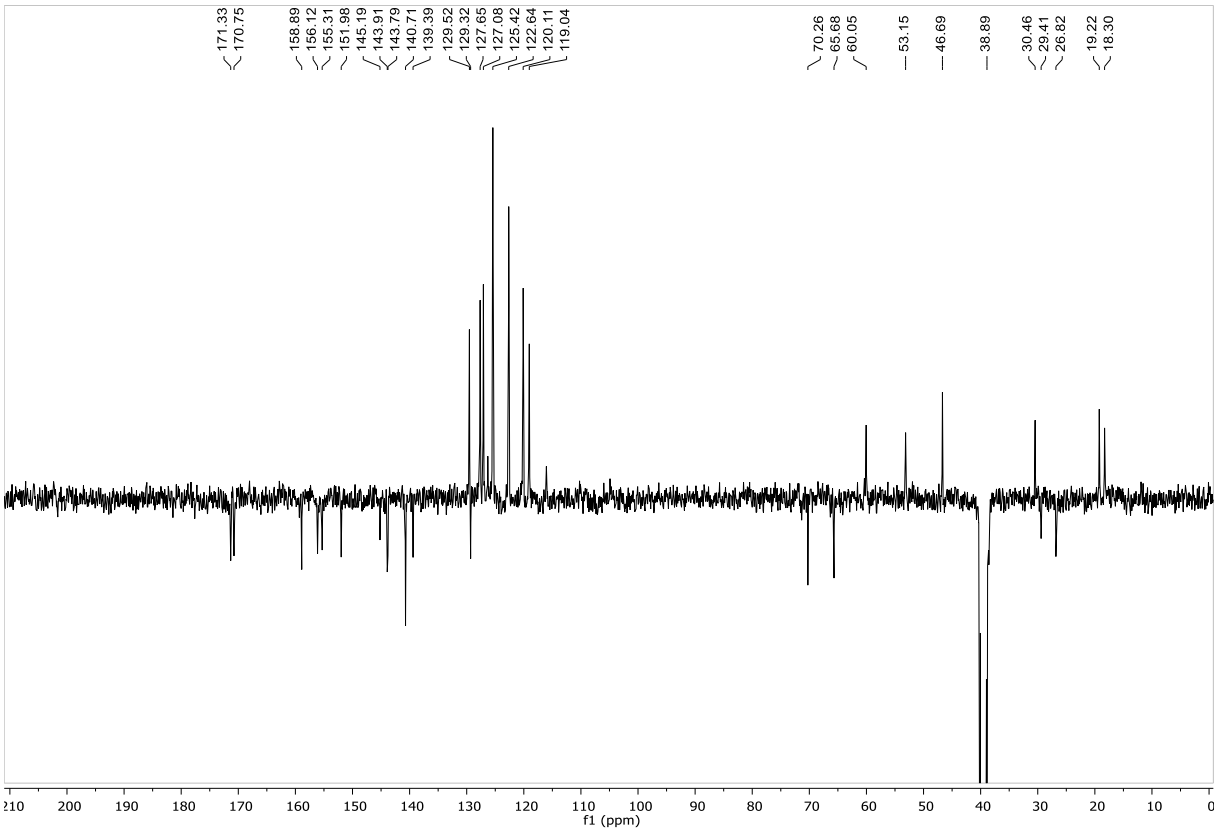

Compound 118

^{1}H NMR (400 MHz, DMSO-d_6)

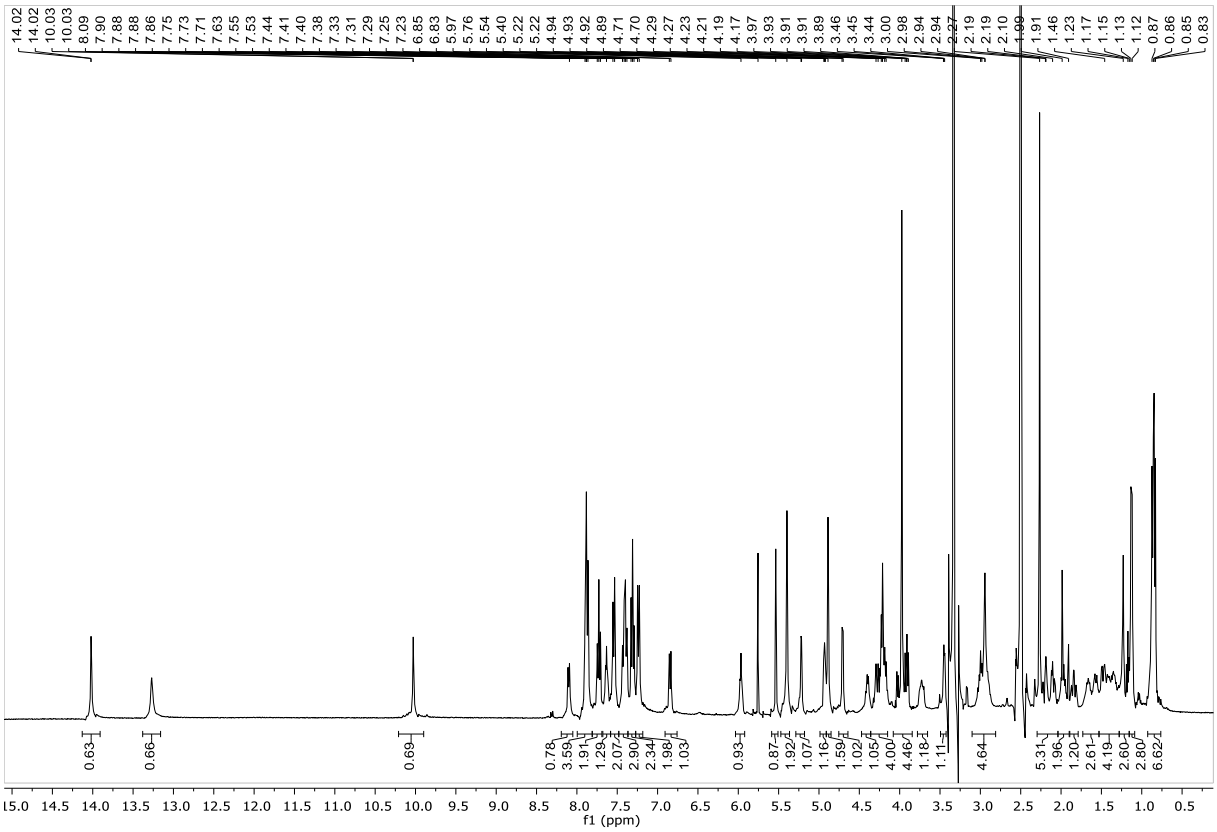

^{13}C NMR (101 MHz, DMSO-d_6)

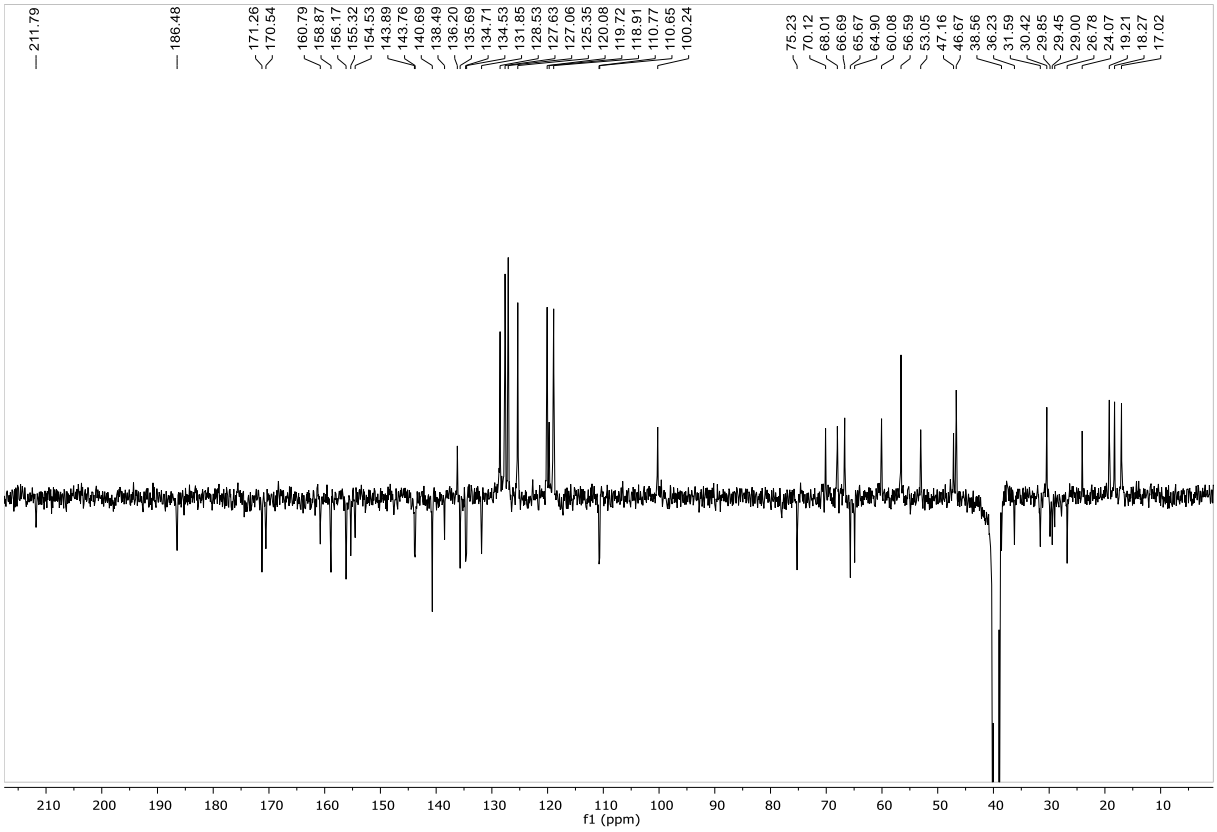

Compound 119

^{1}H NMR (400 MHz, DMSO-d_6)

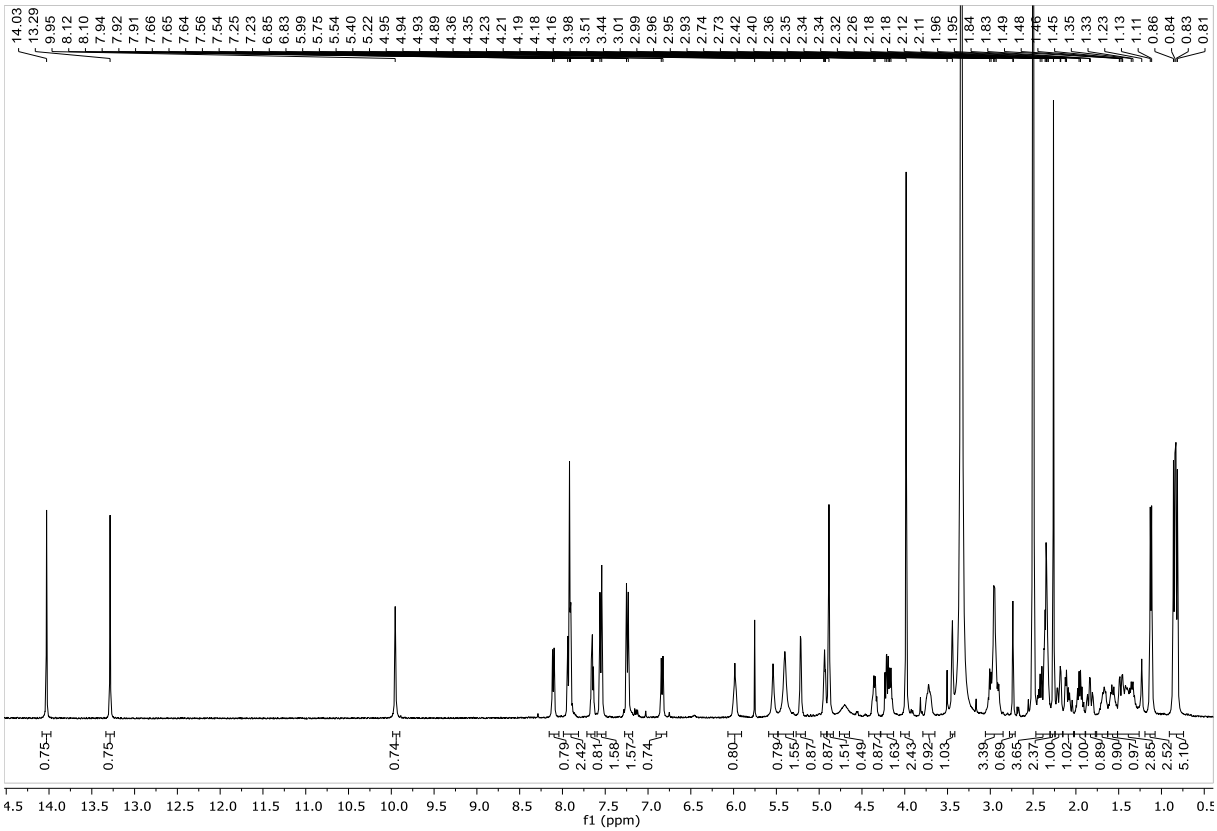

^{13}C NMR (101 MHz, DMSO-d_6)

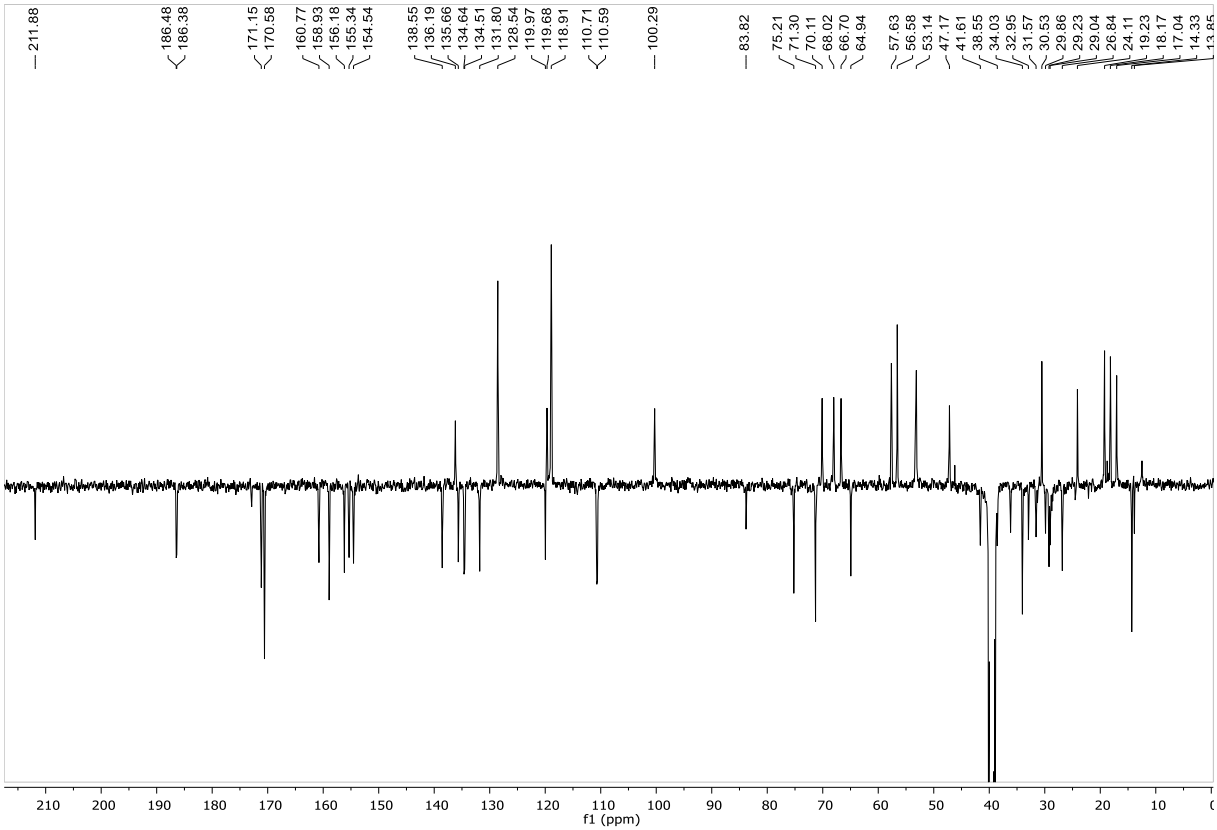

Compound 120

^{1}H NMR (400 MHz, CD_2Cl_2)

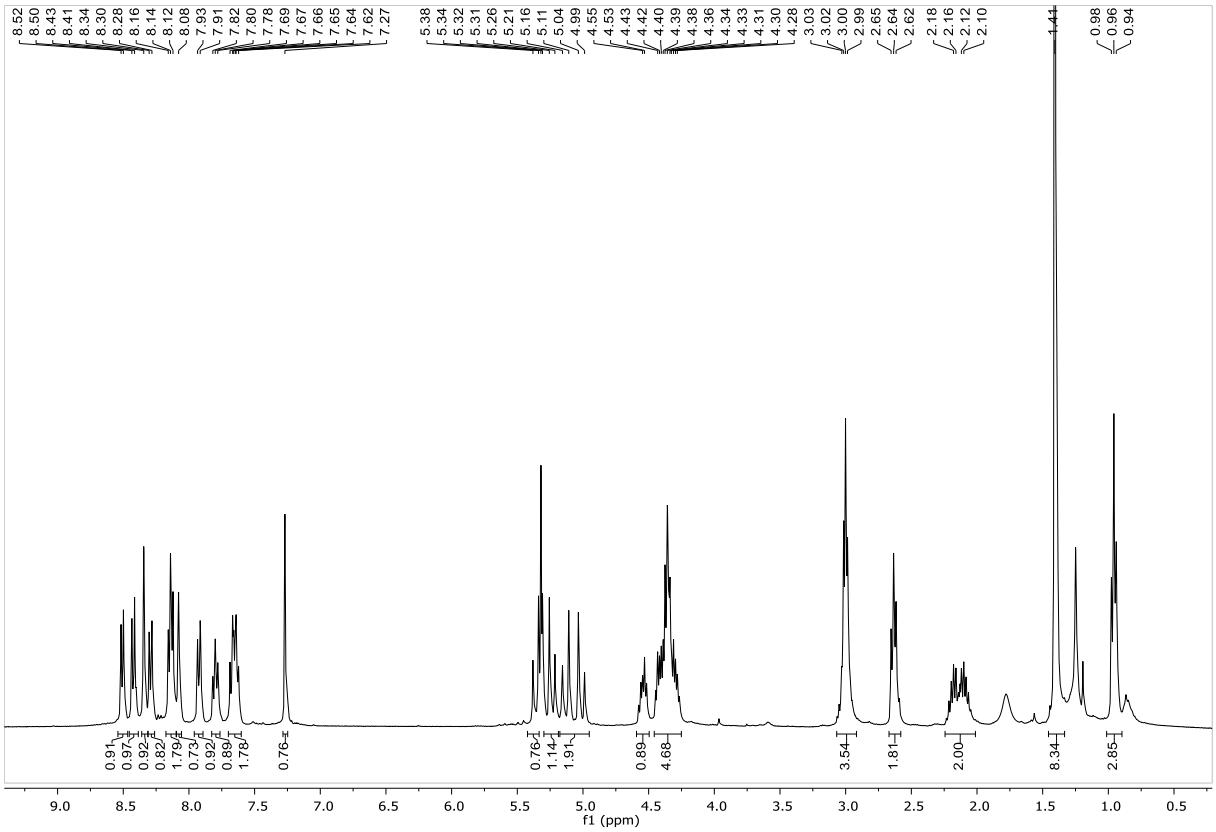

^{13}C NMR (101 MHz, CD_2Cl_2)

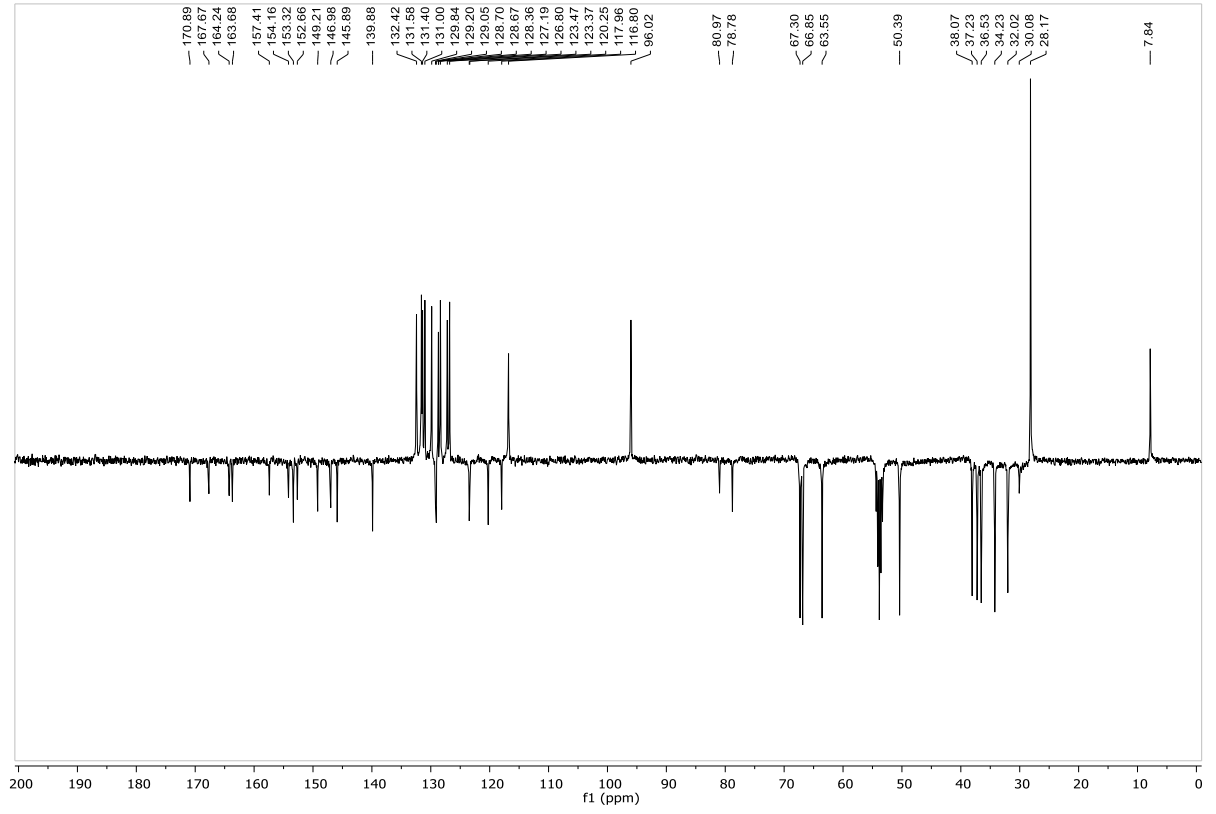

Compound 125

^{1}H NMR (400 MHz, MeOD)

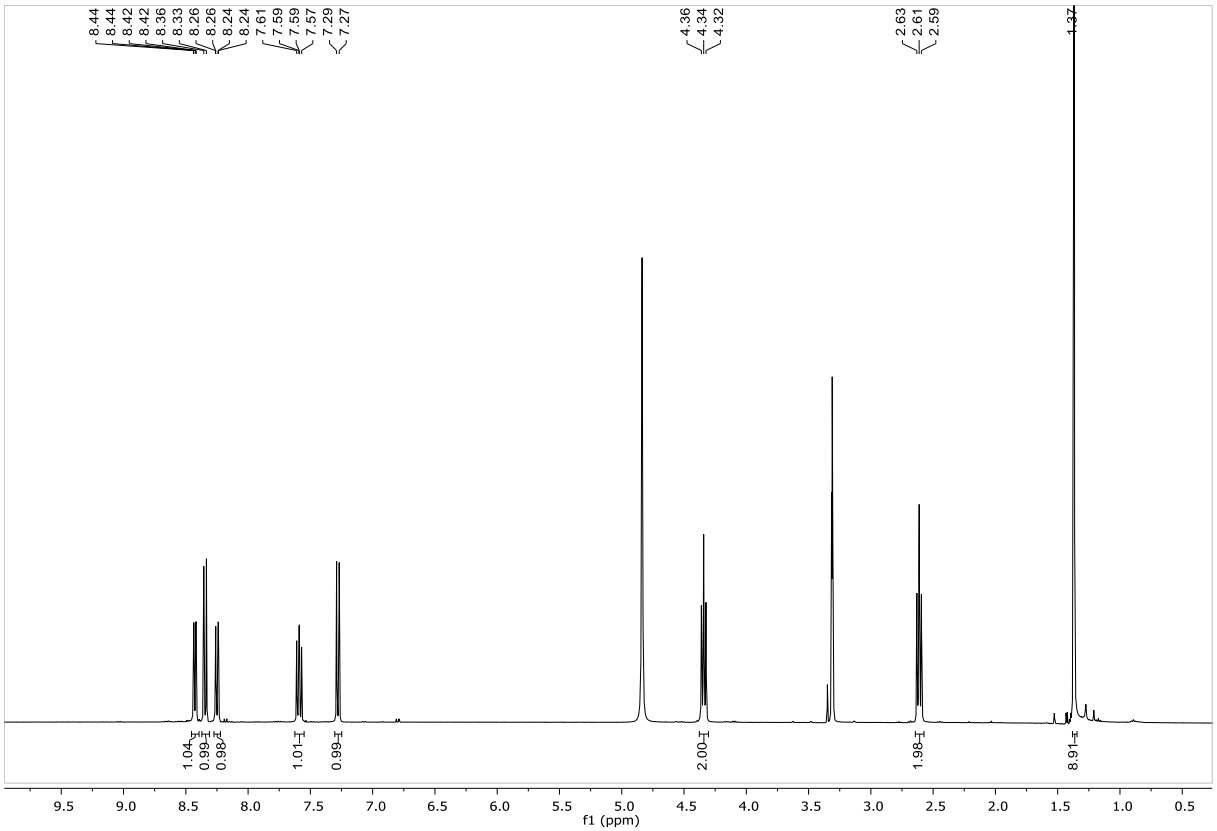

^{13}C NMR (101 MHz, MeOD)

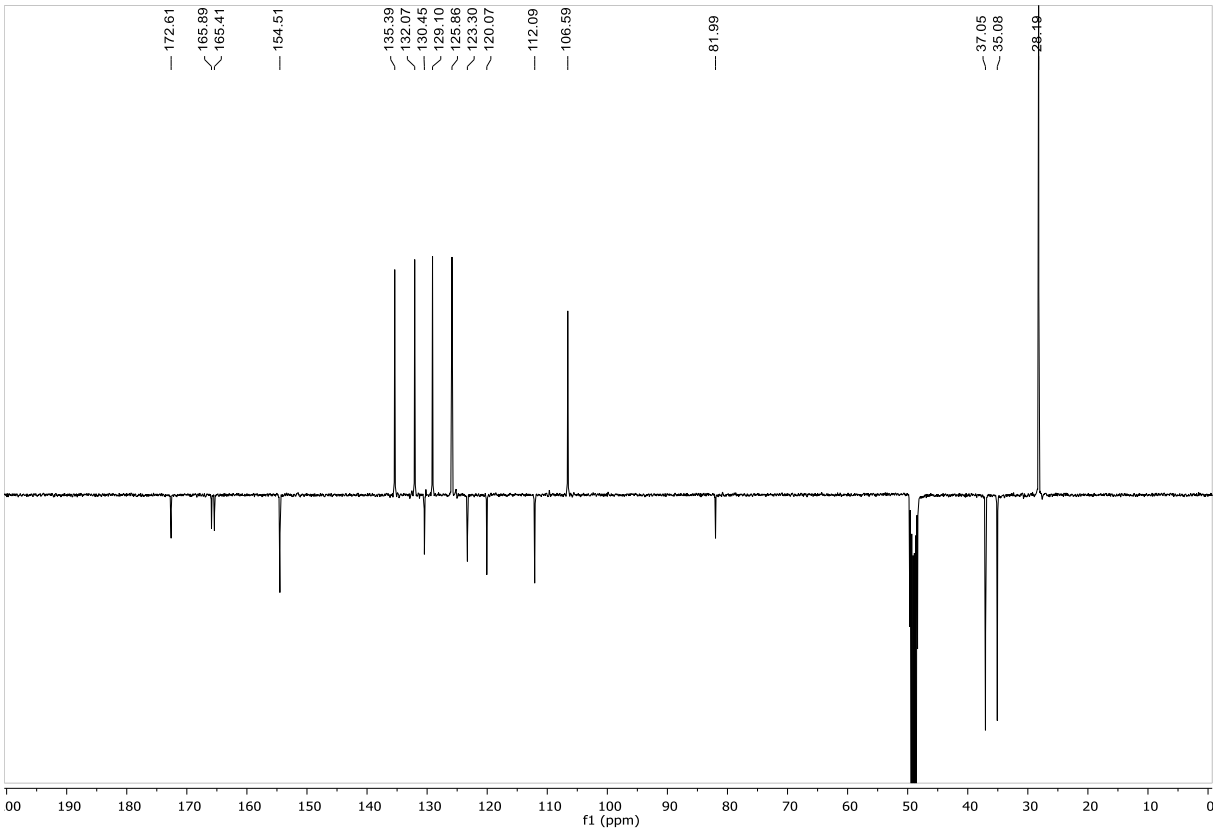

Compound 127

^{1}H NMR (500 MHz, DMSO-d_6 + D_2O)

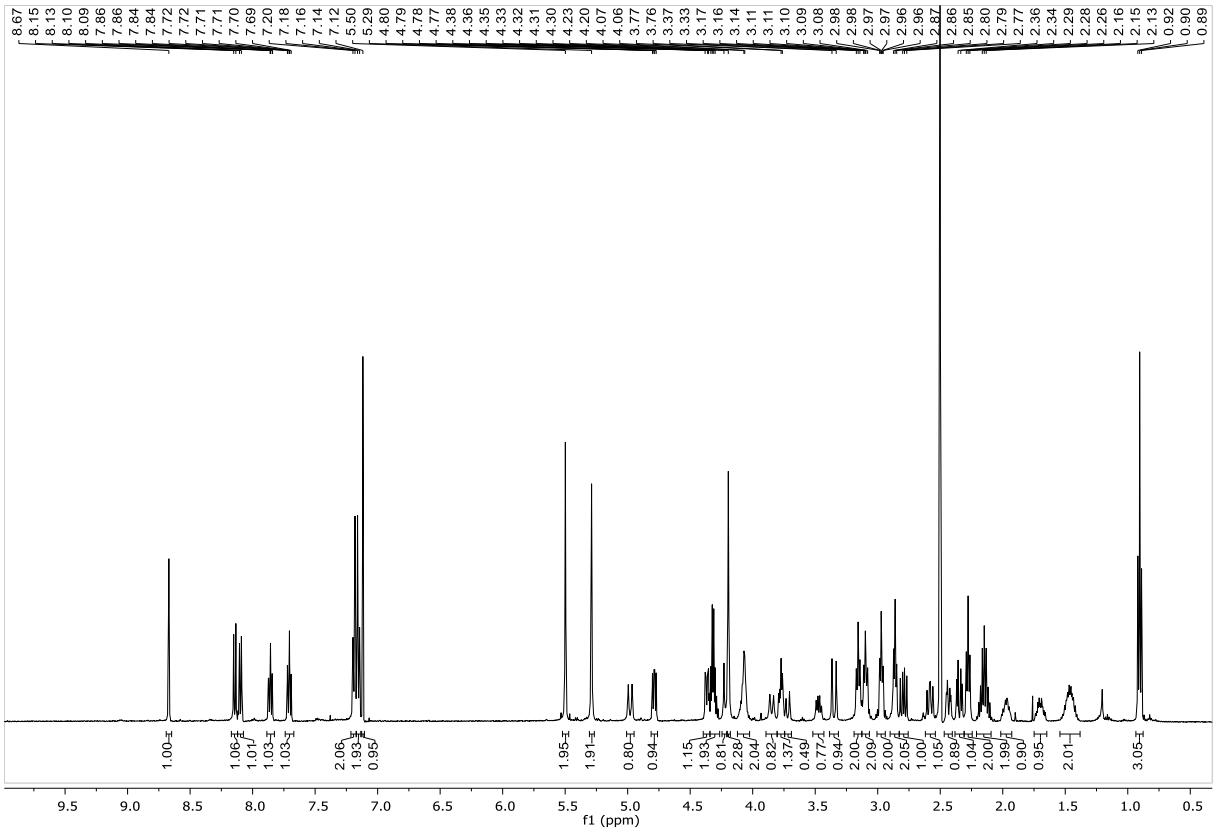

^{13}C NMR (126 MHz, DMSO-d_6 + D_2O)

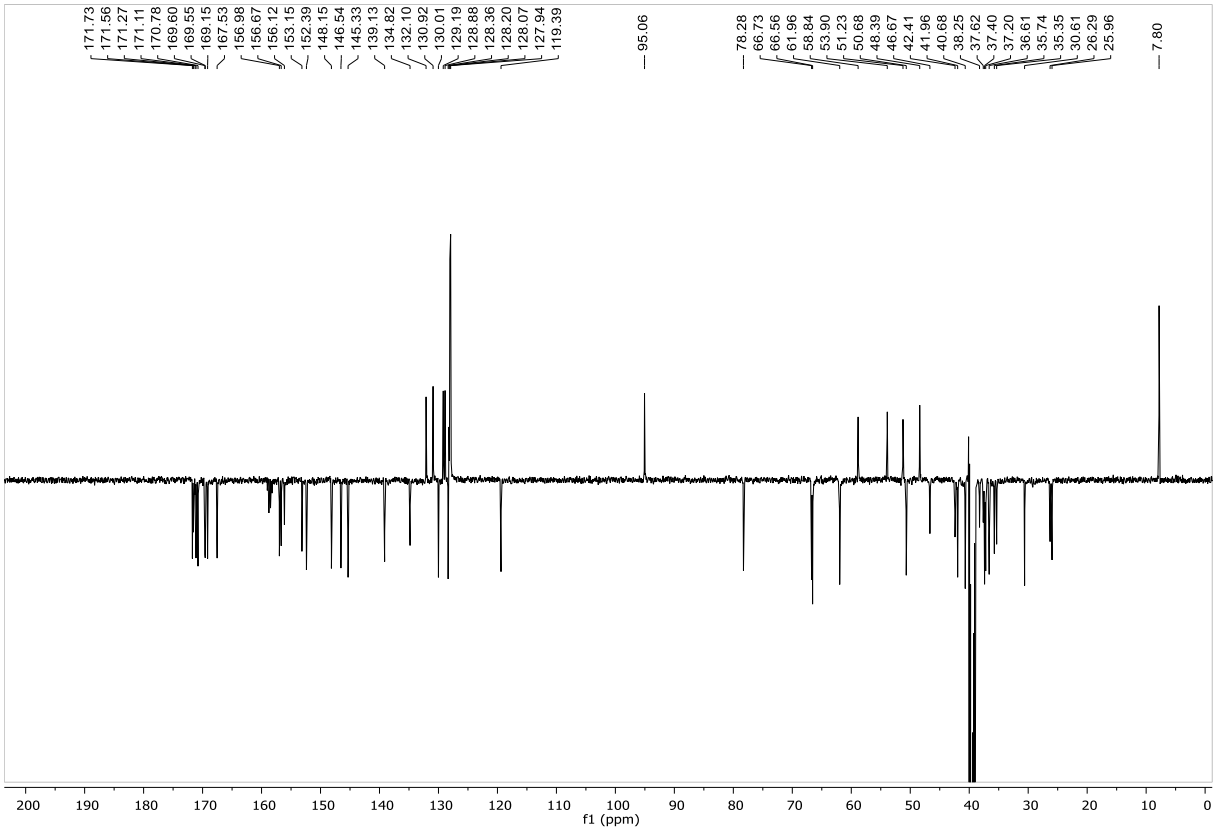

Compound 128

^{1}H NMR (400 MHz, D_2O + CD_3CN)

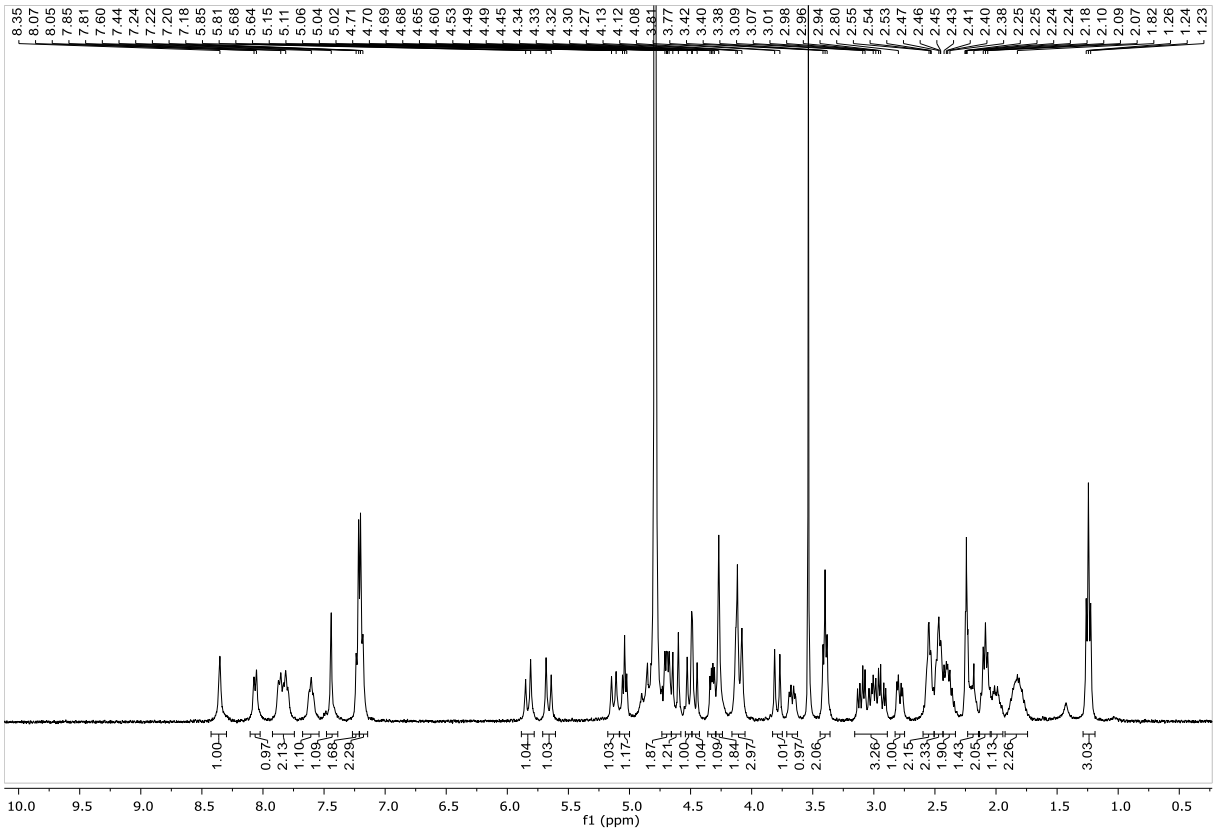

^{13}C NMR (101 MHz, D_2O + CD_3CN)

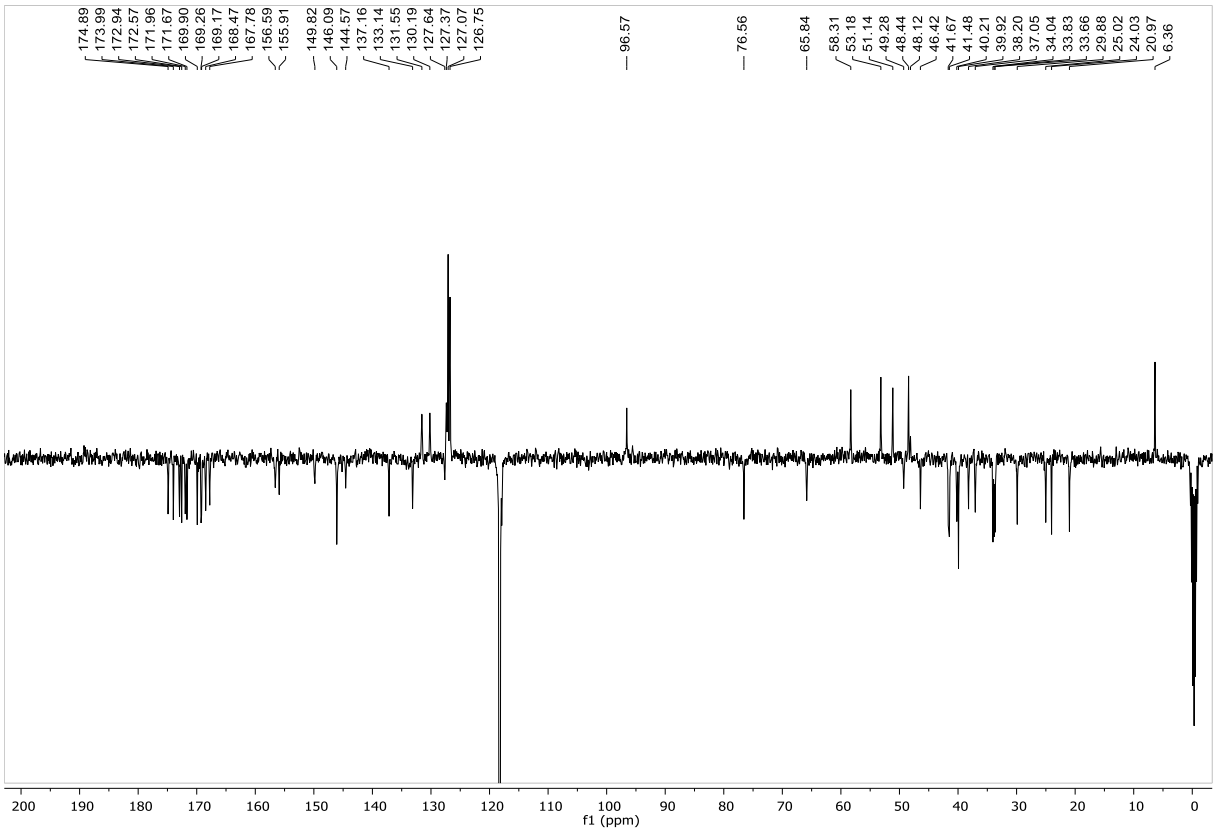

Compound 132

^{1}H NMR (400 MHz, $CDCl_3$)

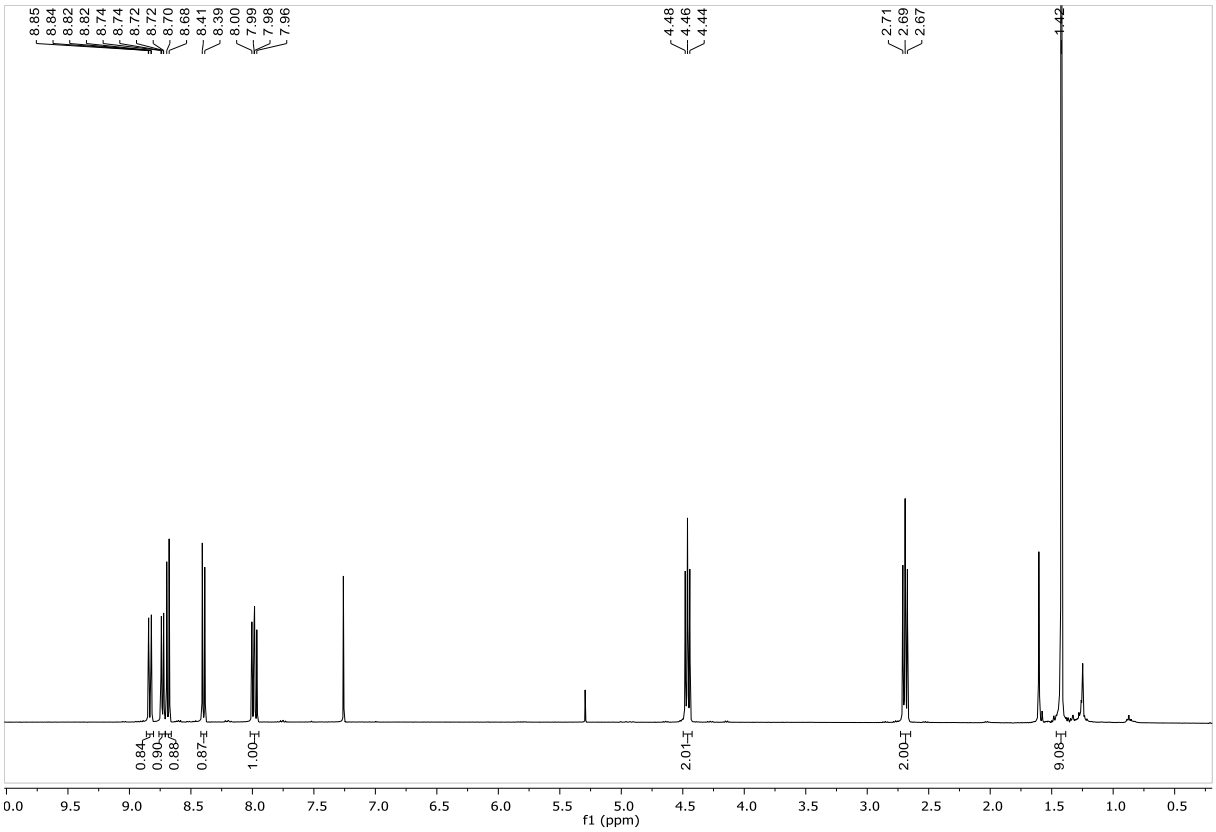

^{13}C NMR (101 MHz, $CDCl_3$)

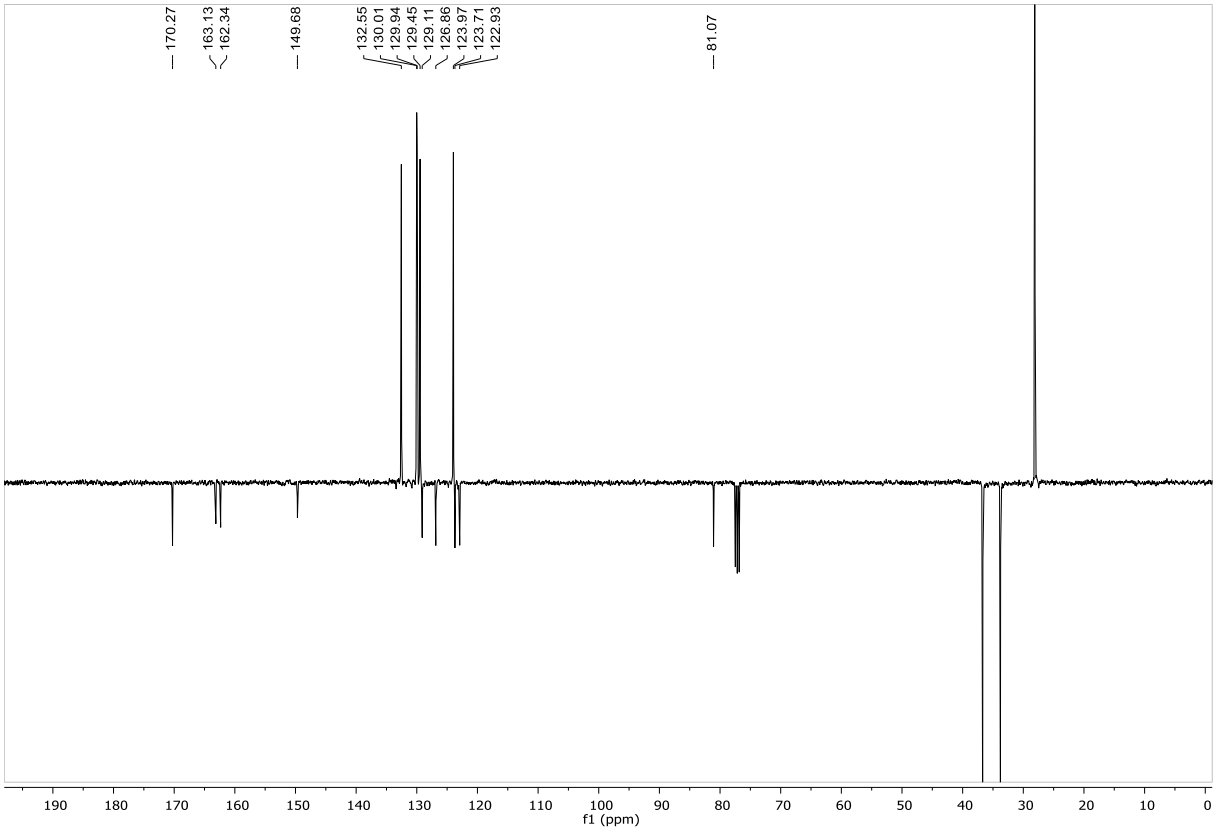

Compound 133

^{1}H NMR (400 MHz, MeOD)

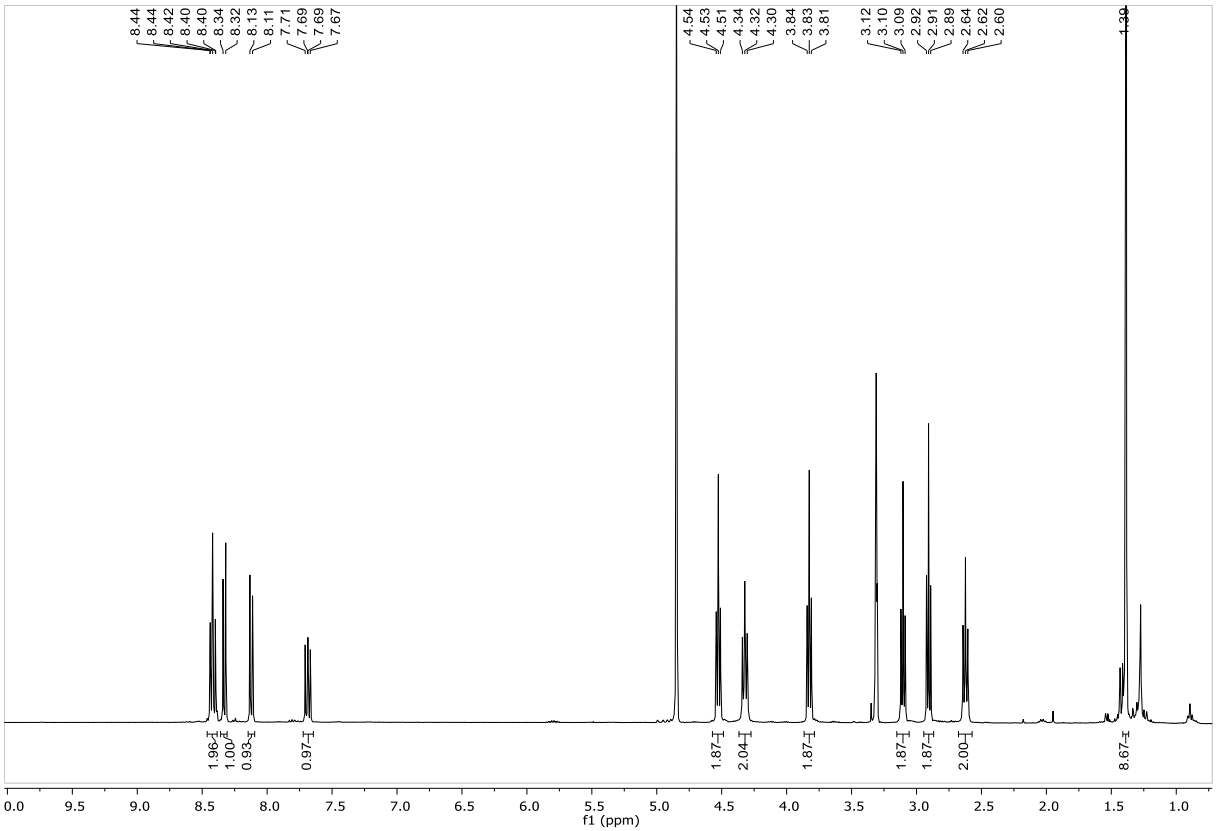

^{13}C NMR (101 MHz, MeOD)

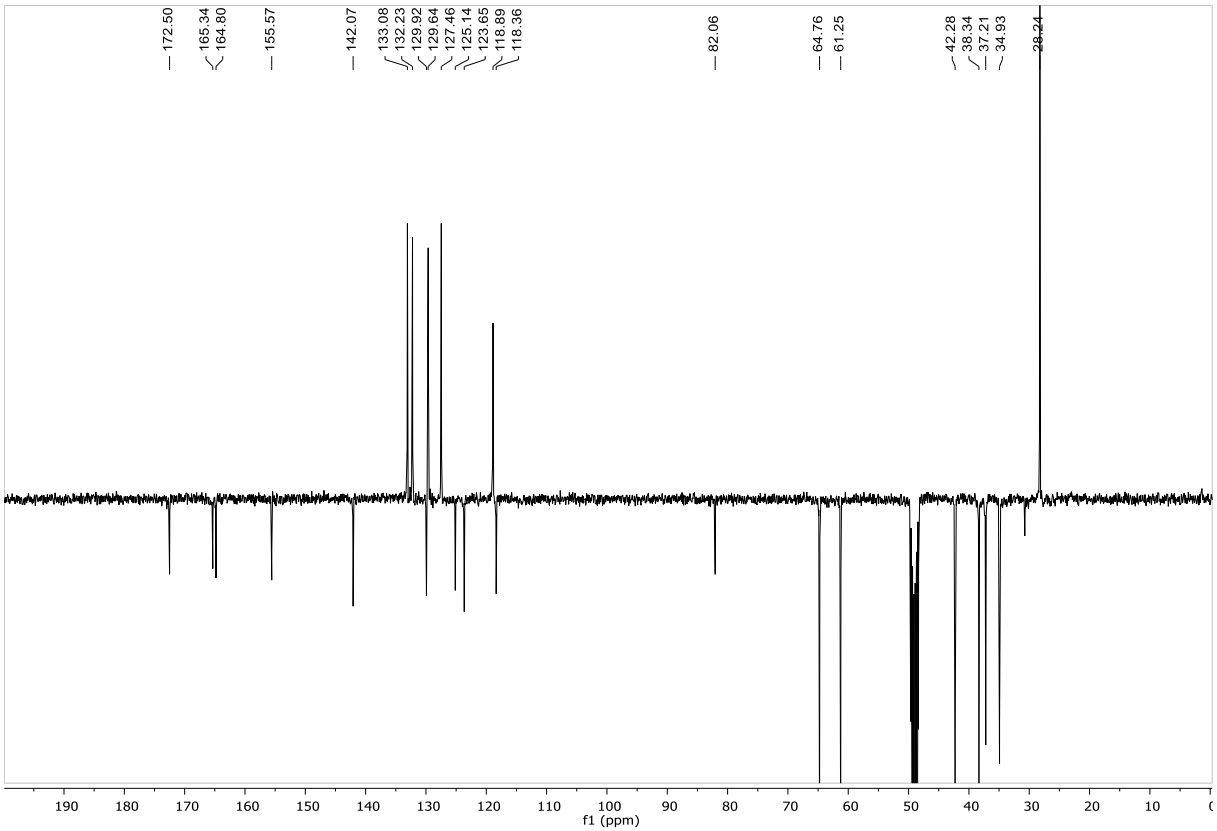

Compound 134

^{1}H NMR (400 MHz, DMSO-d_6)

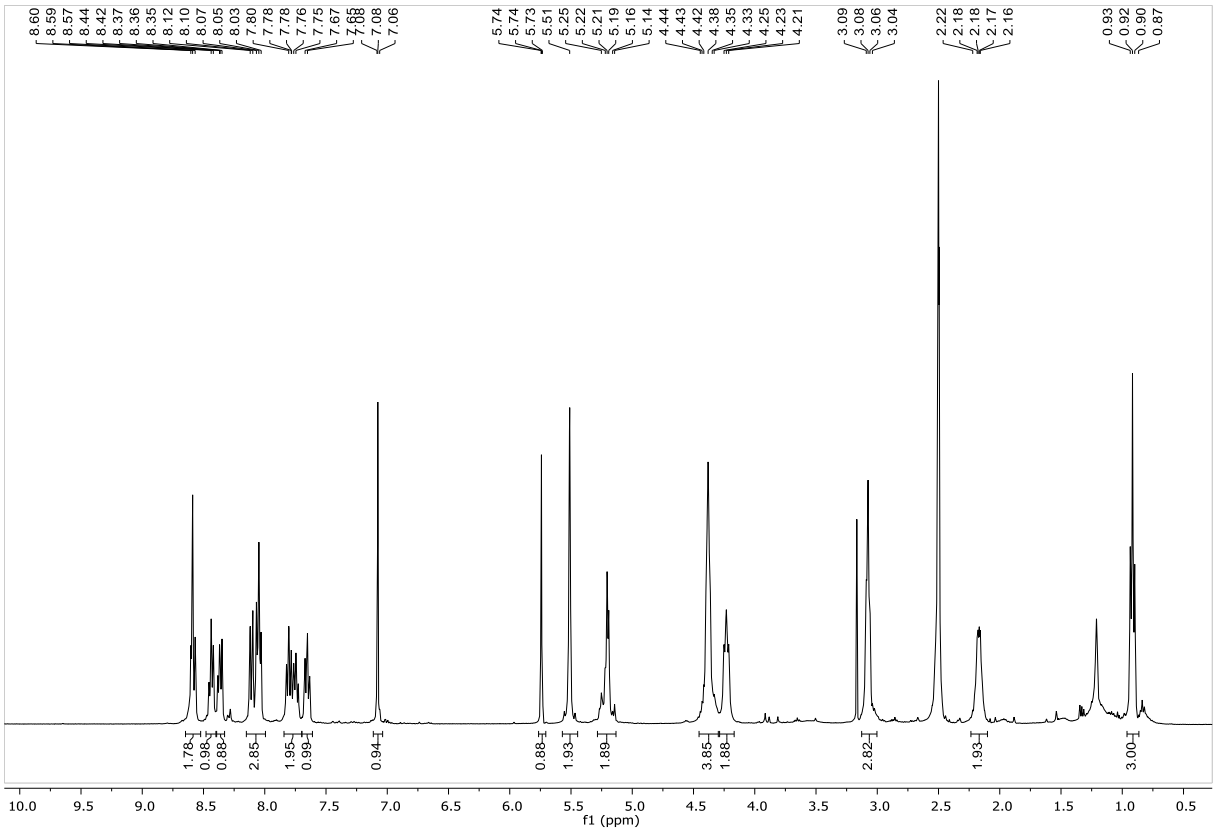

^{13}C NMR (101 MHz, DMSO-d_6)

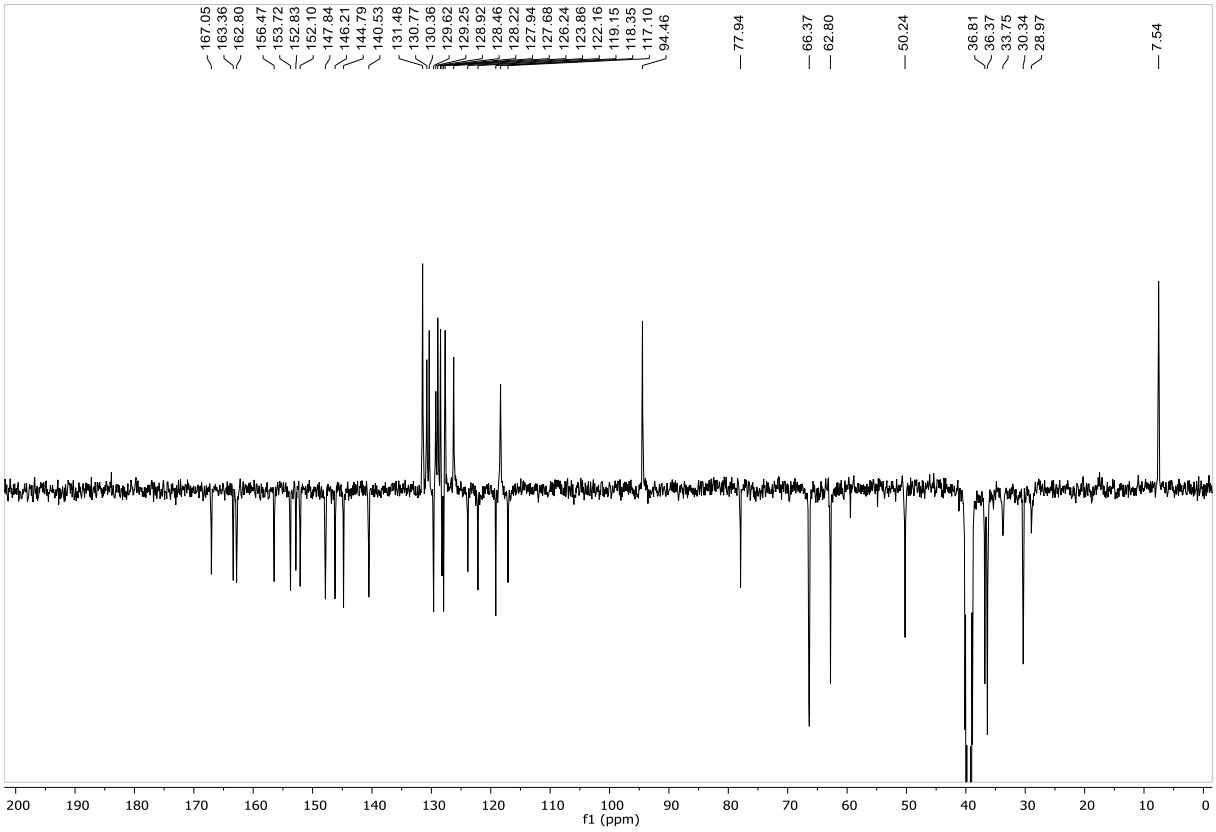

Compound 137

^{1}H NMR (400 MHz, MeOD)

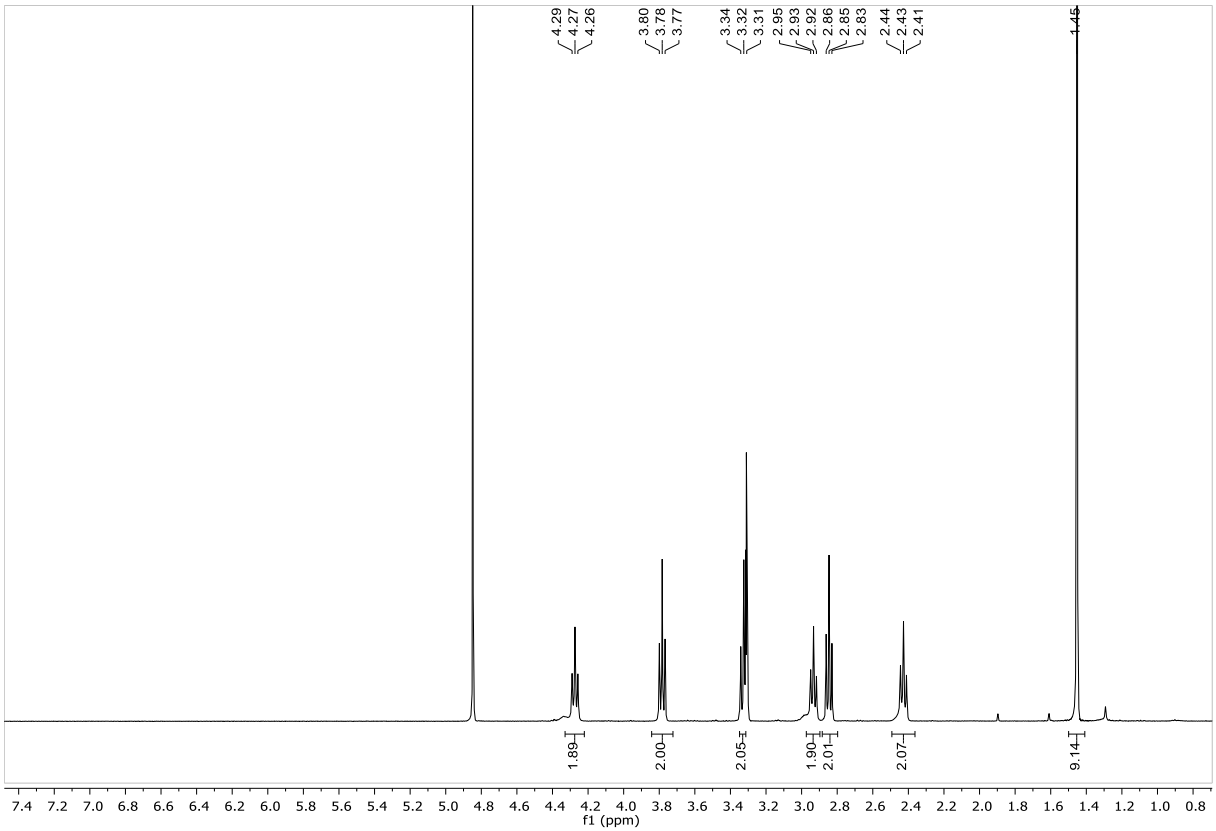

^{13}C NMR (101 MHz, MeOD)

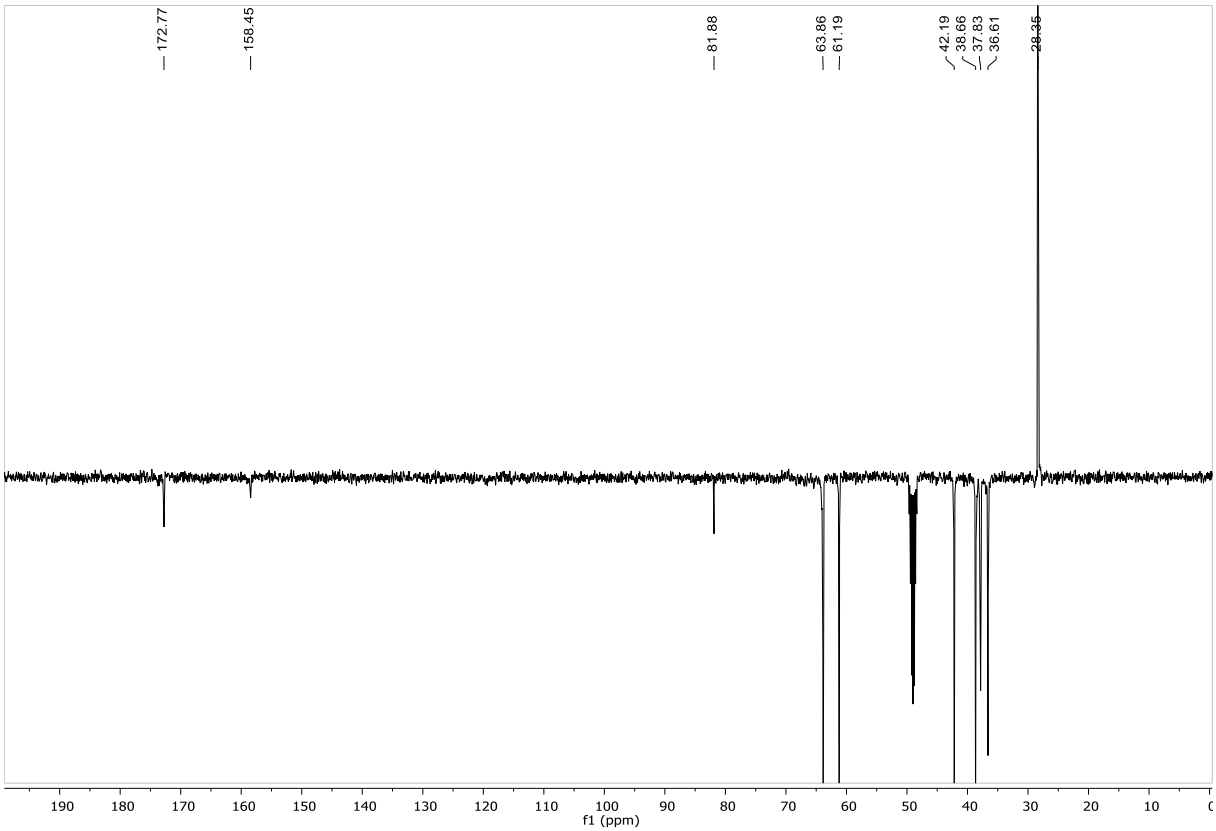

Compound 138

^{1}H NMR (400 MHz, CD_2Cl_2)

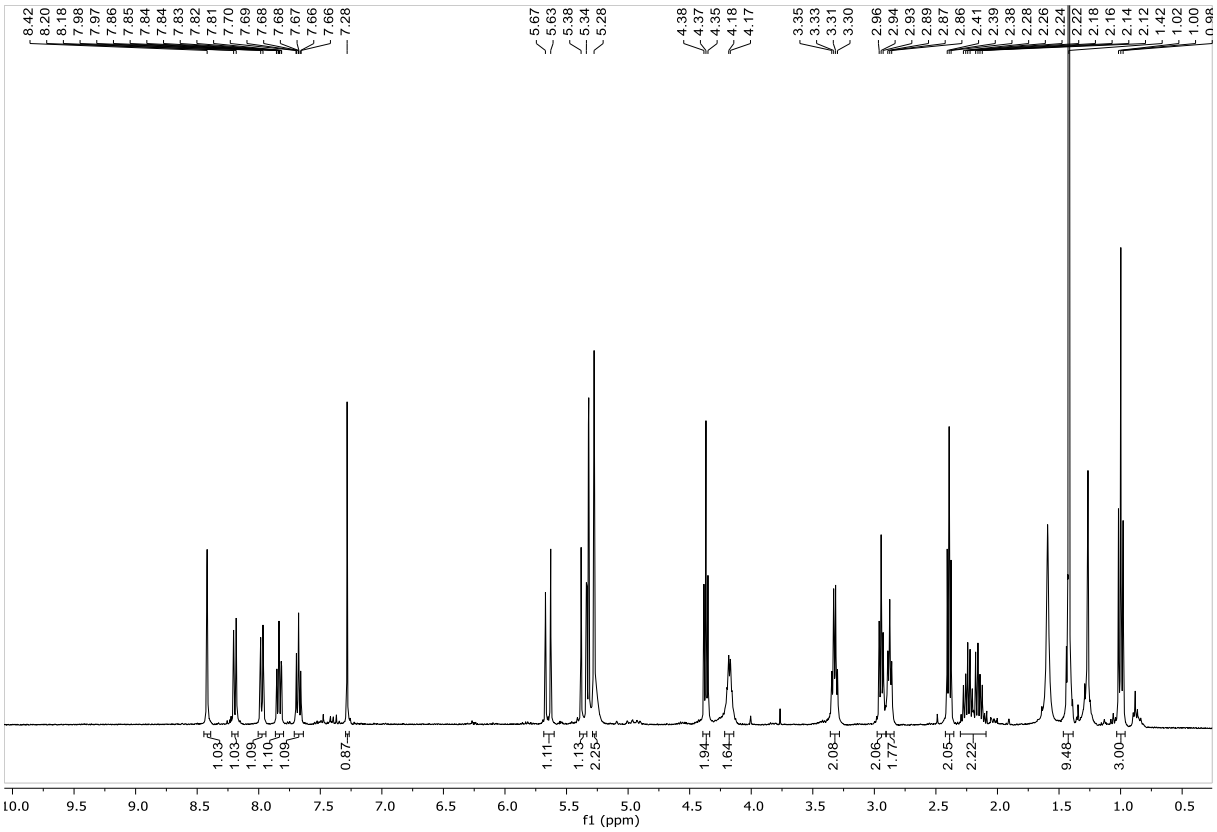

^{13}C NMR (101 MHz, CD_2Cl_2)

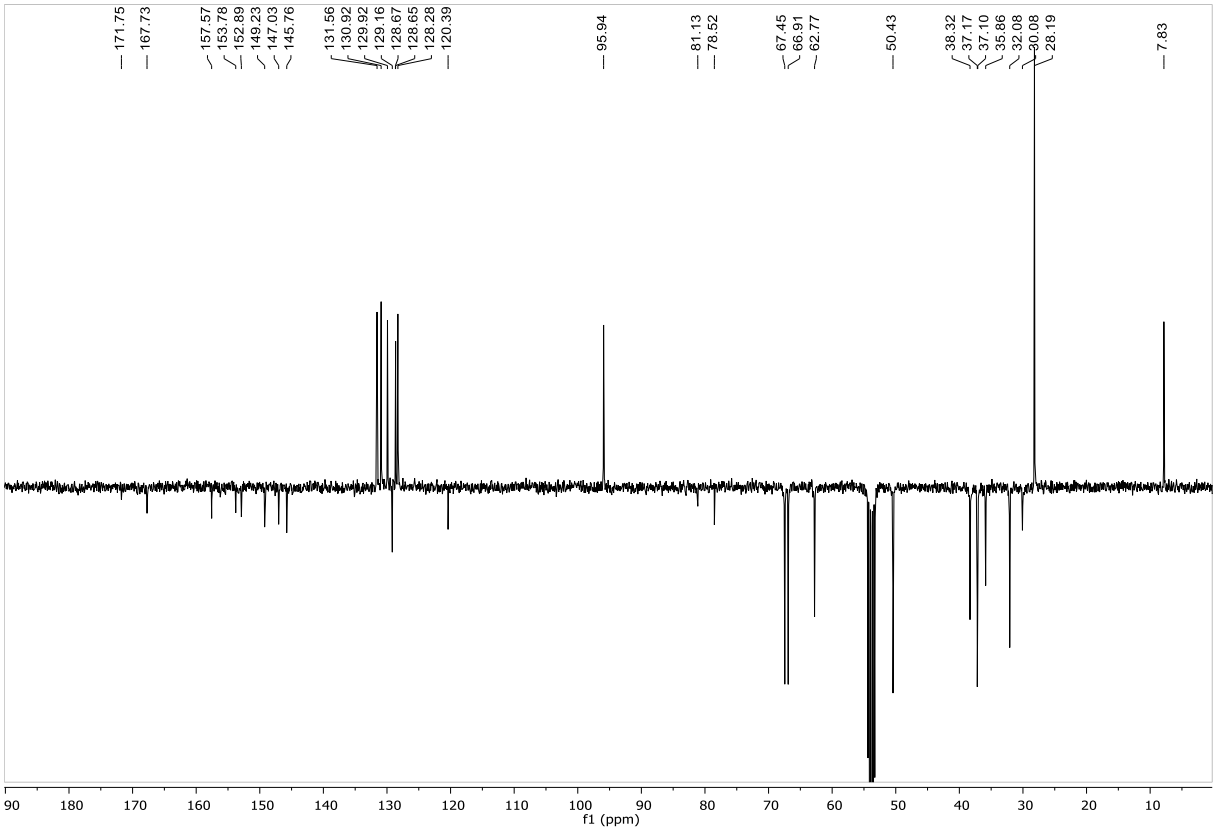

References

[1] For IC_{50} values of methotrexate and doxorubicin see: *Angew. Chem. Int. Ed.* **2013**, *52*, 1384-1402. For IC_{50} values of cisplatin see: *Eur. J. Inorg. Chem.* **2010**, 3441-3448; *Anticancer Drugs* **2000**, *11*, 859-863 and *Anticancer Drugs* **2000**, *11*, 573-578. For IC_{50} values of gemcitabine see: *Int. J. Cancer* **2005**, *114*, 1002-1009; *Thyroid* **2000**, *10*, 865-869 and *Biochem. Pharmacol.* **2008**, *75*, 1901-1911. For IC_{50} values of SN-38 see: *Biochem. Pharmacol.* **2005**, *70*, 1125-1136, *Anticancer Drugs* **2000**, *11*, 573-578 and *Bioconjugate Chem.* **2010**, *21*, 1804-1810.

[2] K. Cheung-Ong, G. Giaever, C. Nislow. DNA-Damaging Agents in Cancer Chemotherapy: Serendipity and Chemical Biology. *Chem Biol.* **2013**, *20*, 648-59.

[3] J. J. Wilson, S. J. Lippard. Synthetic Methods for the Preparation of Platinum Anticancer Complexes. *Chem. Rev.* **2014**, *114*, 4470-4495.

[4] L. G. Dezhenkova, V. B. Tsvetkov, A. A. Shtil. Topoisomerase I and II inhibitors: chemical structure, mechanisms of action and role in cancer chemotherapy. *Russ. Chem Rev.* **2014**, *83*, 82-94.

[5] M. F. Braña, A. Sánchez-Migallón. Anticancer drug discovery and pharmaceutical chemistry: a history. *Clin. Transl. Oncol.* **2006**, *8*, 717-28.

[6] G. Minotti, P. Menna, E. Salvatorelli, G. Cairo, L. Gianni. Anthracyclines: Molecular Advances and Pharmacologic Developments in Antitumor Activity and Cardiotoxicity. *Pharmacol Rev.* **2004**, *56*, 185-229.

[7] For IC_{50} values of vinblastine and paclitaxel see: *Angew. Chem. Int. Ed.* **2013**, *52*, 1384-1402.

[8] W. N. Haita, E. Rubina, E. Alli, S. Goodin. Tubulin Targeting Agents. *Update Cancer Ther.* **2007**, *2*, 1-18.

[9] L. Bildstein, C. Dubernet, P. Couvreur. Prodrug-based intracellular delivery of anticancer agents. *Adv. Drug Deliv. Rev.* **2011**, *63*, 3-23.

[10] For IC_{50} values of maytansine, dolastatin 10, SJG-136, duocarmycin SA and tubulysin D see: *Angew. Chem. Int. Ed.* **2013**, *52*, 1384-1402. For IC_{50} values of monomethyl auristatin E see: *Angew. Chem. Int. Ed.* **2012**, *51*, 11606-11610; *Mol. Pharmaceutics* **2015**, *12*, 1250-1258 and *Blood* **2003**, *102*, 1458-1465. For IC_{50} values of cryptophycin 52 see: *Cancer Chemother. Pharmacol.* **1999**, *43*, 115-125. For IC_{50} values of calicheamicin θ see: *Bioconjugate Chem.* **2009**, *20*, 1587-1594.

[11] M. Hojjat-Farsangi. Small-Molecule Inhibitors of the Receptor Tyrosine Kinases: Promising Tools for Targeted Cancer Therapies. *Int. J. Mol. Sci.* **2014**, *15*, 13768-13801.

[12] Data from firstwordpharma.com.

[13] J. J. Cui. Targeting Receptor Tyrosine Kinase MET in Cancer: Small Molecule Inhibitors and Clinical Progress. *J. Med. Chem.* **2014**, *57*, 4427-4453.

[14] T. Lammers, F. Kiessling, W. E. Hennink, G. Storm. Drug targeting to tumors: Principles, pitfalls and (pre-) clinical progress. *J. Control. Release* **2012**, *161*, 175-187.

[15] G. Casi, D. Neri. Noninternalizing Targeted Cytotoxics for Cancer Therapy. *Mol. Pharmaceutics* **2015**, *12*, 1880-1884.

[16] D. Neri, C. T. Supuran. Interfering with pH regulation in tumours as a therapeutic strategy. *Nat. Rev. Drug Discov.* **2011**, *10*, 767-777.

[17] A. Cambrosio, P. Keating. Between fact and technique: the beginnings of hybridoma technology. *J. Hist. Biol.* **1992**, *25*, 175-230.

[18] G. Köhler, C. Milstein. Continuous cultures of fused cells secreting antibody of predefined specificity. *Nature* **1975**, *256*, 495-497.

[19] P. N. Nelson, G. M. Reynolds, E. E. Waldron, E. Ward, K. Giannopoulos, P. G. Murray. Demystified ...: Monoclonal antibodies. *Mol Pathol.* **2000** *53*, 111-117.

[20] A. M. Scott, J. D.Wolchok, L. J. Old. Antibody therapy of cancer. *Nat. Rev. Cancer* **2012**, *12*, 278-287.

[21] R. V. J. Chari, M. L. Miller, W. C. Widdison. Antibody-Drug Conjugates: An Emerging Concept in Cancer Therapy. *Angew. Chem. Int. Ed.* **2014**, *53*, 3796-3827.

[22] P. D. Senter, E. L. Sievers. The discovery and development of brentuximab vedotin for use in relapsed Hodgkin lymphoma and systemic anaplastic large cell lymphoma. *Nat. Biotechnol.* **2012**, *30*, 631-637.

[23] P. A. Trail. Antibody Drug Conjugates as Cancer Therapeutics. *Antibodies* **2013**, *2*, 113-129.

[24] R. Duncan, R. Gaspar. Nanomedicine(s) under the Microscope. *Mol. Pharmaceutics* **2011**, *8*, 2101-2141.

[25] A. M. Thayer. Building Antibody-Drug Conjugates. *C&EN* **2014**, *92/3*, 13-21.

[26] N. Krall, J. Scheuermann, D. Neri. Small Targeted Cytotoxics: Current State and Promises from DNA-Encoded Chemical Libraries. *Angew. Chem. Int. Ed.* **2013**, *52*, 1384-1402.

[27] B. Q. Shen, K. Xu, L. Liu, H. Raab, S. Bhakta, M. Kenrick, K. L. Parsons-Reponte, J. Tien, S. F. Yu, E. Mai, D. Li, J. Tibbitts, J. Baudys, O. M. Saad, S. J. Scales, P. J. McDonald, P. E. Hass, C. Eigenbrot, T. Nguyen, W. A. Solis, R. N. Fuji, K. M. Flagella, D. Patel, S. D. Spencer, L. A. Khawli, A. Ebens, W. L. Wong, R. Vandlen, S. Kaur, M. X. Sliwkowski, R. H. Scheller, P. Polakis, J. R. Junutula. Conjugation site modulates the in vivo stability and therapeutic activity of antibody-drug conjugates. *Nat. Biotechnol.* **2012**, *30*, 184-189.

[28] P. J. Carter. Potent antibody therapeutics by design. *Nat. Rev. Immunol.* **2006**, *6*, 343-357.

[29] E. Perrino, M. Steiner, N. Krall, G. J. Bernardes, F. Pretto, G. Casi, D. Neri. Curative Properties of Noninternalizing Antibody-Drug Conjugates Based on Maytansinoids. *Cancer Res.* **2014**, *74*, 2569-2578.

[30] P. Strop, S. H. Liu, M. Dorywalska, K. Delaria, R. G. Dushin, T. T. Tran, W. H. Ho, S. Farias, M. G. Casas, Y. Abdiche, D. Zhou, R. Chandrasekaran, C. Samain, C. Loo, A. Rossi, M. Rickert, S. Krimm, T. Wong, S. M. Chin, J. Yu, J. Dilley, J. Chaparro-Riggers, G. F. Filzen, C. J. O'Donnell, F. Wang, J. S. Myers, J. Pons, D. L. Shelton, A. Rajpal. Location Matters: Site of Conjugation Modulates Stability and Pharmacokinetics of Antibody Drug Conjugates. *Chem. Biol.* **2013**, *20*, 161-167.

[31] M. Srinivasarao, C. V. Galliford, P. S. Low. Principles in the design of ligand-targeted cancer therapeutics and imaging agents. *Nat. Rev. Drug Discov.* **2015**, *14*, 203-219.

[32] R. Mahato, W. Tai, K. Cheng. Prodrugs for improving tumor targetability and efficiency. *Adv. Drug Deliv. Rev.* **2011**, *63*, 659-670.

[33] I. R. Vlahov, C. P. Leamon. Engineering Folate-Drug Conjugates to Target Cancer: From Chemistry to Clinic. *Bioconjugate Chem.* **2012**, *23*, 1357-1369.

[34] C. P. Leamon, I. R. Vlahov, J. A. Reddy, M. Vetzel, H. K. R. Santhapuram, F. You, A. Bloomfield, R. Dorton, M. Nelson, P. Kleindl, J. F. Vaughn, E. Westrick. Folate-Vinca Alkaloid Conjugates for Cancer Therapy: A Structure-Activity Relationship. *Bioconjugate Chem.* **2014**, *25*, 560-568.

[35] G. Casi, D. Neri. Antibody-Drug Conjugates and Small Molecule-Drug Conjugates: Opportunities and Challenges for the Development of Selective Anticancer Cytotoxic Agents. *J. Med. Chem.* **2015**, DOI: 10.1021/acs.jmedchem.5b00457.

[36] M. Dyba, N. I. Tarasova, C. J. Michejda. Small Molecule Toxins Targeting Tumor Receptors. *Curr. Pharm. Des.* **2004**, *10*, 2311-2334.

[37] A. Alouane, R. Labruère, T. Le Saux, F. Schmidt, L. Jullien. Self-Immolative Spacers: Kinetic Aspects, Structure-Property Relationships, and Applications. *Angew. Chem. Int. Ed.* **2015**, *54*, 7492-7509.

[38] W. H. Ang, S. Pilet, R. Scopelliti, F. Bussy, L. Juillerat-Jeanneret, P. J. Dyson. Synthesis and Characterization of Platinum(IV) Anticancer Drugs with Functionalized Aromatic Carboxylate Ligands: Influence of the Ligands on Drug Efficacies and Uptake. *J. Med. Chem.* **2005**, *48*, 8060-8069.

[39] D. J. Phillips, M. I. Gibson. Redox-Sensitive Materials for Drug Delivery: Targeting the Correct Intracellular Environment, Tuning Release Rates, and Appropriate Predictive Systems. *Antioxid. Redox Signaling* **2014**, *21*, 786-803.

[40] A. Meister. Glutathione, Ascorbate, and Cellular Protection. *Cancer Res.* **1994**, *54*, 1969s-1975s.

[41] O. H. Aina, R. Liu, J. L. Sutcliffe, J. Marik, C. -X. Pan, K. S. Lam. From Combinatorial Chemistry to Cancer-Targeting Peptides. *Mol. Pharmaceutics* **2007**, *4*, 631-651.

[42] M. Mayr, D. Bojanic. Novel trends in high-throughput screening. *Curr. Opin. Pharmacol.* **2009**, *9*, 580-588.

[43] R. M. Franzini, D. Neri, J. Scheuermann. DNA-Encoded Chemical Libraries: Advancing beyond Conventional Small-Molecule Libraries. *Acc. Chem. Res.* **2014**, *47*, 1247-1255.

[44] P. S. Low, W. A. Henne, D. D. Doorneweerd. Discovery and Development of Folic-Acid-Based Receptor Targeting for Imaging and Therapy of Cancer and Inflammatory Diseases. *Acc. Chem. Res.* **2008**, *41*, 120-129.

[45] T. Legigan, J. Clarhaut, I. Tranoy-Opalinski, A. Monvoisin, B. Renoux, M. Thomas, A. Le Pape, S. Lerondel, S. Papot. The First Generation of β-Galactosidase-Responsive Prodrugs Designed for the Selective Treatment of Solid Tumors in Prodrug Monotherapy. *Angew. Chem. Int. Ed.* **2012**, *51*, 11606-11610.

[46] I. Vergote, Christopher P. Leamon. Vintafolide: a novel targeted therapy for the treatment of folate receptor expressing tumors. *Ther. Adv. Med. Oncol.* **2015**, *7*, 206-218.

[47] W. A. Henne, S. A. Kularatne, J. Hakenjos, J. D. Carron, K. L. Henne. Synthesis and activity of a folate targeted monodisperse PEG camptothecin conjugate. *Bioorg. Med. Chem. Lett.* **2013**, *23* 5810-5813.

[48] Y. Singh, M. Palombo, P. J. Sinko. Recent Trends in Targeted Anticancer Prodrug and Conjugate Design. *Curr. Med. Chem*. **2008**, *15*, 1802-1826.

[49] C. Weiss, B. Sammet, N. Sewald. Recent approaches for the synthesis of modified cryptophycins. *Nat. Prod. Rep.* **2013**, *30*, 924-940.

[50] G. Russell-Jones, K. McTavish, J. McEwan, J. Rice, D. Nowotnik. Vitamin-mediated targeting as a potential mechanism to increase drug uptake by tumours. *J. Inorg. Biochem.* **2004**, *98*, 1625-1633.

[51] S. Maiti, N. Park, J. H. Han, H. M. Jeon, J. H. Lee, S. Bhuniya, C. Kang, J. S. Kim. Gemcitabine-Coumarin-Biotin Conjugates: A Target Specific Theranostic Anticancer Prodrug. *J. Am. Chem. Soc.* **2013**, *135*, 4567-4572.

[52] S. Park, E. Kim, W. Y. Kim, C. Kang, J. S. Kim. Biotin-guided anticancer drug delivery with acidity-triggered drug release. *Chem. Commun.* **2015**, *51*, 9343-9345.

[53] S. Chen, X. Zhao, J. Chen, J. Chen, L. Kuznetsova, S. S. Wong, I. Ojima. Mechanism-Based Tumor-Targeting Drug Delivery System. Validation of Efficient Vitamin Receptor-Mediated Endocytosis and Drug Release. *Bioconjugate Chem.* **2010**, *21*, 979-987.

[54] J. G. Vineberg, E. S. Zuniga, A. Kamath, Y. -J. Chen, J. D. Seitz, I. Ojima. Design, Synthesis, and Biological Evaluations of Tumor-Targeting Dual-Warhead Conjugates for a Taxoid−Camptothecin Combination Chemotherapy. *J. Med. Chem.* **2014**, *57*, 5777-5791.

[55] J. G. Vineberg, T. Wang, E. S. Zuniga, I. Ojima. Design, Synthesis, and Biological Evaluation of Theranostic Vitamin-Linker-Taxoid Conjugates. *J. Med. Chem.* **2015**, *58*, 2406-2416.

[56] S. Bhuniya, S. Maiti, E. -J. Kim, H. Lee, J. L. Sessler, K. S. Hong, J. S. Kim. An Activatable Theranostic for Targeted Cancer Therapy and Imaging. *Angew. Chem. Int. Ed.* **2014**, *53*, 4469-4474.

[57] A. Ghosh, W. D.W. Heston. Tumor Target Prostate Specific Membrane Antigen (PSMA) and its Regulation in Prostate Cancer. *J. Cell. Biochem.* **2004**, *91*, 528-539.

[58] S. A. Kularatne, K. Wang, H. K. R. Santhapuram, P. S. Low. Prostate-Specific Membrane Antigen Targeted Imaging and Therapy of Prostate Cancer Using a PSMA Inhibitor as a Homing Ligand. *Mol. Pharmaceutics* **2009**, *6*, 780-789.

[59] S. A. Kularatne, C. Venkatesh, H. K. R. Santhapuram, K. Wang, B. Vaitilingam, W. A. Henne, P. S. Low. Synthesis and Biological Analysis of Prostate-Specific Membrane Antigen-Targeted Anticancer Prodrugs. *J. Med. Chem.* **2010**, *53*, 7767-7777.

[60] J. Roy, T. X. Nguyen, A. K. Kanduluru, C. Venkatesh, W. Lv, P. V. N. Reddy, P. S. Low, M. Cushman. DUPA Conjugation of a Cytotoxic Indenoisoquinoline Topoisomerase I Inhibitor for Selective Prostate Cancer Cell Targeting. *J. Med. Chem.* **2015**, *58*, 3094-3103.

[61] M. Wichert, N. Krall. Targeting carbonic anhydrase IX with small organic ligands. *Curr. Opin. Chem. Biol.* **2015**, *26*, 48-54.

[62] N. Krall, F. Pretto, W. Decurtins, G. J. L. Bernardes, C. T. Supuran, D. Neri. A Small-Molecule Drug Conjugate for the Treatment of Carbonic Anhydrase IX Expressing Tumors. *Angew. Chem. Int. Ed.* **2014**, *53*, 4231-4235.

[63] M. Wichert, N. Krall, W. Decurtins, R. M. Franzini, F. Pretto, P. Schneider, D. Neri, J. Scheuermann. Dual-display of small molecules enables the discovery of ligand pairs and facilitates affinity maturation. *Nature Chem.* **2015**, *7*, 241-249.

[64] J. C. Reubi. Peptide Receptors as Molecular Targets for Cancer Diagnosis and Therapy. *Endocr. Rev.* **2003**, *24*, 389-427.

[65] J. B. Engel, A. V. Schally, J. Dietl, L. Rieger, A. Hönig. Targeted Therapy of Breast and Gynecological Cancers with Cytotoxic Analogues of Peptide Hormones. *Mol. Pharmaceutics* **2007**, *4*, 652-658.

[66] S. Buchholz, G. Keller, A. V. Schally, G. Halmos, F. Hohla, E. Heinrich, F. Koester, B. Baker, J. B. Engel. Therapy of ovarian cancers with targeted cytotoxic analogs of bombesin, somatostatin, and luteinizing hormone-releasing hormone and their combinations. *Proc. Natl. Acad. Sci. USA* **2006**, *103*, 10403-10407.

[67] C. W. Kwok, O. Treeck, S. Buchholz, S. Seitz, O. Ortmann, J. B. Engel. Receptors for luteinizing hormone-releasing hormone (GnRH) as therapeutic targets in triple negative breast cancers (TNBC). *Target. Oncol.* **2014**, *10*, 365-373.

[68] I. Szabó, S. Bősze, E. Orbán, É. Sipos, G. Halmos, M. Kovácsc, G. Mező. Comparative in vitro biological evaluation of daunorubicin containing GnRH-I and GnRH-II conjugates developed for tumor targeting. *J. Pept. Sci.* **2015**; *21*, 426-435.

[69] C. Wang, Y. Ma, S. Feng, K. Liu, N. Zhou. Gonadotropin-releasing hormone receptor targeted paclitaxel–degarelix conjugate: synthesis and in vitro evaluation. *J. Pept. Sci.* **2015**; *27*, 569-576.

[70] T. Karampelas, O. Argyros, N. Sayyad, K. Spyridaki, C. Pappas, K. Morgan, G. Kolios, R. P Millar, G. Liapakis, A. G. Tzakos, D. Fokas, C. Tamvakopoulos. GnRH-Gemcitabine

Conjugates for the Treatment of Androgen-Independent Prostate Cancer: Pharmacokinetic Enhancements Combined with Targeted Drug Delivery. *Bioconjugate Chem.* **2014**, *25*, 813-823.

[71] M. Volante, R. Rosas, E. Allìa, R. Granata, A. Baragli, G. Muccioli, M. Papotti. Somatostatin, cortistatin and their receptors in tumours. *Mol. Cell. Endocrinol.* **2008**, *286*, 219-229.

[72] H. R. Maecke, J. C. Reubi. Somatostatin Receptors as Targets for Nuclear Medicine Imaging and Radionuclide Treatment. *J. Nucl. Med.* **2011**, *52*, 841-844.

[73] C. -M. Huang, Y. -T. Wu, S. -T. Chen. Targeting delivery of paclitaxel into tumor cells via somatostatin receptor endocytosis. *Chem. Biol.* **2000**, *7*, 453-461.

[74] M. Huo, Q. Zhu, Q. Wu, T. Yin, L. Wang, L. Yin, J. Zhou. Somatostatin Receptor-Mediated Specific Delivery of Paclitaxel Prodrugs for Efficient Cancer Therapy. *J. Pharm. Sci.* **2015**, *104*, 2018-2028.

[75] J. Zhang, W. Jin, X. Wang, J. Wang, X. Zhang, Q. Zhang. A Novel Octreotide Modified Lipid Vesicle Improved the Anticancer Efficacy of Doxorubicin in Somatostatin Receptor 2 Positive Tumor Models. *Mol. Pharmaceutics* **2010**, *7*, 1159-1168.

[76] A. Nagy, P. Armatis, R. -Z. Cai, K. Szepeshazi, G. Halmos, A. V. Schally. Design, synthesis, and in vitro evaluation of cytotoxic analogs of bombesin-like peptides containing doxorubicin or its intensely potent derivative, 2-pyrrolinodoxorubicin. *Proc. Natl. Acad. Sci. USA* **1997**, *94*, 652-656.

[77] A. Plonowski, A. Nagy, A. V. Schally, B. Sun, K. Groot, G. Halmos. *in vivo* inhibition of PC-3 human androgen-independent prostate cancer by a targeted cytotoxic bombesin analogue, AN-215. *Int. J. Cancer*, **2000**, *88*, 652-657.

[78] A. Stangelberger, A. V. Schally, M. Letsch, K. Szepeshazi, A. Nagy, G. Halmos, C. A. Kanashiro, E. Corey, R. Vessella. Targeted chemotherapy with cytotoxic bombesin analogue AN-215 inhibits growth of experimental human prostate cancers. *Int. J. Cancer*, **2006**, *118*, 222-229.

[79] R. Mansi, K. Abiraj, X. Wang, M. L. Tamma, E. Gourni, R. Cescato, S. Berndt, J. C. Reubi, H. R. Maecke. Evaluation of Three Different Families of Bombesin Receptor Radioantagonists for Targeted Imaging and Therapy of Gastrin Releasing Peptide Receptor (GRP-R) Positive Tumors. *J. Med. Chem.* **2015**, *58*, 682-691.

[80] E. Kähkönen, I. Jambor, J. Kemppainen, K. Lehtiö, T. J. Grönroos, A. Kuisma, P. Luoto, H. J. Sipilä, T. Tolvanen, K. Alanen, J. Silén, M. Kallajoki, A. Roivainen, N. Schäfer, R. Schibli, M. Dragic, A. Johayem, R. Valencia, S. Borkowski, H. Minn. *In Vivo* Imaging of Prostate Cancer Using [^{68}Ga]-Labeled Bombesin Analog BAY86-7548. *Clin. Cancer Res.* **2013**, *19*, 5434-5443.

[81] G. Li, P. S. Low. Synthesis and evaluation of a ligand targeting the somatostatin-2 receptor for drug delivery to neuroendocrine cancers. *Bioorg. Med. Chem. Lett.* **2015**, *25*, 1792-1798.

[82] C. Wayua, P. S. Low. Evaluation of a Nonpeptidic Ligand for Imaging of Cholecystokinin 2 Receptor-Expressing Cancers. *J. Nucl. Med.* **2015**, *56*, 113-119.

[83] C. Wayua, J. Roy, K. S. Putt, P. S. Low. Selective Tumor Targeting of Desacetyl Vinblastine Hydrazide and Tubulysin B via Conjugation to a Cholecystokinin 2 Receptor (CCK2R) Ligand. *Mol. Pharmaceutics* **2015**, *12*, 2477-2483.

[84] K. -L. Dao, R. N. Hanson. Targeting the Estrogen Receptor using Steroid-Therapeutic Drug Conjugates (Hybrids). *Bioconjugate Chem.* **2012**, *23*, 2139-2158.

[85] R. N. Hanson, E. Hua, D. Labaree, R. B. Hochberg, K. Proffitt, J. M. Essigmannc, R. G. Croyc. Convergent synthesis of a steroidal antiestrogen-mitomycin C hybrid using “click” chemistry *Org. Biomol. Chem.* **2012**, *10*, 8501-8508.

[86] K. -L. Dao, R. R. Sawant, J. A. Hendricks, V. Ronga, V. P. Torchilin, R. N. Hanson. Design, Synthesis, and Initial Biological Evaluation of a Steroidal Anti-Estrogen-Doxorubicin Bioconjugate for Targeting Estrogen Receptor-Positive Breast Cancer Cells. *Bioconjugate Chem.* **2012**, *23*, 785-795.

[87] D. Cox, M. Brennan, N. Moran. Integrins as therapeutic targets: lessons and opportunities. *Nat. Rev. Drug Disc.* **2010**, *9*, 804-820.

[88] M. Moser, K. R. Legate, R. Zent, R. Fässler. The Tail of Integrins, Talin, and Kindlins. *Science* **2009**, *324*, 895-899.

[89] W. Guo, F. G. Giancotti. Integrin Signalling During Tumor Progression. *Nat. Rev. Mol. Cell Biol.* **2004**, *5*, 816-826.

[90] F. G. Giancotti, G. Tarone. Positional control of cell fate through joint integrin/receptor protein kinase signaling. *Annu. Rev. Cell Dev. Biol.* **2003**, *19*, 173-206.

[91] C. K. Miranti, J. S. Brugge. Sensing the environment: a historical perspective on integrin signal transduction. *Nat. Cell. Biol.* **2002**, *4*, E83-E90.

[92] M. -Y. Hsu, D. -T. Shih, F. E. Meier, P. Van Belle, J. -Y. Hsu, D. E. Elder, C. A. Buck, M. Herlyn. Adenoviral gene transfer of β_3 integrin subunit induces conversion from radial to vertical growth phase in primary human melanoma. *Am. J. Pathol.* **1998**, *153*, 1435-1442.

[93] J. S. Desgrosellier, D. A. Cheresh. Integrins in cancer: biological implications and therapeutic opportunities. *Nat. Rev. Cancer* **2010**, *10*, 9-22.

[94] M. D. Pierschbacher, E. Ruoslahti. Cell attachment activity of fibronectin can be duplicated by small synthetic fragments of the molecule. *Nature*, **1984**, *309*, 30-33.

[95] E. Ruoslahti, M. D. Pierschbacher. New perspectives in cell adhesion: RGD and integrins. *Science*, **1987**, *238*, 491-497.

[96] M. Aumailley, M. Gurrath, G. Müller, J. Calvete, R. Timpl, H. Kessler. Arg-Gly-Asp constrained within cyclic pentapeptides. Strong and selective inhibitors of cell adhesion to vitronectin and laminin fragment P1. *FEBS Lett.* **1991**, *291*, 50-54.

[97] R. S. McDowell, T. R. Gadek, Structural studies of potent constrained RGD peptides. *J. Am. Chem. Soc.* **1992**, *114*, 9245-9253.

[98] R. Pasqualini, E. Koivunen, E. Ruoslahti, α_v Integrins as receptors for tumor targeting by circulating ligands. *Nat. Biotech.* **1997**, *15*, 542-546.

[99] J. -P. Xiong, T. Stehle, T.; Zhang, R.; Joachimiak, A.; Frech, M.; Goodman, S. L.; Arnaout, M. A. Crystal Structure of the Extracellular Segment of Integrin $\alpha_V\beta_3$ in Complex with an Arg-Gly-Asp Ligand. *Science*, **2002**, *296*, 151-155.

[100] K. -E. Gottschalk, H. Kessler. The Structures of Integrins and Integrin-Ligand Complexes: Implications for Drug Design and Signal Transduction. *Angew. Chem. Int. Ed.* **2002**, *41*, 3767-3774.

[101] J. Spiegel, C. Mas-Moruno, H. Kessler, W. D. Lubell. Cyclic Aza-peptide Integrin Ligand Synthesis and Biological Activity. *J. Org. Chem.* **2012**, *77*, 5271-5278.

[102] S. Neubauer, F. Rechenmacher, R. Brimioulle, F. S. Di Leva, A. Bochen, T. R. Sobahi, M. Schottelius, E. Novellino, C. Mas-Moruno, L. Marinelli, H. Kessler. Pharmacophoric Modifications Lead to Superpotent $\alpha_v\beta_3$ Integrin Ligands with Suppressed $\alpha_5\beta_1$ Activity. *J. Med. Chem.* **2014**, *57*, 3410-3417.

[103] L. Auzzas, F. Zanardi, L. Battistini, P. Burreddu, P. Carta, G. Rassu, C. Curti, G. Casiraghi. Targeting $\alpha_v\beta_3$ Integrin: Design and Applications of Mono- and Multifunctional RGD-Based Peptides and Semipeptides. *Curr. Med. Chem.* **2010**, *17*, 1255-1299.

[104] C. C. Suna, X. J. Qua, Z. H. Gao. Integrins: players in cancer progression and targets in cancer therapy. *Anticancer Drugs* **2014**, *25*, 1107-1121.

[105] A. R. Reynolds, I. R. Hart, A. R. Watson, J. C. Welti, R. G. Silva, S. D. Robinson, G. Da Violante, M. Gourlaouen, M. Salih, M. C. Jones, D. T. Jones, G. Saunders, V. Kostourou, F. Perron-Sierra, J. C. Norman, G. C. Tucker, K. M. Hodivala-Dilke. Stimulation of tumor growth and angiogenesis by low concentrations of RGD-mimetic integrin inhibitors. *Nat. Med.* **2009**, *15*, 392-400.

[106] G. C. Alghisi, L. Ponsonnet, C. Rüegg. The Integrin Antagonist Cilengitide Activates $\alpha_V\beta_3$, Disrupts VE-Cadherin Localization at Cell Junctions and Enhances Permeability in Endothelial Cells. *PLoS ONE* **2009**, *4*, e4449.

[107] G. Eisele, A. Wick, A. -C. Eisele, P. Clément, J. Tonn, G. Tabatabai, A. Ochsenbein, U. Schlegel, B. Neyns, D. Krex, M. Simon, G. Nikkhah, M. Picard, R. Stupp, W. Wick, M. Weller. Cilengitide treatment of newly diagnosed glioblastoma patients does not alter patterns of progression. *J. Neurooncol.* **2014**, *117*, 141-145.

[108] S. M. Weis, D. G. Stupack, D. A. Cheresh. Agonizing Integrin Antagonists? *Cancer Cell* **2009**, *15*, 359-361.

[109] S. H. Shabbir, J. L. Eisenberg, M. Mrksich. An Inhibitor of a Cell Adhesion Receptor Stimulates Cell Migration. *Angew. Chem. Int. Ed.* **2010**, *49*, 7706-7709.

[110] S. D. Robinson, K. M. Hodivala-Dilke. The role of β_3-integrins in tumor angiogenesis: context is everything. *Curr. Opin. Cell Biol.* **2011**, *23*, 630-637.

[111] M. S Kim, D. -W. Lee, K. Park, S. -J. Park, E. -J. Choi, E. S. Park, H. R. Kim. Temperature-triggered tumor-specific delivery of anticancer agents by *c*RGD-conjugated thermosensitive liposomes. *Colloids Surf. B Biointerfaces* **2014**, *116*, 17-25.

[112] M. Amin, A. Badiee, M. R. Jaafari. Improvement of pharmacokinetic and antitumor activity of PEGylated liposomal doxorubicin by targeting with N-methylated cyclic RGD peptide in mice bearing C-26 colon carcinomas. *Int. J. Pharm.* **2013**, *458*, 324-333.

[113] L. Battistini, P. Burreddu, A. Sartori, D. Arosio, L. Manzoni, L. Paduano, G. D'Errico, R. Sala, L. Reia, S. Bonomini, G. Rassu, F. Zanardi. Enhancement of the Uptake and Cytotoxic Activity of Doxorubicin in Cancer Cells by Novel *c*RGD-Semipeptide-Anchoring Liposomes. *Mol. Pharmaceutics* **2014**, *11*, 2280-2293.

[114] D. Arosio, L. Manzoni, E. M. V. Araldi, C. Scolastico. Cyclic RGD Functionalized Gold Nanoparticles for Tumor Targeting. *Bioconjugate Chem.* **2011**, *22*, 664-672.

[115] Y. Zhong, F. Meng, C. Deng, Z. Zhong. Ligand-Directed Active Tumor-Targeting Polymeric Nanoparticles for Cancer Chemotherapy. *Biomacromolecules* **2014**, *15*, 1955-1969.

[116] K. Cheng, S. -R. Kothapalli, H. Liu, A. L. Koh, J. V. Jokerst, H. Jiang, M. Yang, J. Li, J. Levi, J. C. Wu, S. S. Gambhir, Z. Cheng. Construction and Validation of Nano Gold Tripods for Molecular Imaging of Living Subjects. *J. Am. Chem. Soc.* **2014**, *136*, 3560-3571.

[117] S. Lanzardo, L. Conti, C. Brioschi, M. P. Bartolomeo, D. Arosio, L. Belvisi, L. Manzoni, A. Maiocchi, F. Maisano, G. Forni. A new optical imaging probe targeting $\alpha_V\beta_3$ integrin in glioblastoma xenografts. *Contrast Media Mol. Imaging* **2011**, *6*, 449-458.

[118] J. Shi, L. Wang, Y. -S. Kim, S. Zhai, Z. Liu, X. Chen, S. Liu. Improving Tumor Uptake and Excretion Kinetics of ^{99m}Tc-Labeled Cyclic Arginine-Glycine-Aspartic (RGD) Dimers with Triglycine Linkers. *J. Med. Chem.* **2008**, *51*, 7980-7990.

[119] A. M. Mozida, M. Holstenssonb, T. Choudhurya, S. Ben-Haimb, R. Allieb, J. Martinc, A. J. Sinusasd, B. F. Huttonb, A. Mathura. Clinical feasibility study to detect angiogenesis following bone marrow stem cell transplantation in chronic ischaemic heart failure. *Nucl. Med. Commun.* **2014**, *35*, 839-848.

[120] Y. Zhou, S. Chakraborty, S. Liu. Radiolabeled Cyclic RGD Peptides as Radiotracers for Imaging Tumors and Thrombosis by SPECT. *Theranostics* **2011**, *1*, 58-82.

[121] M. Janssen, W. J. Oyen, L. F. Massuger, C. Frielink, I. Dijkgraaf, D. S. Edwards, M. Radjopadhye, F. H. Corstens, O. C. Boerman. Comparison of a Monomeric and Dimeric Radiolabeled RGD-Peptide for Tumor Targeting. *Cancer Biother. Radiopharm.* **2002**, *17*, 641-646.

[122] C. Fasting, C. A. Schalley, M. Weber, O. Seitz, S. Hecht, B. Koksch, J. Dernedde, C. Graf, E. -W. Knapp, R. Haag. Multivalency as a Chemical Organization and Action Principle. *Angew. Chem. Int. Ed.* **2012**, *51*, 10472-10498.

[123] W. Wan, N. Guo, D. Pan, C. Yu, Y. Weng, S. Luo, H. Ding, Y. Xu, L. Wang, L. Lang, Q. Xie, M. Yang, X. Chen. First Experience of ^{18}F-Alfatide in Lung Cancer Patients Using a New Lyophilized Kit for Rapid Radiofluorination. *J. Nucl. Med.* **2013**, *54*, 691-698.

[124] C. Yu, D. Pan, B. Mi, Y. Xu, L. Lang, G. Niu, M. Yang, W. Wan, X. Chen. ^{18}F-Alfatide II PET/CT in healthy human volunteers and patients with brain metastases. *Eur. J. Nucl. Med. Mol. Imaging* **2015**, DOI: 10.1007/s00259-015-3118-2.

[125] J. Shi, Y. S. Kim, S. Chakraborty, Y. Zhou, F. Wang, S. Liu. Impact of bifunctional chelators on biological properties of ^{111}In-labeled cyclic peptide RGD dimers. *Amino Acids* **2011**, *41*, 1059-1070.

[126] S. Maschauer, R. Haubner, T. Kuwert, O. Prante. 18F-Glyco-RGD Peptides for PET Imaging of Integrin Expression: Efficient Radiosynthesis by Click Chemistry and Modulation of Biodistribution by Glycosylation. *Mol. Pharmaceutics* **2014**, *11*, 505-515.

[127] Y. Yang, S. Ji, S. Liu. Impact of Multiple Negative Charges on Blood Clearance and Biodistribution Characteristics of ^{99m}Tc-Labeled Dimeric Cyclic RGD Peptides. *Bioconjugate Chem.* **2014**, *25*, 1720-1729.

[128] S. Ji, A. Czerwinski, Y. Zhou, G. Shao, F. Valenzuela, P. Sowinski,́S. Chauhan, M. Pennington, S. Liu. ^{99m}Tc-Galacto-RGD$_2$: A Novel ^{99m}Tc-Labeled Cyclic RGD Peptide Dimer Useful for Tumor Imaging. *Mol. Pharmaceutics* **2013**, *10*, 3304-3314.

[129] P. Caswell, J. Norman. Endocytic transport of integrins during cell migration and invasion. *Trends Cell Biol.* **2008**, *18*, 257-263.

[130] P. T. Caswell, S. Vadrevu, J. C. Norman. Integrins: masters and slaves of endocytic transport. *Nat. Rev. Mol. Cell Biol.* **2009**, *10*, 843-853.

[131] D. J. Burkhart, B. T. Kalet, M. P. Coleman, G. C. Post, T. H. Koch. Doxorubicin-formaldehyde conjugates targeting $\alpha_v\beta_3$ integrin. *Mol. Cancer Ther.* **2004**, *3*, 1593-1604.

[132] X. Chen, C. Plasencia, Y. Hou, N. Neamati. Synthesis and Biological Evaluation of Dimeric RGD Peptide-Paclitaxel Conjugate as a Model for Integrin-Targeted Drug Delivery. *J. Med. Chem.* **2005**, *48*, 1098-1106; Additions and Corrections **2005**, *48*, 5874.

[133] Q. Cao, Z. -B. Li, K. Chen, Z. Wu, L. He, N. Neamati, X. Chen. Evaluation of biodistribution and anti-tumor effect of a dimeric RGD peptide-paclitaxel conjugate in mice with breast cancer. *Eur. J. Nucl. Med. Mol. Imaging* **2008**, *35*, 1489-1498.

[134] C. Ryppa, H. Mann-Steinberg, M. L. Biniossek, R. Satchi-Fainaro, F. Kratz. *In vitro* and *in vivo* evaluation of a paclitaxel conjugate with the divalent peptide E-[*c*(RGDfK)$_2$] that targets integrin $\alpha_v\beta_3$. *Int. J. Pharm.* **2009**, *368*, 89-97.

[135] M. Pilkington-Miksa, D. Arosio, L. Battistini, L. Belvisi, M. De Matteo, F. Vasile, P. Burreddu, P. Carta, G. Rassu, P. Perego, N. Carenini, F. Zunino, M. De Cesare, V. Castiglioni, E. Scanziani, C. Scolastico, G. Casiraghi, F. Zanardi, L. Manzoni. Design, Synthesis, and Biological Evaluation of Novel *c*RGD-Paclitaxel Conjugates for Integrin-Assisted Drug Delivery. *Bioconjugate Chem.* **2012**, *23*, 1610-1622.

[136] A. Bianchi, D. Arosio, P. Perego, M. De Cesare, N. Carenini, N. Zaffaroni, M. De Matteo, L. Manzoni. Design, synthesis and biological evaluation of novel dimeric and tetrameric *c*RGD-paclitaxel conjugates for integrin-assisted drug delivery. *Org. Biomol. Chem.* **2015**, *13*, 7530-7541.

[137] A. Dal Pozzo, M. -H. Ni, E. Esposito, S. Dallavalle, L. Musso, A. Bargiotti, C. Pisano, L. Vesci, F. Bucci, M. Castorina, R. Foderà, G. Giannini, C. Aulicino, S. Penco. Novel tumor-targeted RGD peptide–camptothecin conjugates: Synthesis and biological evaluation. *Bioorg. Med. Chem.* **2010**, *18*, 64-72.

[138] D. Polyak, C. Ryppa, A. Eldar-Boock, P. Ofek, A. Many, K. Licha, F. Kratz, R. Satchi-Fainaro. Development of PEGylated doxorubicin-E-[*c*(RGDfK)$_2$] conjugate for integrin-targeted cancer therapy. *Polym. Adv. Technol.* **2011**, *22*, 103-113.

[139] F. M. H. de Groot, H. J. Broxterman, H. P. H. M. Adams, A. van Vliet, G. I. Tesser, Y. W. Elderkamp, A. J. Schraa, R. Jan Kok, G. Molema, H. M. Pinedo, H. W. Scheeren. Design, Synthesis, and Biological Evaluation of a Dual Tumor-specific Motive Containing Integrin-targeted Plasmin-cleavable Doxorubicin Prodrug. *Mol. Cancer Ther.* **2002**, *1*, 901-911.

[140] C. Ryppa, H. Mann-Steinberg, I. Fichtner, H. Weber, R. Satchi-Fainaro, M. L. Biniossek, F. Kratz. *In Vitro* and *in Vivo* Evaluation of Doxorubicin Conjugates with the Divalent Peptide E-[*c*(RGDfK)$_2$] that Targets Integrin $\alpha_v\beta_3$. *Bioconjugate Chem.* **2008**, *19*, 1414-1422.

[141] J. L. Crisp, E. N. Savariar, H. L. Glasgow, L. G. Ellies, M. A. Whitney, R. Y. Tsien. Dual Targeting of Integrin $\alpha_v\beta_3$ and Matrix Metalloproteinase-2 for Optical Imaging of Tumors and Chemotherapeutic Delivery. *Mol. Cancer Ther.* **2014**, *13*, 1514-1525.

[142] A. Dal Pozzo, E. Esposito, M. Ni, L. Muzi, C. Pisano, F. Bucci, L. Vesci, M. Castorina, S. Penco. Conjugates of a Novel 7-Substituted Camptothecin with RGD-Peptides as $\alpha_v\beta_3$ Integrin Ligands: An Approach to Tumor-Targeted Therapy. *Bioconjugate Chem.* **2010**, *21*, 1956-1967.

[143] Y. Liu, K. M. Bajjuri, C. Liu, S. C. Sinha. Targeting Cell Surface $\alpha_v\beta_3$ Integrin Increases Therapeutic Efficacies of a Legumain Protease-Activated Auristatin Prodrug. *Mol. Pharmaceutics* **2012**, *9*, 168-175.

[144] M. H. Lee, J. Y. Kim, J. H. Han, S. Bhuniya, J. L. Sessler, C. Kang, J. S. Kim. Direct Fluorescence Monitoring of the Delivery and Cellular Uptake of a Cancer-Targeted RGD Peptide-Appended Naphthalimide Theragnostic Prodrug. *J. Am. Chem. Soc.* **2012**, *134*, 12668-12674.

[145] S. Mukhopadhyay, C. M. Barnés, A. Haskel, S. M. Short, K. R. Barnes, S. J. Lippard, Conjugated Platinum(IV)-Peptide Complexes for Targeting Angiogenic Tumor Vasculature. *Bioconjugate Chem.* **2008**, *19*, 39-49.

[146] Y. Yuan, R. T. K. Kwok, R. Zhang, B. Z. Tang, B. Liu. Targeted theranostic prodrugs based on an aggregation-induced emission (AIE) luminogen for real-time dual-drug tracking. *Chem. Commun.* **2014**, *50*, 11465-11468.

[147] W. Arap, R. Pasqualini, E. Ruoslahti. Cancer Treatment by Targeted Drug Delivery to Tumor Vasculature in a Mouse Model. *Science* **1998**, *279*, 377-380.

[148] K. Temming, R. M. Schiffelers, G. Molema, R. J. Kok. RGD-based strategies for selective delivery of therapeutics and imaging agents to the tumour vasculature. *Drug Resist. Updat.* **2005**, *8*, 381-402.

[149] A. D. Borthwick. 2,5-Diketopiperazines: Synthesis, Reactions, Medicinal Chemistry, and Bioactive Natural Products. *Chem. Rev.* **2012**, *112*, 3641-3716.

[150] A. S. M. Ressurreição, A. Vidu, M. Civera, L. Belvisi, D. Potenza, L. Manzoni, S. Ongeri, C. Gennari, U. Piarulli. Cyclic RGD-Peptidomimetics Containing Bifunctional Diketopiperazine Scaffolds as New Potent Integrin Ligands. *Chem. Eur. J.* **2009**, *15*, 12184-12188.

[151] M. Marchini, M. Mingozzi, R. Colombo, I. Guzzetti, L. Belvisi, F. Vasile, D. Potenza, U. Piarulli, D. Arosio, C. Gennari. Cyclic RGD Peptidomimetics Containing Bifunctional Diketopiperazine Scaffolds as New Potent Integrin Ligands. *Chem. Eur. J.* **2012**, *18*, 6195-6207.

[152] R. Fanelli, L. Schembri, U. Piarulli, M. Pinoli, E. Rasini, M. Paolillo, M. C. Galiazzo, M. Cosentino, F. Marino. Effects of a novel cyclic RGD peptidomimetic on cell proliferation, migration and angiogenic activity in human endothelial cells. *Vasc. Cell* **2014**, *6*, 11.

[153] S. Panzeri, S. Zanella, D. Arosio, L. Vahdati, A. Dal Corso, L. Pignataro, M. Paolillo, S. Schinelli, L. Belvisi, C. Gennari, U. Piarulli. Cyclic *iso*DGR and RGD Peptidomimetics Containing Bifunctional Diketopiperazine Scaffolds are Integrin Antagonists. *Chem. Eur. J.* **2015**, *21*, 6265-6271

[154] R. Colombo, M. Mingozzi, L. Belvisi, D. Arosio, U. Piarulli, N. Carenini, P. Perego, N. Zaffaroni, M. De Cesare, V. Castiglioni, E. Scanziani C. Gennari. Synthesis and Biological Evaluation (*in Vitro* and *in Vivo*) of Cyclic Arginine-Glycine-Aspartate (RGD) Peptidomimetic-Paclitaxel Conjugates Targeting Integrin $\alpha_V\beta_3$. *J. Med. Chem.* **2012**, *55*, 10460-10474.

[155] M. Mingozzi, L. Manzoni, D. Arosio, A. Dal Corso, M. Manzotti, F. Innamorati, L. Pignataro, D. Lecis, D. Delia, P. Seneci, C. Gennari. Synthesis and biological evaluation of dual action *cyclo*-RGD/SMAC mimetic conjugates targeting $\alpha_V\beta_3/\alpha_V\beta_5$ integrins and IAP proteins. *Org. Biomol. Chem.* **2014**, *12*, 3288-3302.

[156] S. Zanella, M. Mingozzi, A. Dal Corso, R. Fanelli, D. Arosio, M. Cosentino, L. Schembri, F. Marino, M. De Zotti, F. Formaggio, L. Pignataro, L. Belvisi, U. Piarulli, C. Gennari. Synthesis, characterization and biological evaluation of a dual action ligand targeting $\alpha_V\beta_3$ integrin and VEGF receptors. *ChemistryOpen* **2015**, *4*, 633-641.

[157] M. Nahrwold, C. Weiß, T. Bogner, F. Mertink, J. Conradi, B. Sammet, R. Palmisano, S. Royo Gracia, T. Preuße, N. Sewald. Conjugates of Modified Cryptophycins and RGD-Peptides Enter Target Cells by Endocytosis. *J. Med. Chem.* **2013**, *56*, 1853-1864.

[158] F. M. H. de Groot, L. W. A. van Berkom, H. W. Scheeren. Synthesis and Biological Evaluation of 2'-Carbamate-Linked and 2'-Carbonate-Linked Prodrugs of Paclitaxel: Selective Activation by the Tumor-Associated Protease Plasmin. *J. Med. Chem.* **2000**, *43*, 3093-3102.

[159] F. M. H. de Groot, W. J. Loos, R. Koekkoek, L. W. A. van Berkom, G. F. Busscher, A. E. Seelen, C. Albrecht, P. de Bruijn, H. W. Scheeren. Elongated Multiple Electronic Cascade

and Cyclization Spacer Systems in Activatible Anticancer Prodrugs for Enhanced Drug Release. *J. Org. Chem.* **2001**, *66*, 8815-8830.

[160] A. D. Wong, M. A. DeWit, E. R. Gillies. Amplified release through the stimulus triggered degradation of self-immolative oligomers, dendrimers, and linear polymers. *Adv. Drug Deliv. Rev.* **2012**, *64*, 1031-1045.

[161] K. Hochdörffer, K. Abu Ajaj, C. Schäfer-Obodozie, F. Kratz. Development of Novel Bisphosphonate Prodrugs of Doxorubicin for Targeting Bone Metastases That Are Cleaved pH Dependently or by Cathepsin B: Synthesis, Cleavage Properties, and Binding Properties to Hydroxyapatite As Well As Bone Matrix. *J. Med. Chem.* **2012**, *55*, 7502-7515.

[162] A. Dal Corso, M. Caruso, L. Belvisi, D. Arosio, U. Piarulli, C. Albanese, F. Gasparri, A. Marsiglio, F. Sola, S. Troiani, B. Valsasina, L. Pignataro, D. Donati, C. Gennari. Synthesis and Biological Evaluation of RGD Peptidomimetic-Paclitaxel Conjugates bearing Lysosomally Cleavable Linkers. *Chem. Eur. J.* **2015**, *21*, 6921-6929.

[163] Y. Meyer, J. -A. Richard, B. Delest, P. Noack, P. -Y. Renard, A. Romieu. A comparative study of the self-immolation of para-aminobenzylalcohol and hemithioaminal-based linkers in the context of protease-sensitive fluorogenic probes. *Org. Biomol. Chem.* **2010**, *8*, 1777-1780.

[164] X. Wang, D. Ma, W. C. Olson, W. D. W. Heston. *In Vitro* and *In Vivo* Responses of Advanced Prostate Tumors to PSMA ADC, an Auristatin-Conjugated Antibody to Prostate-Specific Membrane Antigen. *Mol. Cancer Ther.* **2011**, *10*, 1728-1739.

[165] A. Dal Corso, L. Pignataro, L. Belvisi, C. Gennari. $\alpha_v\beta_3$ Integrin-Targeted Peptide /Peptidomimetic-Drug Conjugates: In-Depth Analysis of the Linker Technology. *Curr. Top. Med. Chem.* **2016**, *16*, 314-329.

[166] X. Ma, J. Jia, R. Cao, X. Wang, H. Fei. Histidine−Iridium(III) Coordination-Based Peptide Luminogenic Cyclization and Cyclo-RGD Peptides for Cancer-Cell Targeting. *J. Am. Chem. Soc.* **2014**, *136*, 17734-17737.

[167] D. Boturyn, J. L. Coll, E. Garanger, M. C. Favrot, P. Dumy. Template Assembled Cyclopeptides as Multimeric System for Integrin Targeting and Endocytosis. *J. Am. Chem. Soc.* **2004**, *126*, 5730-5739.

[168] D. S. Choi, H. -E. Jin, S. Y. Yoo, S. -W. Lee. Cyclic RGD Peptide Incorporation on Phage Major Coat Proteins for Improved Internalization by HeLa Cells. *Bioconjugate Chem.* **2014**, *25*, 216-223.

[169] S. Ordanini, N. Varga, V. Porkolab, M. Thépaut, L. Belvisi, A. Bertaglia, A. Palmioli, A. Berzi, D. Trabattoni, M. Clerici, F. Fieschi, A. Bernardi. Designing nanomolar antagonists of DC-SIGN-mediated HIV infection: ligand presentation using molecular rods. *Chem. Commun.* **2015**, *51*, 3816-3819.

[170] D. J. Welsh, P. Posocco, S. Pricl, D. K. Smith. Self-assembled multivalent RGD-peptide arrays - morphological control and integrin binding. *Org. Biomol. Chem.* **2013**, *11*, 3177-3186.

[171] S. S. Kelkar, T. M. Reineke. Theranostics: Combining Imaging and Therapy. *Bioconjugate Chem.* **2011**, *22*, 1879-1903.

[172] K. Y. Choi, M. Swierczewska, S. Lee, X. Chen. Protease-Activated Drug Development. *Theranostics* **2012**, *2*, 156-178.

[173] A. G. Cheetham, Y. -C. Ou, P. Zhang, H. Cui. Linker-determined drug release mechanism of free camptothecin from self-assembling drug amphiphiles. *Chem. Commun.* **2014**, *50*, 6039-6042.

[174] M. H. Lee, J. H. Han, P. -S. Kwon, S. Bhuniya, J. Y. Kim, C. Kang, J. S. Kim. Hepatocyte-Targeting Single Galactose-Appended Naphthalimide: A Tool for Intracellular Thiol Imaging *in Vivo*. *J. Am. Chem. Soc.* **2012**, *134*, 1316-1322.

[175] Z. X. Dong, Y. Shen, J. M. Comstock, S. H. Kim. Somatostatin Vectors. EP1624884 A2, **2004**.

[176] W. C. Still, M. Kahn, A. Mitra. Rapid Chromatographic Technique for Preparative Separations with Moderate Resolution. *J. Org. Chem.* **1978**, *43*, 2923-2925.

[177] G. R. Fulmer, A. J. M. Miller, N. H. Sherden, H. E. Gottlieb, A. Nudelman, B. M. Stoltz, J. E. Bercaw, K. I. Goldberg. NMR Chemical Shifts of Trace Impurities: Common Laboratory Solvents, Organics, and Gases in Deuterated Solvents Relevant to the Organometallic Chemist. *Organometallics* **2010**, *29*, 2176-2179.